METHODS IN MOLECULAR BIOLOGY™ 399

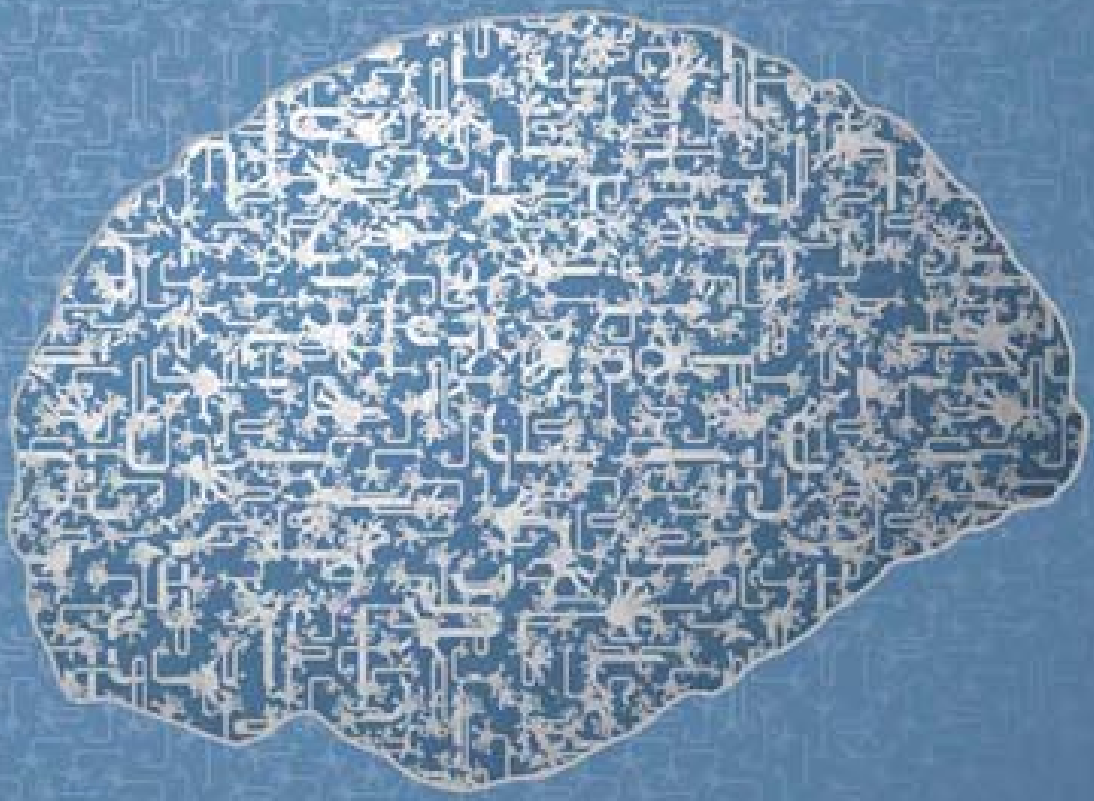

Neuroprotection
Methods and Protocols

Edited by
Tiziana Borsello

HUMANA PRESS

Neuroprotection Methods and Protocols

METHODS IN MOLECULAR BIOLOGY™

John M. Walker, SERIES EDITOR

399. **Neuroprotection Methods and Protocols**, edited by *Tiziana Borsello, 2007*

286. **Transgenic Plants:** *Methods and Protocols,* edited by *Leandro Peña, 2004*

285. **Cell Cycle Control and Dysregulation Protocols:** *Cyclins, Cyclin-Dependent Kinases, and Other Factors,* edited by *Antonio Giordano and Gaetano Romano, 2004*

284. **Signal Transduction Protocols**, *Second Edition,* edited by *Robert C. Dickson and Michael D. Mendenhall, 2004*

283. **Biconjugation Protocols**, edited by *Christof M. Niemeyer, 2004*

282. **Apoptosis Methods and Protocols**, edited by *Hugh J. M. Brady, 2004*

281. **Checkpoint Controls and Cancer, Volume 2:** *Activation and Regulation Protocols,* edited by *Axel H. Schönthal, 2004*

280. **Checkpoint Controls and Cancer, Volume 1:** *Reviews and Model Systems,* edited by *Axel H. Schönthal, 2004*

279. **Nitric Oxide Protocols**, *Second Edition,* edited by *Aviv Hassid, 2004*

278. **Protein NMR Techniques**, *Second Edition,* edited by *A. Kristina Downing, 2004*

277. **Trinucleotide Repeat Protocols**, edited by *Yoshinori Kohwi, 2004*

276. **Capillary Electrophoresis of Proteins and Peptides**, edited by *Mark A. Strege and Avinash L. Lagu, 2004*

275. **Chemoinformatics**, edited by *Jürgen Bajorath, 2004*

274. **Photosynthesis Research Protocols**, edited by *Robert Carpentier, 2004*

273. **Platelets and Megakaryocytes, Volume 2**: *Perspectives and Techniques,* edited by *Jonathan M. Gibbins and Martyn P. Mahaut- Smith, 2004*

272. **Platelets and Megakaryocytes, Volume 1**: *Functional Assays,* edited by *Jonathan M. Gibbins and Martyn P. Mahaut-Smith, 2004*

271. **B Cell Protocols**, edited by *Hua Gu and Klaus Rajewsky, 2004*

270. **Parasite Genomics Protocols**, edited by *Sara E. Melville, 2004*

269. **Vaccina Virus and Poxvirology**: *Methods and Protocols,*edited by *Stuart N. Isaacs, 2004*

268. **Public Health Microbiology**: *Methods and Protocols,* edited by *John F. T. Spencer and Alicia L. Ragout de Spencer, 2004*

267. **Recombinant Gene Expression**: *Reviews and Protocols, Second Edition,* edited by *Paulina Balbas and Argelia Johnson, 2004*

266. **Genomics, Proteomics, and Clinical Bacteriology**: *Methods and Reviews,* edited by *Neil Woodford and Alan Johnson, 2004*

265. **RNA Interference, Editing, and Modification:** *Methods and Protocols,* edited by *Jonatha M. Gott, 2004*

264. **Protein Arrays: Methods and Protocols**, edited by *Eric Fung, 2004*

263. **Flow Cytometry**, *Second Edition,* edited by *Teresa S. Hawley and Robert G. Hawley, 2004*

262. **Genetic Recombination Protocols**, edited by *Alan S. Waldman, 2004*

261. **Protein–Protein Interactions:** *Methods and Applications,* edited by *Haian Fu, 2004*

260. **Mobile Genetic Elements:** *Protocols and Genomic Applications,* edited by *Wolfgang J. Miller and Pierre Capy, 2004*

259. **Receptor Signal Transduction Protocols**, *Second Edition,* edited by *Gary B. Willars and R. A. John Challiss, 2004*

258. **Gene Expression Profiling:** *Methods and Protocols,* edited by *Richard A. Shimkets, 2004*

257. **mRNA Processing and Metabolism:** *Methods and Protocols,* edited by *Daniel R. Schoenberg, 2004*

256. **Bacterial Artifical Chromosomes, Volume 2:** *Functional Studies,* edited by *Shaying Zhao and Marvin Stodolsky, 2004*

255. **Bacterial Artifical Chromosomes, Volume 1:** *Library Construction, Physical Mapping, and Sequencing,* edited by *Shaying Zhao and Marvin Stodolsky, 2004*

254. **Germ Cell Protocols, Volume 2:** *Molecular Embryo Analysis, Live Imaging, Transgenesis, and Cloning,* edited by *Heide Schatten, 2004*

253. **Germ Cell Protocols, Volume 1:** *Sperm and Oocyte Analysis,* edited by *Heide Schatten, 2004*

252. **Ribozymes and siRNA Protocols**, *Second Edition,* edited by *Mouldy Sioud, 2004*

251. **HPLC of Peptides and Proteins:** *Methods and Protocols,* edited by *Marie-Isabel Aguilar, 2004*

250. **MAP Kinase Signaling Protocols**, edited by *Rony Seger, 2004*

249. **Cytokine Protocols**, edited by *Marc De Ley, 2004*

248. **Antibody Engineering: Methods and Protocols**, edited by *Benny K. C. Lo, 2004*

247. **Drosophila Cytogenetics Protocols**, edited by *Daryl S. Henderson, 2004*

246. **Gene Delivery to Mammalian Cells:** *Volume 2: Viral Gene Transfer Techniques,* edited by *William C. Heiser, 2004*

245. **Gene Delivery to Mammalian Cells: Volume 1:** *Nonviral Gene Transfer Techniques,* edited by *William C. Heiser, 2004*

244. **Protein Purification Protocols**, *Second Edition,* edited by *Paul Cutler, 2004*

243. **Chiral Separations: Methods and Protocols**, edited by *Gerald Gübitz and Martin G. Schmid, 2004*

METHODS IN MOLECULAR BIOLOGY™

Neuroprotection Methods and Protocols

Edited by

Tiziana Borsello

HUMANA PRESS TOTOWA, NEW JERSEY

999 Riverview Drive, Suite 208
Totowa, New Jersey 07512

www.humanapress.com

This publication is printed on acid-free paper. ♾
ANSI Z39.48-1984 (American Standards Institute) Permanence of Paper for Printed Library Materials

Cover design and illustration: Graeme Coultrip, coultripdesign.com

Production Editor: Christina Thomas

For additional copies, pricing for bulk purchases, and/or information about other Humana titles, contact Humana at the above address or at any of the following numbers: Tel.: 973-256-1699; Fax: 973-256-8341; E-mail: humana@humanapr.com; or visit our Website: www.humanapress.com

eISBN 978-1-59745-504-6

Printed in the United States of America. 10 9 8 7 6 5 4 3 2 1

Library of Congress Control Number: 2007929657

Preface

Neuroprotection is a topic of great importance in current neuroscience, both basic and clinical. The incidence of age-related neurodegenerative diseases could be expected to rise dramatically in the future owing to an aging population. Consequently, finding the means of retarding or preventing the progression of such diseases becomes increasingly important.

This book focuses on basic perspective on neuroprotective approaches and scientists well recognized for their work have contributed chapters to this volume.

Although findings on neuroprotection in the different pathologies become more and more frequent and detailed, it can be difficult for researchers to orient themselves in such a complicate field. For this reason, this book describes basic science discovery and the application of such research within different laboratories leading to the development of neuroprotective protocols.

The main aim of this volume is thus to give an overview of methods used to study neuronal death and neuroprotection and to offer a really comprehensive step-by-step method in order to make clear not just the procedure but also the principles behind the use of it. At this purpose, the "Notes" section of each chapter represents a useful tool to solve technical problems and to help in reproducing the described methods.

To get through the book easily, the chapters are subdivided in four groups:

1. Methods to assess neuronal degeneration/death
2. Models to study neuronal injury/neuroprotection
3. Methods to identify genes involved in neuronal death/survival
4. Neuroprotective strategies

I hope that this book will serve as a reference for basic neuroscientists (rather than clinical) interested in updating the molecular and cellular biology of neuronal death/neuroprotection and will represent an easy guide to answer technical problems and questions.

Tiziana Borsello

Contributors

Mathias Bähr • *Neurologische Universitätsklinik, Göttingen, Germany*

Myriam Bernaudin • *UMR-CNRS 6185, Centre Cyceron, Neurodégénérescence: Modèles et Stratégies Thérapeutiques, Université de Caen, Caen, France*

Tiziana Borsello • *Biol. Neurodeg. Disorders Lab, Istituto di Ricerche Farmacologiche Mario Negri, Milano, Italy, and Département de Biologie Cellulaire et de Morphologie, Université de Lausanne, Lausanne, Switzerland*

Daniele Bottai • *Stem Cell Research Institute, DIBIT Fondazione Centro San Raffaele del Monte Tabor, Milan, Italy, and Department of Biotechnology and Biosciences, University Milan Bicocca, Milan, Italy*

Concetta Bubici • *The Ben May Institute for Cancer Research, The University of Chicago, Chicago, IL*

Marcus J. Calkins • *School of Pharmacy and Environmental Toxicology Center, University of Wisconsin, Madison, WI*

Hong Cui • *Toronto Western Research Institute, Division of Applied and Interventional Research, Toronto, ON*

Luciano D'Adamio • *Ceinge Biotecnologie Avanzate S.C.ar.l., Napoli, Italy, Dipartimento di Biochimica e Biotecnologie Mediche, Universita' degli Studi di Napoli Federico II Napoli, Italy, and Department of Microbiology and Immunology, Albert Einstein College of Medicine, Bronx, NY*

Ferrari Daniela • *Stem Cell Research Institute, DIBIT Fondazione Centro San Raffaele del Monte Tabor, Milan, Italy*

David L. Deitcher • *Department of Neurobiology and Behavior, Cornell University, Ithaca, NY*

Thomas Deller • *Institute of Clinical Neuroanatomy, J. W. Goethe-University, Frankfurt, Germany*

Domenico Del Turco • *Institute of Clinical Neuroanatomy, J. W. Goethe-University, Frankfurt, Germany*

Gunnar P.H. Dietz • *Neurologische Universitätsklinik, Göttingen, Germany*

John Ewer • *Entomology Department, Cornell University, Ithaca, NY*

Guido Franzoso • *The Ben May Institute for Cancer Research, The University of Chicago, Chicago, IL*
Mark P. Goldberg • *Hope Center for Neurological Disorders and Department of Neurology, Washington University School of Medicine, St. Louis, MO*
Theo Hagg • *Kentucky Spinal Cord Injury Research Center, Department of Neurological Surgery and Department of Pharmacology and Toxicology, University of Louisville, Louisville, KY*
Delinda A. Johnson • *School of Pharmacy, University of Wisconsin, Madison, WI*
Jeffrey A. Johnson • *School of Pharmacy and Environmental Toxicology Center and Waisman Center, University of Wisconsin, Madison, WI*
Jonathan Kipnis • *Department of Neurobiology, The Weizmann Institute of Science, Rehovot, Israel, and Department of Pharmacology and Experimental Neuroscience and Department of Ophthalmology and Visual Sciences, University of Nebraska Medical Center, Omaha, NE*
James R. Knabb • *The Ben May Institute for Cancer Research, The University of Chicago, Chicago, IL*
Christian Kuntzen • *The Ben May Institute for Cancer Research, The University of Chicago, Chicago, IL*
Anthony C. Lau • *Toronto Western Research Institute, Division of Applied and Interventional Research, Toronto, ON, and Department of Physiology, Medical Sciences Building, University of Toronto, Toronto, ON*
Jiang Li • *School of Pharmacy, University of Wisconsin, Madison, WI*
David M. Lin • *Department of Biomedical Sciences, Cornell University, Ithaca, NY*
Brandon Loveall • *Entomology Department, Cornell University, Ithaca, NY*
W. David Lust • *Department of Experimental Neurological Surgery, Case Western Reserve University School of Medicine, Cleveland, OH*
Jean Mariani • *UMR 7102 Neurobiologie des Processus Adaptatifs, Lab. Developpement et Vieillissement du Systeme Nerveux (DVSN), Universite P. et M. Curie, Paris, France*
Salvatore Papa • *The Ben May Institute for Cancer Research, The University of Chicago, Chicago, IL*
Can G. Pham • *The Ben May Institute for Cancer Research, The University of Chicago, Chicago, IL*
Michele Puchowicz • *Department of Anatomy, Case Western Reserve University School of Medicine, Cleveland, OH*

Mariaelena Repici • *Département de Biologie Cellulaire et de Morphologie, Université de Lausanne, Lausanne, Switzerland*
Michal Schwartz • *Department of Neurobiology, The Weizmann Institute of Science, Rehovot, Israel*
Nikolaus J. Sucher • *Department of Neurology, Children's Hospital & Harvard Medical School, Boston, MA*
Yang Tang • *Department of Neurology, University of Minnesota Medical School, Minneapolis, MN*
Tatyana I. Tenkova • *Hope Center for Neurological Disorders and Department of Neurology, Washington University School of Medicine, St. Louis, MO*
Michael Tymianski • *Toronto Western Research Institute, Division of Applied and Interventional Research, Toronto, ON, and Department of Physiology, Medical Sciences Building, University of Toronto, Toronto, ON*
Angelo Luigi Vescovi • *University Milan Bicocca, Department of Biotechnology and Biosciences, Milan, Italy*
Roberta Visconti • *Ceinge Biotecnologie Avanzate S.C.ar.l., Napoli, Italy*
Rikki N. Waterhouse • *Neurobiology and Imaging Program, Department of Biological Psychiatry, New York State Psychiatric Institute, New York, NY*
Francesca Zazzeroni • *Department of Experimental Medicine, The University of L'Aquila, L'Aquila, Italy*
Jennifer Zechel • *Department of Experimental Neurological Surgery, Case Western Reserve University School of Medicine, Cleveland, OH*
Jun Zhao • *Neurobiology and Imaging Program, Department of Biological Psychiatry, New York State Psychiatric Institute, New York, NY*

Contents

1

Neuronal Death and Neuroprotection: A Review

Mariaelena Repici, Jean Mariani, and Tiziana Borsello

Summary

To achieve neuroprotection is one of the main interests for neuroscientist: understanding the control mechanisms of neuronal death allows developing new tools for preventing it. Neuronal death plays a critical role in most of the important neural pathologies, including stroke, epilepsy, Parkinson's disease and Alzheimer's disease.

This review summarizes the three main different types of neuronal death: apoptosis, necrosis and autophagic cell death, although we are conscious that if cell death falls into several categories, the boundaries are not always distinct. We then introduce the current understanding of the relationship between neuronal death types and neuroprotection.

Key Words: Necrosis, apoptosis, autophagy, neuronal cell death, neuroprotective strategies

1. Introduction

The death of neurons is one of the forces that shape the development of the central nervous system (CNS). Neurons establish contact with their targets during development and refine it throughout their life. To achieve the scope of forming and retaining the functional nervous system architecture, neuronal death is finely regulated in development and strictly kept under control in adult systems. Therefore, individual neurons that fail to retain most of their synaptic connections have no reason to further exist and die.

In the mature nervous system, most neurons are postmitotic cells and cannot be easily replaced by cell renewal. For this reason, the death of neurons in

From: *Methods in Molecular Biology, vol. 399: Neuroprotection Methods and Protocols*
Edited by: T. Borsello © Humana Press Inc., Totowa, NJ

the adult CNS is a phenomenon more severe than in other tissues: the number of mature neurons in adult is primarily dependent on the extent of neuronal survival, and their decline in the old age is an important event. In addition, increasing neuronal death induced by damaging insults is also a major risk factor of neurodegenerative disorders and aging among the elderly of the population is another risk factor that can cause neuronal degeneration.

The process called "neurodegeneration" is a progressive loss of structure or function of neurons, culminating in the death of neurons. It is possible to distinguish between acute and chronic neurodegeneration. Acute neurodegeneration is caused by a specific and traumatic event, whereas chronic neurodegeneration is normally a constant disease state with a multifactorial origin that has longer progression. Acute neurodegeneration that accompanies stroke, head trauma, cardiac arrest, and subarachnoid hemorrhage, however, share common mechanisms of neuronal death with chronic forms of neurodegeneration, for example, Alzheimer's and Parkinson's diseases, and also Huntington's disease and amyotrophic lateral sclerosis.

The neurodegeneration field has attracted much deserved attention in recent times, leading to several new and important insights into cell biology. In fact, studying the mechanisms of neuronal death will help in the identification of a possible treatment to prevent it and improve the health and the quality of patient life.

The field on neuroprotection is moving so rapidly and is so massive that it is not possible to cover everything in a small review—there are several recent and more extensive publications to which the interested reader should refer to go deeper in details.

2. Neuronal Death Types

Neurons, such as the other cells, have death machinery: it consists of a set of genes, intracellular pathways, and enzymes, which stand ever ready to self-destruction.

It is now possible to discriminate 11 pathways of cell death ***(1)***, some of which are tissue specific or occur in only one type of cell. However, seven types are observed in CNS. We will further simplify the situation and will focus our attention on the three major known categories of neuronal death: necrosis, apoptosis, and autophagic cell death (**Table 1**). This classification is mainly based on morphological features because in the majority of cases the molecular mechanisms are not well established. In addition, it is well known that neurons can pass from one to the other types of cell death. In other words, neurons all

Table 1
Types of Neuronal Death

Features	Apoptosis	Necrosis	Autophagic cell death
Genetic program	PARP, and other?	No?	Atg-5, Atg-6 (Beclin 1), Atg-7, and other?
Cellular membrane	Intact	Lysed	Intact
Organelles	Subtle changes, notably in mitochondria	Lysed	Often into autophagosomes
Nucleus	Shrinkage, DNA fragmentation, and late fragmentation of nucleus	Swollen and late fragmentation of nucleus	Late DNA fragmentation
Enzymes	Caspases	Calpains	Cathepsins and other lysosomal hydrolases
ATP	Maintained	Depleted	Maintained
Markers	Activated caspase-3 and annexin-5	Ca^{2+}	LC3-II, Monodansylcadaverine? lysosomal markers such as cathepsin D, and LAMP-1
Inhibitors	Caspase inhibitors	Channels blockers and calpain inhibitors	3-Methyladenine and other PI3K inhibitors (e.g., wortmannin)
Time	Hours	Hours	Hours

have virtually the same death machinery, but this may be used differently. The eventual death mode—necrosis, apoptosis, or autophagic cell death—depends on a number of parameters, including metabolic state and energy resources, availability of growth factors, cell maturity, stress stimuli, and many other factors.

2.1. Apoptosis

Apoptosis has come to be used synonymously with the phrase "programmed cell death," as it is a cell-intrinsic mechanism for suicide regulated by a variety of cellular signaling pathways (for a recent review, *see* **ref. *2***). The apoptotic

machinery, initially identified in *Caenorhabditis elegans*, is evolutionarily conserved in higher organisms, and apoptosis represents a default mechanism in mammalian development. It is marked by a well-defined sequence of morphological changes. For neuronal death to be classified as apoptotic, nuclear condensation and fragmentation, cleavage of chromosomal DNA into internucleosomal fragments, and packaging of the deceased cell into apoptotic bodies without plasma membrane breakdown must be observed (**Fig. 1**). Apoptotic bodies are recognized and removed by phagocytic cells; thus, apoptosis is also notable for the absence of inflammation around the dying cell. Other peculiar features of apoptosis result from the activation of caspases (cysteine proteases), which play a crucial role in dismantling the cell structure. Caspases are synthesized as proenzymes with very low intrinsic activity. Their activation can proceed through two distinct mechanisms: one involving the binding of extracellular ligands to their receptors (extrinsic pathway, which culminates in caspase-8 activation) and the other involving the release of cytochrome c from the mitochondria (intrinsic pathway). A crosstalk between these two pathways is provided by Bid, a Bcl-2 family member ***(3)***. Cytosolic cytochrome c is highly proapoptotic and promotes the formation of a complex, called apoptosome, between the protein Apaf-1 and an initiator caspase, procaspase-9. The apoptosome is a caspase-activating structure: it causes, as a final result, the activation of the downstream effector caspases, particularly executors of the cell death program, caspase-3 and caspase-7.

Recent studies have shown that apoptosome may be finally regulated under normal physiological state and may be altered under different pathological conditions ***(4)***. Dying by apoptosis requires energy in the form of ATP and has a very rapid course ***(5)***. The highly stereotyped changes accompanying apoptosis suggested to early workers that this type of cell death was under the control of a strict genetic program and induced them to define this type of cell death as a "programmed or controlled death."

2.2. Necrosis

In contrast to apoptosis, necrosis has been traditionally thought to be a passive form of cell death with more similarities to an incident than to a suicide. Necrosis is the end result of a bioenergetic catastrophe resulting from ATP depletion to a level incompatible with cell survival and was thought to be initiated mainly by toxic insults or physical damage. It is morphologically characterized by vacuolation of the cytoplasm, mitochondrial swelling, dilatation of the endoplasmic reticulum (ER), and breakdown of the plasma membrane (**Fig. 1**) ***(6)***. As a consequence, cellular contents are liberated into the

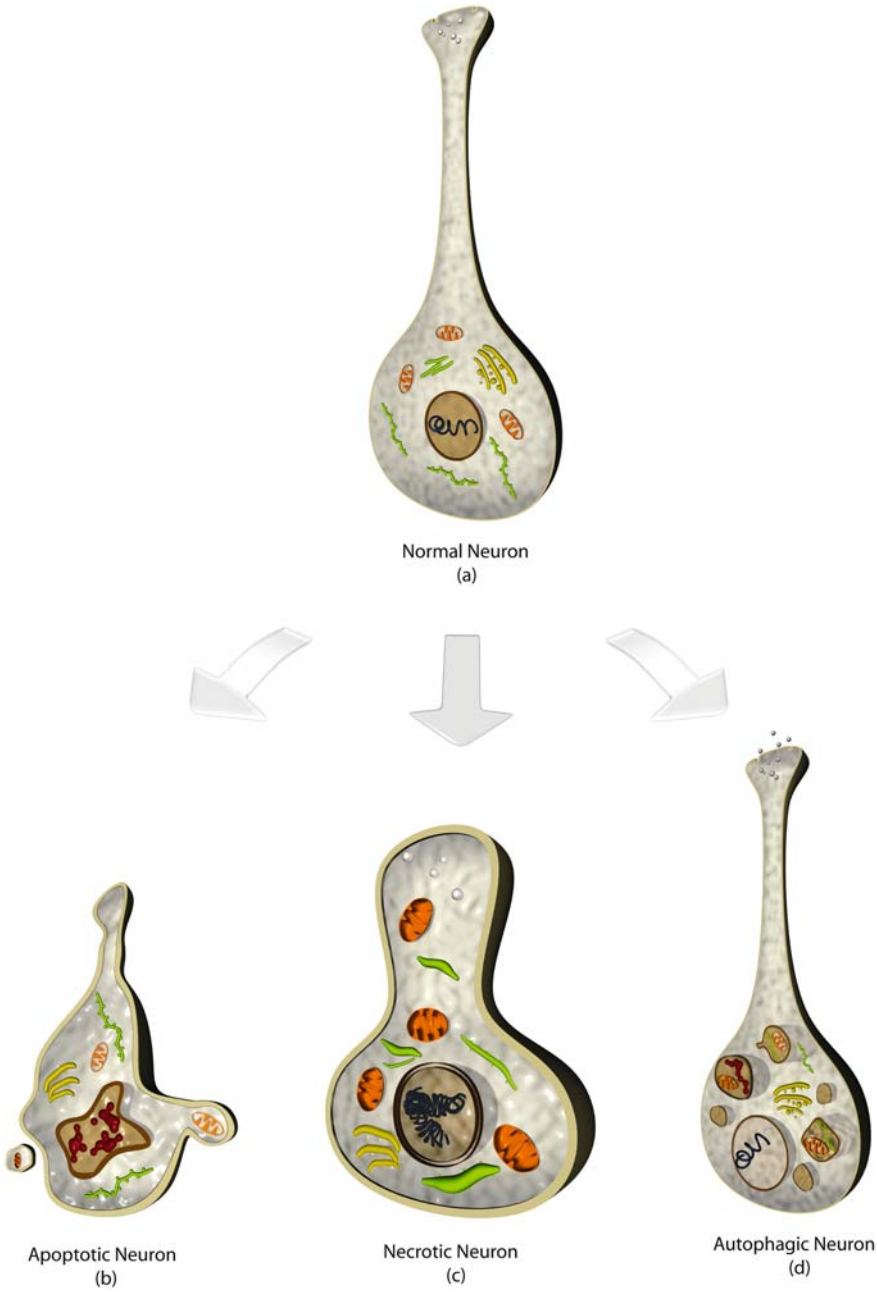
Normal Neuron
(a)
Apoptotic Neuron
(b)
Necrotic Neuron
(c)
Autophagic Neuron
(d)

extracellular space and can damage neighboring cells and evoke inflammatory responses ***(7)***. Although the molecular mechanisms that cause necrotic cell death are not fully elucidated, typically, neurons lose control of their ionic balance, imbibe water, and lyse. Typical necrotic death pathway has been found in acute excitotoxicity. Excitotoxicity results from the release of excess of neurotransmitters and the engagement of cell membrane receptors with excitatory amino acids such as ionotropic *N*-methyl-D-aspartate (NMDA), kainate, and 2-amino-3-propionate (AMPA). The excitatory amino acids induce increased intracellular Ca^{2+} by releasing the ER Ca^{2+} pool and/or inducing transport of extracellular Ca^{2+} through plasma membrane transporters. Persistently elevated cytosolic Ca^{2+} has been implicated in excitotoxic cell death ***(8,9)***. Inhibition of Ca^{2+} uptake by mitochondria can suppress necrotic cell death ***(10)***. Necrosis seems to be dependent on proteolytic system ***(11)***; in fact, the lysosomes damage and the calpain–cathepsin liberation is an active mechanism of this death pathway.

Although necrosis has been traditionally referred to as unregulated pathological cell death, increasing examples of cell death with necrotic features described under normal physiological and/or certain pathological conditions suggest that, at least in some instances, necrosis may also be a regulated cellular mechanism ***(12)***.

Programmed necrosis in response to DNA damage was found to be initiated by the DNA repair protein poly(ADP-ribose) polymerase 1 (PARP-1, the DNA damage-dependent nuclear enzyme) after cerebral ischemia. The nuclear enzyme PARP is activated by DNA strand breaks, resulting in destabilization of the surrounding chromatin and allowing DNA repair enzymes to gain access

Fig. 1. Morphological features of apoptotic, necrotic, and autophagic neuronal death. **(A)** Normal neuron. **(B)** Apoptotic neuron: the execution phase is mediated by the activation of the caspases that induce the degradation of a series of nuclear and cytosolic targets. This phenomenon culminates in the chromatin condensation with the shrinkage and collapse of the neuron that generates the apoptotic bodies. **(C)** Necrotic neuron: the swelling of the entire neuron with grossly swollen organelles is the peculiar feature of this type of death. One of the important steps in necrosis is an excessive influx of intracellular calcium that by damaging the respiratory cycle causes neuronal death. **(D)** Autophagic neuron: cytoplasm is characterized by a number of autophagic vacuoles with a double-membrane vesicle that encapsulates whole organelles and bulk cytoplasm. This autophagosome then fuses with the lysosomes where the contents are degraded and recycled: the neuron digests itself as a suicide strategy.

to the damaged DNA ***(13)***. PARP-1 hyperactivity is causative in postischemic brain damage and turns out to be an active mechanism in necrosis. Also, if much remains to be learned about the genetic and biochemical pathways of necrosis downstream of the individual insults, studies examining excitotoxic neuronal death, including those following ischemia, have proven instructive.

2.3. Autophagic Cell Death

It has been demonstrated in yeast, Dictyostelium, *C. elegans*, and plants that autophagy represents a survival mechanism employed to allow these organisms to survive times of famine starvation ***(14)***, although cultured mammalian cells that are subjected to nutrient deprivation rapidly undergo apoptosis rather than switching to the stationary phase that allows survival in less complex organisms. Nevertheless, in certain disease states, including neurodegenerative disorders such as Alzheimer's and Parkinson's diseases, cells in an advanced state of autophagy are frequently observed. This led to the idea that autophagy is not only an adaptive response to nutrient limitation but also a mechanism for cell suicide ***(12,15,16)***. When autophagy involves the total destruction of the cell, it is called autophagic cell death (also known as cytoplasmic cell death or type II cell death) ***(6)***. This is one of the main types of programmed cell death. This "autophagic death" process has been classified as distinct from apoptotic and necrotic cell death. Autophagic cell death is morphologically characterized by abundant vacuoles in the cytoplasm, mitochondrial dilatation, and enlargement of Golgi and ER without nuclear condensation and fragmentation (**Fig. 1**) ***(6)***. Normally, the degradation of cytoplasmic components including subcellular organelles precedes the nuclear collapse; the integrity of cytoskeletal elements is maintained until the late stages of the process ***(17)***. The most characteristic feature of autophagic cell death is the formation of autophagosomes/vacuoles in the cytosol of neurons; these vacuoles are two-membraned and contain degenerating cytoplasmic organelles or cytosol ***(14)***. A good marker of autophagic cell death is the light chain 3 (LC3), a homolog of yeast Atg-8 (which is a crucial factor for yeast autophagy) that is a constituent of autophagosomal membrane ***(18)***. This type of cell death can be inhibited by 3-methyladenine and wortmannin or by downregulation of the autophagic proteins such as Beclin 1. This implies that autophagic cell death is a program of death dependent on gene and not only a falling survival attempt. Moreover, in the analysis of the three major categories of neuronal death, it must be kept in mind that although apoptosis and necrosis are clearly cell death pathways and autophagy has been associated with neuronal death, autophagy is also considered to be a cell protective mechanism, induced as a major catabolic

pathway to generate intracellular nutrients to maintain energy production and macromolecular synthesis when external nutrients are limited ***(19)***. Two very recent studies performed by inactivating proteins of the autophagic pathway have led to results indicating that the role and importance of autophagy in neuronal death is still an object of debate: inactivation of either protein Atg-7 or Atg-5 in mice leads to behavioral defects and progressive neuronal degeneration ***(20,21)***.

3. Neuroprotection

Neuronal injury contributes significantly to functional impairment in a wide variety of peripheral and central nervous system disorders. Such disorders include acute diseases such as ischemia or head trauma and chronic diseases such as Parkinson's and Alzheimer's diseases. Neurologic impairments characteristic of these disorders include loss of coordination and inability to walk, memory loss, incapability to concentrate, and other cognitive deficits. Such impairments often become progressively worse over weeks and years, thus leading to chronic dysfunction. Current therapies do not adequately treat such dysfunctional neurologic conditions.

Basic research studies provided a great hope for the alleviation of these human diseases. In fact, the treatments that interfere with a specific event in the death-signaling pathway have been reported to produce neuroprotection against neuronal death. However, the existence of multiple cell death pathways with both overlapping and distinct molecular mechanisms, combined with the observation that inhibition of one such pathway may enhance alternative ones, suggests that treatment strategies should optimally be directed at multiple targets/mechanisms.

The optimal neuroprotective approach should therefore include either combination treatment of strategies directed toward multiple cell death pathways or the use of single compounds that may inhibit more than one cell death mechanism (multipotential agents). In this context, we will go over the different inhibitors available for the three neuronal death pathways described in the previous section.

3.1. Neuroprotection Against Apoptotic Cell Death

Owing to the complexity of the apoptotic cascade, apoptotic neuronal death can be modulated at many critical steps: by inhibiting key initiators, by blocking key components of the death cascade, or by enhancing prosurvival factors. Moreover, it is possible to discriminate between strategies to prevent caspase-dependent apoptosis (e.g., caspase inhibitors) and strategies to prevent

caspase-independent apoptosis (e.g., PARP inhibitors). PARP activation has been shown to directly contribute to caspase-independent apoptosis, and PARP inhibitors therefore represent one possible therapeutic strategy against this type of cell death. Caspase inhibitors have been used in several acute experimental paradigms, such as cerebral ischemia and traumatic brain injury, and also in chronic diseases (it has recently been shown that upstream caspase cascade needs to be inhibited if useful neuroprotection is to be achieved in cell culture model of SOD1-related familial amyotrophic lateral sclerosis, *see* **ref. *22***). However, in the neuroprotective approach using caspase inhibitors, it must be kept in mind that (1) by inhibiting caspase-dependent apoptosis the mode of cell death might shift to caspase-independent apoptosis or necrosis and (2) caspase activity may have an important function in some physiological processes ***(23)***.

Positive results have also been obtained by enhancing prosurvival factors: overproduction of Bcl-2 in transgenic mice is associated with reduction in the infarct size following cerebral ischemia ***(24)***, and in vivo virally mediated overexpression of the antiapoptotic gene X chromosome-linked inhibitor of apoptosis protein (XIAP) reduces apoptosis and behavioral deficits following transient forebrain ischemia ***(25,26)***.

Recently, the overproduction of the Apaf-1 interacting protein (AIP), a splice variant of caspase-9 endogenously expressed in the brain, has been shown to promote the survival of hippocampal neurons after transient global ischemia ***(27)***, and AIP overproduction has been proposed as a neuroprotective strategy to prevent neurodegeneration and stroke-induced neuronal death. Finally, it is clear that the continued studies of apoptosomal formation and regulation will make the apoptosome itself a viable therapeutic target in the CNS.

3.2. Neuroprotection Against Necrotic Cell Death

Intracellular calcium is recognized as a central effector of necrosis, and preventing the increase in its concentration has been shown to reduce neuronal death following excitotoxicity. The necrotic pathway initiated by elevated calcium concentration can be blocked at specific points to prevent neuronal death. At a first level, it is possible to block the glutamate-gated channels: by preventing the calcium influx, the membrane depolarization is also prevented and as a consequence neurotoxicity. The MK801 is a potent NMDA blocker and represents an efficient tool to prevent in vitro neuronal death. However, neuroprotective drugs acting at the NMDA receptor level tested in clinical trails have failed because of side effects. More recently, the memantine (NMDA

blocker) is on final clinical trail (phase III), showing efficacies in Alzheimer's disease *(28)*.

At a second level, the control of cytoplasmic calcium may be obtained using specific chelators and has neuroprotective effects in mammalian neurons *(29–31)*. Similarly, overexpression of the calcium sequestering protein Calbindin protects neurons from necrotic insults *(32)*. At a lower level, inhibitors of calcium-activated calpain protease can favor survival *(33)*. Another possible level of intervention is to work at the synapse level: cleaning glutamate by enhancing its uptake.

Considerable progress has been made in combating necrosis, and there is now a more coherent and detailed picture of this type of cell death; however, because of the intricacies of this cascade of events, there is a long way to go before having an effective strategy to prevent it. Understanding this death process will help develop the successful methodology.

3.3. Neuroprotection Against Autophagic Cell Death

It is difficult to propose efficient strategies to inhibit autophagic cell death and neuroprotect the brain because of several uncertainties in the understanding of this process.

First, the drugs proposed to inhibit autophagy such as 3-methyladenine and wortmannin are likely to be nonspecific inhibitors of this type of cell death. Second, because autophagy is also considered to be a cell protective mechanism, its pharmacological manipulation might lead to unexpected or contradictory results. For instance, rapamycin, a lipophilic macrolide antibiotic, induces autophagy by inactivating the protein mammalian target of rapamycin (mTOR). Rapamycin protects against mutant huntingtin-induced neurodegeneration in cell, fly, and mouse models of Huntington's disease *(34,35)*. Third, there is increasing evidence that apoptosis and autophagy represent networks of molecular processes and that there are a number of molecular mechanisms that link the regulation of both processes (reviewed in **ref.** ***36***). Beclin 1 was originally identified as a Bcl-2-interacting protein and was quickly identified as a mammalian ortholog of the yeast autophagy gene, Atg-6/Vps30 *(37)*. A recent study of the interactions between Beclin 1 and Bcl-2 has shown that Bcl-2 can inhibit autophagy in a variety of tissues by binding Beclin 1, and in the absence of Bcl-2, Beclin 1 can overinduce autophagy leading to cell death. The relative levels of Beclin 1 and Bcl-2 may act like a rheostat to set the cellular levels of autophagy. Because Beclin 1 interacts with Bcl-2 and Bcl-2 interacts with Bax, it seems likely that there may be a more complex rheostat where

the relative levels of Beclin 1, Bcl-2, and Bax regulate the cellular status of autophagy and apoptosis induction. Much more work will be needed to understand these intricate mechanisms before any clear neuroprotective strategies could be proposed.

4. Conclusions

The edge at which a neuron commits to die is surely adjusted by metabolic and respiratory factors, which are themselves adjusted by other activities of the cell. In the dying neuron, there is considerable crosstalk among many different metabolic pathways. Cytoplasmic or lysosomal proteases other than upstream caspases can affect the activation of effector caspases, and many other enzymes are often upregulated in dying neurons, playing important roles in the death of the cells. Most commonly, cells follow an apoptotic route to death, but they have many options that can divert to or accentuate autophagic or necrotic pathways. We do not fully understand the extent to which cells can switch between pathways. A better understanding of the genes involved in apoptosis and autophagy should allow future studies to dissect the role of autophagy in neuronal death and survival more thoroughly. However, we are not persuaded that the energy deprivation is the only reason for dying by necrosis and that necrosis is just a passive way without any higher implication.

For instance, we do not know to what extent the metabolic history of a neuron (including activity, neuronal interaction, nutritional reserves, accumulated oxidative damage, and the conversation among its organelles and compartments) can affect the pathway that it follows to death. It is always important to point out that neurons operate more as an ecosystem than as a collection of individual enzymatic pathways. Efforts to establish therapies that are based on the control of neuronal death will eventually incorporate these considerations.

Acknowledgments

T.B. was supported by grants from the Botnar Foundation grant and FNRS (Swiss National Science Foundation) grants 310000-107888. Special thanks to Architettura Laboratorio Communication for the graphic figure (http://www.archilab.it).

References

1. Melino G, Knight RA, Nicotera P. (2005) How many ways to die? How many different models of cell death? *Cell Death Differ*, **12 Suppl 2**:1457–1462.
2. Danial NN, Korsmeyer SJ. (2004) Cell death: critical control points. *Cell*, **116**: 205–219.

3. Luo X, Budihardjo I, Zou H, Slaughter C, Wang X. (1998) Bid, a Bcl2 interacting protein, mediates cytochrome c release from mitochondria in response to activation of cell surface death receptors. *Cell*, **94**:481–490.
4. Schafer ZT, Kornbluth S. (2006) The apoptosome: physiological, developmental, and pathological modes of regulation. *Dev Cell*, **10**:549–561.
5. Kerr JF, Wyllie AH, Currie AR. (1972) Apoptosis: a basic biological phenomenon with wide-ranging implications in tissue kinetics. *Br J Cancer*, **26**:239–257.
6. Clarke PG. (1990) Developmental cell death: morphological diversity and multiple mechanisms. *Anat Embryo (Berl)*, **181**:195–213.
7. Leist M, Jaattela M. (2001) Four deaths and a funeral: from caspases to alternative mechanisms. *Nat Rev Mol Cell Biol*, **2**:589–598.
8. Bennett BL, Sasaki DT, Murray BW, O'Leary EC, Sakata ST, Xu W, Leisten JC, Motiwala A, Pierce S, Satoh Y, et al. (2001) SP600125, an anthrapyrazolone inhibitor of Jun N-terminal kinase. *Proc Natl Acad Sci USA*, **98**:13681–13686.
9. Sattler R, Tymianski M. (2001) Molecular mechanisms of glutamate receptor-mediated excitotoxic neuronal cell death. *Mol Neurobiol*, **24**:107–129.
10. Stout AK, Raphael HM, Kanterewicz BI, Klann E, Reynolds IJ. (1998) Glutamate-induced neuron death requires mitochondrial calcium uptake. *Nat Neurosci*, **1**:366–373.
11. Syntichaki P, Xu K, Driscoll M, Tavernarakis N. (2002) Specific aspartyl and calpain proteases are required for neurodegeneration in C. elegans. *Nature*, **419**:939–944.
12. Yuan J, Lipinski M, Degterev A. (2003) Diversity in the mechanisms of neuronal cell death. *Neuron*, **40**:401–413.
13. de Murcia G, Schreiber V, Molinete M, Saulier B, Poch O, Masson M, Niedergang C, Menissier de Murcia J. (1994) Structure and function of poly(ADP-ribose) polymerase. *Mol Cell Biochem*, **138**:15–24.
14. Levine B, Klionsky DJ. (2004) Development by self-digestion: molecular mechanisms and biological functions of autophagy. *Dev Cell*, **6**:463–477.
15. Baehrecke EH. (2003) Autophagic programmed cell death in Drosophila. *Cell Death Differ*, **10**:940–945.
16. Gozuacik D, Kimchi A. (2004) Autophagy as a cell death and tumor suppressor mechanism. *Oncogene*, **23**:2891–2906.
17. Cuervo AM. (2004) Autophagy: many paths to the same end. *Mol Cell Biochem*, **263**:55–72.
18. Kabeya Y, Mizushima N, Ueno T, Yamamoto A, Kirisako T, Noda T, Kominami E, Ohsumi Y, Yoshimori T. (2000) LC3, a mammalian homologue of yeast Apg8p, is localized in autophagosome membranes after processing. *EMBO J*, **19**:5720–5728.
19. Levine B. (2005) Eating oneself and uninvited guests: autophagy-related pathways in cellular defense. *Cell*, **120**:159–162.

20. Komatsu M, Waguri S, Chiba T, Murata S, Iwata J, Tanida I, Ueno T, Koike M, Uchiyama Y, Kominami E, et al. (2006) Loss of autophagy in the central nervous system causes neurodegeneration in mice. *Nature*, **441**:880–884.
21. Hara T, Nakamura K, Matsui M, Yamamoto A, Nakahara Y, Suzuki-Migishima R, Yokoyama M, Mishima K, Saito I, Okano H, et al. (2006) Suppression of basal autophagy in neural cells causes neurodegenerative disease in mice. *Nature*, **441**:885–889.
22. Sathasivam S, Shaw PJ. (2005) Apoptosis in amyotrophic lateral sclerosis—what is the evidence? *Lancet Neurol*, **4**:500–509.
23. Dash PK, Blum S, Moore AN. (2000) Caspase activity plays an essential role in long-term memory. *Neuroreport*, **11**:2811–2816.
24. Martinou JC, Dubois-Dauphin M, Staple JK, Rodriguez I, Frankowski H, Missotten M, Albertini P, Talabot D, Catsicas S, Pietra C, et al. (1994) Overexpression of BCL-2 in transgenic mice protects neurons from naturally occurring cell death and experimental ischemia. *Neuron*, **13**:1017–1030.
25. Xu D, Bureau Y, McIntyre DC, Nicholson DW, Liston P, Zhu Y, Fong WG, Crocker SJ, Korneluk RG, Robertson GS. (1999) Attenuation of ischemia-induced cellular and behavioral deficits by X chromosome-linked inhibitor of apoptosis protein overexpression in the rat hippocampus. *J Neurosci*, **19**:5026–5033.
26. Renwick J, Narang MA, Coupland SG, Xuan JY, Baker AN, Brousseau J, Petrin D, Munger R, Leonard BC, Hauswirth WW, et al. (2006) XIAP-mediated neuroprotection in retinal ischemia. *Gene Ther*, **13**:339–347.
27. Cao G, Xiao M, Sun F, Xiao X, Pei W, Li J, Graham SH, Simon RP, Chen J. (2004) Cloning of a novel Apaf-1-interacting protein: a potent suppressor of apoptosis and ischemic neuronal cell death. *J Neurosci*, **24**:6189–6201.
28. Lipton SA. (2006) Paradigm shift in neuroprotection by NMDA receptor blockade: memantine and beyond. *Nat Rev Drug Discov*, **5**:160–170.
29. McGinnis KM, Wang KK, Gnegy ME. (1999) Alterations of extracellular calcium elicit selective modes of cell death and protease activation in SH-SY5Y human neuroblastoma cells. *J Neurochem*, **72**:1853–1863.
30. Arataki S, Tomizawa K, Moriwaki A, Nishida K, Matsushita M, Ozaki T, Kunisada T, Yoshida A, Inoue H, Matsui H. (2005) Calpain inhibitors prevent neuronal cell death and ameliorate motor disturbances after compression-induced spinal cord injury in rats. *J Neurotrauma*, **22**:398–406.
31. Araujo IM, Verdasca MJ, Leal EC, Bahr BA, Ambrosio AF, Carvalho AP, Carvalho CM. (2004) Early calpain-mediated proteolysis following AMPA receptor activation compromises neuronal survival in cultured hippocampal neurons. *J Neurochem*, **91**:1322–1331.
32. McMahon A, Wong BS, Iacopino AM, Ng MC, Chi S, German DC. (1998) Calbindin-D28k buffers intracellular calcium and promotes resistance to degeneration in PC12 cells. *Brain Res Mol Brain Res*, **54**:56–63.

33. Bano D, Young KW, Guerin CJ, Lefeuvre R, Rothwell NJ, Naldini L, Rizzuto R, Carafoli E, Nicotera P. (2005) Cleavage of the plasma membrane Na + /Ca2+ exchanger in excitotoxicity. *Cell*, **120**:275–285.
34. Ravikumar B, Duden R, Rubinsztein DC. (2002) Aggregate-prone proteins with polyglutamine and polyalanine expansions are degraded by autophagy. *Hum Mol Genet*, **11**:1107–1117.
35. Ravikumar B, Vacher C, Berger Z, Davies JE, Luo S, Oroz LG, Scaravilli F, Easton DF, Duden R, O'Kane CJ, et al. (2004) Inhibition of mTOR induces autophagy and reduces toxicity of polyglutamine expansions in fly and mouse models of Huntington disease. *Nat Genet*, **36**:585–595.
36. Rubinsztein DC, DiFiglia M, Heintz N, Nixon RA, Qin Z-H, Ravikumar B, Stefanis L, Tolkovsky A. (2005) Autophagy and its possible roles in nervous system diseases, damage and repair. *Autophagy*, **1**:11–22.
37. Liang XH, Jackson S, Seaman M, Brown K, Kempkes B, Hibshoosh H, Levine B. (1999) Induction of autophagy and inhibition of tumorigenesis by beclin 1. *Nature*, **402**:672–676.

2

The Use of Propidium Iodide to Assess Excitotoxic Neuronal Death in Primary Mixed Cortical Cultures

Anthony C. Lau, Hong Cui, and Michael Tymianski

Summary

Neurodegenerative disorders are subjects of intense scrutiny in biomedical research because of their often-debilitating effects. Currently, many laboratories are engaged in developing or testing drugs to prevent neuronal loss in a variety of these pathologies. A key to testing such drugs is the use of a fast, reliable, and easily reproducible model of neurodegeneration and neuroprotection. Our laboratory has previously used propidium iodide (PI) to assess the degree of neurodegeneration and neuroprotection under a variety of conditions. Ultimately, efforts are underway in the laboratory to prevent delayed neuronal loss following acute ischemic insults using drug therapies. It is now believed that a key mechanism of neurodegeneration following acute ischemia or anoxia is a result of excitotoxicity via *N*-methyl-D-aspartate receptors (NMDARs) and subsequent overproduction of nitric oxide via neuronal nitric oxide synthase (nNOS). Thus, for the purposes of this chapter, the insult used to induce cell death will be various concentrations of NMDA and the compound used to demonstrate neuroprotection will be the nonspecific NOS inhibitor *N*ω-nitro-L-arginine methyl ester (L-NAME). Assessment of neuronal death is accomplished by measuring changes in PI fluorescence using a fluorescent plate reader. This chapter will outline the necessary steps required to (1) produce primary mixed cortical cultures, (2) apply PI and NMDA to these cultures, (3) quantify the results obtained from these cultures, and (4) image these cultures in conjunction with Hoechst 33342 and immunocytochemistry using fluorescence microscopy.

Key Words: Cortical cell culture; *N*-methyl-D-aspartate; propidium iodide; excitotoxicity; immunocytochemistry; neurodegeneration; *N*ω-nitro-L-arginine methyl ester; nitric oxide; neuroprotection.

From: *Methods in Molecular Biology, vol. 399: Neuroprotection Methods and Protocols*
Edited by: T. Borsello © Humana Press Inc., Totowa, NJ

1. Introduction

Neurodegenerative diseases are often considered among the most debilitating pathologies capable of causing significant motor and cognitive deficits. Therefore, a large proportion of biomedical research has been devoted to the idea of neuroprotection, the ability to bestow neurons with an increased resistance against cellular degeneration following injury. Much of our research is focused on providing neuroprotection following acute excitotoxic or ischemic insults ***(1,2)***. One of our ultimate goals is to develop drugs that are neuroprotective in a clinical setting. However, before any of these can be considered for clinical utility, it is useful to screen their neuroprotective effects in cell cultures. Thus, as the advancement of biomedical science produces increasing numbers of putative neuroprotective compounds, the need for a fast and reliable method of demonstrating neuroprotection in cell cultures is clear. To this end, we have developed an efficient and robust model system to test compounds for their neuroprotective efficacy in primary murine cortical cultures using propidium iodide (PI) ***(3)***.

The term "excitotoxicity" was first coined by Olney ***(4)*** to reflect the finding that excessive activation of neuronal glutamate receptors with excitatory amino acids is neurotoxic. It is now believed that much of the neurotoxicity of glutamate receptor overstimulation is because of calcium influx via *N*-methyl-D-aspartate glutamate receptors (NMDARs) ***(5)***, and subsequent studies in cell cultures have shown that NMDAR-mediated neuronal death is, in large part, a result of the close association of NMDARs with neuronal nitric oxide synthase (nNOS), an enzyme that mediates the production of the reactive nitrogen species nitric oxide (NO) ***(2)***. NO-mediated neuronal death can be attenuated by the addition of NOS inhibitors such as *N*ω-nitro-L-arginine methyl ester (L-NAME) ***(6)***. Thus, in our model of neurotoxicity, cell cultures are treated with NMDA to induce cell neuronal death, whereas the application of the L-NAME serves as a positive control for neuroprotection. This model of NMDA-induced neurotoxicity is believed to recapitulate some of the key damaging mechanisms that occur in vivo during brain ischemia. Thus, this in vitro approach has utility in screening neuroprotective agents before these are applied to more complex animal models of disease such as stroke ***(1)***.

PI is a fluorophore that interacts directly with dsDNA ***(7)***. PI intercalation into dsDNA enhances its fluorescence over a wide excitation (peak ~ 540 nm) and emission (peak ~ 620 nm) range. PI is a large molecule that is unable to traverse the plasma membrane of healthy cells and thus remains minimally fluorescent. However, during cellular degeneration, a reduction in plasma membrane integrity allows PI to enter the cell, permitting its contact with dsDNA. Thus, in most cases, PI is a reliable index for dead and dying cells

(*see* **Note 1**). The technique described herein quantifies the increased fluorescence of these dying cells 24 h after a 1-h excitotoxic insult. The following outlines the protocols required to (1) generate primary neuronal cell cultures from mouse embryos in 24-well plates, (2) apply NMDA, PI, and L-NAME to these cultures (*see* **Note 2** and **3**), (3) quantify and compare the amount of neuronal death in treated and nontreated wells, and (4) produce qualitative fluorescence images from these cultures. This technique is of a high-throughput nature and has general applicability and reproducibility for neuroprotective drug screens.

2. Materials

2.1. Primary Murine Mixed Cortical Cultures

1. Poly-L-ornithine (PLO) solution: 30 mg/L PLO (Sigma-Aldrich, Oakville, ON, Canada) and 3.6 g/L borax (Invitrogen/Gibco, Burlington, ON, Canada) are dissolved in water (*see* **Notes 3** and **4**). Solution pH is adjusted to 8.4 and is 0.2 μm-filtered. PLO solution is stored at 4° C and is good for up to 2 weeks.
2. Minimum essential medium (MEM): MEM (Invitrogen/Gibco) is purchased with Earle's salts, without L-glutamine, and 0.1 μm-filtered. MEM is stored at 4° C.
3. Phosphate-buffered saline (PBS): PBS (Invitrogen/Gibco) is purchased without calcium chloride ($CaCl_2$) and magnesium chloride ($MgCl_2$) and is 0.1 μm-filtered. PBS for dissections is stored at 4° C until use.
4. Growth medium (GM): GM is made by supplementing MEM with 10% heat-inactivated (*see* **Note 5**) horse serum (Invitrogen/Gibco), 1% GlutaMAX™-1 100× (Invitrogen/Gibco, *see* **Note 6**), and 4.5 g/L D-glucose (Sigma-Aldrich). GM is 0.2 μm-filtered prior to use and stored at 4° C for up to 1 month.
5. Plating medium (PM): PM is made by supplementing MEM with 10% heat-inactivated horse serum, 10% fetal bovine serum (Invitrogen/Gibco), 1% GlutaMAX™-1 100×, and 4.5 g/L D-glucose. PM is 0.2 μm-filtered and stored at 4° C for up to 1 month.
6. Trypsin–EDTA digestion buffer: 0.05% Trypsin–EDTA 1× (Invitrogen/Gibco) is purchased and divided into 4-mL aliquots. Aliquots are stored at −20° C until use.
7. Cell culture plates: Costar 3526 24-well plates (Corning Inc., Corning, NY, USA).
8. E15 embryos: E15 pregnant female mice are purchased from Charles River, Wilmington, MA.
9. (+)-5-Fluor-2′-deoxyuridine (FDU) stock solution: 12.21 mg uridine (Sigma-Aldrich) and 12.39 mg FDU (Sigma-Aldrich) are dissolved in 5 mL water, for a final concentration of 10 mM each; 500-μL aliquots are made and stored at −20° C until use.
10. FDU/GM solution: FDU/GM solution is made by adding 500 μL FDU stock solution to 500 mL GM. FDU/GM is subsequently 0.2 μm-filtered and stored at 4° C for up to 1 month.
11. Trypan blue: Trypan blue stain 0.4% (Invitrogen/Gibco) is kept at room temperature until use.

2.2. NMDA, PI, and Drug Treatments

1. NMDA stock solution: 20 mM NMDA solution is made by dissolving 2.94 mg NMDA (Sigma-Aldrich) in 1 mL water. NMDA solution is made fresh prior to the experiment and kept at 4° C.
2. Nimodipine stock solution: 20 μM nimodipine solution is made by dissolving 8.4 mg nimodipine (RBI, Sigma) in 1 mL dimethylsulfoxide (DMSO, Sigma-Aldrich). Nimodipine is made fresh daily and kept at −20° C.
3. 6-Cyano-7-nitroquinoxaline-2,3-dione (CNQX) stock solution: 25 μM CNQX stock solution is made by adding 5 mg CNQX (Sigma-Aldrich) to 861 μL DMSO and sonicating for 1 h. CNQX stock solution is stored for up to 1 month at −20° C in 200-μL aliquots.
4. PI stock solution (1 mg/mL): 250 mg PI (*see* **Note 7**) (Invitrogen/Molecular Probes, Burlington, ON, Canada) is dissolved in 250 mL PBS for a final concentration of 1 mg/mL. PI stock solution is stored at 4° C until use.
5. HEPES buffer solution: HEPES buffer solution is made by dissolving 7.08 g sodium chloride (121 mM NaCl), 2.34 g HEPES acid (10 mM HEPES), 1.82 g HEPES sodium salt (7 mM HEPES-Na), 3.60 g D-glucose (20 mM D-glucose), 0.372 g potassium chloride (0.5 mM KCl, Sigma-Aldrich), 0.11 g sodium pyruvate (1 mM sodium pyruvate), 0.2 g calcium chloride (1.8 mM $CaCl_2$), 0.252 g sodium bicarbonate (3 mM $NaHCO_3$), and 100 μL100 mM glycine (0.01 mM glycine, *see* **Note 8**) in 1 L water. HEPES buffer solution is kept at 4° C and is made weekly.
6. L-NAME stock solution: 10 mM L-NAME stock solution is made by dissolving 5.4 mg L-NAME (Sigma-Aldrich) in 2 mL water. L-NAME stock is made fresh daily and kept at 4° C until use.

2.3. Quantifying Neuronal Death in PI-Treated Cultures

1. Plate reader: Fluoroskan Ascent FL with Ascent Software v2.6 (Thermo Labsystems, Burlington, ON, Canada). Filters on the plate reader are set at 530 nm excitation and 620 nm emission (*see* **Note 9**).
2. Statistical software: Microsoft Office Excel 2003 with the Analysis ToolPak add-in (Microsoft Canada Co., Mississauga, ON, Canada).
3. Graphing software: SigmaPlot 8.02A (Systat Software, Point Richmond, CA, USA).

2.4. Costaining and Imaging PI-Treated Cultures

1. Fixative solution (*see* **Note 10**): 4% paraformaldehyde and 10% sucrose in PBS. Solution pH: 7.4. Fixative solution is made fresh and stored at 4° C.
2. PBS: PBS is purchased without $CaCl_2$ and $MgCl_2$ and is 0.1 μm-filtered. PBS for immunocytochemistry is stored at room temperature until use.
3. Blocking solution: 2 mL normal rabbit serum is added to 18 mL PBS, resulting in a 10% rabbit serum blocking solution. Blocking solution is made daily and stored at 4° C until use.

4. HEPES buffer solution: HEPES solution in this subheading is identical to that in **Subheading 2.2**.
5. Hoechst 33342 stock solution: 2 mL Hoechst 33342 (10 mg/mL) is diluted into 198 mL water, resulting in a final dilution of 100 μg/mL. Hoechst 33342 stock solution is stored at 4° C until use.
6. Triton X-100 solution: 10% Triton X-100 stock solution is made by mixing 10 mL Triton X-100 with 90 mL water. This stock is kept at room temperature until use.
7. Triton X-100 working solution: 0.2% Triton X-100 working solution is made by diluting 400 μL 10% stock in 20 mL PBS. This solution is made fresh and is kept at room temperature.
8. Primary antibody solution (*see* **Note 11**): 30 μL mouse monoclonal anti-NeuN (1:500 dilution; Chemicon, Temecula, CA, USA) is added to 12.75 mL PBS with 2.25 mL blocking solution. This solution is made fresh and stored at 4° C.
9. Secondary antibody solution (*see* **Note 11**): 15 μL goat antimouse conjugated to fluorescein (1:1000 dilution; Sigma-Aldrich) is added to 12.75 mL PBS with 2.25 mL blocking solution. This solution is made fresh and stored at 4° C.
10. Microscope and camera system (*see* **Note 12**): images are visualized using Nikon Eclipse TE200 inverted microscope with a TE-FM Epi-Fluorescence Attachment (Nikon Canada, Mississauga, ON, Canada). Images are captured using a Hamamatsu C4742-95-12ER Digital CCD camera (Hamamatsu Photonics K.K., Sunayama-Cho, Hamamatsu-City, Japan) with SimplePCI software (Compix Inc., Cranberry Township, PA, USA).

3. Methods

3.1. Primary Murine Mixed Cortical Cultures

1. At least 1 day before beginning dissections, coat four 24-well plates with PLO solution (500 μL per well) and incubate overnight at 37° C with 5% CO_2 (*see* **Note 13**).
2. Aspirate out PLO solution and add 500 μL water per well. Repeat wash with water once. Remove water and allow plates to air-dry (*see* **Note 14**).
3. Place an E15 (*see* **Note 15**) pregnant mouse into an induction chamber with 1:2 oxygen:nitrous oxide supplemented with 2% halothane. Once sufficiently anesthetized (*see* **Note 16**), cervically dislocate the animal. Wash the animal thoroughly (*see* **Note 17**) in 70% ethanol and place into the laminar flow hood on a sterile plate.
4. Make incisions from the uterus laterally along both sides of the body until the thoracic cavity. Retract the skin and remove embryos in the placenta from the animal. Place embryos into a culture dish filled with cold PBS.
5. Carefully remove the placenta and place the embryos in the amniotic sac in a separate culture dish with cold MEM.

6. The following steps should be performed one embryo at a time. Remove embryo from its amniotic sac and place it in a culture dish under a dissection microscope. Make an incision on the occipital bone and another incision along the sagittal suture. Holding the neck, ease out the brain out of the cranium through the incision and place the dorsal side up. Remove the olfactory lobes and spread cortices outward, such that the dorsal sides of the cortices are facing down. Cut off any brain matter below the cortex and ease the cortices out of the dura. Place cortices in cold MEM in a small culture dish.
7. Aspirate out MEM and replace with 2 mL Trypsin–EDTA digestion buffer. Incubate cortices at 37° C with 5% CO_2 for 5 min.
8. Transfer cortices using a 5-mL serological pipette into a sterile 15-mL polypropylene tube containing 10 mL cold MEM.
9. Allow cortices to settle and aspirate MEM leaving approximately 2 mL total volume (cortices + MEM).
10. Triturate cortices 10 times with a normal Pasteur pipette, taking care to avoid bubbles. Flame-polish the opening of another Pasteur pipette approximately 50% of its original size and allow to cool. Using the flame-polished pipette, triturate the cortical homogenate another 10 times, again taking care to avoid bubble formation.
11. Add prewarmed (37° C) GM to the homogenate up to 10 mL.
12. Place the cortical homogenate in a centrifuge (GLC-1, Sorvall, Newtown, CT, USA) at 1000 rpm (200 × g) for 5 min. Then, using a 5-mL serological pipette, triturate gently 10 times (*see* **Note 18**). Allow cellular debris a few seconds to settle and place 50 μL cortical suspension into a mixture of 200 μL Trypan blue and 750 μL PBS. Count cells (*see* **Note 19**).
13. Calculate the total volume necessary for 0.8×10^6 cells per well and dilute the cortical homogenate (without cellular debris) in an appropriate volume of prewarmed (37° C) GM (*see* **Note 20**). Add 250 μL PM to each well prior to the addition of 1 mL cortical homogenate per well. Gently agitate plates manually to promote even distribution of neurons and place into a 37° C incubator supplemented with 5% CO_2.
14. Four days following the dissection, gently aspirate GM and replace with prewarmed (37° C) GM/FDU solution (1 mL) to inhibit further glial growth (*see* **Note 21**).
15. Six days following the dissection, aspirate GM/FDU solution and replace with prewarmed (37° C) GM (1 mL) solution.
16. Conduct experiments on day 11 following dissection (*see* **Note 22**).

3.2. NMDA Application and PI Application

1. Visually inspect the cortical cultures using a ×20 objective and phase-contrast microscopy prior to use (**Fig. 1**).
2. Make serial dilutions of NMDA from the 20 mM stock solution into HEPES solution (*see* **Table 1**).

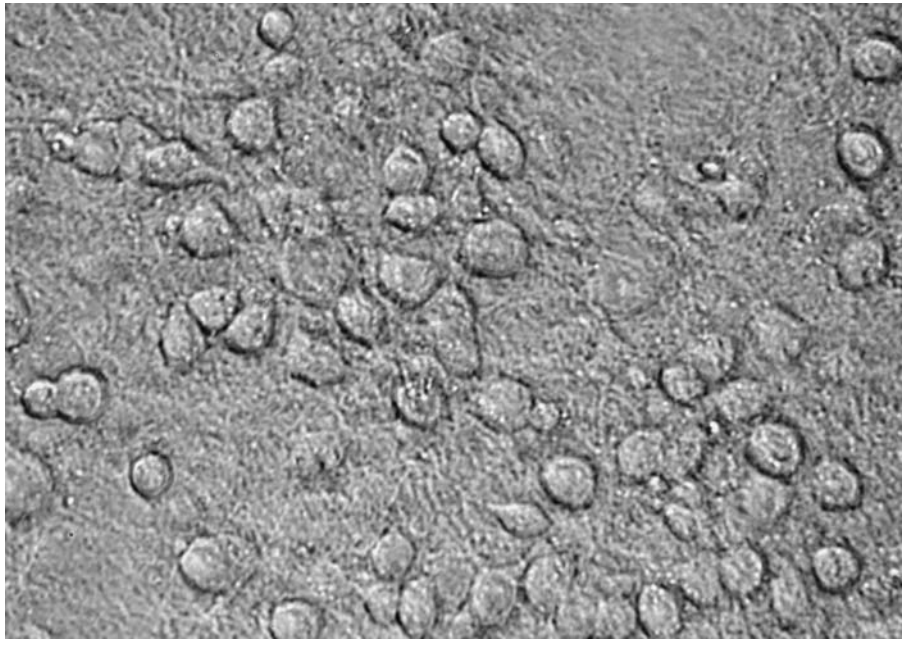

Fig. 1. Appearance of the cell cultures. Healthy neurons should be well rounded, large, and evenly dispersed throughout each well. Images were taken using a ×20 objective.

3. Warm 200 mL HEPES to 37° C (*see* **Note 23**).
4. Add 40 μL CNQX and 10 μL nimodipine to 100 mL prewarmed HEPES solution to a final working concentration of 2 μM CNQX and 10 μM nimodipine.
5. Prepare 100 μM L-NAME working solution by adding 100 μL of the 10 mM L-NAME stock solution to 10 mL CNQX/nimodipine/HEPES buffer.

Table 1
Serial Dilutions of *N*-Methyl-D-Aspartate

Stock dilution	Volume added (mL)	Fill to with HEPES (mL)	Final concentration (μM)
20 mM	1	9	2000
2000 μM	3	7	600
600 μM	6	3	400
N/A	N/A	10	0

6. Remove cultures from the incubator and wash cells twice with 1 mL warm HEPES buffer solution.
7. Gently aspirate HEPES solution from the wells and add warm CNQX/nimodipine/HEPES buffer to 12 wells (1 mL each). Add CNQX/nimodipine/HEPES/L-NAME buffer to the other 12 wells (1 mL each).
8. Add 50 µL NMDA serial dilutions to each appropriate well (**Fig. 2**). The final concentrations of NMDA are 0 µM (50 µL of 0 µM NMDA), 20 µM (50 µL of 400 µM NMDA), 30 µM (50 µL of 600 µM NMDA), and 100 µM (50 µL of 2000 µM NMDA).
9. Return plates to a 37° C/5%CO_2 incubator for 1 h.
10. During the 1 h incubation, make up working PI solution by adding 0.5 mL of 1 mg/mL PI to 45.5 mL of the CNQX/nimodipine/HEPES buffer, resulting in a 10 µg/mL working dilution of PI.
11. Following the 1 h incubation, remove solutions and add 500 µL prewarmed CNQX/nimodipine/HEPES solution with 10 µg/mL PI to each well.
12. Read plates immediately in a plate reader to assess baseline readings (emission 540 nm, excitation 620 nm) (*see* **Note 24**).

3.3. Quantifying Neuronal Death in PI-Treated Cultures

1. Returned plates to the 37° C/5%CO_2 incubator and reassess PI uptake at 20 h following PI treatment. These readings represent the final PI readings.

	1	2	3	4	5	6
A	100µM NMDA 2µM CNQX 10µM nimodipine In HEPES buffer	100µM NMDA 2µM CNQX 10µM nimodipine In HEPES buffer	100µM NMDA 2µM CNQX 10µM nimodipine In HEPES buffer	100µM NMDA 2µM CNQX 10µM nimodipine 100µM L-NAME In HEPES buffer	100µM NMDA 2µM CNQX 10µM nimodipine 100µM L-NAME In HEPES buffer	100µM NMDA 2µM CNQX 10µM nimodipine 100µM L-NAME In HEPES buffer
B	60µM NMDA 2µM CNQX 10µM nimodipine In HEPES buffer	60µM NMDA 2µM CNQX 10µM nimodipine In HEPES buffer	60µM NMDA 2µM CNQX 10µM nimodipine In HEPES buffer	60µM NMDA 2µM CNQX 10µM nimodipine 100µM L-NAME In HEPES buffer	60µM NMDA 2µM CNQX 10µM nimodipine 100µM L-NAME In HEPES buffer	60µM NMDA 2µM CNQX 10µM nimodipine 100µM L-NAME In HEPES buffer
C	30µM NMDA 2µM CNQX 10µM nimodipine In HEPES buffer	30µM NMDA 2µM CNQX 10µM nimodipine In HEPES buffer	30µM NMDA 2µM CNQX 10µM nimodipine In HEPES buffer	30µM NMDA 2µM CNQX 10µM nimodipine 100µM L-NAME In HEPES buffer	30µM NMDA 2µM CNQX 10µM nimodipine 100µM L-NAME In HEPES buffer	30µM NMDA 2µM CNQX 10µM nimodipine 100µM L-NAME In HEPES buffer
D	0µM NMDA 2µM CNQX 10µM nimodipine In HEPES buffer	0µM NMDA 2µM CNQX 10µM nimodipine In HEPES buffer	0µM NMDA 2µM CNQX 10µM nimodipine In HEPES buffer	0µM NMDA 2µM CNQX 10µM nimodipine 100µM L-NAME In HEPES buffer	0µM NMDA 2µM CNQX 10µM nimodipine 100µM L-NAME In HEPES buffer	0µM NMDA 2µM CNQX 10µM nimodipine 100µM L-NAME In HEPES buffer

Fig. 2. Example of the plate layout for an experiment in which there are three repetitions of each condition, and both treatments (control and L-NAME) are applied on the same plate to minimize any potential inter-plate variability. CNQX, 6-cyano-7-nitroquinoxaline-2,3-dione; L-NAME, *N*ω-nitro-L-arginine methyl ester; NMDA, *N*-methyl-D-aspartate.

2. Because the mixed cortical cultures invariably exhibit an endogenous level of cell death, evaluating the extent of neuronal death requires that data obtained at 20 h be compared with baseline readings. The following equation accomplishes this required operation for any given condition:

$$F_x = \frac{\sum_{i=1}^{n} \left[F_{\text{Final}(i)} - F_{\text{Baseline}(i)} \right]}{n},$$

   Where n is the number identical treatment repetitions (3 in this case), F_{Baseline} is the arbitrary fluorescence obtained by the plate reader at 0 h, F_{Final} is the arbitrary fluorescence obtained by the plate reader at 20 h, x is any given condition, and F_x is the mean increase in fluorescence for any given condition.
3. To normalize the data, divide each point obtained above by the mean PI reading at 0 μM NMDA at 20 h of the same drug treatment(*see* **Note 25**).
4. To evaluate the significance of each data point, perform a one-tailed *t*-test on each pair of points (comparing nontreatment with treatment groups), where the alternative hypothesis is "nontreated PI fluorescence" > "treated PI fluorescence." Any *P*-value less than 0.05 is considered significant (*see* **Note 26**).
5. Graph results using SigmaPlot 8.02A (**Fig. 3**) or another suitable graphing software package.

3.4. Costaining and Fluorescence Imaging

3.4.1. Verifying Neuronal Content of the Cell Cultures

1. While still in the PI working solution, add 15 μL 10% Triton X-100 solution to each of the 100 μM NMDA well. Incubate the cells for at least 5 min and assess PI staining using the plate reader.
2. To determine the proportion of neurons compared with other cell types (*see* **Note 27**), the following equation is used:

$$F_{\text{Other}} = \frac{\sum_{i=1}^{n} \left[F_{\text{Triton X}(i)} \right]}{n},$$

   Where n is the number of 100 μM NMDA wells treated with Triton X-100 (3 in this case), $F_{\text{Triton X}}$ is the PI fluorescence obtained following Triton X-100 treatment, and F_{other} is the average PI staining attributed to other cell types in the culture.
3. F_x is divided by F_{Other}, where x is the nontreated 100 μM NMDA condition at 20 h, and a percentage of neuronal cells is obtained (*see* **Note 28**).

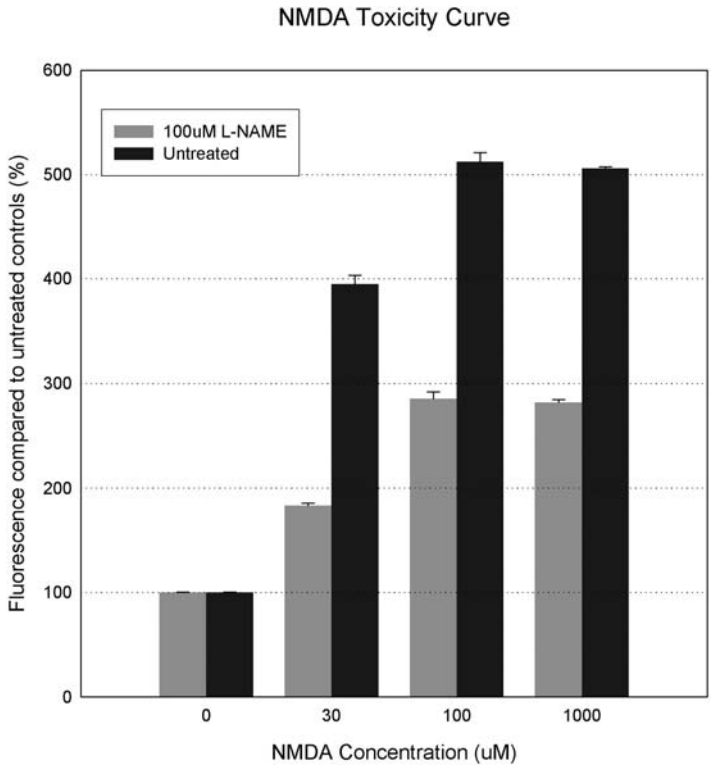

Fig. 3. A representative example of an *N*-methyl-D-aspartate (NMDA) toxicity curve obtained by propidium iodide (PI) staining and quantification of fluorescence increase. Note the similarities in fluorescence staining obtained with 100 and 1000 μM NMDA applications, indicating saturation of neuronal death.

3.4.2. Verifying the Cellular Nature of PI Staining

1. Prior to beginning the experiment, warm 100 mL HEPES buffer to 37° C.
2. Prepare Hoechst 33342 working solution by adding 150 μL stock solution to 15 mL prewarmed HEPES to a final dilution of 1 μg/mL.
3. Wash cell cultures twice with prewarmed HEPES solution followed by an application of 500 μL Hoechst 33342 working solution to each well (*see* **Note 29**).
4. Incubate the plate at 37° C for 5 min and visualize.
5. Visualize PI using excitation 540 nm and emission 620 nm. Visualize Hoechst 33342 staining using excitation 350 nm and emission 460 nm (**Fig. 4**).

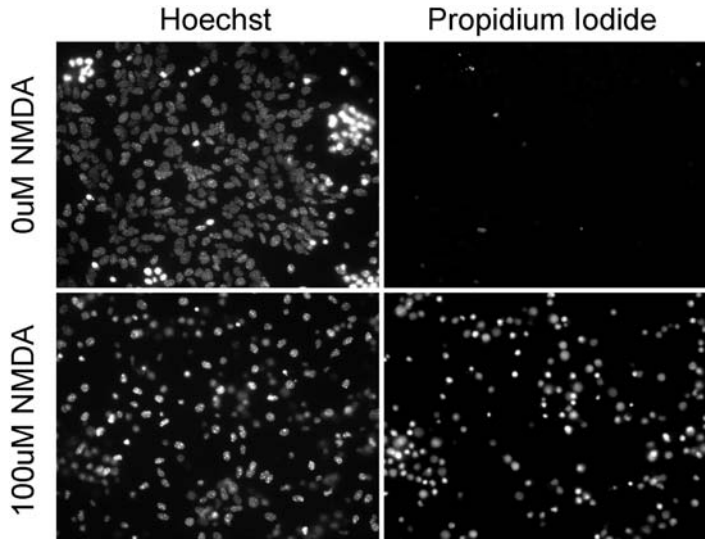

Fig. 4. An example of propidium iodide (PI)-treated (right panels) cell cultures costained with Hoechst 33342 (left panels). Although some fluorescence is observed in the 0 μM *N*-methyl-D-aspartate (NMDA) condition, it is not associated with Hoechst 33342, indicating PI staining from a noncellular source. NMDA (100 μM) treatment induces widespread PI staining, largely localized with Hoechst 33342. Images were taken using a 20× objective.

3.4.3. Costaining Cultures With Immunocytochemistry

1. Remove plates from the incubator and wash twice with 1 mL prewarmed PBS.
2. Apply 500 μL warm fixative solution to each well and leave at room temperature for 50 min.
3. Permeabilize cells using 500 μL 0.2% Triton X-100 in PBS and leave at room temperature for 15 min.
4. Wash wells three times (1 mL each wash) with PBS.
5. Incubate cells with 500 μL 10% normal rabbit serum for 1 h at room temperature to block.
6. Add 200 μL primary antibody solution and leave at 4° C overnight.
7. Wash cells again three times with PBS for 5 min each.
8. Incubate plates in secondary antibody solution at room temperature for 1 h.
9. Wash cells three times with PBS for 5 min each and visualize using the microscope.
10. Visualize PI at excitation 540 nm and emission 620 nm. Visualize fluorescein-conjugated antimouse at excitation 495 nm and emission 520 nm (**Fig. 5**).

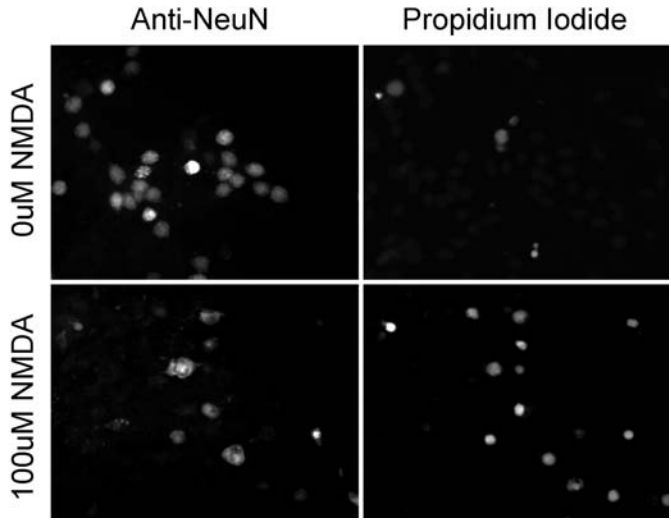

Fig. 5. Propidium iodide (PI)-treated cell cultures costained with immunocytochemistry (anti-NeuN). Note the significant overlapping staining of PI (right panels) and anti-NeuN (left panels) with 100 μM *N*-methyl-D-aspartate (NMDA) compared with little or no staining with 0 μM NMDA. Images were taken using an 40× objective.

4. Notes

1. Although this statement holds true for most types of insults, it should be noted that direct mechanical injuries (such as the stretching of cells) can induce the formation of pores in the plasma membrane large enough to allow PI into the cell. However, subsequent experiments have shown that some of these cells appear healthy after the insult. Thus, results obtained from these types of cultures should be interpreted carefully, as neuronal death using PI staining can be overestimated in these cases.
2. Despite the focus on NMDAR-mediated neuronal death in this chapter, the basic protocol can be applied to almost any type of neuronal insult (with the exception of those listed in the previous note). We have successfully used this method with staurosporine, 3-morpholinosydnonimine (SIN-1), glutamate, and other neurotoxic substances.
3. All solutions for the cell culture preparation must be kept sterile at all times unless otherwise noted. Solutions are filtered into autoclaved glass bottles.
4. For the purposes of this chapter, unless otherwise noted, all references to water refer to distilled, deionized water with a resistance of at least 18.2 MΩ and a total carbon content of less than 5 parts per billion.

5. Horse serum (Invitrogen/Gibco) is inactivated by heating bottle for 1 h in a 56° C water bath; 50-mL aliquots are made and stored at −20° C until use.
6. If GlutaMAX™-1 100× is unavailable, it can be substituted with an equivalent volume of 200 mM L-glutamine dissolved in water.
7. PI has been demonstrated to have mutagenic properties. Handle PI with appropriate protection (i.e., gloves, mask, and fumehood).
8. Glycine stock solution (100 mM) is made by dissolving 75.07 mg glycine (Sigma-Aldrich) in 10 mL water. Glycine stock solution is divided into 500-μL aliquots and kept at −20° C until use.
9. Any plate reader capable of excitation and emission recordings at approximately 530 and 620 nm, respectively, will be sufficient to quantify PI staining provided it has the appropriate sensitivity.
10. Paraformaldehyde is a known carcinogen—use proper protection when handling. Fifteen milliliters of PBS is heated under the fumehood until its temperature reaches approximately 80° C. Once the temperature has reached 80° C, 0.8 g paraformaldehyde (Sigma-Aldrich) is added to the PBS. If the solution does not become clear, drops of 0.1 M sodium hydroxide (NaOH) are added until no precipitate is observed. When the fixative solution has cleared, it is removed from the heating plate and allowed to cool to room temperature. Two grams of sucrose (Sigma-Aldrich) is then dissolved in the solution. The pH is adjusted to 7.4, and water is added to the solution to obtain 20 mL total volume, resulting in 4% paraformaldehyde (w/v) and 10% sucrose (w/v).
11. The volume listed here is sufficient for immunocytochemistry in all 24 wells of the plate. Often, it is not necessary to stain each condition in triplicate (or even each condition), so careful planning should be performed such that no antibody is wasted.
12. Any microscope/camera system with the following filter pairs will be sufficient for visualizing PI, Hoechst 33342, and fluorescein isothiocyanate (FITC), respectively: excitation 540 nm and emission 620 nm, excitation 350 nm and emission 460 nm, and excitation 495 nm and emission 520 nm.
13. Unless otherwise noted, all procedures outlined in the preparation and maintenance of primary mixed cortical cultures should be performed in a sterile environment. Any manipulations on the cortical cultures are performed in a laminar flow hood in our laboratory. Spray bottles with 70% ethanol are used constantly to keep gloved hands clean. All surgical instruments are allowed to sit in 70% ethanol prior to use. Micropipette tips and Pasteur pipettes are autoclaved prior to use.
14. Because the number of embryos is variable, any extra PLO-treated plates can be kept in sterile conditions at 4° C for up to 1 week.
15. Although E15 embryos are usually used in our laboratory, E14–E16 embryos may still be used if necessary.
16. Various behavioral tests (such as tail pinch or toe pinch) are used at this stage to ensure that the animals do not feel pain prior to dislocation.

17. Use a squirt bottle filled with 70% ethanol and squirt against the grain of the fur of the animal to ensure thorough washing.
18. Cellular debris should remain mostly in precipitate form, whereas neurons should be resuspended in solution at this stage. Allowing too long a time to settle will result in an underestimation of the homogenate concentration. Thirty seconds is usually enough to allow cellular debris to settle without neurons settling.
19. Using a cell counter with 0.1 mm depth and 1 mm^2 field areas, our laboratory routinely obtains about 40 cells per field for all embryos from a single pregnant mouse.
20. At a 20× dilution in the Trypan blue solution, 40 cells per field refers to about 80 million cells in the 10 mL cortical homogenate. At a concentration of 0.8×10^6 cells per well, there is enough homogenate to accommodate 100 wells, or four 24-well plates. Because each well requires 1 mL homogenate, 10 mL cortical homogenate should be diluted in 90 mL warm GM. Transfer of cellular debris in the homogenate to the warm GM is avoided.
21. At this and subsequent stages, the plated neurons are extremely fragile and prolonged exposure to air should be avoided at all times. In our laboratory, the technique for changing media is as follows: hold a sterile Pasteur pipette in the left hand and a nose pipettor with an appropriate serological pipette in the right hand; aspirate most of the media (leaving a thin film); and immediately (and gently) place the appropriate amount of solution in the well using the nose pipettor or micropipette.
22. Eleven days following dissection, neurons are sufficiently adhered to the well bottom and have had sufficient time to develop processes. Although it is possible to conduct experiments at earlier times, we have noted that variability in results increases.
23. For the purposes of this chapter, the following volumes cited are necessary for assaying a single 24-well plate. If more plates are required, volumes should be adjusted accordingly.
24. If the plate reader allows, one can also take a kinetic reading of PI as it increases over time. This modification is especially useful when using multiple neurotoxic treatments and can be used to asses whether various treatments have differing time courses of cell death.
25. Alternatively, one can express the extent of cell death as a function of total neuronal death by dividing each point by the average PI reading at 100 μM NMDA at 20 h of the same drug treatment.
26. If more than two treatments are examined, a Bonferroni-corrected one-way ANOVA test could be performed on the data accordingly.
27. This test is based on observations that a 100 μM NMDA treatment kills almost all neurons (similar to a 1 mM NMDA treatment) but leaves other cell types relatively unharmed. Thus, any increase in PI staining from Triton X-100 treatment is a result of the membrane permeabilization of all other cell types.

28. Our cultures routinely result in a proportion of neuronal cells over 85%.
29. PI staining can be so intense that it can be mistaken for unspecific noncellular staining. Hoechst 33342 provides an independent measure to determine whether PI staining is cellular in nature.

References

1. Aarts, M., Liu, Y., Liu, L., Besshoh, S., Arundine, M., Gurd, J. W., Wang, Y. T., Salter, M. W., and Tymianski, M. (2002). Treatment of ischemic brain damage by perturbing NMDA receptor-PSD-95 protein interactions. *Science* **298**, 846–850.
2. Sattler, R., Xiong, Z., Lu, W. Y., Hafner, M., MacDonald, J. F., and Tymianski, M. (1999). Specific coupling of NMDA receptor activation to nitric oxide neurotoxicity by PSD-95 protein. *Science* **284**, 1845–1848.
3. Sattler, R., Charlton, M. P., Hafner, M., and Tymianski, M. (1997). Determination of the time course and extent of neurotoxicity at defined temperatures in cultured neurons using a modified multiwell plate fluorescence scanner. *J. Cereb. Blood Flow Metab*. **17**, 455–463.
4. Olney, J. W. (1969). Brain lesions, obesity, and other disturbances in mice treated with monosodium glutamate. *Science* **164**, 719–721.
5. Sattler, R., Charlton, M. P., Hafner, M., and Tymianski, M. (1998). Distinct influx pathways, not calcium load, determine neuronal vulnerability to calcium neurotoxicity. *J. Neurochem.* **71**, 2349–2364.
6. Dawson, V. L., Dawson, T. M., London, E. D., Bredt, D. S., and Snyder, S. H. (1991). Nitric oxide mediates glutamate neurotoxicity in primary cortical cultures. *Proc. Natl. Acad. Sci. U. S. A*. **88**, 6368–6371.
7. Tas, J. and Westerneng, G. (1981). Fundamental aspects of the interaction of propidium diiodide with nuclei acids studied in a model system of polyacrylamide films. *J. Histochem. Cytochem.* **29**, 929–936.

3

A Modified Silver Technique (de Olmos Stain) for Assessment of Neuronal and Axonal Degeneration

Tatyana I. Tenkova and Mark P. Goldberg

Summary

Silver impregnation histological techniques yield excellent visualization of degenerating neurons and their processes in animal models of neurological diseases. These methods also provide a particularly valuable complement to current immunocytochemical techniques for recognition of axon injury in the setting of brain or spinal cord trauma, ischemia, or neurodegenerative diseases. Despite their utility, silver methods are not commonly used because of complex preparation requirements and inconsistent results obtained by inexperienced histologists. This chapter details a modification of the de Olmos amino-cupric-silver protocol, which has been adapted for efficient processing of large numbers of mouse or rat brains. One author (T.I.T.) has used this method for several years to identify degenerating neurons in adult and neonatal rodent brains. A detailed protocol is provided, with attention to the most critical variables in tissue fixation and solution preparation. Examples are shown of axon injury in the rat brain after focal ischemia.

Key Words: Axon; neuron; histological techniques; stroke; microscopy; neurodegeneration.

1. Introduction

Recognition of injured or degenerating neurons by optical microscopy poses special technical challenges in disease models. Many conventional histological or immunocytochemical methods do not readily distinguish injured cells from the tissue background. On the contrary, highly specific chemical or antibody markers for cellular injury (e.g., labels for DNA damage or caspase activation) may not provide adequate visualization of cellular morphology or structure.

From: *Methods in Molecular Biology, vol. 399: Neuroprotection Methods and Protocols*
Edited by: T. Borsello © Humana Press Inc., Totowa, NJ

Metal impregnation techniques have been used for decades to add contrast to otherwise clear tissue sections, with the specific labeled cellular or subcellular component depending in unpredictable ways on chemical composition of the staining solution, tissue fixative, and staining procedure. A significant advance came with the development of silver stain procedures that label only injured neurons ***(1,2)***. Although the chemical nature of the metal–neuron interaction remains unknown, these silver stain methods provide many valuable benefits for light microscopic analysis of fixed tissue. Degenerating neurons are darkly stained throughout their cell bodies and processes, and even rare, isolated labeled neurons can be easily recognized among large numbers of normal cells and unstained brain or spinal cord.

Silver stain methods may prove especially valuable for identification of injured or degenerating axons in models of acute and chronic disease. Common techniques include immunocytochemical markers for normal or abnormal neurofilament proteins, injectable antegrade or retrograde tract tracers, antibodies to normally transported proteins such as amyloid precursor protein, and visualization of axons in transgenic mice with neuron-specific expression of fluorescent proteins. Currently, no single labeling method is fully satisfactory for axon injury. Silver methods identify darkly stained degenerating axons within unstained white matter tracts; degenerating axons may be potentially visible even after fluorescent proteins or immunocytochemical epitopes have disappeared. **Fig. 2** shows a rat brain 12 h after focal ischemia produced by occlusion of the middle cerebral artery. Low-power micrograph demonstrates the area of degeneration in cortex and subcortical white matter. The higher magnification images (inset) shows regions of axon injury in white matter. The silver stain method demonstrates axon injury even more clearly in rodent models of chronic neurodegeneration.

The technique described here is adapted from the amino-cupric-silver stain developed by de Olmos and colleagues ***(1)***. This method has been used to identify degenerating neurons in retina, cortex, and other nervous system regions of infants and adult rodents ***(3)***. It also works well in nonhuman primate and human brain sections, although background labeling is higher in unperfused human tissue because of intravascular erythrocytes. Some of the most important variables are described in the protocol. It is assumed that the reader is familiar with perfusion fixation; careful fixation is critical for silver staining and especially so for visualizing axons (which are easily damaged by incomplete or cold fixation). The most effective fixative for de Olmos staining is 4% paraformaldehyde in 0.1 M cacodylate buffer, pH 7.4; fortunately, this fixative is also fine for light

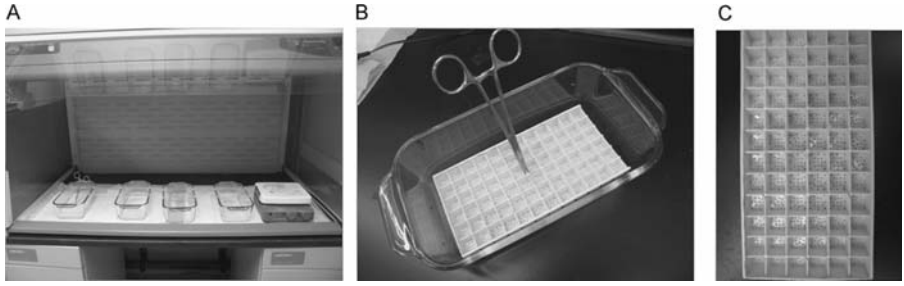

Fig. 1. Some apparatus for de Olmos silver staining of rodent brain sections. **(A)** Arrangement of Pyrex dishes and electric stirrer in chemical safety hood. **(B)** Divided staining tray fitting in Pyrex dish, with appropriate sized chambers for rodent brain sections. The tray is handled using hemostats. **(C)** Perforated bottom of staining tray, which allows thorough solution exchanges without damage to tissue sections.

microscopy and immunocytochemistry. Several of the staining solutions must be measured with some precision, and many of them must be prepared just before use.

2. Materials

2.1. Equipment and Supplies

1. Chemical safety hood.
2. Vibratory microtome (Vibratome) for tissue sections.
3. Four Pyrex dishes, size 8.5 in × 5 in, for use as staining boats (*see* **Fig. 1A**) .
4. One plastic "mini-ice cube tray" with individual wells 1 cm × 1 cm, of the sort usually used for plastic embedding in electron microscopy (*see* **Fig. 1B**). This must fit into the Pyrex dishes and must be resistant to organic solvents. The bottoms of all the 1 cm × 1 cm wells in this "staining tray" should be perforated with many small holes so that they drain rapidly, and these drain holes should be smooth on the inside so that they do not tear the tissue sections (*see* **Fig. 1C**).
5. One thermometer for measuring approximately 20–60° C.
6. Two 250-mL beakers; 10, 25, 50, 100 and 250 ml graduated cylinders.
7. One hemostat.
8. Two stir bars, 2 cm long.
9. Aluminum foil, 18 inches wide.
10. Paper towels.
11. Distilled and deionized water.
12. All chemicals are from Sigma Chemical Co. unless otherwise specified.

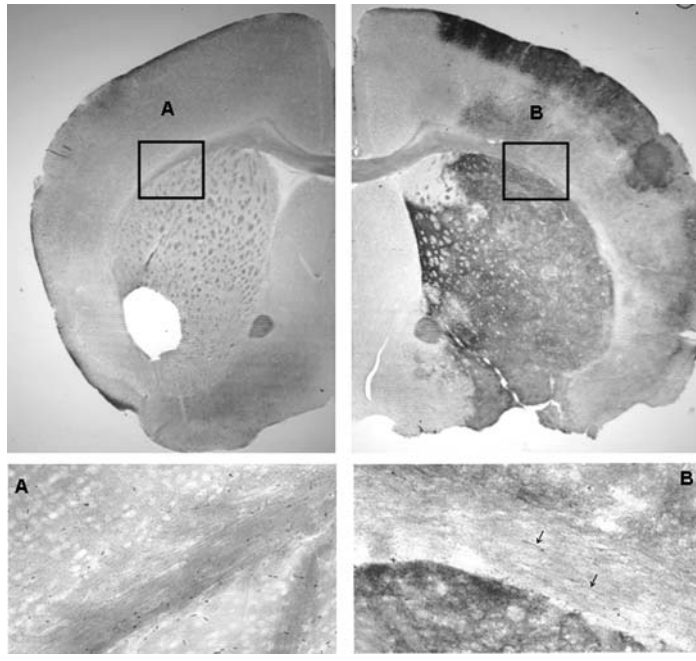

Fig. 2. de Olmos silver stain of ischemic neuronal injury. Adult mouse brains were fixed 12 h after occlusion of the middle cerebral artery (right side). Silver stain identifies extensive region of injury in cortex and striatum. Inset shows higher magnification view of subcortical white matter, with labeling of individual axon fibers (arrows) in ischemic but not control white matter. Note some background labeling on control side is from red blood cells; this is a consequence of incomplete perfusion.

2.2. Stock Solutions

All solutions should be prepared in clean beakers with clean stir bars, then stored in clean glass bottles. We clean all glassware by soaking in 50% nitric acid for at least 1 h (in the hood—dangerous fumes), then rinsing very well with distilled water and finally with deionized water. Use precise measurements in every step. Unless otherwise noted, stock solutions can be stored at room temperature in a chemical cabinet for up to 1 year (*see* **Note 1**).

1. 1% $CuNO_3$ (light sensitive).
2. 0.1% Allantoin.
3. 0.4% NaOH.

4. Ammonium hydroxide, absolute. (We order small 25-mL bottles, because it is no longer good for silver staining after 2–3 months; it does not clear the solution—*see* Note 3).
5. Borate buffer (light sensitive):

   Titrate 0.2 M boric acid (Aldrich) with 0.05 M sodium tetraborate (in deionized water) to pH 8.5.

6. Mounting solution:

   a. 100 mL Distilled water,
   b. 2 g Gelatin, and
   c. 100 mL Absolute ethanol.

Dissolve the gelatin completely on a hot plate, allow it to cool but not solidify, and then add the alcohol very slowly, with continuous mixing, to avoid precipitating the gelatin. This mounting solution can be stored for a long time at 4° C, at which point it is a cloudy gel. Before each use, put approximately 10 mL of this solution in a beaker and warm it enough to redissolve and clarify it.

2.3. Solutions to be Prepared for Each Use

1. Fixative: 4% paraformaldehyde (Fisher Scientific) in 0.1 M cacodylate buffer (Polysciences, Inc.), pH 7.4. For perfusion, make up the fixative solution fresh, or at least use it within the first 24 h after preparation.
2. Cupric-silver solution: Make fresh in the hood for each use, with the hood lights off, as it is light sensitive.

   a. 120 mL Deionized water,
   b. 1.05 g $AgNO_3$,
   c. 1 mL 1% $CuNO_3$,
   d. 10 mL 0.1% Allantoin,
   e. 6 mL Pyridine,
   f. 12 mL Absolute ethanol, and
   g. 6 mL Borate buffer.

3. Silver diamine incubation solution:

   a. 60 mL Deionized water,
   b. 12 g $AgNO_3$,
   c. 30 mL 0.4% NaOH (upon addition of this, the solution should turn very brown),
   d. 15 mL NH_4OH (upon addition of this, the solution should clear completely again; *see* **Note 2**), and
   e. 60 mL Deionized water (total 120 mL).

   Make fresh for each use, in the hood with the hood lights off.

4. Reducing agent solution:
   a. 135 mL Deionized water,
   b. 15 mL Absolute ethanol (or 16 mL of 95% ethanol) (*see* **Note 3**),
   c. 180 µL 37% w/w Formaldehyde, and
   d. 10.5 mg Anhydrous citric acid (or 11.5 mg citric acid if it is monohydrous); measure this precisely.
5. Ferricyanide bleaching solution, 0.3% $K_3Fe(CN)_6$:

   450 mg $K_3Fe(CN)_6$ in 150 mL distilled water (*see* **Note 4**).
   Make fresh for each use.
6. Thiosulfate solution:

   150 mg Sodium thiosulfate in 150 mL distilled water.
   Make fresh for each use.

3. Methods

Clean all dishes with 50% nitric acid as described in Section 2.2. All steps should be done in a fume hood (*see* **Note 1**). Prepare solutions listed in **Subheading 2.3.**, just before use.

3.1. Tissue Preparation

1. Fix rodent brains or spinal cord by intracardiac perfusion. Warm the fixative (4% paraformaldehyde in 0.1 M cacodylate buffer, pH 7.4; *see* **Note 5**) to room temperature before perfusion. Use good perfusion technique, including a preflush with buffer to remove all red blood cells. (If any red blood cells remain behind, they will also become impregnated with silver and create a confusing background.) For adult mice, the following perfusion method is effective:
   a. 20-ga Needle, gravity or pump perfusion,
   b. 20 mL Cacodylate buffer with 0.002 g heparin, and
   c. 80 mL Fixative.
2. After perfusion fixation, remove the brains or spinal cords and store them in the same fixative for at least 24 h at 4° C. For faster perfusion, fix in 8% paraformaldehyde at room temperature overnight, with gentle agitation on shaker.
3. Prepare 50-µm thick vibratome sections. Silver staining works also on 40-µm to 100-µm thick brain, spinal cord, or retina sections. Store tissue sections in 4% paraformaldehyde at 4° C for up to 6 months.

3.2. Staining

1. Put approximately 150 mL of deionized water into each staining boat, enough to float the brain sections in the staining tray but not to overflow its wells so that the sections get mixed up.

2. Distribute not more than three to four brain sections in each well of the staining tray (*see* **Note 6**) and make sure to note on paper which row (horizontally or vertically) corresponds to which section and which brain or spinal cord (*see* **Note 7**).
3. Wash the sections five times with deionized water for 1–5 min each, by transfer through five successive dishes, shaking the tray occasionally in each dish. (Hold the tray in the middle with a hemostat.) Blot the tray well on paper towels (but be careful not to dry it) before the next step.
4. Place the tray in a dish of cupric-silver solution, wrap the dish in aluminum foil, and insert a thermometer into it through the foil, then place the dish on a hot plate at 40° C for 1 h, then remove it from the hot plate and leave it in the hood at room temperature overnight.
5. The next day, blot the tray well on paper towels (but again, be careful not to dry it).
6. Dip the staining tray in a dish of 100% acetone for 30–90 s (again, make sure not to overflow the tray and risk mixing up the brain slices).
7. Quickly transfer the staining tray to a dish of silver diamine incubation solution and incubate for 35 min. Wrap the dish in Aluminium foil.
8. Remove the tray from the silver diamine incubation solution and blot it very well with paper towels (again, be careful not to dry it).
9. Transfer the staining tray to a dish of reducing agent solution for 90 s to 5 min (*see* **Note 8**). (From this point on, blot the staining tray between each step with a lot of paper towels.)
10. Transfer the tray to a dish of ferricyanide bleaching solution and incubate for approximately 10 min with continuous gentle agitation (*see* **Note 9**). Watch this step very carefully. The tissue should end up a dark straw color. If the tissue remains too dark, it can be left in this solution for up to 30 min. Blot well.
11. Transfer the staining tray through three distilled water washes in three clean dishes, spending 30 s to 1 min in each dish. Blot well between each transfer.
12. Transfer to a stabilizing solution composed of 0.1% sodium thiosulfate for 1 min. Blot well.
13. Again transfer the staining tray through three distilled water washes in three clean dishes, spending approximately 1 min in each dish. Blot well between each transfer.
14. Mount the tissue sections on prewarmed "+ treated" glass slides with gelatin/alcohol mounting solution (Section 2.2.6). Place a group of sections in the solution for approximately 5 min to impregnate them, then use a small soft paint brush to transfer them onto a slide and orient them as desired. Then leave the sections to dry on the slide overnight, without a coverslip.
15. "Dehydrate" the mounted sections through graded alcohols (50, 70, $2 \times 90\%$, and $2 \times 100\%$) for 5 min each, transfer to xylene for three exchanges for 5 min.

16. Coverslip with Permount before the xylene dries out.
17. Examine slides under bright-field microscopy (*see* **Note 10**).

4. Notes

1. Many of the solutions are toxic, volatile, corrosive, and/or carcinogenic. Use appropriate precautions for safety, storage, and disposal at all stages. Do not remove the preincubation cupric-silver solution from the hood; it contains pyridine (a carcinogen). Store the silver waste solutions and potassium ferricyanide solution in disposable containers. The glassware, stir bars, thermometer, and hemostat should be cleaned by soaking in 50% nitric acid for at least 1hr, followed by rinsing with distilled then dionized water.
2. All the measurements should be very precise. If this solution does not clear completely, it may mean that the ammonium hydroxide is not fresh (the most common reason) or that the water or dishes are not clean.
3. Use 15 mL alcohol only if the bottle has been opened for the first time, otherwise use 16 mL.
4. From this point in the procedure on, deionized water does not need to be used; ordinary distilled water is adequate.
5. The best fixative for de Olmos staining is 4% paraformaldehyde in 0.1 M cacodylate buffer, pH 7.4; this fixative is also perfectly fine for light microscopy and immunocytochemistry. Alternatively, 4% paraformaldehyde in 0.1 M Tris buffer, pH 7.4, is also effective and less toxic than cacodylate buffer. Other tested buffers resulted in unacceptably high backgrounds.
6. If the sections are overcrowded, the quality of the staining is not good—especially, the bleaching step is perturbed.
7. The sections can be distributed horizontally or vertically, so every row or every column corresponds to sections from one brain. Placement of the sections in rows allows processing of 12 sections from six brains at the same time.
8. You should watch the color of the sections. The color should be dark brown velvet. Sometimes, the color does not correspond to the time.
9. This is the most critical step referring to the background of the staining. Watch the color of the sections and continuously agitate the tray. The bleaching of young tissue generally proceeds much faster (for neonatal mouse brains, ≤ 2 min).
10. Sections from experimental brains should be compared with age-matched control brains that are processed in parallel.

Acknowledgments

This protocol was developed in the laboratory of Dr. John Olney at Washington University. Preparation of this manuscript was supported by NIH grants (to M.P.G.) P01 NS032636 and R01 NS36265.

References

1. Carlsen, J. and de Olmos, J.S. (1981) A modified cupric–silver technique for the impregnation of degenerating neurons and their processes. Brain Res. **208**, 426–431.
2. Switzer, R.C. (2000) Application of silver degeneration stains for neurotoxicity testing. Toxicol Pathol. **28**, 70–83.
3. Tenkova, T., Young, C., Dikranian, K., Labruyere, J., and Olney, J.W. (2003) Ethanol-induced apoptosis in the developing visual system during synaptogenesis. Invest Ophthalmol Vis Sci. **44**, 2809–2817.

4

Model of Acute Injury to Study Neuroprotection

Michal Schwartz and Jonathan Kipnis

Summary

A major causative factor in the paralysis that often follows an acute injury to the central nervous system (CNS) is the paradoxical inability of the CNS to tolerate its own mechanism of self-repair. The dismal result is often a wider spread of damage (part of the inevitable "secondary" or "delayed" degeneration) rather than contribution toward a cure. Ever since the phenomenon of posttraumatic damage spread in the CNS was first recognized, neuroscientists have attempted to identify the players in this destructive process and have sought ways to neutralize or bypass them with the object of rescuing any neurons that are still viable. This approach is collectively termed neuroprotection. In this chapter, we present a view of experimental paradigms used to study neuroprotection.

Key Words: Neuroprotection; CNS degeneration; partial injuries; protective autoimmunity.

1. Introduction

1.1. Central Nervous System Injuries

The central nervous system (CNS) has been referred to as an immune privileged site in which local immune responses are restricted ***(1–6)***. Unlike most peripheral tissues, the CNS functions through a network of postmitotic cells (neurons) that are incapable of regeneration, and hence, any immune activity might interfere with cell function. The CNS is vulnerable to damage that might be caused by the same means that the immune system uses to defend peripheral tissues from pathogens. Consequently, immune privilege in the CNS might be interpreted as an evolutionary adaptation developed to protect the intricate neuronal networks of the CNS from incursion by the immune system ***(7,8)***.

From: *Methods in Molecular Biology, vol. 399: Neuroprotection Methods and Protocols*
Edited by: T. Borsello © Humana Press Inc., Totowa, NJ

An early definition of CNS immune privilege was based on the assumption that access of the immune system into the CNS is restricted. This assumption was supported by the observation that the rejection of allografts is very slow in the CNS ***(9,10)***. Any penetration of leukocytes into the CNS was viewed as evidence of pathology. Several observations have challenged this definition. First, CNS antigens drain into peripheral (cervical) lymph nodes and induce immune responses in the host ***(11,12)***. Second, activated T cells have been found to enter the CNS in the absence of discernible neuropathology ***(13,14)***. Third, leukocyte recruitment into the CNS appears to successfully resolve some CNS viral infections, such as Sindbis virus encephalitis, without the development of any apparent long-term bystander effects ***(15,16)***. Fourth, based on the relatively prolonged survival of xenografts (tissue grafts from different species) in immunosuppressed individuals, it was suggested that the immune system participates in CNS xenograft rejection ***(17)***. Taken together, these findings indicate that the CNS is accessible to immune cells and that local immune responses within the CNS are regulated by a number of mechanisms. It seems likely that some of these mechanisms help limit immune responses, with meaningful consequences for the functioning of the healthy CNS. However, these mechanisms are altered following injury or under neurodegenerative disorders, making the CNS more accessible to immune cells. This includes upregulation of MHC class I and II molecule expression ***(18)***.

1.2. Why Neuroprotection?

Acute insults to CNS neurons often cause direct damage to their cell bodies, their axons, or both. Damage to the cell body will inevitably cause death of the neuron. Damage to the axon will result in its degeneration, but the cell body might survive for a while, and during that time, it is potentially capable of being rescued from death ***(19)***. Rescued cell bodies will not have the capacity to confer functional recovery, however, unless they undergo the regenerative process of sprouting new axons capable of forming new connections.

The overall damage and resulting disability caused by a CNS injury is often worse than would be expected from the severity of the insult. This is because degeneration of axons and damage to cell bodies are not confined to the neurons that sustained the primary injury; additional neurons in the vicinity of the directly injured cells are often affected as well. Studies over the last 15 years have suggested that the major agents of posttraumatic damage spread are neurotransmitters such as glutamate and NO ***(20–28)***. These physiological compounds, although normally pivotal for proper functioning of neural tissue, become neurotoxic when their physiological levels are exceeded,

for example, after an acute insult or under chronic CNS neurodegenerative conditions (**Fig. 1**). Based on these findings, it was reasonable to assume that by restoring such compounds to physiological levels it should be possible to prevent the postinjury loss of neural tissue. Experiments showing that a transient increase in their levels occurs within hours of an acute insult led scientists to focus their studies of neuroprotection in animal models on a therapeutic window spanning only the first few hours after the insult ***(25,29,30)***. Their assumption was supported by observations that any postinjury intervention based on blocking or neutralizing glutamate or NO was beneficial only if applied within that time window ***(25,31)***.

Over the years, it was shown, however, that CNS insults also trigger the operation of other mechanisms. One such mechanism, in which the infiltration of immune cells is required, has been interpreted in different, even conflicting, ways mostly in terms of its destructive effect ***(32–34)***. Nevertheless, understanding that the same compounds might exert their adverse effects at different dosages and different stages and that the same cells might behave differently under different conditions have led to the recognition that (1) the therapeutic window for neuroprotection in acute insults is wider than originally thought, (2) the optimal timing of an intervention is critically dependent on the nature of the manipulation, (3) a similar mechanism operates in both acute and chronic conditions, and (4) many of the devastating mechanisms represent physiological self-repair processes that are out of control and have consequently become distorted.

1.3. Model of Partial Insult to the CNS Leads to Further Findings

Several years ago, we developed a novel model of partial injury of the rat optic nerve ***(19,35–37)***, which enabled us to distinguish quantitatively between

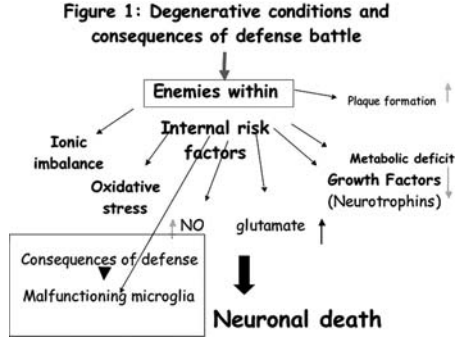

Fig. 1. Degenerative conditions and consequences of defense battle.

axons that have survived the primary injury and those that have survived secondary degeneration. Using calibrated forceps to inflict a controlled crush injury, we were able to calibrate the force of the insult in such a way that it left a desired proportion of axons undamaged. We next injected a fluorescent dye at the site of injury and then counted the axons that were retrogradely labeled distal to the lesion site, that is, those that were still viable. This procedure made it possible to demonstrate quantitatively that even axons that escape the primary lesion subsequently undergo degeneration ***(19)***. The model also proved useful in screening candidate compounds for their neuroprotective effects ***(19)***.

Use of this model opened the way to several important developments in connection with neurodegenerative diseases. First, it led us to propose that glaucoma, a chronic disease of the visual system, might benefit from a neuroprotective treatment strategy ***(38)***. This suggestion has substantially influenced current research on glaucoma. Second, it led to the discovery that the systemic immune system plays a key role in the ability of the CNS to withstand injurious conditions and, in particular, to fight off delayed degeneration ***(32,39)***. The latter finding led in turn to the discovery that the therapeutic window after acute insults is wider than the few hours suggested by the observed postinjury increase in neurotransmitters. Several useful models of acute CNS injury have been adapted over the years to study neuroprotection. Examples of such models are given below. (*see* **Subheadings 3.1.**, **3.2.**, **3.3.**)

2. Material

2.1. Tools

1. Cross-acting forceps.
2. Precalibrated cross-acting (self-closing) forceps that open when the handles are pressed and close when the handles are released.
3. Binocular operating microscope.
4. Stereotactic device.
5. 10-μL Hamilton syringe with a 30-ga needle.
6. 27-ga Syringe.
7. Fluorescent microscope.

2.2. Reagents

1. Fluro-Gold (5% solution in saline: Flurochrome, Denver CO).
2. Pentobarbitone.
3. Ketamine.
4. Xylazine.
5. Neurotracer 4-(4-(didecylamino)styryl)-*N*-methylpyridinium iodide (4-Di-10-Asp) (Molecular Probes, Invitrogen, Europe BV).

6. L-Glutamate (Sigma-Aldrich, St. Louis, MO).
7. Paraformaldehyde (4%).
8. Hydrogen peroxide.

3. Methods

3.1. Partial Crush Injury of the Rat Optic Nerve

Use of the model has made it possible to demonstrate self-propagating secondary degeneration ***(35)***, identify some of the mediators of degeneration common to many neurodegenerative disorders ***(40)***, study the molecular mechanisms underlying retinal ganglion cell (RGC) death, and discover processes of neuroprotection ***(1,41–44)***. Molecular mechanisms can also be studied in the severely crushed optic nerve of the mouse (*see* **Subheading 3.2.**), an easily obtained model in which the availability of transgenic mice can be exploited for studies of the effects of relevant genes on RGC survival ***(45,46)***.

3.1.1. Surgical Exposure of the Optic Nerve Intraorbitally

The intraorbital part of the optic nerve is longer in rodents than in other species, making it relatively easy to carry out experimental manipulations without impinging on adjacent tissues or harming the nerve itself. All surgical procedures are done under general anesthesia. We use a binocular operating microscope. The conjunctiva is incised lateral to cornea; the retractor bulbi muscles are separated using curved blunt forceps; and the optic nerve is identified and exposed near the eyeball by blunt dissection for 2.5–3 mm. Care is taken not to stretch the nerve (*see* **Notes 1** and **2**).

3.1.2. Calibrated Crush Injury

A reproducible crush injury of graded severity is inflicted on the optic nerve by the use of precalibrated cross-acting (self-closing) forceps that open when the handles are pressed and close when the handles are released ***(35)***. The force exerted by the grasping jaws, and thus the severity of the crush lesion inflicted, is adjusted by varying the number of revolutions of the screw attached to the handle.

Using the forceps, a moderate, mild, or very mild crush injury is inflicted on the exposed optic nerve about 1 mm distal to the eye, for 30 s (**Fig. 2**).

3.1.3. Retrograde Labeling of RGCs

Because of the anatomical construction of the visual system, RGC survival at any time after axonal injury can be quantified by the use of retrograde neuronal

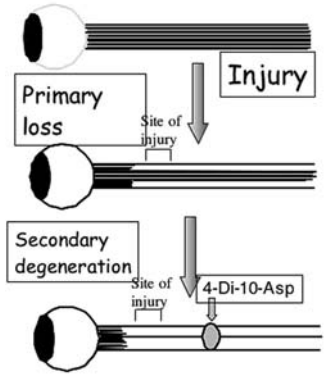

Fig. 2. Partial crush injury of the rat optic nerve: a model for secondary degeneration.

tracers. Properties of the tracers selected for this purpose should include (1) lack of any effect on neuronal viability and activity, (2) intense fluorescence, (3) resistance to fading, (4) absence of diffusion from labeled cells, and (5) relatively prolonged survival time (**Fig. 2**).

The RGCs that survive an optic nerve crush injury and are potentially capable of being rescued by neuroprotective therapy are the cell bodies of the damaged fibers and of intact fibers that escaped the injury. To determine the total number of surviving RGCs, the protocol of choice is to label prior to the injury. To assess the number of surviving RGCs with still-intact fibers, the protocol of choice is the postinjury labeling. These two protocols are done by employing the retrograde labeling procedures, as described in the following section. (*see* **Subheading 3.1.4.**)

3.1.4. Labeling of All RGCs Prior to Injury

The total number of RGCs in the retina is determined after sterotactic injection of a fluorescent dye to the superior colliculus of both hemispheres, where almost all of the optic axons form synapses. This technique is performed in order to assay the total number of surviving RGCs of the injured and intact fibers in the retina. Two weeks prior to the crush injury, rats are deeply anesthetized and placed in the stereotactic instrument. The skull is exposed and kept dry and clean using 3% hydrogen peroxide. Bregma is identified and marked. A hole is drilled above the superior colliculus (6 mm behind and 1.2 mm in front of bregma). Using a stereotactic measuring device and Hamilton injection, Fluoro-Gold is injected (2 μL/2 min for each point, at three points in the superior colliculus, at depths of 3.8, 4, and 4.2 mm from the bony surface of the brain).

3.1.5. Postinjury Labeling of Cell Bodies of Rescued Fibers

Postinjury application of the fluorescent lipophilic dye 4-Di-10-Asp ***(47)*** (Molecular Probes, Europe BV) distal to the site of optic nerve lesion results in the labeling of RGCs with intact axons, as only axons whose continuity is preserved across the site of injury are capable of transferring the dye to RGC bodies (*see* **Note 3**).

At different times after crush injury, the optic nerve is re-exposed intraorbitally as described above (*see* **Subheading 3.1.**). With the use of a 27-ga syringe, a small hole is made in the dura 1 mm from the distal border of the site of injury, and the axons are cut to allow dye uptake. Solid crystals (0.2–0.4 mm diameter) of the dye are deposited at the cut edge of the optic nerve. Five days after dye application, the number of labeled RGCs is determined. The dye application procedure had no effect on RGC survival during the period until retinal excision ***(19)***.

3.1.6. Counting of RGCs

At the end of experimental period, the rats are killed and their eyes are excised into Petri dishes containing phosphate-buffered saline (PBS). The retina is detached from the eye without the vitreous body and fixed in freshly prepared 4% paraformaldehyde. Four cuts are made in the fixed retina to allow flattening of the retina onto a nitrocellulose filter (**Fig. 3**).

Labeling RGCs are counted using the fluorescent microscope (*see* **Note 4**). It should be noted that RGC density across the rat retina ranges from about 1000 cells/mm^2 at the periphery to 6000 cells/mm^2 in the center. However, over most

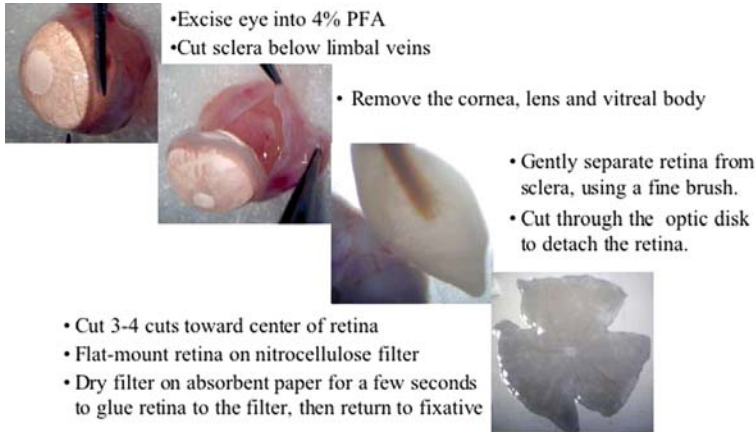

Fig. 3. Whole-mount retina.

of the retina, except at the outer periphery, the average density is about 3000 cells/mm^2 ***(19,48)***. Nevertheless, after optic nerve injury, the rate of RGC death is higher at the periphery than at the center of the retina ***(19)***. Accordingly, labeled RGCs are counted in four to six fields at the same distance from the center of the retina, at a magnification of ×250. The numbers of labeled RGCs per field are averaged, and the mean number of RGCs per square millimeter is calculated (*see* **Note 5**).

3.2. Mouse Optic Nerve Injury Model

3.2.1. Crush Injury of the Mouse Optic Nerve

To identify and characterize the molecule participation in the process of RGC death, it is necessary to devise an animal model that allows molecular manipulation. Establishment of the mouse model makes it possible to study the effects of severe optic nerve injury in genetically manipulated mice. For this purpose, all RGCs must be labeled 72 h before optic nerve crush. With the aid of a binocular operating microscope, the conjunctiva over the posterior pole of the eye of the anesthetized mouse is incised. The optic nerve is exposed by gentle blunt dissection between the surrounding muscle and the retrobulbar region, as described above for the rat (*see* **Subheading 3.1.**). Using cross-acting forceps and taking care not to interfere with the blood supply, we then crush the nerve for 2 s.

3.2.2. RGC Labeling in Mice

RGCs are labeled 72 h before excision with a fluorescent dye injected stereotactically into superior colliculus. For this purpose, mice are anesthetized and placed in a stereotactic device. The skull is exposed and kept dry and clean, and the bregma is identified and marked. The designated point of injection is 2.92 mm posterior to the bregma, 0.5 mm lateral to the midline, and at a depth of 2 mm from the brain surface. A window is drilled in the scalp above the designated coordinates in the right and left hemispheres. The neurotracer dye Fluoro-Gold (5% solution in saline) is applied (1 μL, at a rate of 0.5 μL/min in each hemisphere) using a Hamilton syringe, and the skin over the wound was sutured.

3.2.3. Assessment of RGC Survival

At the end of the experiment period, the mice are given a lethal dose of pentobarbitone. The eyes are enucleated, and the retinas are detached and prepared as flattened whole mounts in 4% paraformaldehyde in PBS. Labeled cells from four to six fields of identical size are counted, all located at the same distance from the optic disk (**Fig. 3**).

3.3. Glutamate Eye Intoxication

This model simulates the process of secondary degeneration itself, because glutamate is a common mediator of self-perpetuating degeneration ***(49)*** (*see* **Note 6**). The right eye of the anesthetized mouse or rat is punctured with a 27-ga needle in the upper part of the sclera, and a 10-μL Hamilton syringe with a 30-ga needle was inserted as far as the vitreal body. Mice are injected with a total volume of 1 μL (200 nmol) of L-glutamate dissolved in saline. Rats are injected with 2 mL (375 nmol) of L-glutamate ***(45,46)***. The model of eye intoxication is convenient and accurate and can be used with other mediators of neurodegeneration ***(50)***.

4. Notes

1. When incising the conjunctiva, make sure that it is done as far as possible from the limbal area, which has abundant vasculature. An incision at this site might cause massive bleeding, obscuring the area close to the optic nerve.
2. While exposing the optic nerve, separate it as much as possible from the adjacent fat and fascia.
3. While labeling the RGCs with a lipophilic fluorescent dye such as 4-Di-10-Asp, make sure that the dye is completely immersed in the hole that has been made in the dura sheath by injecting a drop of incomplete Freund's adjuvant.
4. If the view of the retina under the microscope is too blurred to count the cells, the problem might be caused by one or more of the following:
   a. The vitreous body is still attached to the retina.
   b. The paraformaldehyde solution in which the retina is soaked is not fresh.
   c. Dye application process went wrong.
5. For complete objectivity, the RGCs should be counted by someone who does not know which animal the retinas were taken from. The therapeutic window may vary among paradigms and the tested neuroprotective approaches. For example, immune-mediated neuroprotection is exerted not at the hyperacute or the acute phase after a CNS injury, but at the subacute phase. When the neuroprotective approach is immune based, it is critically dependent on the choice of the antigen and the adjuvant. If the immune response is too strong or persists, its adverse side effects override the potential benefit. An immune-based approach also leads to neurogenesis.
6. Use of different models may not always point to similar conclusions.

Acknowledgments

M.S. holds the Maurice and Ilse Katz Professorial Chair in Neuroimmunology. The work was supported by Proneuron Ltd., Industrial Park, Ness-Ziona, Israel.

References

1. Schwartz, M., Moalem, G., Leibowitz-Amit, R., and Cohen, I. R. (1999) Innate and adaptive immune responses can be beneficial for CNS repair. *Trends Neurosci* **22**, 295–299.
2. Villoslada, P., and Genain, C. P. (2004) Role of nerve growth factor and other trophic factors in brain inflammation. *Prog Brain Res* **146**, 403–414.
3. Pachter, J. S., de Vries, H. E., and Fabry, Z. (2003) The blood-brain barrier and its role in immune privilege in the central nervous system. *J Neuropathol Exp Neurol* **62**, 593–604.
4. Neumann, H. (2000) The immunological microenvironment in the CNS: implications on neuronal cell death and survival. *J Neural Transm Suppl* **59**, 59–68.
5. Hailer, N. P., Heppner, F. L., Haas, D., and Nitsch, R. (1998) Astrocytic factors deactivate antigen presenting cells that invade the central nervous system. *Brain Pathol* **8**, 459–474.
6. Hatterer, E., Davoust, N., Didier-Bazes, M., Vuaillat, C., Malcus, C., Belin, M. F., and Nataf, S. (2006) How to drain without lymphatics? Dendritic cells migrate from the cerebrospinal fluid to the B-cell follicles of cervical lymph nodes. *Blood* **107**, 806–812.
7. Lotan, M., and Schwartz, M. (1994) Cross talk between the immune system and the nervous system in response to injury: implications for regeneration. *FASEB J* **8**, 1026–1033.
8. Lotan, M., Solomon, A., Ben-Bassat, S., and Schwartz, M. (1994) Cytokines modulate the inflammatory response and change permissiveness to neuronal adhesion in injured mammalian central nervous system. *Exp Neurol* **126**, 284–290.
9. Broadwell, R. D., Charlton, H. M., Ebert, P., Hickey, W. F., Villegas, J. C., and Wolf, A. L. (1990) Angiogenesis and the blood-brain barrier in solid and dissociated cell grafts within the CNS. *Prog Brain Res* **82**, 95–101.
10. Broadwell, R. D., Baker, B. J., Ebert, P. S., and Hickey, W. F. (1994) Allografts of CNS tissue possess a blood-brain barrier: III. Neuropathological, methodological, and immunological considerations. *Microsc Res Tech* **27**, 471–494.
11. Cserr, H. F., Harling-Berg, C. J., and Knopf, P. M. (1992) Drainage of brain extracellular fluid into blood and deep cervical lymph and its immunological significance. *Brain Pathol* **2**, 269–276.
12. Cserr, H. F., and Knopf, P. M. (1992) Cervical lymphatics, the blood-brain barrier and the immunoreactivity of the brain: a new view. *Immunol Today* **13**, 507–512.
13. Flugel, A., Berkowicz, T., Ritter, T., Labeur, M., Jenne, D. E., Li, Z., Ellwart, J. W., Willem, M., Lassmann, H., and Wekerle, H. (2001) Migratory activity and functional changes of green fluorescent effector cells before and during experimental autoimmune encephalomyelitis. *Immunity* **14**, 547–560.
14. Hickey, W. F. (1999) Leukocyte traffic in the central nervous system: the participants and their roles. *Semin Immunol* **11**, 125–137.

15. Griffin, D., Levine, B., Tyor, W., Ubol, S., and Despres, P. (1997) The role of antibody in recovery from alphavirus encephalitis. *Immunol Rev* **159**, 155–161.
16. Griffin, D. E., and Hardwick, J. M. (1997) Regulators of apoptosis on the road to persistent alphavirus infection. *Annu Rev Microbiol* **51**, 565–592.
17. Czech, K. A., Ryan, J. W., Sagen, J., and Pappas, G. D. (1997) The influence of xenotransplant immunogenicity and immunosuppression on host MHC expression in the rat CNS. *Exp Neurol* **147**, 66–83.
18. Moalem, G., Monsonego, A., Shani, Y., Cohen, I. R., and Schwartz, M. (1999) Differential T cell response in central and peripheral nerve injury: connection with immune privilege. *FASEB J* **13**, 1207–1217.
19. Yoles, E., and Schwartz, M. (1998) Degeneration of spared axons following partial white matter lesion: implications for optic nerve neuropathies. *Exp Neurol* **153**, 1–7.
20. Yurkewicz, L., Weaver, J., Bullock, M. R., and Marshall, L. F. (2005) The effect of the selective NMDA receptor antagonist traxoprodil in the treatment of traumatic brain injury. *J Neurotrauma* **22**, 1428–1443.
21. Belli, A., Sen, J., Petzold, A., Russo, S., Kitchen, N., Smith, M., Tavazzi, B., Vagnozzi, R., Signoretti, S., Amorini, A. M., Bellia, F., and Lazzarino, G. (2006) Extracellular N-acetylaspartate depletion in traumatic brain injury. *J Neurochem* **96**, 861–869.
22. Matute, C., Domercq, M., and Sanchez-Gomez, M. V. (2006) Glutamate-mediated glial injury: mechanisms and clinical importance. *Glia* **53**, 212–224.
23. Xu, G. Y., Hughes, M. G., Zhang, L., Cain, L., and McAdoo, D. J. (2005) Administration of glutamate into the spinal cord at extracellular concentrations reached post-injury causes functional impairments. *Neurosci Lett* **384**, 271–276.
24. McAdoo, D. J., Hughes, M. G., Nie, L., Shah, B., Clifton, C., Fullwood, S., and Hulsebosch, C. E. (2005) The effect of glutamate receptor blockers on glutamate release following spinal cord injury. Lack of evidence for an ongoing feedback cascade of damage → glutamate release → damage → glutamate release → etc. *Brain Res* **1038**, 92–99.
25. Parsons, C. G., Danysz, W., and Quack, G. (1998) Glutamate in CNS disorders as a target for drug development: an update. *Drug News Perspect* **11**, 523–569.
26. Rosin, C., Bates, T. E., and Skaper, S. D. (2004) Excitatory amino acid induced oligodendrocyte cell death in vitro: receptor-dependent and -independent mechanisms. *J Neurochem* **90**, 1173–1185.
27. Sargsyan, S. A., Monk, P. N., and Shaw, P. J. (2005) Microglia as potential contributors to motor neuron injury in amyotrophic lateral sclerosis. *Glia* **51**, 241–253.
28. Kim, S. U., and de Vellis, J. (2005) Microglia in health and disease. *J Neurosci Res* **81**, 302–313.

29. Croxford, J. L., and Miller, S. D. (2003) Immunoregulation of a viral model of multiple sclerosis using the synthetic cannabinoid R+WIN55,212. *J Clin Invest* **111**, 1231–1240.
30. Stieg, P. E., Sathi, S., Warach, S., Le, D. A., and Lipton, S. A. (1999) Neuroprotection by the NMDA receptor-associated open-channel blocker memantine in a photothrombotic model of cerebral focal ischemia in neonatal rat. *Eur J Pharmacol* **375**, 115–120.
31. Nagafuji, T., Sugiyama, M., Matsui, T., and Koide, T. (1993) A narrow therapeutical window of a nitric oxide synthase inhibitor against transient ischemic brain injury. *Eur J Pharmacol* **248**, 325–328.
32. Moalem, G., Leibowitz-Amit, R., Yoles, E., Mor, F., Cohen, I. R., and Schwartz, M. (1999) Autoimmune T cells protect neurons from secondary degeneration after central nervous system axotomy. *Nat Med* **5**, 49–55.
33. Popovich, P. G., Yu, J. Y., and Whitacre, C. C. (1997) Spinal cord neuropathology in rat experimental autoimmune encephalomyelitis: modulation by oral administration of myelin basic protein. *J Neuropathol Exp Neurol* **56**, 1323–1338.
34. Rapalino, O., Lazarov-Spiegler, O., Agranov, E., Velan, G. J., Yoles, E., Fraidakis, M., Solomon, A., Gepstein, R., Katz, A., Belkin, M., Hadani, M., and Schwartz, M. (1998) Implantation of stimulated homologous macrophages results in partial recovery of paraplegic rats. *Nat Med* **4**, 814–821.
35. Assia, E., Rosner, M., Belkin, M., Solomon, A., and Schwartz, M. (1989) Temporal parameters of low energy laser irradiation for optimal delay of post-traumatic degeneration of rat optic nerve. *Brain Res* **476**, 205–212.
36. Rosner, M., Caplan, M., Cohen, S., Duvdevani, R., Solomon, A., Assia, E., Belkin, M., and Schwartz, M. (1993) Dose and temporal parameters in delaying injured optic nerve degeneration by low-energy laser irradiation. *Lasers Surg Med* **13**, 611–617.
37. Duvdevani, R., Lavie, V., Segel, L., and Schwartz, M. (1993) A new method for expressing axonal size: rat optic nerve analysis. *J Electron Microsc (Tokyo)* **42**, 412–414.
38. Schwartz, M., Belkin, M., Yoles, E., and Solomon, A. (1996) Potential treatment modalities for glaucomatous neuropathy: neuroprotection and neuroregeneration. *J Glaucoma* **5**, 427–432.
39. Hauben, E., Agranov, E., Gothilf, A., Nevo, U., Cohen, A., Smirnov, I., Steinman, L., and Schwartz, M. (2001) Posttraumatic therapeutic vaccination with modified myelin self-antigen prevents complete paralysis while avoiding autoimmune disease. *J Clin Invest* **108**, 591–599.
40. Yoles, E., and Schwartz, M. (1998) Elevation of intraocular glutamate levels in rats with partial lesion of the optic nerve. *Arch Ophthalmol* **116**, 906–910.
41. Schwartz, M., and Cohen, I. R. (2000) Autoimmunity can benefit self-maintenance. *Immunol Today* **21**, 265–268.

42. Yoles, E., Belkin, M., and Schwartz, M. (1996) HU-211, a nonpsychotropic cannabinoid, produces short- and long-term neuroprotection after optic nerve axotomy. *J Neurotrauma* **13**, 49–57.
43. Kipnis, J., Yoles, E., Porat, Z., Cohen, A., Mor, F., Sela, M., Cohen, I. R., and Schwartz, M. (2000) T cell immunity to copolymer 1 confers neuroprotection on the damaged optic nerve: possible therapy for optic neuropathies. *Proc Natl Acad Sci USA* **97**, 7446–7451.
44. Moalem, G., Yoles, E., Leibowitz-Amit, R., Muller-Gilor, S., Mor, F., Cohen, I. R., and Schwartz, M. (2000) Autoimmune T cells retard the loss of function in injured rat optic nerves. *J Neuroimmunol* **106**, 189–197.
45. Levkovitch-Verbin, H., Harris-Cerruti, C., Groner, Y., Wheeler, L. A., Schwartz, M., and Yoles, E. (2000) RGC death in mice after optic nerve crush injury: oxidative stress and neuroprotection. *Invest Ophthalmol Vis Sci* **41**, 4169–4174.
46. Fisher, J., Levkovitch-Verbin, H., Schori, H., Yoles, E., Butovsky, O., Kaye, J. F., Ben-Nun, A., and Schwartz, M. (2001) Vaccination for neuroprotection in the mouse optic nerve: implications for optic neuropathies. *J Neurosci* **21**, 136–142.
47. Fritzsch, B., and Wilm, C. (1990) Dextran amines in neuronal tracing. *Trends Neurosci* **13**, 14
48. Linden, R., and Perry, V. H. (1983) Massive retinotectal projection in rats. *Brain Res* **272**, 145–149.
49. Schori, H., Kipnis, J., Yoles, E., WoldeMussie, E., Ruiz, G., Wheeler, L. A., and Schwartz, M. (2001) Vaccination for protection of retinal ganglion cells against death from glutamate cytotoxicity and ocular hypertension: implications for glaucoma. *Proc Natl Acad Sci USA* **98**, 3398–3403.
50. Schori, H., Robenshtok, E., Schwartz, M., and Hourvitz, A. (2005) Post-intoxication vaccination for protection of neurons against the toxicity of nerve agents. *Toxicol Sci* **87**, 163–168.

5

Organotypic Entorhino-Hippocampal Slice Cultures—A Tool to Study the Molecular and Cellular Regulation of Axonal Regeneration and Collateral Sprouting In Vitro

Domenico Del Turco and Thomas Deller

Summary

Organotypic slice cultures of the brain are widely used as a tool to study fundamental questions in neuroscience. In this chapter, we focus on a protocol based on organotypic slice cultures of mouse entorhinal cortex and hippocampus that can be employed to study axonal regeneration and collateral sprouting in the central nervous system in vitro. Using pharmacological as well as genetic approaches, axonal regeneration and sprouting can be influenced, and some of the molecular and cellular mechanisms involved in these processes can be identified. The protocol describes in detail (1) the generation of organotypic entorhino-hippocampal slice cultures, (2) the conditions needed for the analysis of axonal regeneration and collateral sprouting, respectively, (3) the lesioning technique, (4) tracing techniques to visualize regenerating entorhinal axons, and (5) an immunohistochemical technique to visualize sprouting fibers.

Key Words: Hippocampus; dentate gyrus; entorhinal cortex lesion; mossy cells; axonal regeneration; axonal sprouting; plasticity; calretinin; NeuN; mini-ruby.

1. Introduction

Slice cultures of the rodent hippocampus are widely used as a tool to study fundamental questions of nervous system development, cell biology, and neuronal and glial function ***(1–9)***. In addition, they have been employed to model neurological disease conditions and to investigate putative molecular and

From: *Methods in Molecular Biology, vol. 399: Neuroprotection Methods and Protocols*
Edited by: T. Borsello © Humana Press Inc., Totowa, NJ

cellular mechanisms and treatment strategies ***(10–14)***. In this chapter, we will focus on one of these aspects and will detail a protocol based on organotypic entorhino-hippocampal slice cultures (OEHSCs) that can be used to analyze regenerative mechanisms in neural tissues.

Entorhino-hippocampal cultures of rodents prepared by the interface culture method ***(15,16)*** appear to be an almost ideal instrument to study the lesion-induced reorganization of the brain ***(17–21)***. These cultures preserve much of the cyto and fiber architecture of the entorhinal cortex and hippocampus in vivo ***(22)***. Their particular advantage, however, is the formation of the perforant pathway in vitro, a distinct fiber tract that can readily be transected with a scalpel blade. It is part of the beauty of the model that this culture system can be used to study axonal regeneration following axotomy as well as collateral sprouting following denervation. For both questions, entorhino-hippocampal slice cultures are generated from mouse brain between postnatal (P) day 0 and 5. In these freshly explanted slice cultures, entorhino-dentate fibers are either preserved or quickly regenerated with a very high degree of layer specificity ***(23–25)***. Thus, within a few days after explantation, an intact entorhino-hippocampal projection is present in vitro. If this fiber projection is lesioned early, that is, between 5 and 10 days in vitro (DIV), regeneration of entorhinal axons occurs and can be studied ***(26)***. In contrast, if the entorhino-hippocampal projection is lesioned late, that is, between DIV 14 and 16, entorhinal fibers mature and lose their regenerative potential. In this case, transection of the perforant pathway denervates the outer molecular layer of the dentate gyrus, and associational fibers sprout and reinnervate the former termination zone of the entorhino-hippocampal projection ***(21)***. Thus, entorhino-hippocampal slice cultures can be used to study a variety of questions related to the molecular and cellular regulation of axonal regeneration and collateral sprouting.

It is now of particular interest to understand the role of the various cellular players during these regenerative events and to test the role of candidate regulatory molecules. This interest in mechanisms rather than phenomenology has resulted in the more widespread use of organotypic slices generated from mice rather than from rats, making it possible to take advantage of the mutant mouse resources that are available today ***(27–34)***. Accordingly, the protocol reported here is based on mouse organotypic slice cultures.

In the following, we will first describe in detail the slice culture procedure and then concentrate on the application of the transection technique, a potential tracing method to visualize the entorhino-hippocampal projection in vitro, and an immunostaining protocol frequently used in these studies to demonstrate sprouting fibers.

2. Materials

2.1. Animals

C57BL/6 and CB6F1 mouse pups (Charles River, Sulzfeld, Germany) at postnatal day 0–5 (P0–P5) were used for the preparation of OEHSCs in our studies ***(21,26)***. No differences among these mouse strains with regard to the experimental model system were observed. In principle, the method outlined below (*see* **Subheading 3.1.**) should be applicable to all available mouse strains. Strain differences might occur, however, and it is strongly suggested to re-validate the model if other mouse strains are being used.

2.2. Instruments

1. Scissors; medium and small size.
2. Forceps; fine, curved, and straight shape.
3. Spatulas; straight, medium, and small size.
4. Scalpels; with razorblades, curved and straight shape.
5. Pasteur pipettes and glass micropipettes; cut, fire-polished.
6. Tissue culture hood (Heraeus/Kendro Laboratory Products, Hanau, Germany).
7. Stereo microscope (Olympus, Hamburg, Germany).
8. Vibratome (Leica, Bensheim, Germany).
9. CO_2 incubator (Heraeus/Kendro Laboratory Products).

2.3. Tissue Culture Reagents

1. Tissue culture plastic: six-well plates, 35-mm plastic dishes; sterile (BD Falcon, Heidelberg, Germany).
2. Tissue culture inserts: Millicell-CM, 0.4 μm pore size, 30 mm diameter (Millipore, Schwalbach, Germany).
3. Cyanoacrylate glue and agar (sterile).
4. Preparation medium (sterile; use within days, at 4° C): 100% HEPES-buffered minimum essential medium (MEM), 0.65% glucose, 0.1 mg/mL streptomycin, 100 U/mL penicillin, and 2 mM Glutamax; adjusted to pH 7.3.
5. Slice culture medium (sterile; keep at 4° C for 1–2 weeks): 50% MEM, 25% heat-inactivated normal horse serum, 25% Hanks' balanced salt solution, 0.65% glucose, 0.1 mg/mL streptomycin, 100 U/mL penicillin, and 2 mM Glutamax; adjusted to pH 7.2.

All tissue culture solutions were obtained from Gibco (Invitrogen, Karlsruhe, Germany).

2.4. Tracing and Immunostaining

1. Mini-ruby (Molecular Probes, Invitrogen, Karlsruhe, Germany).
2. 4% Paraformaldehyde (PFA).

3. 0.1 M Phosphate-buffered saline (PBS) (pH 7.4).
4. 50 mM Tris-buffered saline (TBS) (pH 7.4).
5. Triton X-100 detergent.
6. Blocking solution: 5% serum, 0.5% Triton X-100, in 50 mM TBS.
7. Staining solution: 1% serum, 0.1% Triton X-100, in 50 mM TBS.
8. Rabbit anticalretinin (Swant, Bellinzona, Switzerland).
9. Mouse anti-NeuN (Chemicon, Temecula, CA, USA).
10. Biotinylated antimouse and antirabbit IgG (Linaris, Wertheim, Germany).
11. Peroxidase-conjugated avidin–biotin complex (Linaris).
12. Nickel/cobalt-intensified diaminobenzidine (DAB) solution: 0.05% DAB, 0.025% cobalt chloride, 0.02% ammonium nickel sulfate, in 50 mM TBS.
13. Toluol (100%) and ethanol (70, 80, 90, and 100%).
14. Xylene-based or toluol-based permanent mounting medium.

All other reagents and solutions were obtained from Sigma-Aldrich (München, Germany) or Merck (Darmstadt, Germany).

3. Methods

The experimental methods described in this chapter outline (1) the slice culture preparation, (2) the transection of the entorhino-hippocampal projection in vitro, (3) the labeling of entorhino-hippocampal fibers by an anterograde tracer in vitro, and (4) an immunostaining protocol for slice cultures to monitor sprouting following denervation.

3.1. Slice Culture Preparation

The static slice culture method was used to maintain brain tissue for long-term culture on membrane filter inserts at the interface between the culture medium and an oxygenated atmosphere ***(15)***.

1. Rapidly decapitate a mouse pup (P0–P5) with a scissor and place the head into a plastic dish (sterile conditions, tissue culture hood).
2. Using small scissors, quickly remove the skin and neck muscles. Make a cut along the midline of the head and carefully open the skull with the forceps.
3. Remove the brain with the spatulas and glue it on a vibratome base plate with the ventral surface of the brain directed upward. Cut small blocks of agar and glue them around the brain tissue. Agar blocks should not be glued on the side of the brain facing the vibratome blade.
4. Immerse the base plate in a vibratome chamber containing preparation medium (4° C). Then cut 350-μm to 400-μm thick horizontal brain sections including the hippocampus and cortical areas with a vibratome at slow speed and high frequency (*see* **Note 1**).

5. Transfer sections with a cut, fire-polished Pasteur pipette into a plastic dish containing 3–5 mL ice-cold preparation medium and use the scalpels to dissect pieces of hippocampus together with the adjacent entorhinal cortex.
6. Use the spatulas to gently transfer three to four selected slices into a membrane filter insert in a preincubated six-well plate containing slice culture medium (1 mL each well). Place the six-well plate into a humidified incubator (95% air, 5% CO_2, at 35° C).
7. Replace the culture medium completely on DIV 1 after explantation and then every DIV 2 (to DIV 3) until further processing.

3.2. Transection of the Entorhino-Hippocampal Projection In Vitro

In entorhino-hippocampal slice cultures, the perforant pathway is present ***(25,26,35)***. Entorhinal fibers terminate in the dentate gyrus in a highly laminated pattern in the outer molecular layer. To study regeneration, that is, the regenerative competence of axotomized entorhinal fibers, slice cultures from mouse brain at P0–P5 were used and lesioned between DIV 5 and 10 (*see* **Fig. 1**) ***(26)***. To study sprouting, that is, collateral sprouting of associational fibers, slice cultures were lesioned between DIV 14 and 16 (*see* **Fig. 2**) ***(21)***.

The mechanical lesioning technique used to axotomize the entorhinal fiber projection in vitro is described in this part of the protocol.

1. (a) Axonal regeneration of entorhinal fibers: Incubate selected slice cultures (P0–P5) until DIV 5–10 prior to lesioning; or (b) collateral sprouting of associational fibers: Incubate selected slice cultures (P0–P5) until DIV 14–16 prior to lesioning.
2. Use a sterile scalpel blade to transect slices completely from the rhinal fissure to the hippocampal fissure under visual control using a stereo microscope (*see* **Note 2**).
3. Place slice cultures back into the incubator immediately after the transection has been performed to avoid secondary damage.
4. Change the culture medium on DIV 1 after transection and then every DIV 2 until processing.

3.3. Anterograde Tracing of Entorhinal Fibers In Vitro

For labeling of entorhinal axons in vitro, different anterograde tracers, for example, biotinylated dextran amine (BDA) ***(26)***, biocytin ***(5)***, and mini-ruby ***(21,25)***, have been employed. In the following, the application of the anterograde tracer mini-ruby, a 10,000 MW conjugate of tetramethylrhodamine and biotin with dextran, is described in detail. This tracer has been used successfully to visualize the entorhinal fiber projection to the dentate gyrus in living and fixed entorhino-hippocampal slice cultures (*see* **Fig. 1**) ***(25)***.

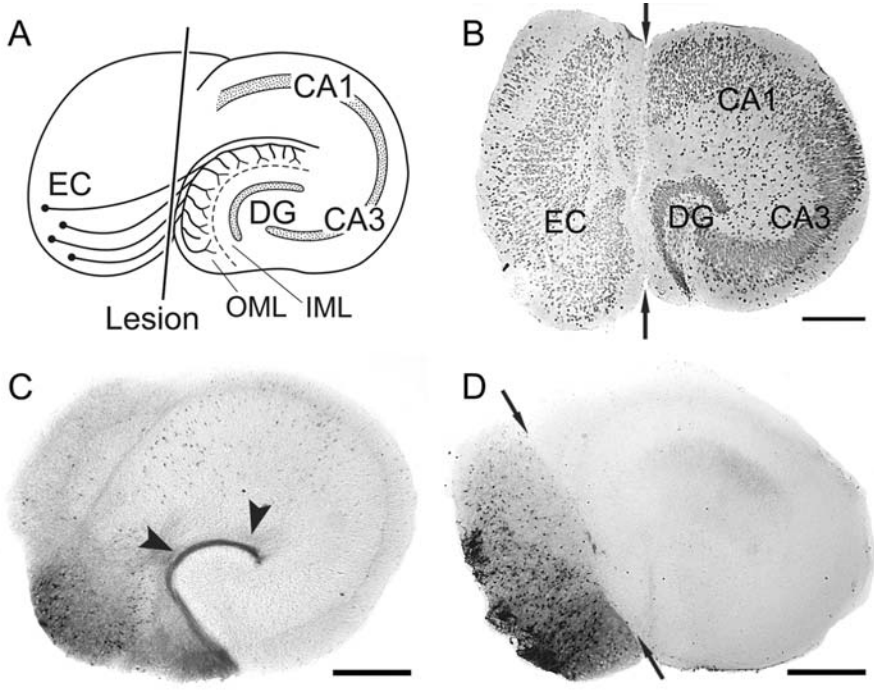

Fig. 1. Transection of the entorhino-hippocampal pathway in vitro. **(A)** Schematic representation of a lesioned entorhino-hippocampal slice culture. The entorhino-dentate fibers originate from the entorhinal cortex (EC) and terminate within the outer molecular layer (OML) of the dentate gyrus (DG). A scalpel blade is used to transect the culture from the rhinal sulcus to the hippocampal fissure, separating the EC from the hippocampus. IML, inner molecular layer. **(B)** The neuronal cytoarchitecture of a lesioned entorhino-hippocampal culture (DIV 25) is revealed using NeuN-immunohistochemistry. Note that the neuronal architecture of EC and DG are well preserved in spite of the lesion. **(C)** Anterograde tracing of entorhinal fibers with mini-ruby reveals a normal entorhino-dentate projection in an unlesioned entorhino-hippocampal slice culture (DIV 25). Entorhinal fibers terminate in a layer-specific fashion in the OML (arrowheads). **(D)** Anterograde tracing of entorhinal fibers with mini-ruby in a lesioned entorhino-hippocampal culture (DIV 24). The entorhino-hippocampal fiber tract was lesioned at DIV 14. Note that entorhinal fibers fail to regenerate into the dentate gyrus. Scale bars: 300 μm (Reprinted from **ref. *23*** with permission from Elsevier).

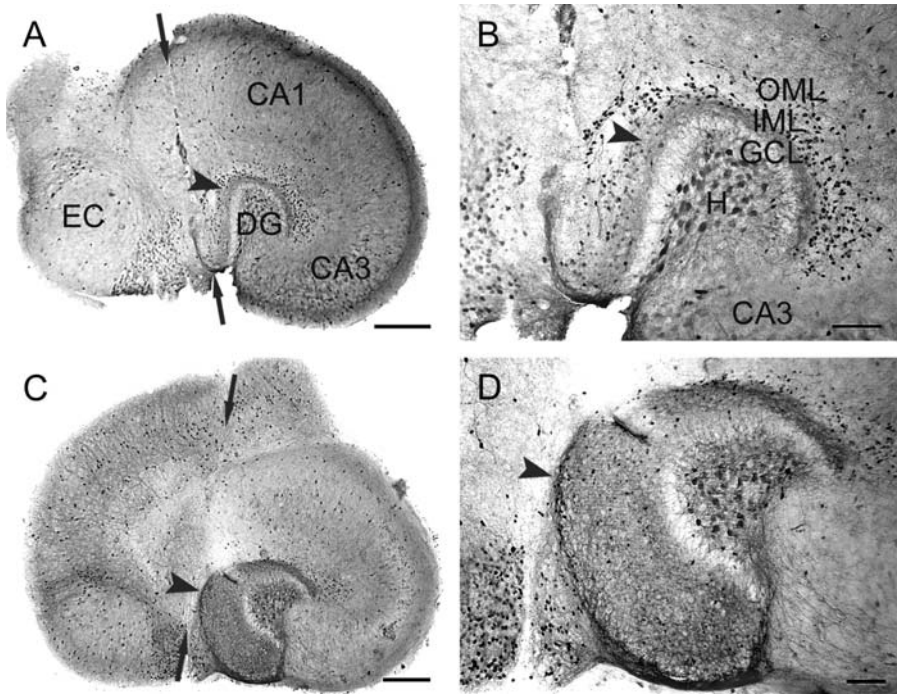

Fig. 2. Associational fiber sprouting after transection of the entorhino-dentate projection. (**A** and **B**) Entorhino-hippocampal slice culture 1 day postlesion (DIV 17). Calretinin-positive fibers (arrowhead) form a dense fiber plexus in the inner molecular layer, which is indistinguishable from the one observed in controls. Arrows indicate the lesion site. CA1, CA3, hippocampal subfields; DG, dentate gyrus; EC, entorhinal cortex; GCL, granule cell layer; H, hilus; IML, inner molecular layer; OML, outer molecular layer. (**C** and **D**) Entorhino-hippocampal culture 10 days postlesion (DIV 26). Calretinin-positive associational fibers (arrowhead) terminate throughout the entire width of the molecular layer. The former inner molecular layer can often still be discerned because of a stronger immunolabeling. Arrows indicate the lesion site. Scale bars: A, C: 300 μm; B, D: 100 μm (Reprinted from **ref. *23*** with permission from Elsevier).

1. Under visual control, place small crystals of mini-ruby under sterile conditions on the surface of the entorhinal cortex of intact or lesioned entorhino-hippocampal cultures (DIV 3 postlesion) using a glass micropipette. Wash slices after 2 h and place slices into the incubator for 2–3 days before further processing (*see* **Note 3**).
2. Fix slices in 4% PFA in 0.1 M PBS (pH 7.4) for 2–3 h at room temperature (RT).
3. After several washes with 50 mM TBS (pH 7.4), incubate slices with peroxidase-conjugated avidin–biotin complex in TBS with 0.1% Triton X-100 for 2 h at RT.

4. For visualization of labeled fibers, process the slices using a nickel/cobalt-intensified DAB solution. Start reaction by adding H_2O_2 (final concentration: 0.001%) and monitor development under visual control. Stop reaction by several rinses in ice-cold TBS.
5. Remove slice cultures carefully from the underlying membrane and mount on glass slides. Let slides dry for 30 min to several hours at RT.
6. Dehydrate in ethanol series (70, 80, 90, and 100%) and twice in toluol (100%).
7. Coverslip slides with a xylene-based or toluol-based mounting medium and examine slice cultures using a light microscope with an imaging system attached.

3.4. Immunostaining of Slice Cultures

An immunohistochemical protocol that can be used to stain organotypic slice cultures is described. It was employed for the antibodies used in our studies ***(21)*** but should also work well for other antibodies of interest.

To visualize the cytoarchitecture of entorhino-hippocampal slice cultures, an antibody against the neuron-specific marker neuronal nuclei (NeuN) was used (*see* **Fig. 1**). To detect sprouting associational fibers in the dentate gyrus, immunohistochemistry against the calcium-binding protein calretinin was employed. This simple immunohistochemical detection method is effective to monitor sprouting in mice because in this species associationally projecting hilar mossy cells contain calretinin ***(36,37)***. In unlesioned (control) slice cultures, mossy cell axons terminate predominantly in the inner molecular layer of the dentate gyrus, whereas robust sprouting of these fibers into the adjacent outer molecular layer was observed in slice cultures lesioned between DIV 14 and 16 (*see* **Fig. 2**).

1. Fix slice cultures in 4% PFA solution in 0.1 M PBS (pH 7.4) for 2–3 h at RT. Wash several times with 50 mM TBS (pH 7.4) (*see* **Note 4**).
2. To reduce unspecific staining, immerse cultures in 3% H_2O_2 in TBS for 30 min at RT. Wash several times in TBS.
3. Preincubate cultures in blocking solution for 1 h at RT.
4. Incubate slices in rabbit anticalretinin (1:10,000) or mouse anti-NeuN (1:1000) staining solution for 24–48 h at 4° C.
5. Wash several times with TBS.
6. Incubate slices for 2 h with the appropriate secondary antibody (1:200; biotinylated antirabbit or antimouse IgG) staining solution at RT.
7. Following subsequent washes in TBS, incubate the slices for additional 2 h in the avidin–biotin–peroxidase complex (1:100; in TBS with 0.1% Triton X-100) at RT.
8. Wash several times in TBS.
9. Proceed as described in **Subheading 3.3., steps 4–7**.

4. Notes

1. Using a vibratome rather than a tissue chopper for the preparation of mouse entorhino-hippocampal cultures is advantageous, because temporal slices of entorhinal cortex and hippocampus can be selected. In these slices, the entorhino-hippocampal projection will be largely preserved. Up to six to eight slice cultures might be obtained from one mouse brain and not more than three to four selected cultures should be plated on a single filter insert. After plating, the hippocampal layers will spread out moderately and cultures will flatten from a thickness of 350–400 to 100–150 μm over time. If possible, cultures should be made from mice younger than P7. Cultures made from older animals are more susceptible to necrotic tissue damage after incubation for several weeks. All slice cultures that show signs of microbial contamination should be discarded. Prior to changing the culture medium, the culture medium should be slowly heated to 35° C and the pH should be adjusted to 7.2. Incubation temperatures between 33 and 36° C are optimal for long-term maintenance of slice cultures and well established.
2. Only entorhino-hippocampal slice cultures without any detectable loss of neuronal cell layers should be used. Because slices may adhere to metal instruments, immerse the scalpel blade in serum-containing medium prior to transecting the slices. Do not use excess pressure while cutting the culture to avoid damaging the underlying membrane. Damage to the membrane will disrupt the interface between the slice culture and the culture medium. To ensure a complete and reproducible transection of the entorhinal fibers, separate the entorhinal cortex from the hippocampus by shifting the entorhinal cortex away from the hippocampus. For regeneration studies, rejoin the two tissue pieces under visual control. Make sure that contact at the cutting edges is regained. For sprouting studies, the entorhinal cortex can also be discarded.
3. Substitute glass micropipettes for mini-ruby application frequently, as labeling efficacy of fibers decreases after multiple use. The culture medium should be replaced soon after the tracer application, because glial cells (primarily microglia) tend to phagocytose tracer crystals located at the surface of the slice cultures. Before further processing, incubate slices for at least 2–3 days to allow for the anterograde transport of the tracer. After fixing the slice cultures, they can be counterstained with cresyl violet or toluidine blue to show labeled entorhinal axons in relation to the different layers of the hippocampus. The anterograde tracing technique can also be combined with the immunostaining protocol, for example, for NeuN to visualize the neuronal cell layers in fixed organotypic slice cultures.
4. Leave slice cultures on the membrane inserts during fixation and the whole immunostaining procedure. 4% PFA solution should be made fresh each time and warmed up to 35° C before use. Always add solutions slowly. Do not place fixative directly onto the slice cultures, as they might easily detach from the membrane filter. The use of a nickel/cobalt-intensified DAB solution will lead to a dark blue staining product after a short reaction time. If combined with a second staining,

for example, to visualize the entorhinal fiber projection after tracing, omit the intensification reagents to obtain a brownish staining product. Monitor the intensity of the staining after addition of H_2O_2 under a stereo microscope and stop the reaction when staining intensity is satisfactory.

Acknowledgments

Some of the studies reviewed in this chapter were done in collaboration with Drs. Peter Prang and Josef Kapfhammer. We would like to thank Ute Fertig for excellent technical assistance. This work was supported by DFG (DE 551/8-1), German Israeli Foundation (GIF), and Gisela Stadelmann-Stiftung (Frankfurt/M., Germany).

References

1. Frotscher, M., Zafirov, S., and Heimrich, B. (1995). Development of identified neuronal types and of specific synaptic connections in slice cultures of rat hippocampus. *Prog. Neurobiol.* **45**, vii–xxviii.
2. Del Rio, J. A., Heimrich, B., Borrell, V., Forster, E., Drakew, A., Alcantara, S., Nakajima, K., Miyata, T., Ogawa, M., Mikoshiba, K., Derer, P., Frotscher, M., and Soriano, E. (1997). A role for Cajal-Retzius cells and reelin in the development of hippocampal connections. *Nature* **385**, 70–74.
3. Dusart, I., Airaksinen, M. S., and Sotelo, C. (1997). Purkinje cell survival and axonal regeneration are age dependent: an in vitro study. *J. Neurosci.* **17**, 3710–3726.
4. Gahwiler, B. H., Capogna, M., Debanne, D., McKinney, R. A., and Thompson, S. M. (1997). Organotypic slice cultures: a technique has come of age. *Trends Neurosci.* **20**, 471–477.
5. Frotscher, M., Drakew, A., and Heimrich, B. (2000). Role of afferent innervation and neuronal activity in dendritic development and spine maturation of fascia dentata granule cells. *Cereb. Cortex* **10**, 946–951.
6. Gimsa, U., Peter, S. V., Lehmann, K., Bechmann, I., and Nitsch, R. (2000). Axonal damage induced by invading T cells in organotypic central nervous system tissue in vitro: involvement of microglial cells. *Brain Pathol.* **10**, 365–377.
7. Kapfhammer, J. P. (2004). Cellular and molecular control of dendritic growth and development of cerebellar Purkinje cells. *Prog. Histochem. Cytochem.* **39**, 131–182.
8. Nagerl, U. V., Eberhorn, N., Cambridge, S. B., and Bonhoeffer, T. (2004). Bidirectional activity-dependent morphological plasticity in hippocampal neurons. *Neuron* **44**, 759–767.
9. Raineteau, O., Rietschin, L., Gradwohl, G., Guillemot, F., and Gahwiler, B. H. (2004). Neurogenesis in hippocampal slice cultures. *Mol. Cell Neurosci.* **26**, 241–250.

10. Duport, S., Robert, F., Muller, D., Grau, G., Parisi, L., and Stoppini, L. (1998). An in vitro blood-brain barrier model: cocultures between endothelial cells and organotypic brain slice cultures. *Proc. Natl. Acad. Sci. U. S. A.* **95**, 1840–1845.
11. Dehghani, F., Conrad, A., Kohl, A., Korf, H. W., and Hailer, N. P. (2004). Clodronate inhibits the secretion of proinflammatory cytokines and NO by isolated microglial cells and reduces the number of proliferating glial cells in excitotoxically injured organotypic hippocampal slice cultures. *Exp. Neurol.* **189**, 241–251.
12. Radojevic, V. and Kapfhammer, J. P. (2004). Repair of the entorhino-hippocampal projection in vitro. *Exp. Neurol.* **188**, 11–19.
13. Huuskonen, J., Suuronen, T., Miettinen, R., van Groen, T., and Salminen, A. (2005). A refined in vitro model to study inflammatory responses in organotypic membrane culture of postnatal rat hippocampal slices. *J. Neuroinflammation* **2**, 25.
14. Noraberg, J., Poulsen, F. R., Blaabjerg, M., Kristensen, B. W., Bonde, C., Montero, M., Meyer, M., Gramsbergen, J. B., and Zimmer, J. (2005). Organotypic hippocampal slice cultures for studies of brain damage, neuroprotection and neurorepair. *Curr. Drug Targets. CNS. Neurol. Disord.* **4**, 435–452.
15. Stoppini, L., Buchs, P. A., and Muller, D. (1991). A simple method for organotypic cultures of nervous tissue. *J. Neurosci. Methods* **37**, 173–182.
16. Bergold, P. J. and Casaccia-Bonnefil, P. (1997). Preparation of organotypic hippocampal slice cultures using the membrane filter method. *Methods Mol. Biol.* **72**, 15–22.
17. Stoppini, L., Buchs, P. A., and Muller, D. (1993). Lesion-induced neurite sprouting and synapse formation in hippocampal organotypic cultures. *Neuroscience* **57**, 985–994.
18. Diekmann, S., Nitsch, R., and Ohm, T. G. (1994). The organotypic entorhinal-hippocampal complex slice culture of adolescent rats. A model to study transcellular changes in a circuit particularly vulnerable in neurodegenerative disorders. *J. Neural Transm. Suppl.* **44**, 61–71.
19. Li, D., Field, P. M., and Raisman, G. (1996). Connectional specification of regenerating entorhinal projection neuron classes cannot be overridden by altered target availability in postnatal organotypic slice co-culture. *Exp. Neurol.* **142**, 151–160.
20. Stoppini, L., Parisi, L., Oropesa, C., and Muller, D. (1997). Sprouting and functional recovery in co-cultures between old and young hippocampal organotypic slices. *Neuroscience* **80**, 1127–1136.
21. Prang, P., Del Turco, D., and Deller, T. (2003). Associational sprouting in the mouse fascia dentata after entorhinal lesion in vitro. *Brain Res.* **978**, 205–212.
22. van Groen, T., Miettinen, P., and Kadish, I. (2003). The entorhinal cortex of the mouse: organization of the projection to the hippocampal formation. *Hippocampus* **13**, 133–149.
23. Heimrich, B. and Frotscher, M. (1993). Slice cultures as a model to study entorhinal-hippocampal interaction. *Hippocampus* **3 Spec No**, 11–17.

24. Li, D., Field, P. M., Yoshioka, N., and Raisman, G. (1994). Axons regenerate with correct specificity in horizontal slice culture of the postnatal rat entorhino-hippocampal system. *Eur. J. Neurosci.* **6**, 1026–1037.
25. Kluge, A., Hailer, N. P., Horvath, T. L., Bechmann, I. and Nitsch, R. (1998). Tracing of the entorhinal-hippocampal pathway in vitro. *Hippocampus* **8**, 57–68.
26. Prang, P., Del Turco, D., and Kapfhammer, J. P. (2001). Regeneration of entorhinal fibers in mouse slice cultures is age dependent and can be stimulated by NT-4, GDNF, and modulators of G-proteins and protein kinase C. *Exp. Neurol.* **169**, 135–147.
27. Muller, D., Djebbara-Hannas, Z., Jourdain, P., Vutskits, L., Durbec, P., Rougon, G., and Kiss, J. Z. (2000). Brain-derived neurotrophic factor restores long-term potentiation in polysialic acid-neural cell adhesion molecule-deficient hippocampus. *Proc. Natl. Acad. Sci. U. S. A.* **97**, 4315–4320.
28. Schwab, M. H., Bartholomae, A., Heimrich, B., Feldmeyer, D., Druffel-Augustin, S., Goebbels, S., Naya, F. J., Zhao, S., Frotscher, M., Tsai, M. J., and Nave, K. A. (2000). Neuronal basic helix-loop-helix proteins (NEX and BETA2/Neuro D) regulate terminal granule cell differentiation in the hippocampus. *J. Neurosci.* **20**, 3714–3724.
29. Schrenk, K., Kapfhammer, J. P., and Metzger, F. (2002). Altered dendritic development of cerebellar Purkinje cells in slice cultures from protein kinase Cgamma-deficient mice. *Neuroscience* **110**, 675–689.
30. Teter, B., Xu, P. T., Gilbert, J. R., Roses, A. D., Galasko, D., and Cole, G. M. (2002). Defective neuronal sprouting by human apolipoprotein E4 is a gain-of-negative function. *J. Neurosci. Res.* **68**, 331–336.
31. Zhao, S., Forster, E., Chai, X., and Frotscher, M. (2003). Different signals control laminar specificity of commissural and entorhinal fibers to the dentate gyrus. *J. Neurosci.* **23**, 7351–7357.
32. Sole, M., Fontana, X., Gavin, R., Soriano, E., and Del Rio, J. A. (2004). Bcl-2 overexpression does not promote axonal regeneration of the entorhino-hippocampal connections in vitro after axotomy. *Brain Res.* **1020**, 204–209.
33. Zhao, S., Chai, X., Forster, E., and Frotscher, M. (2004). Reelin is a positional signal for the lamination of dentate granule cells. *Development* **131**, 5117–5125.
34. Zhao, S., Chai, X., Bock, H. H., Brunne, B., Forster, E., and Frotscher, M. (2006). Rescue of the reeler phenotype in the dentate gyrus by wild-type coculture is mediated by lipoprotein receptors for reelin and disabled 1. *J. Comp Neurol.* **495**, 1–9.
35. Frotscher, M. and Heimrich, B. (1993). Formation of layer-specific fiber projections to the hippocampus in vitro. *Proc. Natl. Acad. Sci. U. S. A.* **90**, 10400–10403.
36. Blasco-Ibanez, J. M. and Freund, T. F. (1997). Distribution, ultrastructure, and connectivity of calretinin-immunoreactive mossy cells of the mouse dentate gyrus. *Hippocampus* **7**, 307–320.
37. Del Turco, D., Woods, A. G., Gebhardt, C., Phinney, A. L., Jucker, M., Frotscher, M., and Deller, T. (2003). Comparison of commissural sprouting in the mouse and rat fascia dentata after entorhinal cortex lesion. *Hippocampus* **13**, 685–699.

6

Role of Nrf2-Dependent ARE-Driven Antioxidant Pathway in Neuroprotection

Jiang Li, Marcus J. Calkins, Delinda A. Johnson, and Jeffrey A. Johnson

Summary

The promoter regions of many detoxification enzymes contain a *cis*-acting enhancer known as the antioxidant response element (ARE). NF-E2-related factor 2 (Nrf2) is considered as one of the major transcription factors for the ARE. Nrf2-dependent transcriptional activation by means of the ARE is known to coordinate the upregulation of these antioxidant enzymes involved in combating oxidative stress and has been shown to be protective against neural toxicants. The mitochondrial complex II inhibitor malonate causes striatal damage reminiscent of Huntington's disease and is known to involve oxidative stress in its pathogenesis. In order to achieve a systemic upregulation of antioxidant potential in local striatal region, a cell-based, Nrf2-dependent antioxidant gene therapy is performed to attenuate malonate-induced neuronal cell death. The details for generating Nrf2-overexpressing astrocytes and grafting them onto the lesion model are described in this chapter.

Key Words: Malonate; antioxidant response element; astrocytes; grafting; adenovirus; neuroprotection.

1. Introduction

Transcriptional activation of the major phase II detoxification enzymes and/or antioxidant genes by quinone compounds has been traced to a*cis*-acting element (RTGACnnnGC) called the antioxidant response element (ARE) or the electrophile response element (EpRE) that regulates constitutive and inducible gene expression ***(1–2)***. Several ARE-binding proteins have been proposed and/or identified ***(3)***. NF-E2-related factor 2 (Nrf2) has been demonstrated to

From: *Methods in Molecular Biology, vol. 399: Neuroprotection Methods and Protocols*
Edited by: T. Borsello © Humana Press Inc., Totowa, NJ

play a central role in the gene expression of these detoxification enzymes and antioxidant genes. Microarray-based gene expression profiling has identified a pool of genes that are responsive to Nrf2 activation ***(4–6)***. Genes commonly regulated by the overexpression of Nrf2 include multiple detoxification enzymes and antioxidant genes, which coordinate to promote glutathione synthesis, NADPH production, and free-radical scavenging (**Table 1**). Together, these mechanisms are thought to protect cells from oxidative stress-induced cell death.

Table 1
Nrf2-Upregulated Genes in Glial-Enriched Cultures and Mixed Neuronal/Glial Cultures

Detoxification	Antioxidant/reducing potential/metabolism
NAD(P)H : quinone oxidoreductase	Glutamate-cysteine ligase, modifier subunit (γGCS)
Glutathione S transferase A1 or 2	Glutathione reductase 1
Glutathione S transferase A3	Thioredoxin reductase 1
Glutathione S transferase A4	Ferritin H subunit H
Glutathione S transferase P2	Cu/Zn superoxide dismutase
Metallothionein 1 or 2	Catalase
p-Glycoprotein/multi-drug resistance protein (MDR2)	Heme oxygenase 1
Multidrug resistance protein (MRP1)	Peroxiredoxin 1
Signal transduction	Peroxiredoxin 6 (1-Cys peroxiredoxin)
Src-related tyrosine kinase	Acyl-coenzyme A dehydrogenase, medium chain
Protein tyrosine phosphatase receptor E	Aldose reductase 1
c-raf	Transaldolase
E2F-5 transcription factor	Mitochondrial intermediate peptidase
cAMP-responsive element modulator	Cytochrome b5
Inflammation	S-100 calcium-binding protein β
FK506 binding protein	Solute carrier family 39 (iron-regulated transporter)
CD59 antigen	
Cyclooxygenase 1	

Source: From Shih et al. ***(6)*** with permission.

We hypothesize that Nrf2-dependent ARE activation is a novel neuroprotective pathway that confers resistance to a variety of oxidative stress-related neurodegenerative insults. Hence, neural cells may avoid excessive oxidative stress through prompt and extensive activation of the Nrf2–ARE pathway. In a recent study, primary neuronal cultures treated with chemical activators of the Nrf2–ARE pathway displayed significantly greater resistance to hydrogen peroxide-induced and glutamate-induced neurotoxicity ***(5,7)***. In addition, similar cultures generated from ARE–human placental alkaline phosphatase (hPAP) reporter mice demonstrated selective activation of the Nrf2–ARE pathway in astrocytes ***(6–7)***. Furthermore, in a model of striatal degeneration that is similar to Huntington's disease, Nrf2-overexpressing astrocytes prior to lesioning conferred dramatic protection against malonate-induced neurotoxicity ***(8)***. We hypothesize that the activation of the Nrf2–ARE pathway early in the pathologic process is a neuroprotective response manifested principally by astrocytes to attenuate the pending neuronal cell death. Nrf2-dependent ARE activation primarily in astrocytes coordinates the upregulation of cytoprotective genes involved in enhancing detoxification and antioxidant potential, maintaining $[Ca^{2+}]$ homeostasis, promoting glucose utilization, promoting neurotrophic factor secretion, and attenuating glutamate-induced toxicity.

Here, we describe a method of astrocyte-based, Nrf2-dependent, antioxidant gene therapy that confers dramatic protection against malonate-induced neuronal cell death.

2. Materials

2.1. Animals

The ARE–hPAP transgenic mice were created using 51 bp of the rat NAD(P)H : quinone oxidoreductase (NQO1) promoter upstream of a heat-stable hPAP reporter construct ***(9)***.

2.2. Vectors and Adenovirus

Recombinant adenovirus (ad) for enhanced green fluorescent protein (eGFP) (ad-GFP), Nrf2-GFP (ad-Nrf2), and DN-Nrf2-GFP (ad-DN-Nrf2) were prepared, in collaboration with Dr. Tim Murphy at the University of Vancouver (Vancouver, British Columbia, Canada), and were available from the Adenovirus Core Facility (Canadian Stroke Network Core Facility, University of Ottawa, Ottawa, Ontario, Canada).

2.3. Surgical Device

1. Stoelting stereotaxic injection apparatus with a mouse gas anesthesia platform (Cat. No. 53310, Stoelting, Wood Dale, IL, http://www.stoeltingco.com) as shown in **Fig. 1A** and **B**.
2. Sterile surgical supplies: sterile drapes, sterile cotton applicators, and gauze.
3. Instruments: No. 10 scalpel blade and holder, one fine straight scissors (8 cm), one curved scissors (10 cm), one blunt spatula (12 cm), four small towel clamps (12 cm), two curved forceps (12 cm), and two fine forceps (e.g., Dumont® forceps). All instruments should be autoclaved before use such that they are sterile.
4. Dremel two speed multi-pro tool with a carving/engraving bit (Cat. No. 2850-02, Dremel Racine, WI).
5. A 27-ga, 2/3-inch needle (Cat. No. 7762-05) attached to a Hamilton 700 series syringe (Cat. No. 7634-01) for cell injections (Reno, USA, NV). Alternatively, a finer gauge needle or pulled glass pipette may be used to minimize damage associated

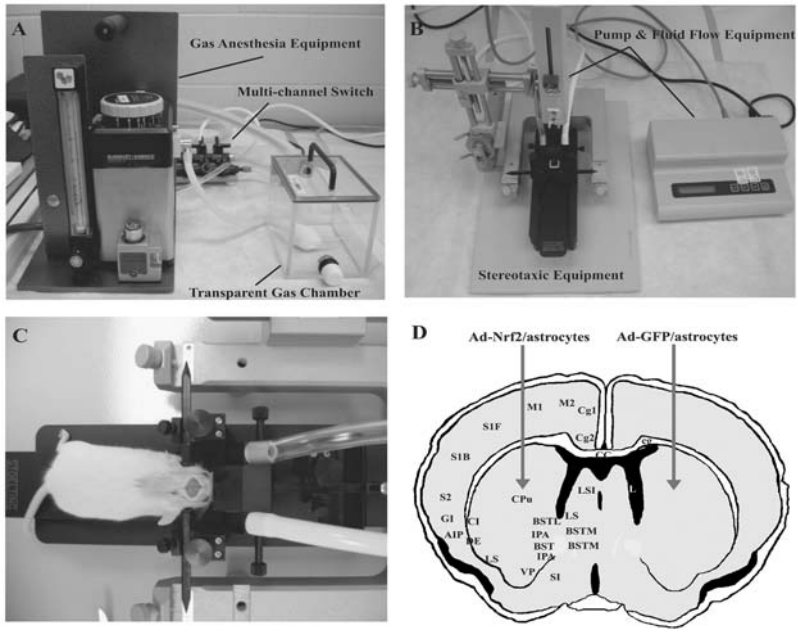

Fig. 1. A typical setup of Stoelting stereotaxic injection apparatus with a mouse gas anesthesia platform. **(A–C)** Parts of gas anesthesia equipment, transparent gas chamber, pump and fluid flow equipment, and stereotaxic equipment. **(D)** Coronal section of the injection site.

with injection. Our laboratory uses a 32-ga, 2/3-inch needle (Cat. No. 7762-01) attached to a Hamilton 700 series syringe for chemical injections.
6. Stoelting 9-mm autoclip wound clips with clip applying forceps (Cat. No. 59020, Stoelting).

2.4. Solutions

1. 1 × Hanks' balanced salt solution (HBSS; Cat. No. 14025, Invitrogen).
2. 0.05% Trypsin in HBSS and 200 μL10× trypsin (Cat. No. 15400054, Invitrogen Carlsbad, CA, USA) in 2 mL HBSS.
3. Eagle's minimum essential medium (Eagle's MEM; Cat. No. 21063, Invitrogen) containing 10% heat-inactivated fetal calf serum (Cat. No. 10082), 10% horse serum (Cat. No. 26050), and 2 mM glutamine.
4. MTS assay kit was commercially available from Promega (Cat. No. G3580).
5. Triadine and 70% ethanol.
6. Malonate (sodium malonate dibasic monohydrate) was purchased from Sigma (Cat. No. 63411, St. Louis, MO, USA), 0.5 M malonate (pH 7.4 in 0.9% NaCl).

3. Methods

3.1. Nrf2-Overexpressing Astrocytes

3.1.1. Primary Astrocyte Cultures

Prepare primary astrocyte cultures from postnatal day 1 or 2 ARE–hPAP or wild-type pups.

1. Anesthetize P1 or P2 pups with isoflurane in a transparent chamber. Cut off head and pin down on paraffin plate with needles (22 ga, 1.5 inch). Remove tail for genotyping.
2. For each head, remove the skin with a curved forceps and a curved scissors, and cut along the scalp in the midline with a fine straight scissors (8 cm). Make a similar midline cut in the calvarium. Clear away meninges, deflect the calvarium with a blunt spatula, and scoop the brain into another 10 cm dish containing 2 mL1 × HBSS on ice.
3. Dissect the cortices: place the brain ventral side up. Place the spatula in the medial aspect of the ventral cortex and midbrain and cut the cortices off.
4. Break up tissue (cortex or midbrain) with a 1-mL pipette tip. One trituration should be sufficient. Over-trituration prior to the posttrypsinization washes will lead to poor yield. Centrifuge 300 rpm (300 g) for 2 min.
5. Replace media with ice-cold 0.05% trypsin in HBSS and 200 μL10 × trypsin in 2 mL HBSS.
6. Transfer to 37 °C shaking water bath for 13 min and then spin tubes at 300 rpm (300 g) for 2 min. After removing tubes from the centrifuge, a floating viscous debris indicates over-trypsinization and will indicate that a poor yield is imminent.

7. Wash dissociated cells three times with ice-cold HBSS and then resuspend in 2 mL prewarmed Eagle's MEM containing 10% heat-inactivated fetal calf serum, 10% horse serum, and 2 mM glutamine (CEMEM). Triturate into a single-cell suspension. Typically, this will require 10 triturations with a 1-mL pipette tip.
8. Pass the suspension through a 70-μm mesh filter (Cat. No. 35-2350, BD Falcon Bedford, MA, USA) into a 50-mL conical tube (Cat. No. 35-2070, BD Falcon Bedford, MA, USA).
9. Using sterile technique, aliquot 5 μL of filtered cell suspension from each tube into 45 μL Trypan blue (Cat. No. 15250-061, Invitrogen). Count cells on hemocytometer and dilute cells to approximately 1×10^5 cells/mL with CEMEM.
10. Plate 3 mL cell suspension in one well of six-well plate. Allow cells to expand in CEMEM at 37 °C in a humidified incubator (95% air, 5% CO_2).
11. Change media (CEMEM) after 24 h and every 3 days thereafter. Typically, it will take 5–7 days for astrocytes to grow to confluence.
12. Cells may be passaged using 0.25% trypsin. In order to passage, wash cells with 1× phosphate-buffered saline (PBS) at least two times to remove serum-containing medium. Add enough 0.25% trypsin to just cover the bottom of the plate. Monitor cells with a microscope, and once they begin to detach, dilute trypsin with CEMEM. Wash cells off the bottom of plate and centrifuge 300 rpm (300 g) for 2 min. Aspirate medium and resuspend cells in three times the original volume of medium. Plate 3 mL of cells per well of a six-well plate.
13. A representative sample of the cells should be immunostained for the astrocyte marker GFAP after 7 days in culture. Typically, nearly all of the cells are positive for GFAP (>95%). This step is essential to demonstrate that cultures are predominantly astrocytes.

3.1.2. Adenovirus Infection

1. Once astrocyte cultures reach about 85% confluence, infect with adenovirus for 1 h in Eagle's MEM. Dilute adenovirus in an appropriate volume of MEM. Remove CEMEM from cells and reserve in another six-well plate. Add 1 mL MEM containing adenovirus onto cells. Incubate cells at 37 °C in a humidified incubator. After 1 h of incubation, replace the virus-containing medium with conditioned CEMEM and placed in a 37 °C humidified atmosphere of 5% CO_2 in air (*see* **Note 1**).
2. Use cultures for grafting 24 h later. Up to 200 multiplicity of infection (MOI) have been used, and no toxicity was observable by visual inspection of the cells 24 h later.
3. Determine the infection rate by the percentage of GFP-positive cells. The modified constructs contained Nrf2 (or DN-Nrf2) and GFP in separate expression cassettes. Therefore, we assume that any infected cell will be labeled with GFP after 24 h. Visualize cells with an inverted fluorescent microscope. Photograph cells using a green filter set and again using phase contrast. To determine infection rate,

count green cells and divide by the total number of cells, then multiply by 100. Additionally, we surmised that GFP-positive cells also overexpressed Nrf2 (*see* **Note 2**).

4. The toxicity of this replication-deficient adenovirus was evaluated on astrocyte cultures by MTS assay. According to our experience, the virus applied at a titer of 25–200 MOI resulted in over 90% infection rate in astrocytes with no significant increase in viral toxicity.

3.2. Grafting

1. Mice will be preanesthetized with 4% isoflurane, 0.5 L/min O_2 in a transparent chamber, until they are no longer responsive to toe or tail pinch. Mount mice on the stereotaxic injection apparatus (Stoelting) with a mouse gas anesthesia platform (Stoelting) (**Fig. 1C**). Maintain the anesthetic level at approximately 1.5–2.5% isoflurane, 0.5 L/min O_2 throughout the injection procedure. Adjust isoflurane percentage if animal becomes responsive to tail pinch or begins gasping, which is indicative of too much anesthetic. Correct placement of mice in the stereotactic frame (Stoelting) is critical to anesthesia and intracranial surgery. In order to locate a specific three-dimensional structure, all the calculations are based on a coordinate system relative to a predefined landmark (bregma). First, insert the incisor bar gently. Make sure the nose is completely contained within the nose cone. Adjust the platform relative to the ear bars, such that the ear bars may be inserted and then fix. Fix one ear bar and hold the head to insert the fixed bar into the ear canal. Holding the head, insert the other ear bar slowly until one is unable to move the head laterally. Then fix the ear bar.
2. Moisten the eyes with Akwa tears eye lubricant to prevent over-drying during the procedure and subsequent damage to the animal's eye. Disinfect the scalp with triadine and 70% ethanol. It is not necessary to shave the scalp, as the short hair should not interfere with the incision or injection once it is wetted with triadine. Make an incision along the midline of the scalp beginning slightly posterior to the eyes and ending at the back of the skull. Open the skin and push away the membrane covering the skull with two sterile cotton-tipped applicators. At this point, bregma will be exposed. Bregma is the junction of the coronal and sagittal sutures at the top of the skull **(Fig. 1)**.
3. Using the stereotaxic apparatus, locate bregma with the needle on the mounted syringe. Bregma can be difficult to establish because of individual variations in skull plate fusion. In the case that bregma is not easily identifiable, project the coronal suture toward the sagittal suture (midline) and establish an imaginary point at the intersection. It may take considerable experience with the apparatus and surgeries before one develops a high level of proficiency with this sort of estimation. Fortunately, the majority of mice have bregma that is easily identified.
4. From bregma, measure out injection coordinates and mark with pencil on the skull. The coordinates we use for injection into the striatum are as

follows (*see* **Note 3**): 0.5 mm anterior to bregma and 2.1 mm lateral to midline (either dextral or sinistral). It is essential that each laboratory conducts pilot experiments in which coordinates derived from the atlas are evaluated.

5. Drill through the skull at these coordinates using a Dremel two speed multipro tool with a carving/engraving bit. Be careful to drill just through the skull without penetrating the dura. This is difficult but possible with practice and patience.
6. Inject mice in the striatum using a Hamilton syringe with a 27-ga, 2/3-inch needle for cell transplantation and according to the following coordinates: 0.5 mm anterior to bregma, 2.1 mm lateral to midline, and 3.8 mm ventral to bone surface. Alternatively, a finer gauge needle or pulled glass pipette may be used to minimize damage associated with injection. In our laboratory, we use a 32-ga, 2/3-inch needle attached to a Hamilton 700 series syringe to inject chemicals and have seen a great reduction in postsurgical damage doing so. A diagram of coronal section illustrates the injection site (**Fig. 1D**).
7. Inject 100,000 astrocytes in a total volume of 1 μL culture media. Astrocytes will be infected with either GFP-expressing or Nrf2/GFP-expressing adenovirus 24 h prior to surgery. Cells will be lifted from plates by trypsinization (0.05% trypsin in HBSS for 2 min), pelleted, washed, and then resuspended at 1×10^8 cells/mL (*see* **Note 4**).
8. One or two minutes after insertion of the needle, administer the injection over the course of 2 min and the needle slowly withdrawn at 2 mm/min. We use a motorized stereotaxic injector to ensure that the injection is continuous and precise (**Fig. 1B**). Wait several minutes (depending on volume injected and region) before withdrawal to avoid backflow.
9. Disinfect skin with triadine and 70% ethanol. Then, suture using two 9-mm autoclip wound clips.
10. Allow mice to recover from anesthesia under a warm lamp for approximately 30 min. Monitor mice for signs of distress. Wound clips will be removed after 7 days (*see* **Notes 5** and **6**).

3.3. Lesioning

1. Lesioning experiments will be performed at least 2 weeks after transplantation. This allows grafting cells to completely integrate into the local region. After cell grafting, inject mice that are at least 18 weeks old intrastriatally with malonate. For malonate injections, the protocol will be the same as above (*see* **Subheading 3.2.6.**), except that instead of cells, 0.5 M malonate (pH 7.4 in 0.9% NaCl) will be injected 0.5 mm anterior to bregma, 2.1 mm lateral to midline, and 3.8 mm ventral to bone surface.
2. After 48 h of malonate administration, kill mice and harvest brains for histochemical staining and lesion quantification (**Fig. 2**).

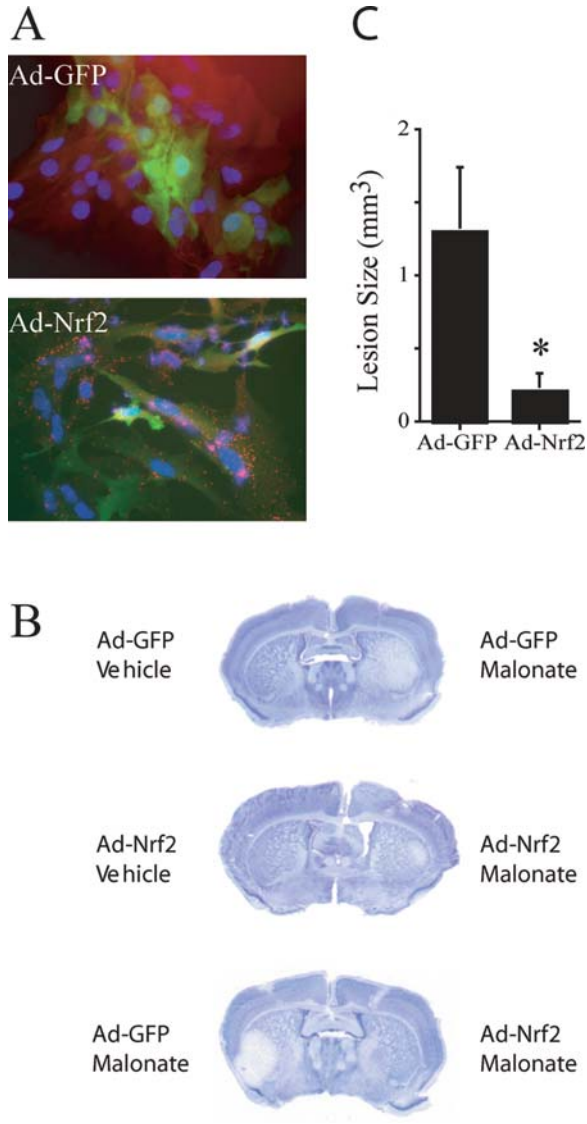

Fig. 2. Adenovirus (ad)-Nrf2-infected astrocyte transplants protect from malonate-induced lesions. Human placental alkaline phosphatase (hPAP) + astrocytes were infected with ad-GFP or ad-Nrf2-GFP. GFP expression and hPAP histochemistry were visualized **(A)**. Mice were lesioned 5 weeks posttransplant with malonate (1 μL, 0.5 M, pH 7.4, in 0.9% NaCl). Lesions were visualized by cresyl violet **(B)** and quantified **(C)**. $^{*}P < 0.05$ compared with hemispheres receiving GFP-infected astrocytes.
Source: From Calkins et al. ***(8)*** with permission.

3.4. Quantification of Lesion Size

1. Perfuse mice with heparinized saline (0.9% w/v NaCl) followed by 4% w/v paraformaldehyde and 15% saturated picric acid in 0.1 M phosphate buffer (PB) (pH 7.4). Incubated brains in 20% w/v sucrose in 0.1 M PB (24 h at 4 °C) followed by freezing in isopentane (−40 °C).
2. Cryosections (20 μm) were made by Leica Cryostat CM 3050S. Take at least two sets of coronal cryosections 200 μm apart and select one set randomly to stain with cresyl violet (Cat. No. C5042, Sigma).
3. Use the stained sections for lesion volume quantification using the nonbiased Cavalieri estimator in the Stereoinvestigator™ program (Microbrightfield, Williston, VT). Lesion area for each section is estimated, and volume is interpolated (*see* **Notes 7** and **8**).
4. In order to estimate the lesion area in each section, use the software to define the boundary of the lesion and then to randomly place a grid over an image of the section. Count grid points contained within the boundary and estimate area.
5. In general, counting greater than 50 points, using the Cavalieri estimator on roughly circular areas, will ensure that the coefficient of error associated with the volume estimation for each lesion remains below 5%.

4. Notes

1. Handling of adenovirus: store at −80 °C in sealed microcentrifuge tubes. Add small aliquots of virus particles to culture plates in a bio-safety cabinet vented to the exterior of the building. Clean the cell culture area with bleach (5%) and soak disposable items in dilute bleach (5%) and then discard them. To ensure a safe working environment, we follow the guidelines detailed by Health Canada (http://www.hc-sc.gc.ca/pphb-dgspsp/msds-ftss/index.html).
2. Nrf2-cDNA was excised from the pEF/Nrf2 ***(10)*** using *Not*I and *Hin*dIII. The replication-deficient constructs were created using the Cre-lox system ***(11)*** and were titered on human embryonic kidney 293 cells ***(6)***. For this experiment, the tracking of gene delivery and expression can be achieved by using either the transgenic reporter mice or the virus constructs with two separate expression cassettes for target gene and reporter gene (e.g., GFP). The commercially available small-molecule cell tracers may potentially activate Nrf2-dependent ARE pathway. This would influence our results, and hence, we avoid using them.
3. It is very important to become familiar with the general anatomy of the specific region where one will inject. Some brain atlases or online sources (http://www.mbl.org) will assist in correctly locating the target for surgical intervention. In this experiment, coordinates are determined from a mouse brain atlas ***(12)***—individual laboratories should determine coordinates that are repeatable and appropriate for their purposes.
4. A major concern when grafting cells is maintaining good health of the cells to be grafted. Therefore, preparation, handling, and delivery need to be fast, clean, and

gentle. We recommend two people: one in charge of anesthesia and intracranial surgery and the other responsible for cell preparation. Once cells are isolated, they are always kept in ice.

5. Graft rejection is rare with allografts. However, xenografts will be rejected unless the animals are given appropriate immunosuppressive therapy. Cyclosporin may be given (10 mg/kg; ~0.2–0.5 mL depending on weight) on a daily basis by intraperitoneal injection in order to achieve immunosuppression.
6. Handling of grafted animals: grafted mice are isolated from their respective colonies. Any remaining virus-infected astrocytes and used syringes are decontaminated by bleach (5%). After injection, animals are monitored daily for any changes in overt signs of discomfort. The viruses are all rendered replication-deficient prior to transfer to the laboratory and injection into host animals. No adverse reactions are anticipated. If mice appear to be experiencing pain or discomfort because of the surgery, they will be immediately euthanized by CO_2 because stress of this type also can cause genetic changes that could confuse the interpretation of the data. In our experience, it is extremely rare for a mouse to exhibit signs of infection, discomfort, or pain.
7. For lesions that were approximately 1 mm^3, the grid size was set at 100 μm, and lesion area was measured in five to eight sections separated by 200 μm. This resulted in at least 100 total points being counted for relatively small lesions ($100\,\mu m \times 100\,\mu m \times 200\,\mu m \times 100 points = 0.2\,mm^3$).
8. Infected neural progenitor cells demonstrated better migration away from the needle tract and better integration into the local region than infected astrocytes. According to a quantitative study, hemispheres receiving Nrf2-infected progenitors or astrocytes showed significant resistance to malonate-induced lesions. (The lesion size decreased from 1.303 ± 0.443 to $0.212 \pm 0.123\,mm^3$ for astrocyte transplant, $P < 0.05$; from 0.428 ± 0.067 to 0.135 ± 0.029 for neural progenitors transplant, $n = 4$.) The protocol for isolating and culturing of neural progenitor cells is available from Wu et al. 2002 ***(13)***.

References

1. Rushmore, T. H., Morton, M. R., and Pickett, C. B. (1991) The antioxidant responsive element. Activation by oxidative stress and identification of the DNA consensus sequence required for functional activity. *J Biol Chem* 266, 11632–11639.
2. Wasserman, W. W. and Fahl, W. E. (1997) Functional antioxidant responsive elements. *Proc Natl Acad Sci USA* 94, 5361–5366.
3. Motohashi, H., O'Connor, T., Katsuoka, F., Engel, J. D., and Yamamoto, M. (2002) Integration and diversity of the regulatory network composed of Maf and CNC families of transcription factors. *Gene* 294, 1–12.
4. Li, J., Stein, T. D., and Johnson, J. A. (2004) Genetic dissection of systemic autoimmune disease in Nrf2-deficient mice. *Physiol Genomics* 18, 261–272.

5. Lee, J. M., Calkins, M. J., Chan, K., Kan, Y. W., and Johnson, J. A. (2003) Identification of the NF-E2-related factor-2-dependent genes conferring protection against oxidative stress in primary cortical astrocytes using oligonucleotide microarray analysis. *J Biol Chem* 278, 12029–12038.
6. Shih, A. Y., Johnson, D. A., Wong, G., Kraft, A. D., Jiang, L., Erb, H., Johnson, J. A., and Murphy, T. H. (2003) Coordinate regulation of glutathione biosynthesis and release by Nrf2-expressing glia potently protects neurons from oxidative stress. *J Neurosci* 23, 3394–3406.
7. Kraft, A. D., Johnson, D. A., and Johnson, J. A. (2004) Nuclear factor E2-related factor 2-dependent antioxidant response element activation by tert-butylhydroquinone and sulforaphane occurring preferentially in astrocytes conditions neurons against oxidative insult. *J Neurosci* 24, 1101–1112.
8. Calkins, M. J., Jakel, R. J., Johnson, D. A., Chan, K., Kan, Y. W., and Johnson, J. A. (2005) Protection from mitochondrial complex II inhibition in vitro and in vivo by Nrf2-mediated transcription. *Proc Natl Acad Sci USA* 102, 244–249.
9. Johnson, D. A., Andrews, G. K., Xu, W., and Johnson, J. A. (2002) Activation of the antioxidant response element in primary cortical neuronal cultures derived from transgenic reporter mice. *J Neurochem* 81, 1233–1241.
10. Alam, J., Stewart, D., Touchard, C., Boinapally, S., Choi, A. M., and Cook, J. L. (1999) Nrf2, a Cap'n'Collar transcription factor, regulates induction of the heme oxygenase-1 gene. *J Biol Chem* 274, 26071–26078.
11. Hardy, S., Kitamura, M., Harris-Stansil, T., Dai, Y., and Phipps, M. L. (1997) Construction of adenovirus vectors through Cre-lox recombination. *J Virol* 71, 1842–1849.
12. Paxinos, G. and Franklin, K. B. J. (2001) *The Mouse Brain in Stereotaxic Coordinates*, 2nd edn. Academic Press, San Diego, CA.
13. Wu, Y. Y., Mujtaba, T., and Rao, M. S. (2002) Isolation of stem and precursor cells from fetal tissue, in *Methods in Molecular Biology, Vol 198: Neural Stem Cells: Methods and Protocols* (Zigova, T., Sanberg, P. R., and Sanchez-Ramos, J. R., eds.), Humana Press, Totowa, NJ, pp. 29–40.

7

Biochemical Methods to Assess the Coupling of Brain Energy Metabolism in Control and Disease States

Jennifer Zechel, W. David Lust, and Michele Puchowicz

Summary

Mitochondrial dysfunction has been increasingly shown as a critical process that makes certain areas of the brain more susceptible not only to neurological disease but also to aging. Quantitative histochemistry is a series of procedures for measuring select metabolites in discrete regions of the brain, as they exist in vivo. The development of this method has been useful in establishing energy imbalance following ischemia but more recently has become useful in studying those processes related to the mitochondria which make the brain more susceptible to a variety of neurological insults. The relatively inexpensive cost to assay a given brain metabolite makes this methodology useful in the interpretation of molecular and biochemical responses in terms of the condition of the tissue following a neurological insult.

Key Words: Brain; high-energy phosphates; redox states; pathologically induced-energy imbalance.

1. Introduction to Balancing of Brain Metabolism

The regulation of metabolic pathways in the production of energy equivalents is the essence of balancing brain energy metabolism. Energetic regulation is inherently very complex and requires feedback control as well as the stabilization of redox state. It is well established that the brain is very metabolically active and that compromising the blood flow and its constituents eventually leads to loss of function, cell injury, and death. The production and utilization

From: *Methods in Molecular Biology, vol. 399: Neuroprotection Methods and Protocols*
Edited by: T. Borsello © Humana Press Inc., Totowa, NJ

of brain energy is tightly coupled, and the disruption of the delicate balance has been implicated in a number of neurological insults. The early findings that ischemia caused the depletion of energy stores and essentially stopped all energy-dependent processes eventually led to the evaluation of energy balance in a number of neurological diseases. In recent years, it has become apparent that mitochondrial dysfunction is a relatively common feature in a number of experimental neurological diseases including Parkinson's disease, dementia, and type II diabetes, which could also lead to cell damage. The primary purpose of this chapter is to present technically feasible assays to complement other experimental findings during and after a neurological insult.

Since the development of enzymatic measurements of pyridine nucleotides by spectrophotometry ***(1,2)*** and the adenylates (ATP, ADP, and 5′ AMP) and phospho-creatine (P-creatine) ***(3,4)*** by luminescence, a host of critical metabolites including glucose, glycogen, lactate, pyruvate, and ketones (*R*-β-hydroxybutyrate and acetoacetate) have been useful in assessing key regulatory points of oxidative and glycolytic pathways, both in normal and in pathological conditions. These assays have been shown to be straightforward, reliable, sensitive, and specific for a given metabolite. For example, the ratios of energy-related metabolites such as lactate to pyruvate and *R*-β-hydroxybutyrate to acetoacetate have been used to assess cytosolic and mitochondrial redox states, respectively. Thus, shifts in redox are often an indicator of metabolic perturbations.

The assays for each metabolite are presented in a step-by-step fashion with a critical section on brain fixation, which is essential for measuring cerebral energy metabolites, as they exist in vivo. A number of in-depth reviews have been published on these topics ***(5–9)***. However, for this chapter, we will simplify the methodological approach and highlight the main points of interest with respect to the accuracy and avoidance of artifactual measurements.

2. Materials

2.1. Animals (See Note 1)

2.1.1. Anesthetics and Drugs

1. Gas mixture containing 2–5% halothane (Halocarbon Laboratories, River Edge, NJ) and 70% N_2O in O_2.
2. Lidocaine hydrochloride, 2% (Abbot Laboratories, North Chicago, IL).
3. Marcaine hydrochloride, 0.25% (Astra Pharmaceutical Products, Westborough, MA).

2.1.2. Surgical Supplies

1. Polyethylene tubing, PE 50, 0.023 inch ID, 0.038 inch OD (Becton Dickinson and Co., Sparks, MD).
2. Silastic catheter, 0.025 inch ID, 0.047 inch OD (Fisher Scientific, Pittsburgh, PA).
3. Heparinized microhematocrit capillary tubes (Fisher Scientific).
4. Stopcock grease.
5. Liquid nitrogen.
6. Tracheal tube. In our laboratory, we used a 14-ga blunted Angiocath needle.
7. Plastic 30-mL cup with the bottom removed.

2.1.3. Equipment

1. Rectal or temporalis thermistor probe (Yellow Springs Instrument Co., Yellow Springs, OH).
2. Blood gas analyzer (ABL5, Radiometer, Copenhagen, Denmark).
3. Blood pressure monitor (DigiMed BPA3000, Micro-Med, Louisville, KY).
4. Rodent ventilator (#683, Harvard Apparatus, Cambridge, MA).

2.2. Sample Preparation

2.2.1. Equipment

1. Glove box or other environment capable of maintaining temperatures of at least -20° C.
2. Pneumatic autopsy saw (Stryker model 277-30, Kalamazoo, MI) with blades (Stryker #1100).
3. Cryo-gloves (Temp-Shield, Mount Desert, ME).
4. Polytron homogenizer (PowerGen 125; Fisher Scientific) with a 5 mm $\times$ 95 mm tip (#15-338-203, Fisher Scientific).
5. Scalpels.
6. Refrigerated centrifuge at 4° C, capable of $10,000 \times g$.
7. Nitrogen gas.
8. Cryo-microtome capable of maintaining temperatures of at least -20° C.

2.2.2. Acid Extraction Reagents

1. 0.3 N Perchloric acid (PCA) with 1 mM EGTA.
2. 3 N PCA with 10 mM EGTA.
3. Distilled water (ddH_2O).
4. 2 M $KHCO_3$ (potassium bicarbonate).
5. 1 N NaOH.
6. pH paper.

2.2.3. Glycogen Extraction Reagents

1. 0.1 N HCl in absolute methanol.
2. Dry ice.
3. 100% Ethanol.
4. 3 N PCA with 10 mM EGTA.
5. 2 N $KHCO_3$.
6. 1 N NaOH.
7. 0.016 N HCl.

2.3. Adenylate and P-Creatine Measurement

1. AXP reagent: 50 mM imidazole–HCl (pH 7.0) (30 mM imidazole base, 20 mM imidazole–HCl), 2 mM $MgCl_2$, 75 mM KCl, and 3 mM phosphoenolpyruvic acid (PEP).
2. Luciferin/Luciferase reagent: 50 mM glycylglycine buffer (pH 8.1) (25 mM glycylglycine base, 25 mM glycylglycine–HCl) (#G1127, Sigma, St. Louis, MO), 2 mM DTT, 2 mM EGTA; 0.02% bovine serum albumin (BSA), 10 nM Ap5A (P^1, P^5-Di(adenosine-5′-)pentaphosphate—Roche Applied Science, Indianapolis, IN, #10161624), 5 μg/mL luciferase (#L5256, Sigma), and 20 μg/mL luciferin (#L9504, Sigma).
3. P-Creatine reagent: 50 mM imidazole–HCl (pH 7.0) (30 mM imidazole base, 20 mM imidazole–HCl), 1 mM $MgCl_2$, 60 μM ADP (#A6521, Sigma), 0.02% BSA (#A7409, Sigma), and 10 nM Ap5A.
4. 50 μg/mL Pyruvate kinase from rabbit muscle (#128163, Roche Applied Science).
5. 25 μg/mL Myokinase from rabbit muscle (#127949, Boehringer Mannheim, Indianapolis, IN).
6. 10 μg/mL Creatine kinase (#127566, Roche Applied Science); take 5 μL and mix with 2 mL P-creatine reagent.
7. Pyruvate kinase enzyme mix: add 200 μL pyruvate kinase (from a 10 mg/mL stock) to 2 mL AXP reagent.
8. 6 mm × 50 mm Glass tubes (#14-958-A, Fisher Scientific).
9. 10 mm × 75 mm Glass tubes (#14-961-25, Fisher Scientific).
10. Luminometer (Lumi-Vette, ChronoLog Corp., Havertown, PA).
11. ATP, ADP, and 5′ AMP standards.

2.4. Lactate Measurement

1. Reagent: 50 mM 5′ 2-amino-2-methylpropanol (5′ AMP) buffer (pH 9.9) (25 mM free base, 25 mM hydrochloride), 1.5 mM NAD^+ (grade V-C, #N8129, Sigma), 50 mM glutamate (pH 9.8) (from 1 M stock of monosodium glutamate) (*see* **Note 2**).
2. 100 μg/mL Lactate dehydrogenase from beef heart (#106-984, Boehringer Mannheim).
3. 100 μg/mL Glutamate pyruvic transaminase from pig heart (#G9880, Sigma).

2.5. Pyruvate Measurement

1. Reagent: 50 mM phosphate buffer, (pH 7.0) (30 mM K_2HPO_4, 20 mM NaH_2PO_4), 2 mM $MgCl_2$, 200 μM ADP, 50–150 μM NADH (minimum of 20% excess).
2. 0.2 U/mL Lactate dehydrogenase from beef heart (#106-984, Boehringer Mannheim).

2.6. Glucose Measurement

1. Reagent: 50 mM Tris–HCl (pH 8.1); 1 mM $MgCl_2$, 500 μM ATP, 500 μM $NADP^+$ (#0505, Sigma), 0.2 μg/mL glucose-6-P dehydrogenase (yeast, #0127710, Roche Applied Science).
2. 250 μg/mL Hexokinase (yeast, #127809, Boehringer Mannheim). Dilute 25 μL hexokinase stock with 975 μL glucose reagent.

2.7. Glycogen Measurement

1. Glucose reagent.
2. 250 μg/mL Amyloglucosidase (#10102857, Roche Applied Science), diluted 1:50 with ddH_2O, final concentration 0.5 μg/mL.
3. 45 mM Sodium acetate.
4. 0.016 N HCl.
5. 0.03 N HCl.
6. pH paper.
7. 250 μg/mL Hexokinase. Dilute 25 μL hexokinase stock with 975 μL glycogen reagent.
8. 1 mM Glucose standard (#635-100, Sigma).
9. 1 mM Glycogen standard (#G4011, Sigma).
10. Heater capable of maintaining a temperature of 60° C.

2.8. R-β-Hydroxybutyrate

1. Alpha mix: 0.1 M Tris, 10 mM $MgSO_4$, and 5 mM EDTA (pH 8.5).
2. Tris–hydrazine buffer: 25 mL alpha mix with 1.18 g hydrazine hydrate (*see* **Note 3**).
3. Reagent 1:25 mL Tris–hydrazine buffer plus 455 μL of an 80 mg/mL NAD stock solution.
4. 5 mg/mL BHB dehydrogenase (BHB-DH) (#0127841, Roche Applied Science).

2.9. Acetoacetate

1. Reagent: 860 μL of a 2 mg/mL NADH stock, 10 mL 0.1 M monobasic phosphate buffer (pH 7.0).
2. 5 mg/mL BHB-DH.

2.10. General Equipment

1. Vortex.
2. Spectrophotometer capable of reading 340 nm.
3. Cuvettes with a 10-mm light path, either quartz or plastic.

3. Methods

Brain is particularly susceptible to postmortem changes in concentrations of cerebral labile energy metabolites (glycolytic and TCA cycle intermediates and adenylates), and if the tissue is not properly fixed, artifactual data may result. Because postmortem changes occur rapidly, within seconds ***(10)***, the stability of certain enzymes or metabolites of interest will also change. The goal of fixation is to trap the metabolites, as they exist in vivo, by rapidly stopping metabolic processes. There are many methods that describe fixation of brain tissue (for detailed review, *see* **ref. *9***). Because the assays described in the following subheadings require the use of rapid fixation and therefore are consistent with certain molecular methods that require intact, active proteins, we describe the rapid freezing technique ***(7,9,11)***. This method has been viewed for its advantages for studying cerebral energy metabolism, as there is little evidence for autolytic changes (hence avoidance of autolytic artifact) in energy-related metabolites.

To ensure proper oxygenation and ventilation, various physiological parameters are measured: arterial blood gases (pO_2, pCO_2) and pH are measured, and routinely glucose and lactate from the same blood sample metabolites are also measured if relevant; body temperature is monitored by rectal thermometer or by a temporalis muscle thermistor and maintained at 37° C with a heating pad or heat lamp for the entire procedure.

3.1. Funnel Freezing Procedure

1. Animal is placed in small box designed for administering volatile anesthetics (5% halothane, 70% nitrous oxide in oxygen); once anesthetized, the animal can be connected to a nose cone during the surgical placement of the cannula or directly by orotracheo-catheter and maintained on gas mixture (2% halothane, 70% nitrous oxide in 30% oxygen).
2. For placement of arterial tail cannula, the animal is turned on its back and the tail artery is exposed and cannulated with PE 50 tubing and sutured both distal and proximal to the incision (*see* **Note 4**). The arterial line is then connected to the blood pressure monitor and recorded. The incision site is infiltrated with a local anesthetic such as 2% Lidocaine hydrochloride or for longer acting anesthesia 0.25% Marcaine hydrochloride is used.

3. Once the animal is orotracheotomized and stabilized on the gas mixture, the placement of the funnel is performed by surgically opening the skin midline to the scalp exposing the surface of the cranium. Stopcock grease is applied to the bottom of the funnel (to seal the funnel to the scalp to prevent the leakage of liquid nitrogen) and is fitted over the skull with the posterior lip approximating the lambdoidal suture (*see* **Note 5**).
4. Just prior to freezing, the blood gases and blood pressure are checked (*see* **Note 6**). The anesthetizing gas is reduced to 1%, and liquid nitrogen is poured into the funnel, filling the funnel approximately three-fourths of the way (*see* **Note 7**). Freezing is continued by replenishing the funnel with liquid nitrogen as required until the mBP is about 50% of baseline ($\approx$ 40 mmHg), after which the entire animal is plunged into a container of 1–2 L liquid nitrogen and stored in a -70° C freezer. Freezing should not continue for more than 6 min (*see* **Note 8**).

3.2. Tissue Preparation and Extraction

3.2.1. Sample Removal

1. Place the animal in the glove box or similar temperature environment to equilibrate to -20° C (*see* **Note 9**) for 1 h prior to use.
2. Using a scalpel, scrape tissue away from top of skull, exposing the parietal ridges.
3. Scrape away muscle and connective tissue around skull.
4. Remove the brain from the skull using a pneumatic surgical saw driven by nitrogen gas (*see* **Note 10**).
5. Once removed from the skull, the tissue is sectioned either by refrigerated microtome (-20° C) (*see* **Note 11**) to a thickness of 5–20 μm or by gross dissection using a surgical blade or cork borer.

3.2.2. Tissue Extraction of Metabolites

The purpose of chemical extraction (acid/alkaline; *see* **Note 12**) is to quantitatively remove endogenous compounds from the tissue into a medium such that they are not irreversibly lost by precipitating the enzymes and structural proteins of the tissue. The medium should have the following critical characteristics: (1) the metabolite should be soluble and stable in the reagent; (2) the extractant should not interfere with enzymatic assay; and (3) the extraction of the metabolite(s) from the tissue should be complete (*see* **Note 13**).

3.2.3. Acid Extraction

The following steps describe the extraction process for most of the acid-soluble metabolites in brain tissue:

1. The brain sample (~ 40–100 mg wet weight [w/w] tissue; *see* **Notes 14** and **15**) is pulverized using mortar and pestle over dry ice or can be minced and homogenized in a test tube kept in ice.
2. 0.3–0.6 mL ice-cold 0.3 N PCA with 0.1 mM EGTA is added to the tissue sample and vortexed (if powdered) or homogenized on ice using a polytron until the sample is dispersed.
3. The resultant acid extract is neutralized with 0.15 mL of 2 N $KHCO_3$/mL of acid (*see* **Note 16**) extract resulting in the formation of insoluble potassium perchlorate. The supernatant is tested to ensure that the pH is between 6.8 and 7.2.
4. The protein pellet can be dissolved in 1 N NaOH for the analysis of protein content ***(12)***.

3.2.4. Extraction for Glycogen Analysis

1. Brain sample (~ 100 mg w/w of tissue) is added to 0.1 mL of 0.1 N HCl in absolute methanol (1:10, 1 part tissue w/w to 10 parts HCl solution) in a −20° C ethanol–dry ice bath and incubated for 20 min.
2. 500 µL Aqueous 0.016 N HCl is added and the tissue homogenized using a polytron. Remove a 100-µL aliquot for the measurement of glycogen and glucose, store below −20° C.
3. To the remaining extract (0.5 mL), 50 µL of 3 N PCA with 10 mM EGTA is added, and ddH_2O is added to a final volume of 1 mL.
4. The sample is mixed and centrifuged at $10,000 \times g$ for 10 min, and the supernatant (free of protein) is removed.
5. To measure acid-soluble metabolites, the remaining sample is processed as for acid extraction, *see* **Subheading 3.2.3., steps 3** and **4** (*see* **Note 17**).

3.3. Luminometric Measurement of Adenylates and P-Creatine

The indicator-step method for measuring adenylates and P-creatine (as ATP) using light emitted from the Luciferin/Luciferase reaction imposes increased sensitivity for smaller tissue sample. The measurement of adenylates and P-creatine in tissue is accomplished by the enzymatic conversion to ATP by the use of myokinase, pyruvate kinase, and creatine kinase by transfers of the phosphate moiety from P-creatine to ADP to form ATP ***(3)*** (*see* **Flowchart 1**).

There are certain tenets that apply to each of the assays described. Generally, the assays are initiated with the addition of the final enzyme in the reaction. The critical step is to ensure that the blank is small relative to the sample reading. Then, the reaction should be tested prior to running the assay to ensure the reaction mixture is properly prepared.

3.3.1. Individual Adenylates (ATP, ADP, and 5′ AMP)

1. Prepare adenylate standards using 10 mm × 75 mm glass test tubes: add 5 µL ATP, ADP, or 5′ AMP standard (in the range of ≈ 1 mM) to 100 µL AXP reagent; vortex 15 s. For each standard, perform a fourfold serial dilution with a final volume of 50 µL per tube.
2. Measuring AXP standards:
   a. In three new sets of test tubes individually labeled for ATP, ADP, and 5′ AMP standards, pipette 50 µL AXP reagent. Be sure to include a blank tube containing only buffers. Pipette 10 µL of each of the ATP, ADP, and 5′ AMP standards as prepared in step 1 into the corresponding sets of test tubes.
   b. To each of the ADP standards, add 10 µL pyruvate kinase enzyme mix prepared (**Subheading 2.3., item 7**). Incubate mixture for 60 min.
   c. To each of the 5′ AMP standards, add 5 µL myokinase enzyme and 10 µL pyruvate kinase enzyme, and incubate mixture for 60 min.
   d. Pipette 10 µL of each of the prepared AXP standards into 6 mm × 50 mm test tubes and add 250 µL Luciferin/Luciferase reagent. Vortex and read *immediately* using a luminometer (*see* **Note 18**).
   e. A typical AXP standard curve is shown in **Fig. 1**.
3. Measuring sample adenylates:
   a. Pipette 10 µL sample prepared in **Subheading 3.2.2.** to a new 6 mm × 50 mm test tube.
   b. Add 100 µL AXP reagent and vortex.
   c. Pipette 10 µL of the sample (in reagent) to a new 6 mm × 50 mm tube and add 250 µL Luciferin/Luciferase reagent. Vortex briefly and read *immediately* on a luminometer. This allows the calculation of the total ATP in the sample.
   d. To the remaining sample (from step c), add 5 µL pyruvate kinase stock solution, vortex, and let the reaction continue for 60 min.
   e. Pipette 10 µL of the sample from step d (in reagent) to a new 6 mm × 50 mm tube and add 250 µL Luciferin/Luciferase reagent. Vortex briefly and read on a luminometer. This allows the calculation of the amount of ATP plus ADP in the sample.
   f. Add 5 µL myokinase stock solution (*see* **Note 19**), vortex, and let the reaction continue for 60 min.
   g. Pipette 10 µL of the sample (in reagent) from step f to a new 6 mm × 50 mm tube and add 250 µL Luciferin/Luciferase reagent. Vortex briefly and read using a luminometer. This allows the calculation of the total amount of adenylates in the sample.

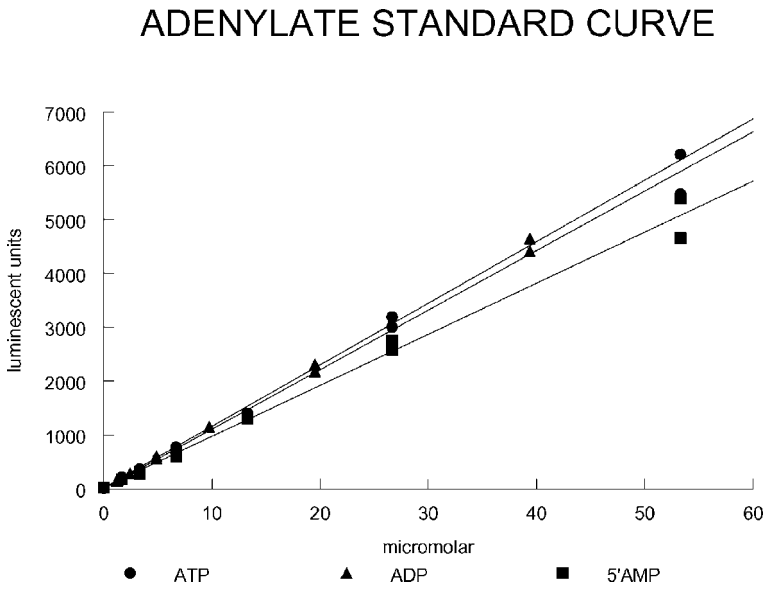

Fig. 1. Standard curve for ATP, ADP, and 5′ AMP. The standards were linear up to 60 μM, and the correlation coefficient for each standard approached 1 for all the standards. The slope of the standards ranged from 94 to 100 luminescent units/μM.

3.3.2. ATP and P-Creatine

1. Prepare and measure ATP standards as described in **Subheading 3.3.1**.
2. Prepare P-creatine standards using 10 mm × 75 mm glass test tubes: add 5 μL of 1 mM standard to 100 μL neutralized PCA; vortex 15 s. For each standard, perform a fourfold serial dilution with a final volume of 50 μL per tube.
3. Measuring P-creatine standards:
   a. In a new set of test tubes labeled for P-creatine standards, pipette 50 μL P-creatine reagent. Be sure to include a blank tube containing only buffers. Pipette 10 μL of each of the standard mixes of ATP and P-creatine (as prepared in **Subheading 3.3.1.**) into the corresponding test tubes.
   b. Pipette 10 μL of each of the standards (as described in **Subheading 3.3.1.**) into 6 mm × 50 mm test tubes and add 250 μL Luciferin/Luciferase reagent. Vortex and read using a luminometer.
4. Measuring ATP and P-creatine samples:
   a. To 100 μL P-creatine reagent, add 10 μL sample and vortex.
   b. Aliquot 10 μL of this mixture to a new 6 mm × 50 mm tube and add 250 μL

Luciferin/Luciferase reagent. Vortex and read using a luminometer. This reading allows the calculation of the amount of ATP contained in the sample.

c. Add 5 μL creatine kinase solution to the remaining sample, vortex, and allow to react for 30 min.
d. Aliquot 10 μL from step 4c into a new 6 mm × 50 mm tube and add 250 μL Luciferin/Luciferase reagent. Vortex and read using a luminometer. This reading allows the calculation of the ATP from the P-creatine contained in the sample.

3.3.3. Calculations

1. Standards:

a. $$\frac{(5\,\mu\text{L})(1\,\text{mM ATP or PCr standard})}{(100\,\mu\text{L AXP reagent} + 5\,\mu\text{L standard})} = [\mu\text{M}]\,\text{of high standard}$$

b. $$([\mu\text{M}]\,\text{high})\left(\frac{10\,\mu\text{L}}{6\,\text{mm} \times 50\,\text{mm tube}}\right)\left(\frac{10\,\mu\text{L standard}}{110\,\mu\text{L in } 10\,\text{mm} \times 75\,\text{mm tube}}\right)$$
$$= \text{pmol standard in} 10\,\text{mm} \times 75\,\text{n}$$

c. $$\frac{(\Delta\text{standard} - \Delta\text{blank})}{\text{pmol of ATP in tube}} = \text{luminescence/pmol ATP} = \Delta/\text{pmol}$$

2. Calculation of sample ATP (**Fig. 2** demonstrates ATP measurements from brain following middle cerebral artery occlusion and reperfusion):

a. $$\left(\frac{\Delta\text{sample} - \Delta\text{blank}}{\Delta\text{pmol}}\right)(\text{Dilution factor})\left(\frac{1}{\text{mg protein}}\right) = \frac{\text{nmol ATP}}{\text{mg protein}}$$

b. $$\text{Dilution factor}: \left(\frac{110\,\mu\text{L } \textit{sample} + \text{reagent}}{10\,\mu\text{L indicator tube}}\right)$$
$$\left(\frac{\text{volume transferred supernatant} + \text{volume of 3 N } KHCO_3}{10\,\mu\text{L to assay}}\right)\left[\frac{\text{total extraction volume}(\mu\text{L})}{\text{transferred supernatant}(\mu\text{L})}\right]$$

For PCr and ATP, the dilution factor must account for the addition of 10 μL creatine kinase.

	ATP	ATP+ADP	AMP	ATP + P-Creatine
Reactions	L/L+ATP↔ Luciferin-AMP-enzyme+O_2→light	ADP+PEP $\xrightarrow{PK}$ ATP + pyruvate	AMP+ATP $\xrightarrow{myo}$ 2ADP	P-creatine +ADP $\xrightarrow{CrK}$ creatine +ATP

	Stock Conc.	Reagent	Volume	Final Conc.	Stock	Reagent	Volume	Final
Base Reagent	1M	Imidizole-HCl pH 7.0	2.5mL	50mM	1M	Imidizole-HCl pH 7.0	2.5mL	50mM
	1M	$MgCl_2$	100µL	2mM	1M	$MgCl_2$	50µL	1mM
	1M	KCl	3.75mL	75mM	10mM	ADP	300µL	60µM
	0.1M	PEP	1.5mL	3mM	10mM	Ap5A	0.5µL	0.1µM
			Final volume:	*50mL*			*Final volume:*	*50mL*
Enzyme mix		5µL of PK (10mg/mL stock)	5µL of PK (10mg/mL stock)		50mg/mL	CrK	5µL	125µg/mL
			5µL of myo*(5mg/mL stock)			P-creatine reagent	2mL	
							Final volume	*2mL*

Step 1	Add 10µl prepared sample (section 3.2.2.) or standard into a 10x75 mm test tube, add 100µl AXP base reagent and vortex.	Add 10µl prepared sample to 100µl p-creatine reagent.
Step 2	Pipette 10µl from step 1 to a new 6x50mm tube and add to 250µl luciferin-luciferase reagent (2.3.2.). Vortex and read immediately on a luminometer.	Pipette 10µl into a new 6x50mm tube, add to 250µl luciferin/luciferase reagent, vortex and read on a luminometer.
Step 3	Add 5µL pyruvate kinase stock to the remaining sample, vortex and let react 60 min.	To the remaining sample add 10µl of a 125µg/ml solution of creatine kinase, incubate 30 minutes at room temperature.
Step 4	Pipette 10µl from step 3 to a new 6x50mm tube and add to 250µl luciferin-luciferase reagent. Vortex and read immediately on a luminometer.	Pipette 10µl into a new 6x50mm tube, add to 250µl luciferin-luciferase reagent, vortex and read immediately on a luminometer.
Step 5	Add 5µL myokinase stock to the remaining sample, vortex and let react 60 min.	
Step 6	Pipette 10µl from step 5 to a new 6x50mm tube and add to 250µl luciferin-luciferase reagent. Vortex and read immediately on a luminometer.	
Brain conc.	ATP = ~3.00, ADP =~0.26 and 5'AMP =~0.04 µmol/mL	P-creatine = ~4.5 µmol/mL

Abbreviations used: PEP- phosphoenolpyruvic acid; Ap5A- P^1, P^5-Di(adenosine-5'-)pentaphosphate; PK-pyruvate kinase; myo-myokinase; Crk- creatine kinase; L/L- luciferin/luciferase;

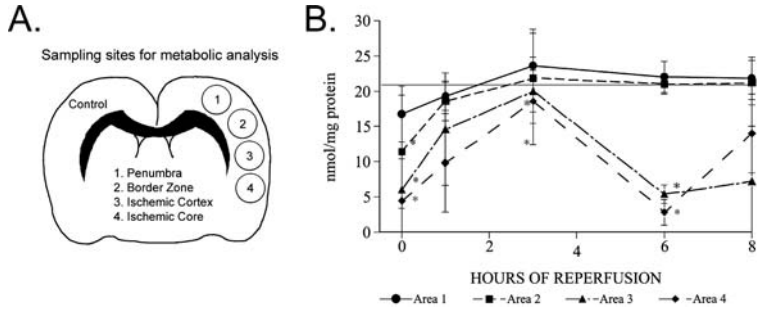

Fig. 2. **(A)** Schematic of a coronal section of an ischemic brain and the sampling sites used for metabolite analysis. The severity of the insult increases from areas 4 to 1 which is considered the penumbra. (**B**) ATP concentrations in regions of the cortex at various reflow times after a 2-h middle cerebral artery occlusion. The levels of ATP were significantly depressed at the end of the focal ischemia and onset of reperfusion. After 3 h of reflow, the ATP levels were not significantly different from control in the four groups, but in the subsequent 3 h, the ATP levels declined significantly in areas 1 and 2. It must be emphasized that the energy depletion occurred during reperfusion and therefore does not reflect a loss of cerebral blood flow. We speculate that the secondary energy failure is another type of delayed reperfusion injury. In contrast, the tissue adjacent to the penumbra and the penumbra itself maintained the energy state. The effect in areas 3 and 4 has been defined as secondary energy failure, which occurs in the presence of blood flow and glucose. The metabolite profile at the various times of reflow reflects the cellular condition when a number of proteins and mRNAs are being expressed. Clearly, the energy-depleted cells are incapable of active processes, including protein synthesis and mRNA transcription and are eventually destined to die by necrosis. The fate of the other two regions may be either survival or apoptotic brain death. The interpretation of the results is that reflow may be able to reverse damage, but alone, it cannot ensure the homogeneous survival of tissue. Asterisk denotes a significant change, $P < 0.05$.

3.4. Spectrophotometric Measurement of Metabolites

Spectrophotometric methodology is based on the absorbance of light because of the reduced pyridine nucleotides at 340 nm. These test reactions should be run with both standards and samples in order to determine the volume of sample required to achieve the optimal change in optical density. Although each reaction should be initially followed using a time course to determine the time required for the completion, reactions should not be left overly long to avoid drift.

It is essential that the user understands that some of the metabolites cannot be measured directly and requires a conversion to a detectable equivalent form

of that metabolite. Therefore, the conversion processes and the assays are described together as a comprehensive group of steps. See the reactions in the flowcharts as a guide.

It is important to note that the sample volumes described here are a guide and that users should ensure that they use sample volumes that result in the optimal optical density change (*see* **Flowcharts 2–4**).

3.4.1. Lactate Measurement (See **Note 20**)

1. Spin down 100 µL of the LDH (lactate dehydrogenase) and the GPT (glutamate pyruvic transaminase) in a centrifuge at 4° C for 10 min. Aspirate the supernatant and reconstitute the enzymes with 100 µL ddH_2O (*see* **Note 21**) .
2. Dilute the GPT to a final concentration of 10 µg/mL.
3. Add 10 µL of the prepared sample to 1 mL lactate reagent and vortex.
4. Add 10 µL of the diluted GPT to the tube and mix.
5. Take the first reading at 340 nm.
6. Add 10 µL LDH and allow the reaction to continue to completion.
7. Take the second reading at 340 nm.
8. Calculations (*see* **Note 22**): These calculations also apply to ketone bodies, pyruvate and lactate measurements. They are based on a molar extinction coefficient of 6270 at 340 nm for NADH and NADPH. **Fig. 3** demonstrates lactate measurement from brains following middle cerebral artery occlusion and reperfusion.

   a. $$\Delta\mu M = \Delta\text{Optical Density} - \text{blank} \times \frac{1}{0.00627} \times \frac{\text{total volume of reaction}}{\text{volume of sample added}}$$

   b. $\Delta\mu M \times$ total sample extraction volume(mL)* = total nmol in sample (*from **Subheading 3.2.3., step 3**).
   c. To calculate the concentration, the total amount of metabolite can be expressed in terms of wet weight, dry weight, or protein.

3.4.2. Pyruvate Measurement

1. Spin down 100 µL of the LDH in a centrifuge at 4° C for 10 min. Aspirate the supernatant and reconstitute with 100 µL of ddH_2O (*see* **Note 21**).
2. Add 10 µL of the prepared sample to 900 µL of pyruvate reagent and vortex.
3. Take an initial reading at 340 nm.
4. Add 10 µL of LDH, vortex, and allow the reaction to continue to completion.
5. Take a second reading at 340 nm.

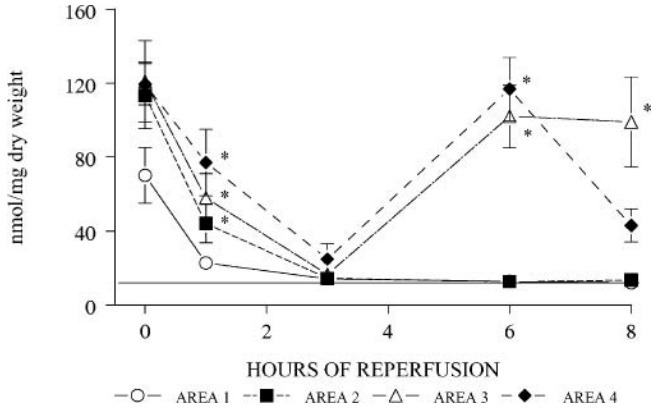

Fig. 3. Lactate levels in regions of the cortex as described in **Fig. 2**. The lactate was elevated at the onset of reflow and normalized by 3 h of reperfusion. In spite of near-normal glucose and blood flow, the lactate in areas 3 and 4 was significantly elevated, which mirrored the finding for ATP. Although the spectrophotometric assay was not as sensitive as that for Luciferin/Luciferase, a sample for analysis could be dissected of sufficient size to reliably measure the lactate. The extent of cell damage or death is indicated in **Fig. 2**. Asterisk denotes a significant change, $P < 0.05$.

3.4.3. Glucose Measurement

1. Dilute the hexokinase 1:40 (25 µL hexokinase stock [10 mg/mL] with 975 µL ddH_2O).
2. Add 10 µL of the prepared sample (from **Subheading 3.2.3., step 2**) to 1 mL glucose reagent and vortex.
3. Take the first reading at 340 nm.
4. Add 10 µL diluted hexokinase, vortex, and incubate until the reaction reaches completion.
5. Take the second reading at 340 nm.

3.4.4. Glycogen Measurement (See ***Note 23***)

1. Thaw 100 µL homogenate prepared in **Subheading 3.2.3.** and heat at 60° C for 10 min. Vortex.
2. Add 100 µL of 45 mM sodium acetate, vortex, and check pH with pH paper (should be ~ 4.9).
3. Remove two 40-µL aliquots for endogenous glucose assay, keep in ice.
4. To the remaining 120 µL sample, add 3 µL of the 1:50 diluted amyloglucosidase and vortex, and allow the amyloglucosidase to convert the glycogen to glucose moieties for 60 min.

Flow chart for lactate and pyruvate:

	Lactate				Pyruvate			
Reactions	Lactate + $NAD^+ \xrightarrow{LDH}$ pyruvate + NADH + H^+ Pyruvate + glutamate $\xrightarrow{GPT}$ alanine + αKG				NADH + pyruvate + $H^+ \xrightarrow{LDH}$ NAD^+ + lactate			
Reagent	**Stock Conc.**	**Reagent**	**Volume**	**Final Conc.**	**Stock Conc.**	**Reagent**	**Volume**	**Final Conc.**
	1M	AMP buffer pH 9.9	1mL	50mM	1M	Phosphate buffer pH 7	1mL	50mM
	0.1M	NAD^+	100µL	0.5mM	1M	$MgCl_2$	40µL	2mM
	1M	glutamate	20µL	1mM	10mM	ADP	400µL	200µM
			Final volume:	*20mL*	2mg/mL	NADH		50-150µM
	10µg/mL	GPT	10µL	100µg/mL			*Final volume*	*20mL*
	0.5mg/mL	LDH	2µL	1µg/mL	0.5mg/mL	LDH	2µL	1µg/mL
Step 1	Add 10µL sample to 1mL of lactate reagent, vortex.				Add 10µL sample to 1mL of pyruvate reagent, vortex.			
Step 2	Add 10µL of diluted GPT.				First reading at 340nm.			
Step 3	First reading at 340nm.				Add 2µL LDH and vortex.			
Step 4	Add 10µL of LDH, allow reaction to continue until completion.				Take second reading at 340nm.			
Step 5	Take second reading at 340nm.							
Rxn time	8-12 min				10-15 min			
Brain conc.	~1.3 mM				~0.08 mM			

Abbreviations used: LDH- lactate dehydrogenase; GPT- glutamate-pyruvic transaminase; AMP- 2-amino-2-methylpropanol

5. Remove two more 40-µL aliquots for glycogen assay, keep in ice.
6. Make blanks by adding 100 µL of 0.03 N HCl to 100 µL of 45 mM sodium acetate; take two 40-µL aliquots.
7. Add 1 mL glucose reagent (**Subheading 2.6., step 1**) to each of the 40-µL aliquots.
8. Take an initial reading at 340 nm (R1).
9. Add 10 µL of the diluted hexokinase (**Subheading 2.7., step 7**) to start the reaction; vortex.
10. Take a second reading at 340 nm (R2).
11. Calculations:

a. $$\Delta\mu M = \Delta \text{Optical density} - \text{blank} \times \frac{1}{0.00627} \times \left(\frac{\text{total volume of reaction}}{\text{volume of sample added}}\right)^{*}$$

b. * For example, Dilution factor $= \left(\frac{1050}{40}\right)\left(\frac{200}{100}\right) \times 0.6^{**}$

** The total volume in milliliters of **steps 1** and **2** from **Subheading 3.2.3**.

c. To calculate the concentration, the total amount of metabolite can be expressed in terms of wet weight, dry weight, or protein.

d. Total glycogen content = (glucose + glycogen) measurement − glucose measurement.

Flow Chart for glucose and glycogen:

	Glucose	**Glycogen**
Reactions	Glucose + ATP $\xrightarrow{HK}$ G6P + ADP G6P + $NADP^+$ $\xrightarrow{G6PDH}$ 6-PG + NADPH + H^+	Glycogen $\xrightarrow{AG}$ glucose Glucose + ATP $\xrightarrow{HK}$ G6P − ADP G6P + $NADP^+$ $\xrightarrow{G6PDH}$ 6-PG + NADPH
Glycogen to glucose reagent		**Stock Conc.** / **Reagent** / **Volume** / **Final Conc.** 45mM Na acetate 250µg/mL AG 1µL 0.5µg/mL ddH_2O 49µL *Final volume: 50µLs*
Glucose reagent	**Stock Conc.** / **Reagent** / **Volume** / **Final Conc.** 1M Tris-HCl pH 8.0 500µL 50mM 1M $MgCl_2$ 50µL 5mM 0.1M $NADP^+$ 40µL 400µM 0.1M ATP 50µL 500µM 5mg/mL G6PDH 1µL 0.5µg/mL *Final volume: 10mLs* 10mg/mL hexokinase 25µL 250µg/mL : Glucose reagent 975mL *Final volume: 1mL*	
Step 1	Add 10µL of sample to 1mL of glucose reagent, vortex.	Heat homogenate at 60°C for 10min.
Step 2	Take an initial reading at 340nm.	Add 100µL 45mM Na acetate.
Step 3	Add 10µL hexokinase and vortex. Allow reaction to go to completion	Remove two 40µL aliquots.
Step 4	Take a second reading at 340nm.	Add 3µL AG.
Step 5		Remove two 40µL aliquots, incubate 60min.
Step 6		Add 1mL conversion reagent to aliquots.
Step 7		Take an initial reading at 340nm.
Step 8		Add 10µL hexokinase and vortex.
Step 9		Take a second reading at 340nm.
Rxn time	4-6 min	glycogen hydrolysis 60 min glucose assay 4-6 min
Brain conc.	~1.82 mM	~1.72 mM

Abbreviations used: HK- hexokinase; AG- amylo-α-1,4-α-1,6-glucosidase; G6PDH- glucose-6-phosphate dehydrogenase

3.4.5. R-β-Hydroxybutyrate Measurement (See ***Note 24****)*

1. Add 30 µL of the prepared sample to 1 mL reagent 1 plus 1 mL ddH_2O. Vortex.
2. Take an initial reading at 340 nm.
3. Add 20 µL BHB-DH; vortex. Incubate for 20 min.
4. Take a second reading at 340 nm.

3.4.6. Spectrophotometric Acetoacetate Measurement

1. Add 250 µL of the prepared sample (*see* **Note 25**) to 1 mL acetoacetate reagent plus 1 mL ddH_2O; vortex.

2. Take an initial reading at 340 nm.
3. Add 20 µL BHB-DH (*see* **Note 26**); vortex. Incubate for 20 min.
4. Take a second reading at 340 nm.

	Beta-hydroxybutyrate (BHB)				Acetoacetate (AcAc)			
Reactions:	3-hydrobutyrate + NAD^+ $\xrightarrow{\text{BHB-DH}}$ acetoacetate + NADH				Acetoacetate+NADH $\xrightarrow{\text{BHB-DH}}$ 3-hydrobutyrate +NAD^+			
Reagents:	**Stock Con.**	**Reagent**	**Volume**	**Final Conc.**	**Stock Con.**	**Reagent**	**Volume**	**Final Conc.**
	1M	Tris*	2.5mL	0.1M	0.1M	phosphate buffer	10mL	0.1M
	1M	$MgSO_4$*	250µL	10mM	2mg/mL	NADH	860µL	158µg/mL
	0.1M	EDTA*	1.25mL	5mM		*Qs to final volume:*		*10.86mL*
		Hydrazine hydrate	1.18g	1.47M	5mg/mL	BHB-DH	40µL	0.2mg/mL
		Qs to final volume:		*25mL*				
	80mg/mL	NAD	455µL	1.5mg/mL				
	5mg/mL	BHB-DH	40µL	0.2mg/mL				
Step 1	Add 30µL sample to 1mL of BHB reagent 1, plus 1mL of ddH_2O, vortex.				Add 250µL of prepared sample to 1mL of acetoacetate reagent plus 1mL of ddH_2O vortex.			
Step 2	Take an initial reading at 340nm.				Take an initial reading at 340nm.			
Step 3	Add 20µL BHB-DH, vortex. Allow the reaction to proceed to completion.				Add 20µL BHB-DH, vortex. Allow the reaction to proceed to completion.			
Step 4	Take a second reading at 340nm.				Take a second reading at 340nm.			
Rxn time	20min				20min			
Brain conc.	~0.01µM baseline to 0.1µM in a ketotic state				~0.01µM - 0.1µM in a ketotic state			

Abbreviations used: BHB-DH- betahydroxybutyrate dehydrogenase; * components of alpha mix.

4. Notes

1. These assays are generally performed in our laboratory using male Wistar rats, 100–400 g in weight.
2. Glutamate is made by adding 0.9 M NaOH to bring the pH to 9.8.
3. The hydrazine hydrate buffer is made fresh, otherwise the lactate is unstable.
4. During placement of the arterial line cannula, ensure that the sutures are not too tight and check if blood flows by opening the distal end of the cannula.
5. The funnel may be secured by using a purse string suture around the funnel to the skin.
6. Depending on anesthetic used, arterial mBP should be about 85–125 mmHg; if it is below this range, then reduce the anesthetic and wait until BP is within range; if it is above this range, then check blood gases to ensure proper oxygenation and ventilation and if necessary increase the amount of anesthetic.
7. To avoid freezing of the airway, the liquid nitrogen should be poured in a manner by which the overflow does not occur around the orotracheo-cannula area.
8. If mBP is not half of baseline at 6 min, then this could be due to artifact as a result of obstructed line; after 6 min, the animal should be immersed in liquid nitrogen.

9. Inadvertent warming of the tissue may result in changes in metabolites (restoration of metabolism in situ) ***(12)***.
10. All instruments should be chilled to −20° C prior to use, and care should be taken to avoid heating by handling or from the friction of the gas driven saw.
11. Brains tend to shatter in temperatures below −20° C.
12. Oxidation of the reduced forms of pyridine nucleotides in tissue extract may be avoided by using an alkaline extraction technique.
13. If complete extraction of metabolites is a concern, then the multiple extraction method can be used. This is accomplished by re-extracting the resulting protein pellet from the first extraction and centrifugation.
14. When referring to literature values, they are often reported in different units. The relationship of these units is approximately 11 mg protein in 100 mg of wet weight tissue and 20 mg of dry weight in 100 mg of wet weight tissue.
15. At no point should the extracts be exposed to temperatures above 4° C.
16. An alternate neutralizing solution can be used (0.29 mL of a 2 N KOH, 0.4 M imidazole base, and 0.4 M KCl mixture) per milliliter of acid extract.
17. The pH of these neutralized extracts should be determined before enzymatic analysis to ensure the proper neutralization range of pH 5.0–8.0 for amyloglucosidase.
18. It is important that blanks, standards, and samples have identical final volumes, because the reagent volume affects the emitted light.
19. The myokinase is in a suspension, which may contain contaminants that could hinder the reaction. This may be minimized by centrifuging the solution, removing the supernatant, and reconstituting with ddH_2O.
20. Because skin contains high amounts of lactate, it is extremely important to minimize lactate contamination by using glassware that has been thoroughly rinsed with ddH_2O and to wear gloves at all times during the analysis.
21. Centrifugation and reconstitution of the LDH and GPT helps to remove any contamination and to minimize background.
22. Calculations: Ideally, metabolite assays should be designed so that the change in optical density at 340 nm will allow a maximal Δ OD and other reagents, other than the metabolite to be measured, should not be limiting in concentration. For example, if measuring NAD, the $\Delta OD < 1.2$, then NAD is the limiting factor rather than the substrate. If measuring NADH, the $\Delta OD < 0.3$, then NADH is the limiting factor rather than the substrate. It is essential that any potentially interfering reagents be treated to minimize background.
23. It is important that all reagents are kept in ice until reading and that reactions are run at room temperature.
24. Note that all *R*-BHB reactions should be done at 37° C. Owing to the broad range of ketone bodies in brain, *see* **ref. *13*** for reference.
25. Owing to low endogenous levels of acetoacetate, additional sample volume may be required to produce a measurable reaction.

26. Note that *R*-BHB is the endogenous form of ketone; thus, it is essential to verify the *R*-specificity and *S*-specificity of the BHB-DH (as well as standards). If the enzyme is not pure, then a conversion factor may be necessary for calculation.

Acknowledgment

Preparation of this chapter was supported in part by USPHS grants NS38632 and GM066309.

References

1. Greengard P (1956) Determination of intermediary metabolites by enzymic fluorimetry. *Nature* **178**: 632–4.
2. Lowry OH, Passonneau JV (1972) *A Flexible System of Enzymatic Analysis.* New York: Academic Press.
3. Lust WD, Feussner GK, Barbehenn EK, Passonneau JV (1981) The enzymatic measurement of adenine nucleotides and P-creatine in picomole amounts. *Anal. Biochem.* **110**: 258–66.
4. Lundin A, Richardsson A, Thore A (1976) Continuous monitoring of ATP-converting reactions by purified firefly luciferase. *Anal. Biochem.* **75**: 611–20.
5. Siesjo BK (1978) Brain energy metabolism and catecholaminergic activity in hypoxia, hypercapnia and ischemia. *J. Neural Transm. Suppl.* 17–22.
6. Lenox RH, Kant GH, Meyerhoff JL (1982) Rapid enzyme inactivation. In: Lajtha A, ed. *Handbook of Neurochemistry*. New York: Plenum, pp. 77–102.
7. Lust WD, Passonneau JV, Veech RL (1973) Cyclic adenosine monophosphate, metabolites, and phosphorylase in neural tissue: a comparison a methods of fixation. *Science* **181**: 280–2.
8. Lust WD, Murakami N, de Azeredo F, Passonneau JV (1980) A comparison of methods for brain fixation. In: Passonneau JV, Hawkins RA, Lust WD, Welsh RA, eds. *Cerebral Metabolism and Neural Function*. Baltimore: Williams and Wilkins, pp. 10–9.
9. Lust WD, Ricci AJ, Selman WR, Ratcheson RA (1989) Methods of fixation of nervous tissue for use in the study of cerebral energy metabolism. In: Boulton, AA; Baker, GB; Butterworth, RF, eds. *Carbohydrates and Energy Metabolism*. Totowa, NJ: Humana Press, pp. 1–42.
10. Goldberg ND, Passonneau JV, Lowry OH (1966) Effects of changes in brain metabolism on the levels of citric acid cycle intermediates. *J. Biol. Chem.* **241**: 3997–4003.
11. Ponten U, Ratcheson RA, Salford LG, Siesjo BK (1973) Optimal freezing conditions for cerebral metabolites in rats. *J. Neurochem.* **21**: 1127–38.
12. Mrsulja BB, Ueki Y, Lust WD (1986) Regional metabolite profiles in early stages of global ischemia in the gerbil. *Metab. Brain Dis.* **1**: 205–20.
13. Harik SI, al Mudallal AS, LaManna JC, Lust WD, Levin BE (1997) Ketogenic diet and the brain. *Ann. N. Y. Acad. Sci.* **835**: 218–24.

8

A Method for Isolating Prosurvival Targets of NF-κB/Rel Transcription Factors

Christian Kuntzen, Francesca Zazzeroni, Can G. Pham, Salvatore Papa, Concetta Bubici, James R. Knabb, and Guido Franzoso

Summary

NF-κB/Rel transcription factors are critical regulators of immunity, inflammation, development, and cell survival. Activation of NF-κB inhibits programmed cell death (PCD) triggered by tumor necrosis factor α (TNFα) and several other stimuli. The prosurvival activity of NF-κB is also crucial to lymphopoiesis, neuroprotection, tumorigenesis, and cancer chemoresistance. The characterization of the downstream targets that mediate the prosurvival activity of NF-κB is therefore a topic of intense investigation. Early screens aimed at identifying these genes were mainly based on expression criteria and so were poised to only isolate genes already known to have protective effects. Here, we describe a new method for the identification of these genes, whereby expression libraries are screened for their ability to halt PCD in NF-κB-deficient cells. This complementation approach provides substantial advantages over other approaches, as it enables functional assessment of isolated genes without any preconceived notion about their sequence or presumed role. Expression libraries are generated from cells that are resistant to TNFα-induced cytotoxicity and are then enriched in prosurvival genes upon selection with TNFα in *NF-κB/RelA*-null cells, which are highly susceptible instead to this cytotoxicity. Upon enrichment, libraries are screened through a randomized two-step approach, whereby cDNAs are first tested for cytoprotective function and then for differential expression in NF-κB-proficient and NF-κB-deficient cells.

Key Words: NF-κB; RelA; TNFα; apoptosis; programmed cell death; library screen; transcriptional regulation; spheroplasts.

From: *Methods in Molecular Biology, vol. 399: Neuroprotection Methods and Protocols*
Edited by: T. Borsello © Humana Press Inc., Totowa, NJ

1. Introduction

Transcription factors of the NF-κB/Rel family are central regulators of inflammation, immunity, development, and cell survival ***(1–3)***. Activation of NF-κB blocks programmed cell death (PCD) triggered by the proinflammatory cytokine tumor necrosis factor α (TNFα) and various other stimuli. The prosurvival activity of NF-κB is essential for lymphopoiesis, osteogenesis, neuroprotection, and tissue response to injury ***(1–3)***. When deregulated, this activity may also contribute to the pathogenesis of human diseases such as chronic inflammatory illnesses and various cancers and represents therefore a major target for therapeutic intervention ***(1–4)***. By and large, the NF-κB-mediated protective function is mediated through upregulation of target genes, and so, the characterization of these genes is a topic of intense investigation ***(1,2)***.

Early screens aimed at identifying these genes were mainly based on expression criteria, and consequently, although they have led to the identification of important targets of NF-κB, such as the Bcl-2-family members Bcl-x_L and A1/Bfl1, the adaptors TRAF1 and TRAF2, and the caspase blockers c-IAP1, c-IAP2, and c-$FLIP_L$, these screens were poised to isolate genes that were already known to have protective activity ***(1,2,5–11)***. Such screens involved methods such as differential display, serial analysis of gene expression (SAGE), and gene-array hybridization and were designed to identify genes that were differentially expressed in NF-κB-proficient and NF-κB-deficient cells, regardless of function. Thus, an inherent complication of these screens was the concomitant isolation of genes that are under the control of NF-κB but are not necessarily involved in blocking PCD.

To overcome these problems, and selectively pursue the specific subset of NF-κB-regulated genes that inhibit cell death, we have developed an approach whereby expression libraries are screened for the ability to block PCD in NF-κB-deficient cells ***(12,13)***. This functional approach provides substantial advantages over the aforementioned methods. First, it ensures that isolated genes have antiapoptotic activity (intended here as synonymous of protective activity). Second, unlike other methodologies, it enables a functional assessment of candidate genes without any preconceived notion about their sequence or presumed physiological role and therefore represents an unbiased approach ***(1,2,12,13)***. Third, because isolated genes are already contained in a mammalian expression vector, it allows for direct use of these genes in functional assays, without a need for laborious and time-consuming subclonings.

In this protocol, expression libraries are generated using mRNA from cells that are refractory to TNFα-induced cytotoxicity and are subsequently enriched in prosurvival genes upon selection with TNFα in *NF-κB/RelA*-null cells,

which are highly susceptible to this cytotoxicity *(12–14)* (**Figs. 1** and **2**). Upon enrichment, libraries are screened through a randomized two-step approach, whereby isolated cDNAs are first tested for function in cytoprotection assays and then for basal and TNFα-inducible expression in NF-κB-proficient and NF-κB-deficient cells (**Figs. 3 and 4**). We outline both theoretical considerations and practical suggestions that are critical for the success of the screen.

2. Materials

2.1. Cell Treatment

1. Dulbecco's modified Eagle's medium (DMEM) (Invitrogen/Gibco, Carlsbad, CA), supplemented with 10% fetal bovine serum (Sigma-Aldrich, St. Louis, MO), Penicillin/Streptomycin 100 U/mL/100 μg/mL (Invitrogen), and 2 mM L-Glutamine (Invitrogen) for *RelA*$^{-/-}$ 3T3 cells. For *RelA*$^{-/-}$ mouse embryonic fibroblasts (MEFs), 1 × HEPES buffer (Invitrogen) is also added. Gentamicin sulfate 15 μg/mL (Invitrogen) is used for spheroplast transfections.
2. Trypsin/EDTA (0.25%/1 mM) (Cellgro, Herndon, VA).
3. Phosphate-buffered saline (PBS), pH 7.4 (Invitrogen/Gibco).
4. T175 tissue culture flasks (BD Falcon, Bedford, MA).
5. Murine TNFα (Peprotech, Rocky Hill, NY). Dissolve 100 μg (1×10^6 U) in 1 mL ice-cold H_2O, mix by pipetting, and freeze in aliquots at −80° C. Do not refreeze upon use. Prepare dilutions on ice and work quickly.
6. NIH-3T3 cells (ATCC, Manassas, VA).

2.2. RNA Extraction and cDNA Synthesis and Preparation

1. Falcon 2096 and 2059 tubes (BD Falcon).
2. Trizol (Invitrogen); Diethyl Pyrocarbonate (DEPC)-treated ddH_2O (Ambion, Austin, TX).
3. Phenol Ultra Pure, buffer saturated (Invitrogen). Store at 4° C. The phenol/chloroform solution (1:1) is also stored at 4° C. Protect from light.
4. Chloroform (J. T. Baker, Phillipsburg, NJ). Store at room temperature.
5. DEPC-treated ddH_2O (Ambion). Store at room temperature.
6. Isopropanol (J. T. Baker). Store at room temperature.
7. Superscript™ Choice System for cDNA Synthesis (Invitrogen/Gibco).
8. Oligotex Direct mRNA Mini Kit (Qiagen, Valencia, CA).
9. Poly dT-primer: 5′-GGATAGTCCAACA<u>GCGGCCGC</u>T_{30}(A/C/G)N-3′ (the *Not*I restriction site is underlined).
10. *Sfi*I adapters: 5′-GAAGCCCTCG-3′ (sense); 5′-GGGCTTC-3′ (antisense). Order PAGE-purified with 5′-phosphate. Dissolve in ddH_2O to 100 μM and measure concentration using a spectrophotometer (OD_{260}).
11. Annealing buffer (10×): 100 mM Tris–HCl (pH 7.5), 1 M NaCl, and 10 mM EDTA (pH 8.0). Stable at room temperature for several months.

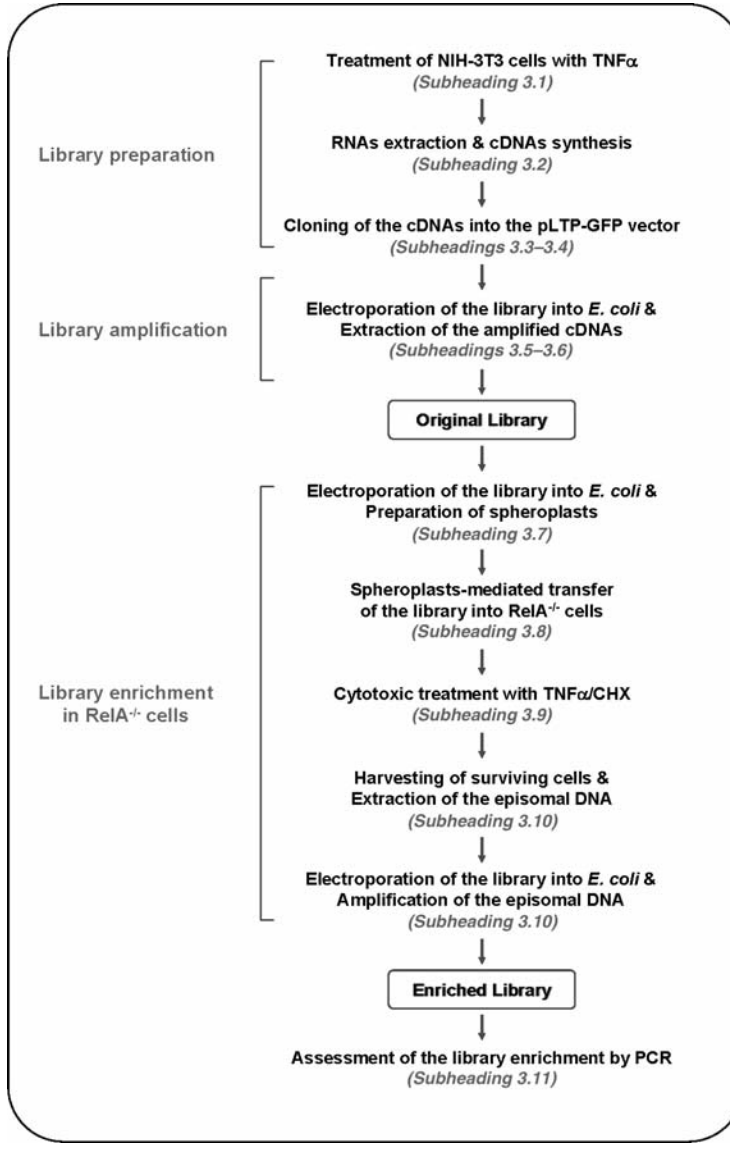

Fig. 1. Schematic overview of the library generation and the multistep enrichment protocols. mRNA pools are enriched in NF-κB target genes through treatment of NF-κB-proficient, NIH-3T3 cells with tumor necrosis factor α (TNFα). cDNA is synthesized from these mRNA pools via reverse-transcriptase reaction and cloned into the pLTP-GFP vector to generate the "original library." After amplification in

2.3. Preparation of the pLTP-GFP Vector

1. pEGFP-N1 (Clontech, Palo Alto, CA).
2. *Sfi*I (20,000 U/mL), *Not*I (10,000 U/mL), *Eco*RV (20,000 U/mL), *Bsr*GI (4000 U/mL), BSA (10 μg/μL), NEB2 buffer (10×) (50 mM NaCl, 10 mM Tris–HCl, 10 mM $MgCl_2$, and 1 mM Dithiothreitol (DTT), and NEB3 buffer (10×) (100 mM NaCl, 50 mM Tris–HCl, 10 mM $MgCl_2$, and 1 mM DTT (New England Biolabs, Ipswitch, MA).
3. EluQuick DNA Purification Kit (Whatman/Schleicher & Schuell, Florham Park, NJ).
4. Calf intestinal phosphatase (CIP) (10,000 U/mL) (New England Biolabs).
5. pLTP ***(15)***.
6. Sodium acetate (pH 5.2) (Sigma-Aldrich). Prepare a 3 M solution in ddH_2O and adjust the pH to 5.2 using acetic acid. Filter through 0.22 μm and store at room temperature.
7. 200-Proof ethanol (Aaper Alcohol and Chemical Co., Shelbyville, KY).

2.4. Ligation of the cDNA to pLTP-GFP

1. T4 ligase (2,000,000 U/mL), T4 ligase buffer (Invitrogen).
2. Glycogen (5 mg/mL) (Ambion). Store at −20° C.
3. Ammonium acetate (Sigma-Aldrich). Prepare a 7.5 M solution in ddH_2O. Filter through 0.22 μm and store at room temperature.
4. 200-Proof ethanol (Aaper Alcohol and Chemical Co.).
5. Tris–EDTA solution (TE), 100× concentrate, for Molecular Biology (Sigma-Aldrich). Prepare 1× stocks in ddH_2O. Store at room temperature.

2.5. Electroporation of the Library

1. ElectroMAX™ DH10B™ Competent Cells (Invitrogen). Store at −80° C.
2. SOC medium (Invitrogen). Store at room temperature.
3. BTX Electro Cell Manipulator 600 (Harvard Apparatus, Holliston, MA).
4. BTX Electroporation cuvettes plus 640 (Harvard Apparatus).
5. 250-mL Centrifuge tubes (Corning, Corning, NY).

◀

Fig. 1. (Continuation) *Escherichia coli*, this library is transfected into $RelA^{-/-}$ 3T3 cells by the use of the spheroplast method, and cells are subjected to cytotoxic treatment with TNFα plus cycloheximide (CHX). Episomal plasmids are then recovered from surviving cells (likely to express antiapoptotic library cDNAs) and amplified in *E. coli* for a subsequent round of enrichment in $RelA^{-/-}$ cells. The "enriched library" is obtained after a total of four cycles of selection in $RelA^{-/-}$ cells. Enrichment of this library in protective cDNAs is finally verified by the use of standard semiquantitative PCR.

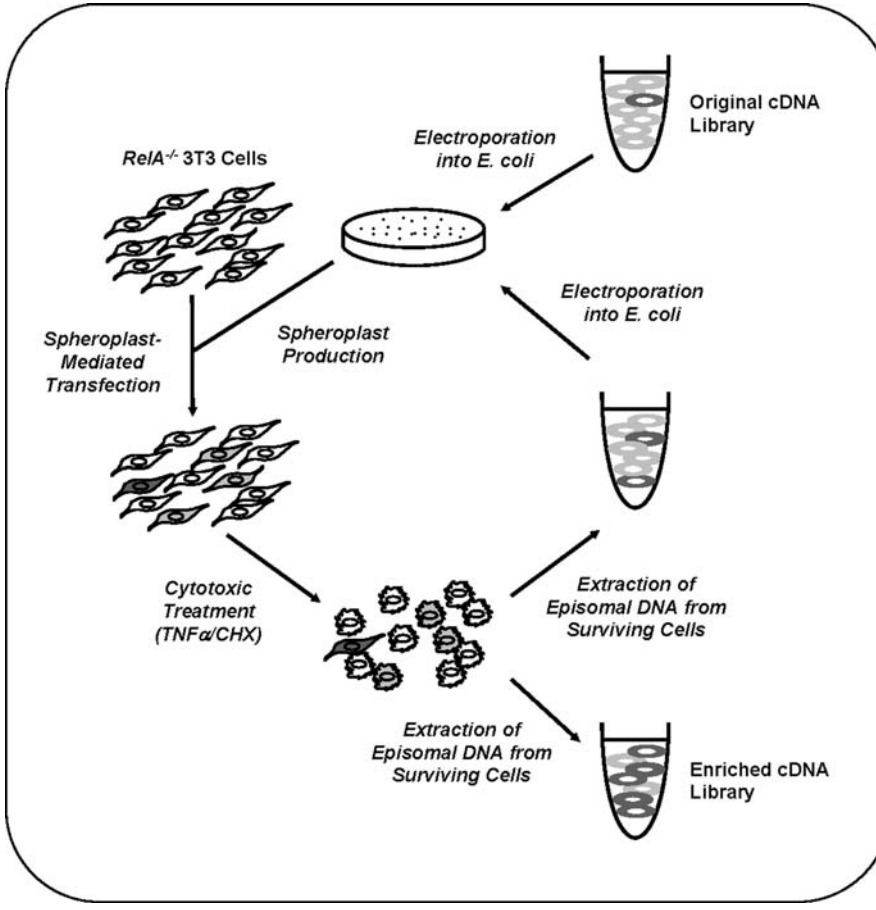

Fig. 2. Schematic representation of the library enrichment protocol. The cDNA library is electroporated into *Escherichia coli*, and spheroplasts are prepared for transfection of this library into $RelA^{-/-}$ 3T3 cells. Cell death is then induced with tumor necrosis factor α (TNFα) and cycloheximide (CHX), and the library is isolated from surviving cells, amplified, and then used for either the next cycle of selection in $RelA^{-/-}$ cells or the randomized analysis of its cDNAs. Protective cDNAs (empty ovals) and cells expressing these cDNAs are in dark gray. Cell containing nonprotective cDNAs and these cDNAs are in light gray.

2.6. Cell Plating and DNA Extraction

1. Carbenicillin (Sigma-Aldrich). Prepare 100 mg/mL stocks in ddH_2O. Store in aliquots at −20° C.

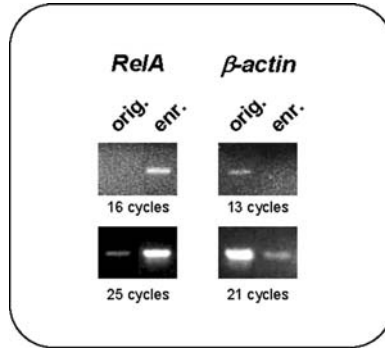

Fig. 3. Successful enrichment of the library in protective genes following selection with tumor necrosis factor α (TNFα). PCR assays showing *RelA*-specific and *β-actin*-specific PCR products in the original (orig.) and enriched (enr.) libraries. Ethidium bromide staining of PCR products isolated from different cycles of PCR amplification is as indicated. The assays show that upon selection with TNFα, the library is enriched in *RelA*-specific cDNAs (compare the signal intensities yielded by original and enriched library templates at the same cycle of amplification and those yielded by 16 cycles of amplification with the enriched library and 25 cycles of amplification with the original library). Upon selection, *β-actin*-specific cDNAs are concomitantly impoverished (compare the signal intensities yielded by original and enriched library templates at the same cycle of amplification and those yielded by 13 cycles of amplification with the original library and 21 cycles of amplification with the enriched library).

2. Ampicillin (Sigma-Aldrich). Prepare 100 mg/mL stocks in ddH_2O. Store in aliquots at −20° C.
3. LB agar (Lennox L agar) and LB broth base (Invitrogen).
4. 150 mm × 15 mm Polystyrene dishes (Fisher Scientific, Pittsburgh, PA).

2.7. Preparation of Spheroplasts

1. ElectroMAX™ DH10B™ Competent Cells (Invitrogen). Store at −80° C.
2. Trizma (Sigma-Aldrich). Use concentrated (37%) HCl to prepare 1 M Tris–HCl solutions. Accurately measure the pH at room temperature. Filter through 0.22 μm and store at room temperature.
3. Sucrose (Sigma-Aldrich). Store at room temperature.
4. Solution I: 20% sucrose (w/v) and 50 mM Tris–HCl (pH 8.0). Store at 4° C.
5. Solution II: 5 mg/mL lysozyme (Sigma-Aldrich); prepare fresh in 250 mM Tris–HCl (pH 8.0). Lysozyme is ineffective at a pH < 8.0.
6. Solution III: 250 mM EDTA (Sigma-Aldrich). Store at room temperature.
7. Solution IV: 50 mM Tris–HCl (pH 8.0). Store at room temperature.

8. Solution V: 10% sucrose (w/v) and 10 mM $MgCl_2$ in DMEM without fetal calf serum (FCS). Filter through 0.45 μm. Store at 4° C.
9. Chloramphenicol (CAP) (Sigma-Aldrich). Prepare stock solution at 50 mg/mL in ddH_2O and store at room temperature. It may lose 50% of activity within 9 months.
10. 500-mL Polypropylene bottles (Beckman #355605, Fullerton, CA).
11. 850 cm^2 Roller bottles (2 L), polystyrene (Corning).
12. JLA-10.500 rotor and J2-HS Beckman high-speed centrifuge.

2.8. Spheroplast-Mediated Transfer of the Library Into RelA$^{-/-}$ Cells

1. Adapters for 100-mm plates in CS-6R centrifuge (Beckman #359474).
2. PEG-1000 solution (Sigma-Aldrich): 50% (w/v) in DMEM without FCS (pH 7.0). Melt PEG-1000 by heating at 60° C and aliquot in 50-mL tubes at 25 mL per tube. Weigh and store tubes at 4° C. Prior to use, thaw aliquots at 60° C and add DMEM without FCS to a final concentration of 50% (w/v). Filter through 0.45 μm. Adjust the pH, a critical parameter, by using DMEM from an unopened bottle.

2.9. Cytotoxic Treatment With TNFα

1. Cycloheximide (CHX; Sigma-Aldrich). Prepare a 10 mg/mL stock in ethanol and store in aliquots at −80° C.

2.10. Extraction of Episomal DNA From Surviving Cells

1. Lympholyte M (Ficoll, Accurate Chemical and Scientific Corp., Westbury, NY).
2. Trypsin/EDTA (0.25%/1 mM) (Cellgro).
3. EDTA (Sigma-Aldrich). Prepare a 0.5 M stock in ddH_2O, adjust pH to 8.0 using NaOH, and filter through 0.22 μm. Store at room temperature. Dilute in ddH_2O to obtain a 10 mM solution.
4. 10% SDS solution (lauryl sulfate/sodium dodecyl sulfate; Sigma-Aldrich). Prepare 10% (w/v) stock solution in water. Store at room temperature.
5. Tris–SDS (10 mM Tris–HCl [pH 8.0], 1.2% SDS). Prepare from stock solutions and filter through 0.22 μm. Store at room temperature.
6. NaCl (Sigma-Aldrich). Prepare a 5 M stock solution. Store at room temperature.
7. Sodium acetate (pH 5.2) (Sigma-Aldrich). Prepare a 3 M solution in ddH_2O and adjust the pH to 5.2 using acetic acid. Filter through 0.22 μm and store at room temperature.

2.11. Assessment of Library Enrichment by PCR

1. *Taq* polymerase (Sigma-Aldrich), 25 mM $MgCl_2$ stock solution (Sigma-Aldrich), and 100 mM dNTP mix (Amersham Biosciences, Piscataway, NJ). Dilute the dNTPs to 10 mM in H_2O. Store in 10-μL aliquots at −20° C.
2. Primers: *β-actin*, 5′-GATGACGATATCGCTGCGCTG-3′ (sense), 5′-GTA CGACCAGAGGCATACAGG-3′ (antisense); *RelA*, 5′-CCTTTCAATGGACCA ACTGAACCC-3′ (sense), 5′-CTCAGCTGTGGAGTGAGACATGG-3′ (antisense).

2.12. Step 1: Cytoprotection Assays in $RelA^{-/-}$ Cells

1. QiaPrep Spin Mini Prep Kit (Qiagen).
2. SuperFect transfection reagent (Qiagen).

3. Methods

The protocol described is aimed at identifying novel protective targets of NF-κB *(1,2)*. This protocol involves generation of expression libraries and their enrichment in prosurvival cDNAs through consecutive cycles of transfection into immortalized *NF-κB/RelA*$^{-/-}$ fibroblasts, induction of cytotoxicity with TNFα, recovery of plasmids from surviving *RelA*$^{-/-}$ cells, and amplification of isolated libraries in *Escherichia coli* (**Figs. 1** and **2**). The success of the screen depends on at least four critical parameters (*see also*: **Note 15**) (1): high expression of the libraries in *RelA*$^{-/-}$ cells; (2) inefficient co-transfection of multiple library plasmids into a single cell; (3) low background viability following cytotoxic treatment; and (4) efficient recovery of episomal DNA from surviving cells. For the success of the screen, it is vital that these parameters are carefully optimized beforehand.

Owing to the wide availability of suitable libraries from several vendors (e.g., Clontech, Stratagene, and Life Technologies) and of excellent commercial kits for cDNA synthesis and cloning, we do not describe in detail the procedures involved in the library construction. To this end, we have successfully used the SuperScript™ Choice System for cDNA Synthesis (*see* **Subheading 2.2.**) and therefore refer to this kit and the enclosed instruction manual. The source of the mRNA used for cDNA synthesis and the choice of the vector used for library construction, however, should be carefully considered (*see* **Note 1**).

3.1. Cell Treatment

1. Maintain NIH-3T3 cells in three T175 tissue culture flasks in 30 mL complete DMEM with supplements (*see* **Heading 2.**) per flask. At near-confluence, aspirate the medium, wash once with ice-cold PBS, add 2 mL trypsin/EDTA, and incubate for 3 min at room temperature. Tap the flasks to detach the cells and add 10 mL complete DMEM to each flask. Pool cells into a sterile 50-mL Falcon tube and centrifuge for 5 min at $350 \times g$ at room temperature.
2. Aspirate the supernatant and resuspend the pellet in 5 mL complete DMEM at room temperature. Pipette gently to break up cell clumps, add an additional 20 mL medium, and dispense 1 mL into each of 24 T175 flasks (1:8 dilution or $\sim 2 \times 10^6$ cells per flask). Add 30 mL warm DMEM to each flask, mix gently, and incubate at 37° C in 5% CO_2 for 48 h.

3. When cells are approximately 90% confluent, reduce the volume of medium in each flask to 9 mL (*see* **Note 2**). Return the flasks to the incubator and allow cells to rest for at least 2–4 h (*see* **Note 3**).
4. Resuspend 1 vial of mouse recombinant TNFα (10^6 U) in 1 mL sterile water, mix vigorously by pipetting, and dilute 1:100 using prewarmed, complete DMEM to a total volume of 25 mL (10× stock; 10,000 U/mL). Mix and immediately add 1 mL 10× TNFα solution to each of the 24 T175 flasks (final TNFα concentration of 1000 U/mL), keeping the flasks inside the incubator (*see* **Note 3**). Stimulate six or fewer flasks at a time (*see* **Note 4**).
5. Incubate at 37° C for 2.5 or 5.5 h. The purpose of this treatment is to induce upregulation of NF-κB target genes ***(1,2,10)***.

3.2. RNA Extraction and cDNA Synthesis and Preparation

1. Label all necessary 15-mL Falcon 2096 tubes. Harvest 12 flasks for each time point in two consecutive groups of six flasks. Carefully aspirate the medium, draining by gravity all residual medium present in the flask, and add 5 mL Trizol to each flask. Ensure that this covers the entire surface of the flask and leave at room temperature for 2–5 min, until all cells are lysed. Collect the Trizol lysates by pipetting and transfer into 15-mL tubes. Wash each flask with an additional 3 mL Trizol and add to the same 15-mL tube. These may now be stored indefinitely at −80° C, provided that the caps are protected with parafilm, or used immediately for extraction of the RNA.
2. Add 0.2 mL chloroform for each milliliter of Trizol (i.e., 1.6 mL for 8 mL Trizol), mix vigorously for approximately 20 s, and centrifuge at 3200 × *g* for 1 h at room temperature (Beckman tabletop centrifuge with GH 3.8 rotor).
3. Collect the aqueous phase from each tube (∼ 6 mL), without disturbing the interphase, and distribute it equally into two separate 10-mL Falcon 2059 tubes (*see* **Note 5**). Add 0.5 mL isopropanol for each milliliter of Trizol used. Tubes should not be filled with a volume greater than 5 mL.
4. Cover tubes with parafilm, vortex, and incubate for 10 min at room temperature.
5. Centrifuge samples at 15, 000 × *g* for 10 min at 4° C using a Beckman high-speed centrifuge and a JA 20.1 rotor.
6. Retrieve the tubes without disturbing the RNA pellets, aspirate the supernatants, and wash the pellets once with 70% (v/v) ethanol in DEPC-treated ddH_2O.
7. Transfer samples to 1.5-mL Eppendorf tubes, pooling into each tube, the RNA pellets from six 15-mL tubes (or three T175 tissue culture flasks), and centrifuge at 7500 × *g* for 5 min at 4° C using an Eppendorf *5417C* microfuge.
8. Aspirate the supernatants and perform one additional wash with 70% ethanol.
9. Aspirate the supernatant and air-dry the pellet under a laminal flow hood for 5–10 min. Avoid excessive drying.

10. Dissolve the RNA using 100 µL DEPC-treated ddH_2O for each T175 flask of NIH-3T3 cells. Leave for 10 min at room temperature and then pipette vigorously to ensure complete solubilization of the RNA.
11. Further pool the samples and measure RNA concentrations using a spectrophotometer (OD_{260}). Twelve T175 flasks of NIH-3T3 cells typically yield 2.5 mg total RNA. If desired, the procedure can be scaled back by starting from fewer cells.
12. For cDNA synthesis, the total RNAs from cells stimulated for 2.5 and 5.5 h are pooled at a 1:1 ratio, and poly-A^+ RNA is isolated through two consecutive rounds of purification with the Oligotex Direct mRNA Kit, following the manufacturer's instructions; 1.5 mg of total RNA usually yields 10–15 µg poly-A^+ RNA.
13. The first cDNA strand is synthesized by reverse-transcriptase (RT) reaction using 5 µg pooled poly-A^+ RNA, 5 µg oligo(dT) primer (containing a *Not*I restriction site; *see* **Subheading 2.2., item 9**), 5 µL SuperScript™ II RT, and the SuperScript™ Choice System, following the instructions in the enclosed manual.
14. After the creation of blunt ends, the double-stranded cDNA is ligated to annealed *Sfi*I adapters (*see* **Subheading 2.2., item 10**) and then digested with *Not*I, in order to create sticky ends for directional cloning between the *Sfi*I and *Not*I restriction sites of pLTP-GFP (*see* **Subheading 3.3., item 3**). These procedures, as well as those involved in cDNA synthesis and poly-A^+ RNA purification (*see* **step 12**), are described in detail in the respective kit manuals. For these procedures, we refer therefore to these manuals.

3.3. Preparation of the pLTP-GFP Vector

1. The pLTP mammalian expression vector has been described previously by D'Adamio and colleagues ***(15)***. Key features of this vector are detailed in **Note 1**. This vector can be used for the generation of expression libraries. However, for some applications, it can be modified by the introduction of the DNA sequence encoding enhanced green fluorescent protein (eGFP) ***(16)***, resulting in the generation of pLTP-GFP and expression of library products as eGFP-fusion proteins ***(13)***. An advantage of this modification is that it enables direct visualization of the library products in transfected cells, *in vivo*. It also supplies a polypeptide sequence that can be targeted by commercial antibodies, to enable an initial biochemical characterization of encoded products (*see* also **Note 6**).
2. To generate pLTP-GFP, the 715-bp *Sma*I–*Bsr*GI fragment of pEGFP-N1 is ligated between the *Eco*RV and *Not*I sites of pLTP-Luc ***(15)***, along with the following oligonucleotide linker: 5′-*GTACA*AGGCCTCGAGGGCCTCATGAATCAGTCAGCGGCCGC**TGACTAA**CG**TAG***TG*-3′ (sense strand: partial *Bsr*GI and destroyed *Not*I sites are italicized; stop codons are in boldface; and internal *Sfi*I, *Xho*I, *Bsp*HI, and *Not*I sites are underlined).

3. To prepare pLTP-GFP for ligation of the cDNA, digest 30 μg of the vector with *Not*I, using 20 μL NEB3 buffer (10×), 2 μL BSA (10 μg/μL), 6 μL *Not*I, and ddH_2O to 200 μL.
4. Incubate at 37° C for 2 h and then verify complete digestion by analyzing a 3-μL aliquot of the reaction via standard agarose gel electrophoresis.
5. Load the digestion mix onto a 1% agarose gel and perform preparative agarose gel electrophoresis. Visualize with ethidium bromide (0.5 μg/mL) and excise the DNA band corresponding to the linearized vector (~7.5 kb).
6. Extract *Not*I-digested pLTP-GFP using the EluQuick Kit or an equivalent kit, following the manufacturer's instructions.
7. Add to the same 1.5-mL Eppendorf tube the linearized pLTP-GFP from **step 6, Subheading 3.3.**, 40 μL NEB2 buffer, 4 μL BSA, 8 μL *Sfi*I, and ddH_2O to 400 μL.
8. Incubate at 50° C for 2 h.
9. Verify digestion by performing standard agarose gel electrophoresis, using 6 μL of the reaction mix. If necessary, add an additional 2 μL *Sfi*I to the mix and let the reaction proceed for another hour.
10. Purify the digested pLTP-GFP vector by performing one phenol/chloroform (1:1; v/v) extraction followed by two extractions with chloroform.
11. Add 1/10 volume of 3 M sodium acetate (pH 5.2), mix, and then add 2.5 volumes of 200-proof ethanol. Incubate at −20° C for 15 min.
12. Spin using an Eppendorf microfuge at 20,000 × *g* for 15 min at room temperature, discard the supernatant, and wash the pellet twice with 70% ethanol.
13. Aspirate the supernatant, air-dry the DNA pellet under a laminal flow hood, and add 50 μL ddH_2O. Incubate at room temperature for approximately 10 min and pipette vigorously to achieve complete resuspension of the DNA.
14. Add to the same Eppendorf tube 10 μL NEB3 buffer, 30 μL ddH_2O, and 10 μL CIP.
15. Incubate for 1 h at 37° C.
16. Stop the reaction by incubating the sample at 72° C for 10 min and then purify the DNA by repeating steps 11–14. Finally, resuspend the DNA in 50 μL ddH_2O. pLTP-GFP is now ready for ligation to the cDNA from **Subheading 3.2., step 14**.

3.4. Ligation of the cDNA to pLTP-GFP

1. Label all necessary 0.5-mL tubes and place them on ice. Add 1 μL cDNA from **Subheading 3.2., step 14**, 1 micro L digested pLTP-GFP (50 ng/μL) from **Subheading 3.3, step 16**, 4 microlitro 5× T4 DNA ligase buffer, and ddH_2O to 19 μL. Mix by pipetting and then add 1 μL T4 DNA ligase. For further information, *see* **Note 7**.
2. Mix by pipetting and incubate at 12° C for 16 h.
3. To prevent arching during electroporation (*see* **Subheading 3.5.**), the conductivity of the ligation samples must be minimized. The most effective method for achieving

this goal is performing ethanol precipitation, which also enables concentration of the DNA. To each 20-μL ligation mix, add sequentially 1 μg glycogen, 12.5 μL 7.5 M ammonium acetate, and 70 μL 200-proof ethanol, mixing at each time.
4. Incubate at −20° C for 20 min. Then, spin samples using an Eppendorf microfuge at $20,000 \times g$ for 15 min at room temperature.
5. Remove the supernatant without disturbing the pellet and wash this using 0.4 mL 70% ethanol. Centrifuge for 1 min at $20,000 \times g$, remove the supernatant, and air-dry the DNA pellet at room temperature for approximately 10 min.
6. Add 5 μL TE, leave at room temperature for 10 min, and then dissolve the DNA by pipetting. Samples can now be stored at −20° C or used immediately for electroporation.

3.5. Electroporation of the Library

1. Label all the necessary 10-mL Falcon 2059 tubes and 1.5-mL Eppendorf tubes (one each per transformation). Add 1 μL ligated DNA to each Eppendorf tube and place on ice. To determine transformation efficiency of the electrocompetent cells, set up one tube with 10 pg circular plasmid DNA. This will help troubleshoot potential problems with the cDNA cloning *(17)*.
2. Label all the necessary 1-mm gap electroporation cuvettes (one per each ligation) and place on ice.
3. Thaw the electrocompetent ElectroMAX™ DH10B™ cells on ice (efficiency > 10^{10} colonies/μg DNA). Mix gently to avoid mechanical damage to the cells and transfer 40 μL of cells to a prechilled microfuge tube containing the DNA.
4. Mix gently by pipetting and immediately transfer to a prechilled electroporation cuvette kept between the electrode bosses of a BTX model 640 or equivalent apparatus.
5. Pulse the cell mix at room temperature using predetermined conditions. There is significant variability between different lots of electrocompetent cells, and so, optimal conditions need to be established beforehand with each lot (*see* **Note. 8**) With most lots of DH10B cells, however, the following conditions are used: resistance 129 Ω (R5), capacitance 50 μF, potential 1.9 kV, and pulse length 5 ms.
6. Immediately after the electric pulse, add to the DNA–cell mix 200 μL SOC medium at room temperature to allow for rapid recovery of the cells. Pipette gently, using a thin pipette tip, and then transfer to the designated Falcon 2059 tube. Gently rinse the electroporation cuvette two more times with SOC medium to collect remaining cells and combine into the same Falcon tube to a final volume of 1 mL.
7. Repeat steps 4–6 with each DNA sample, using each time a new electroporation cuvette. Do not refreeze unused cells, as these will yield a significantly lower transformation efficiency.
8. Incubate the 10-mL tubes containing SOC for 1 h at 37° C in a shaker incubator at 220 rpm and then proceed as detailed in the **Subheading 3.6**.

3.6. Cell Plating and DNA Extraction

1. Place the 10-mL tubes from **step 8, Subheading 3.5.**, on ice. Add 0.5 mL LB medium to each tube, mix, and then transfer 300 µL of the transformation mix to the middle of each of five 150-mm LB agar plates containing 100 µg/mL carbenicillin (*see* **Note 9**). Spread uniformly on the plate by using a sterile bacterial spreader. Uniform spreading is important to avoid formation of bacterial colonies of different sizes.
2. Incubate plates for approximately 16 h at 37° C.
3. Count the number of colonies on the plates and determine size of the cDNA library (total colonies per ligation) and cloning efficiency (colonies per ng cDNA in the transformation). Further information on how to calculate these values can be found in **ref. *17***. For troubleshooting purposes, transformation efficiency (colonies per ng control plasmid DNA) should also be calculated. With small vectors (< 4 kb), the size of the library is usually between 5×10^6 and 5×10^7 colonies per ligation ***(17)***. With larger plasmids, such as pLTP-GFP (~7.5 kb), however, cloning efficiency is usually lower, partly because of a lower transformation efficiency (*see* **Note 6**). Thus, with this plasmid, additional ligations may have to be set up to achieve a desired library size of 2×10^6 to 4×10^6 colonies.
4. Scrape colonies from the LB agar plates using 10 mL ice-cold LB medium and a bacterial scraper and pool the bacterial suspension into sterile 250-mL conical tubes on ice. Wash the plate with an additional 10 mL LB medium and pool into the same tube. Do not fill tubes with more than 175 mL LB.
5. Centrifuge at $3200 \times g$ for 30 min at 4° C.
6. Discard the supernatant and extract the plasmid DNA from the pellets using standard purification methods such as CsCl gradient centrifugation. Commercial plasmid purification kits (e.g., from Promega or Qiagen) can also be used.
7. Determine the average insert size of the library by digesting individual plasmids with *Bsr*GI and *Not*I (*see* **Subheading 3.12., step 8**). This size should be approximately 1.2–1.7 kb.

3.7. Preparation of Spheroplasts

1. The method of choice for transfection of the library into *RelA*$^{-/-}$ fibroblasts is the spheroplast method (so called because it involves the use of spheroplasts—that is, bacteria without the cell wall—for delivery of the cDNA library into *RelA*$^{-/-}$ cells via fusion with these cells) ***(18–20)***. With these cells, this method was found to minimize the number of plasmid species that are introduced into a single cell—a crucial element for the success of the screen (*see* **Note 10**). To begin, thaw a vial of *RelA*$^{-/-}$ 3T3 fibroblasts ***(14)*** and maintain them in culture in complete DMEM supplemented with 10% FCS at 37° C and 5% CO_2. Split cells 1:12 every other day, as detailed in **Subheading 3.1., steps 1** and **2**.
2. To prepare spheroplasts, transform ElectroMAX™ DH10B™ cells by electroporation, as detailed in **Subheading 3.5.**, using 10 ng library DNA.

3. After 1 h incubation in SOC at 37° C, place the tube in ice and make serial 1:10 dilutions of the SOC culture using LB medium.
4. Plate 100 μL of each dilution onto 100-mm LB agar plates containing 100 μg/mL carbenicillin and incubate at 37° C overnight. Store the original SOC culture at 4° C (titer loss during these first 24 h is minimal).
5. On the following day (i.e., day 2), count colonies to determine the bacterial titer of the SOC culture. Plate this culture onto 150-mm LB agar plates (containing 100 μg/mL carbenicillin) at a density of approximately 50,000 colonies per plate and incubate at 37° C for 16 h. Seed 40–80 plates (depending on the size of the library), or a total of 2×10^6 to 4×10^6 colonies.
6. On day 3, trypsinize 12 T175 flasks of near-confluent *RelA*$^{-/-}$ 3T3 cells, as detailed in **Subheading 3.1., steps 1** and **2**, and seed cells into approximately 100-mm tissue culture dishes at a density of 1.4×10^6 cells per dish.
7. Incubate at 37° C in 5% CO_2 for 16–24 h.
8. On the same day (day 3), retrieve the LB agar plates from the incubator and scrape colonies as detailed in **Subheading 3.6., step 4**, using ice-cold LB medium. Pool the bacterial suspension from these plates into a sterile 2-L plastic bottle on ice.
9. Mix the suspension and determine the OD_{600} using a spectrophotometer. Then, dilute to a final OD_{600} of 0.25–0.3 using LB medium (without antibiotic) at room temperature in a total volume of 1 L. Set up six of such 1-L cultures.
10. Incubate at 37° C in a shaker incubator at 220 rpm and allow to grow to a final OD_{600} of 0.5 (~1–2 h).
11. Add CAP to a final concentration of 50 μg/mL and continue incubating at 37° C at 220 rpm for an additional 12–13 h.
12. On day 4, transfer each 1-L culture into two autoclaved 500-mL polypropylene bottles and centrifuge at $4000 \times g$ for 15 min at 4° C using a Beckman high-speed centrifuge and a JLA-10.500 rotor.
13. Discard the supernatants and reduce the bacterial pellet from each 500-mL bottle to single-cell suspensions by pipetting, using 25 mL ice-cold solution I.
14. Add 5 mL solution II, mix gently, and incubate on ice for 5 min.
15. Add 10 mL solution III, mix, and incubate on ice for an additional 10 min.
16. Add 10 mL solution IV, mix, and incubate at 37° C for 10 min, shaking gently every 30–60 s. Then, place on ice.
17. Transfer to a tissue culture hood and add drop-wise 100 mL solution V while swaying the solution gently.

3.8. Spheroplast-Mediated Transfer of the Library Into RelA$^{-/-}$ Cells

1. Remove the medium from the dishes containing *RelA*$^{-/-}$ cells and slowly add to each of these dishes 12.5 mL of the spheroplast solution from **Subheading 3.7., step 17**.

2. Centrifuge the dishes at $100 \times g$ for 10 min at room temperature, using a tabletop Beckman CS-6R centrifuge and appropriate adaptors. Do not stack more than three dishes per adaptor.
3. Carefully remove the supernatants with vacuum, without disturbing the bacterial layer at the bottom of the dish (*see* **Note 11**). Do not incline the dishes.
4. Add 5 mL 50% (w/v) PEG-1000 solution very slowly, positioning the pipette tip at the edge of the dish. Aspirate the solution in excess and incubate for 2 min at room temperature under the hood.
5. Wash by adding 10 mL prewarmed DMEM without FCS, adding the medium very slowly from the edge of the dish to avoid disturbing the cell layer, and aspirate as before. Wash one more time with DMEM without serum, and then aspirate with vacuum as described in **Subheading 3.1.**
6. Add 10 mL complete DMEM supplemented with 10% FCS and 15 μg/mL gentamicin sulfate and incubate at 37° C for approximately 4 h.
7. Replace the medium with fresh DMEM supplemented with 10% FCS and incubate at 37° C for an additional 24 h.
8. Transfection efficiency (i.e., percent $eGFP^+$ cells) can now be determined by performing standard flow cytometry (FCM) using at least two dishes (*see* **Subheading 3.3., step 1**) ***(12,13)***. With $RelA^{-/-}$ cells, this efficiency is typically 0.1–0.5%. Accounting for cell growth, at the time of incubation with spheroplasts, each dish of $RelA^{-/-}$ cells contains approximately 3×10^6 cells, resulting in an average of approximately 9000 $eGFP^+$ cells per dish (at a 0.3% efficiency) or approximately 900,000 cells per 100 dishes. Thus, to transfect at least 2×10^6 to 4×10^6 library cDNAs—a number needed to preserve library representation ***(17)***—it is necessary to repeat the transfection procedure with one to three additional sets of 100 dishes of $RelA^{-/-}$ cells (*see* **Note 12**).

3.9. Cytotoxic Treatment With TNFα

1. For cytotoxic treatment, on day 5, reduce the medium from transfected $RelA^{-/-}$ cells to 4.5 mL per dish (*see* **Note 2**) and incubate for at least 2–4 h at 37° C without disturbance (*see* **Note 3**).
2. Prepare a 10× solution containing 3000 U/mL TNFα and 2.5 μg/mL CHX, as described in **Subheading 3.1., step 4**. For CHX, prepare first a 1:100 dilution (100 μg/mL) from the 10 mg/mL stock in 2 mL DMEM in a 2059 Falcon tube (*see* **Note 13**). Vortex and then dilute 1:40 to make up the 10× solution together with TNFα.
3. Add 0.5 mL 10× solution to each 100-mm tissue culture dish to final concentrations of 300 U/mL TNFα and 0.25 μg/mL CHX. Minimize cooling of the medium by treating no more than 6–12 dishes at a time.
4. Gently swirl the dishes and incubate at 37° C in 5% CO_2 for approximately 21 h.

3.10. Extraction of Episomal DNA From Surviving Cells

1. $RelA^{-/-}$ fibroblasts are highly susceptible to TNFα-induced PCD ***(14)***, and so, on day 6, only few cells should appear viable at light microscopy inspection. To remove dead (i.e., detached) cells, vacuum-aspirate the medium and extensively wash the dishes with 10 mL ice-cold PBS, applying a gentle swirl. Aspirate and perform two additional washes with PBS.
2. Add 2 mL trypsin/EDTA and incubate for 3–5 min at room temperature. Then, tap the dish and ensure detachment of residual (i.e., live) cells by direct observation of these dishes under an inverted light microscope.
3. Add 3 mL complete DMEM and transfer detached cells to a 50-mL Falcon tube on ice. Perform two additional washings with 3 mL complete DMEM and pool cells into the same 50-mL tube.
4. Repeat steps 1–3 with each plate, handling approximately 12 plates at the time.
5. Centrifuge 50-mL tubes at $350 \times g$ for 10 min at 4° C.
6. Discard the supernatants, resuspend pellets in 1 mL ice-cold DMEM, and pool cells into two 50-mL tubes. Repeat the washings two more times using 0.5 mL ice-cold DMEM and combine cells into one tube.
7. Centrifuge tubes at $350 \times g$ for 10 min at 4° C, resuspend pellets in 1 mL DMEM at room temperature reducing them to single-cell suspensions by gentle pipetting, and transfer to a 15-mL Falcon tube. Wash twice with 2 mL DMEM and combine into one tube.
8. Using a 2-mL disposable pipette, slowly lay 2 mL of lympholyte M at the bottom of each tube, creating two distinct phases.
9. Centrifuge at $900 \times g$ for 20 min at room temperature, using a tabletop Beckman centrifuge, and allow the run to stop slowly without the brake.
10. Collect the layer of live cells at the lympholyte M/DMEM interface and transfer them to a new 15-mL tube.
11. Add DMEM to a volume to approximately 5 mL, mix, and repeat lympholyte M purification as described in **Subheading 3.10., items 8–10**.
12. Transfer the layers of live cells to a single 15-mL tube, add DMEM to 12 mL, and centrifuge at $350 \times g$ for 10 min at 4° C.
13. Discard the supernatant and wash once with ice-cold PBS.
14. Resuspend the pellet in 400 μL ice-cold PBS and transfer to a sterile 1.5-mL Eppendorf tube. Wash the 15-mL tube two more times with 400 μL PBS and pool the cells into one Eppendorf tube.
15. Spin at $150 \times g$ for 10 min at 4° C using an Eppendorf microfuge, discard the supernatant, and resuspend the pellet in 200 μL 10 mM EDTA (pH 8.0). Then, lyse the cells by adding 200 μL of a Tris–HCl (20 mM, pH 8.0) SDS (1.2%) solution for extraction of episomal DNA.
16. Rotate the tube on a wheel for 30 min at 4° C and then add 100 μL 5 M NaCl. All solutions should be sterile and handled with care to avoid plasmid contamination.

17. Mix and incubate overnight at 4° C.
18. On day 7, centrifuge tubes for 30 min at $20,000 \times g$ at room temperature using an Eppendorf centrifuge and then transfer the supernatant into a new Eppendorf tube without disturbing the pellet.
19. Perform at least two consecutive phenol/chloroform extractions, until the aqueous/organic interface is clear, and then perform two extractions with chloroform alone.
20. Transfer to a new Eppendorf tube and precipitate DNA by adding 1/10 volume of 3 M sodium acetate (pH 5.2) and then 2.5 volumes of 200-proof ethanol. Vortex and allow to precipitate overnight at 4° C.
21. Centrifuge for 30 min at $20,000 \times g$ at 4° C using an Eppendorf centrifuge, discard the supernatant, and wash twice with 70% ethanol as detailed in **Subheading 3.4., step 5**.
22. Air-dry the pellet for 5 min at room temperature and then dissolve it in 100 µL TE. Store at −20° C or proceed as detailed in **Subheading 3.10., items 23–25**.
23. Amplify the library by electroporating ElectroMAX™ DH10B™ cells with 1 µL episomal DNA, as described in **Subheading 3.5.** (*see* **Note 14**).
24. Plate electroporated bacteria onto 150-mm LB agar plates (containing 100 µg/mL carbenicillin) and incubate at 37° C for approximately 16 h.
25. Harvest colonies by scraping and extract plasmid DNA from a minimum of 0.5×10^6 colonies, as detailed in **Subheading 3.6., steps 4–6**. The library is now ready for the following cycle of selection in $RelA^{-/-}$ cells.

3.11. Assessment of Library Enrichment by PCR

1. At each cycle, enrichment of the library is verified by standard semiquantitative PCR (**Fig. 3**), using original and enriched libraries as templates and primer sets specific for *RelA* (or another protective gene enriched by selection) and *β-actin* (or another "housekeeping" gene impoverished by this process) ***(1,2,12,13)***. We outline here specific PCR steps. Label all necessary 0.5-mL PCR tubes and set up reactions in a total volume of 50 µL, using 100 ng of either original or enriched library, 1.5 mM $MgCl_2$, and *RelA*-specific or *β-actin*-specific primer sets (*see* **Subheading 2.11., item 2**).
2. Cover samples with mineral oil, transfer tubes to a Perkin-Elmer DNA Thermal Cycler 480 (or equivalent apparatus), and set up the amplification reactions as follows: 45 s at 94° C, denaturation; 45 s at 62° C, annealing; 45 s at 72° C, elongation.
3. Stop reactions at 13 amplification cycles for *β-actin* and at 16 amplification cycles for *RelA*, collect 5 µL of each sample from underneath the oil layer, and store in ice.
4. Restart the thermal cycler and repeat the operation at every three cycles of amplification, until reactions have reached a plateau.

5. Analyze samples from the original and enriched libraries at different cycles of amplification by performing standard agarose gel electrophoresis, using a 2% agarose gel containing 0.5 μg/mL ethidium bromide.
6. Compare the relative intensity of *β-actin*-specific and *RelA*-specific bands in the original and enriched libraries (**Fig. 3**). At a predicted theoretical doubling of the concentration of PCR product with each amplification cycle, the relative abundance of this product is expected to increase by eightfold with each three cycles, thereby enabling a rapid semiquantitative estimate of the efficiency of the library enrichment process (**Fig. 3**). Four cycles of library selection normally enable a 500-fold to 2000-fold enrichment of the library in RelA-coding plasmids and a concomitant approximately 1000-fold impoverishment in those encoding *β-actin*. This is sufficient to begin the analysis of individual cDNAs ***(12,13)*** (*see* **Subheading 3.12.**). For a precise assessment of the selection process, more quantitative methods such as real-time PCR and colony hybridization assays should be used. If sufficient enrichment is not achieved by cycle 4, it is likely that conditions used for library selection are suboptimal and therefore need to be re-evaluated. Proceeding beyond this selection cycle is usually unproductive.

3.12. Step 1: Cytoprotection Assays in RelA$^{-/-}$ Cells

1. Once enrichment is verified, proceed with the analysis of individual cDNAs. The screen for the identification of NF-κB-inducible, protective targets is a two-step process (**Fig. 4**). The first step is confirming the ability of isolated cDNAs to inhibit TNFα-induced PCD in NF-κB-deficient cells. Transform ElectroMAX™ DH10B™ cells as in **Subheading 3.5.** using 5 ng of the enriched library and plate 1:10 serial dilutions of the SOC culture onto one 150-mm LB agar plate (containing 100 μg/mL carbenicillin) per dilution.
2. Incubate at 37° C for approximately 16 h.
3. Label the necessary 10-mL 2059 Falcon tubes and add 1 mL LB medium containing 100 μg/mL ampicillin.
4. Pick 50–100 well-isolated colonies using autoclaved toothpicks and inoculate individual tubes.
5. Incubate at 37° C in a shaker incubator at 220 rpm overnight.
6. Label the necessary Eppendorf tubes and transfer bacterial cultures into these tubes. Spin at $20,000 \times g$ for 10 min at 4° C.
7. Discard the supernatants and extract the plasmid DNAs using commercial kits such as the Promega or Qiagen plasmid mini kits for mini preparation. Elute DNAs using 20 μL ddH_2O and determine DNA concentrations using a spectrophotometer.
8. Digest 0.3 μg plasmid DNA with *Not*I and *Bsr*GI and determine the cDNA insert size by performing standard agarose gel electrophoresis. DNA bands of 5.4 and 2.1 kb are derived from pLTP-GFP ***(13,15)***. Other bands are from the insert. Discard mini prep samples that appear to have no insert and store the other

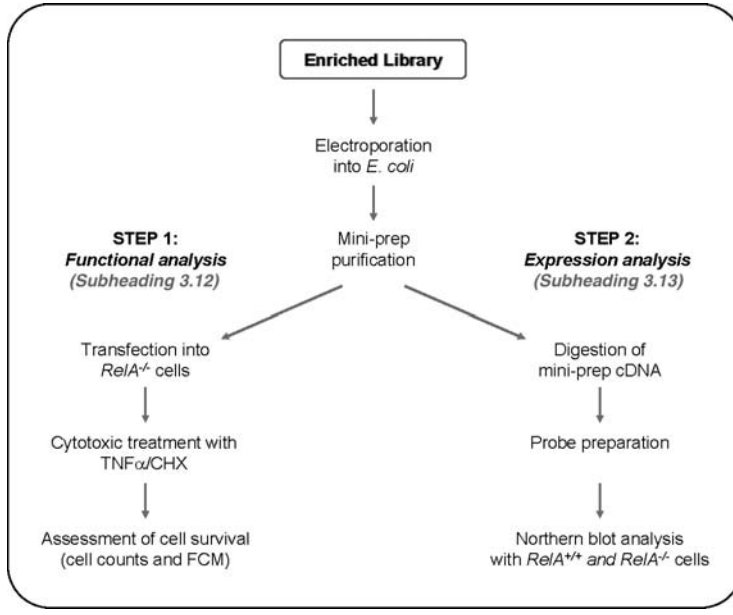

Fig. 4. Schematic representation of the two-step screening process involved in the identification of NF-κB protective targets in the enriched library. Step 1 involves a functional assay for cytoprotective activity in $RelA^{-/-}$ cells. Step 2 involves an assessment of the pattern of basal and/or tumor necrosis factor α (TNFα)-inducible expression of the protective genes in $RelA^{-/-}$ and $RelA^{+/+}$ fibroblasts.

samples at −20° C until needed. It is recommended that a total of at least 200–500 independent DNA clones are ultimately prepared and tested in cytoprotection assays.

9. For these assays, seed exponentially growing $RelA^{-/-}$ 3T3 cells, as described in **Subheading 3.7., step 6**, in 60-mm dishes at a density of 1.5×10^5 per dish. Seed at least two dishes per each library plasmid.
10. Incubate at 37° C in 5% CO_2 for approximately 20 h.
11. On the following day, label the necessary 10-mL 2059 Falcon tubes and the corresponding dishes of $RelA^{-/-}$ cells (two per DNA sample). For transient transfection of the library plasmids, use SuperFect, which typically yields a transfection efficiency of 10–15% in these cells.
12. Add 12 μg plasmid DNA into each tube followed by 300 μL DMEM (without supplements) and mix. Use pLTP-GFP-RelA and insert-less pLTP-GFP as positive and negative controls, respectively.
13. Add 60 μL SuperFect, mix by pipetting, and incubate for 10 min at room temperature. Then, remove the medium from the appropriate dishes of $RelA^{-/-}$ cells

(saving this medium in sterile 50-mL tubes for later use), add 2 mL complete DMEM to the tubes containing the DNA/SuperFect mix, and immediately transfer 1 mL of this mix to each of two appropriately labeled dishes of $RelA^{-/-}$ cells, pointing the pipette tips to the edge of these dishes.

14. Incubate at 37° C in 5% CO_2 for 3 h.
15. Replace the transfection mix with the medium saved in **Subheading 3.12., step 13** (*see* **Note 2**).
16. Incubate at 37° C in 5% CO_2 for an additional 24 h.
17. On the following day, reduce the volume of the medium in the 60-mm dishes to 2 mL and allow to rest at 37° C for at least 2–4 h.
18. Prepare 5× solutions of CHX alone (1.25 μg/mL) and CHX (1.25 μg/mL) plus TNFα (1500 U/mL) in DMEM, similar to what is described in **Subheading 3.9., step 3**, and add 0.5 mL of either solution to the corresponding dishes of $RelA^{-/-}$ cells, to final concentrations 300 U/mL TNFα and 0.25 μg/mL CHX.
19. Incubate at 37° C in 5% CO_2 for 14–16 h.
20. Aspirate the medium, wash dishes twice with ice-cold PBS, and trypsinize cells, as detailed in **Subheading 3.10., step 2**, using 0.5 mL trypsin/EDTA.
21. Transfer to 15-mL Falcon tubes using complete DMEM, centrifuge at 350 × *g* for 5 min at 4° C, and resuspend pellets in 0.5 mL complete medium. Keep tubes on ice.
22. Count cells by using a hemocytometer and analyze the remaining cells by FCM using standard methods and apparatuses (e.g., FACSCalibur, FACScan, and FACSCanto). Gate on live cells at a forward-scatter (FSC) versus sideward-scatter (SSC) plot and determine the percentage of viable $eGFP^+$ cells in this gate, at FL-1. Based on this value and the total cell count, extrapolate the total number of adherent (i.e., live) $eGFP^+$ cells present in each 60-mm dish (*see* **Note 15**). Then, calculate the percent survival in TNFα/CHX-treated cultures relative to control cultures treated with CHX alone, using the following formula:

$$\text{Percent survival} = \frac{\text{total number of adherent GFP}^+\text{cells in TNF}\alpha\text{/CHX-treated dishes} \times 100}{\text{total number of adherent GFP}^+\text{cells in CHX-treated dishes}}$$

Compare the percent survival seen with test plasmids with those seen with pLTP-GFP-RelA (positive control) and insert-less pLTP-GFP (negative control). Approximately 30% of the library cDNAs are expected to have some protective activity in RelA-null cells after four cycles of library selection ***(12,13)***. For further information. These transient transfection assays enable analysis of a large number of cDNAs with relatively little effort. Ultimately, the protective activity of each cDNA needs to be confirmed using nonepisomal plasmids (e.g., pcDNA), and their physiological relevance needs to be established via loss-of-function analyses.

3.13. Step 2: Expression Analysis in $RelA^{-/-}$ and $RelA^{+/+}$ Cells

1. Once protective activity is established, the transcriptional dependence of the isolated genes on NF-κB must be verified through a secondary screen (**Fig. 4**) (*see* **Note 17**). Grow early-passage MEFs from $RelA^{-/-}$ and $RelA^{+/+}$ mice ***(14)*** in complete DMEM supplemented with 10% FCS. At near-confluence, trypsinize these cells and seed them in 100-mm dishes, essentially as described in **Subheading 3.7., step 6**, at a density of 1.8×10^6 cells per dish in 10 mL complete DMEM.
2. Incubate at 37° C in 5% CO_2 overnight.
3. Label all necessary dishes of $RelA^{-/-}$ and $RelA^{+/+}$ cells and stimulate with TNFα (at a final concentration of 1000 U/mL) for 0.5, 1, 2, 4, 6, and 8 h, as detailed in **Subheading 3.1., steps 3–5**, in a total volume of 5 mL. Maintain at least 1 dish per line in the absence of TNFα.
4. At the appropriate time, retrieve dishes from the incubator and extract the total RNA as detailed in **Subheading 3.2., steps 1–10**. Measure RNA concentrations using a spectrophotometer and store samples at −80° C.
5. Assess the pattern of gene expression by performing standard northern blots, RT–PCR, or using other appropriate methods. To prepare probes for northern blots, gel-purify cDNA inserts excised from pLTP-GFP by double digestion with *Not*I and *Bsr*GI (*see* **Subheading 3.12., step 8**), by using commercial gel extraction kits such as QiaQuick, and then label probes with [^{32}P]dCTP using standard methods. To design primers for RT–PCR, sequence the cDNA inserts using oligonucleotides specific for either the 3′-terminal end of eGFP or the DNA-binding sequence of the SP6 RNA polymerase, which flanks the multicloning site of pLTP-GFP ***(13,15)***, and utilize appropriate software. NF-κB targets should be induced by TNFα in $RelA^{+/+}$, but not $RelA^{-/-}$ cells.

4. Notes

1. The library is chosen based on (1) the source of the cDNA and (2) the type of vector. The mRNA must originate from cells expressing high levels of the genes under investigation. We used mRNA from TNFα-treated NF-κB-proficient fibroblasts ***(12,13)***. The vector must yield high cDNA expression and replicate episomally in the chosen cell system. With pLTP ***(15)***, these conditions are met in mouse cells by the presence of the cytomegalovirus (CMV) immediate early promoter, and the polyomavirus origin of replication and large-T-coding sequences, respectively. These latter sequences are key to further enhance gene expression and enable plasmid recovery from surviving cells following cytotoxic treatment. With human cells, however, different viral systems must be chosen (e.g., SV40 or EBV systems) ***(21,22)***. It is worth noting that with viral vectors, gene delivery is usually much more efficient. This advantage of viral vectors, however, is often offset by a much lower expression—a key feature for this type of screens—and a more problematic recovery of the library from rescued cells ***(23,24)***.

2. Do not use fresh medium, as this causes *RelA*$^{-/-}$ 3T3 cells to detach from the flask.
3. Precautions must be taken to allow the temperature of the culture medium to return to 37° C prior to carrying out the stimulation with TNFα. If available, multiple CO_2 incubators should be used for treatment of different subsets of flasks, in order to avoid exposing the cells to unnecessary opening of the incubator door. When absolute sterility is not necessary (e.g., with short time points), treat cells directly in the incubator, without recapping the flasks.
4. At least one flask should be left untreated to establish basal gene expression and verify adequate induction of TNFα-responsive genes in RT–PCR assays.
5. From this point on, all procedures must be performed under RNase-free conditions, using DEPC-treated solutions when appropriate.
6. The presence of eGFP, however, also has disadvantages. First, it causes two-thirds of the cDNAs to be translated in the wrong frame. Second, it increases the size of library plasmids, thereby reducing both the efficiency of transfection into *RelA*$^{-/-}$ cells and that of transformation of *E. coli*. For these (and other reasons), in some cases, it is therefore advisable to generate libraries directly in the pLTP vector without introduction of the *eGFP* cassette ***(17)***.
7. Ligation efficiency depends on the molar vector-to-cDNA ratio ***(17)***. Thus, to maximize colony number, the ligation reaction must be first optimized by titrating the cDNA (e.g., using 0.25, 0.5, 1, and 2 μL cDNA) while keeping constant the amount of the vector (50 ng).
8. Electroporation is the most efficient method for bacterial transformation ***(17)***. It is also relatively unselective against plasmid size, and so, it facilitates introduction into bacteria of larger plasmids—a key feature for preserving library representation ***(17)***. Owing to a great deal of lot-to-lot variability in conductivity of the ElectroMAX™ DH10B™ cells, electroporation conditions must be optimized with each lot. With a BTX 640 apparatus, resistance, capacitance, and pulse length are usually kept constant, whereas different voltages beginning from 1.5 to 2.5 kV are tested, using 0.1-kV increments. Low voltages usually yield suboptimal transformation efficiency, whereas high voltages cause excessive cell death and greatly increase the risk of arching.
9. When ligation efficiency is unknown, it is helpful to titrate the transformation (*see* **Subheading 3.7., step 3**).
10. The method of transfection is crucial for the success of the library screen. Foremost, this must minimize co-transfection efficiency (i.e., the introduction of different plasmid species into a single cell). The method of choice depends on the specific cell system, and with *RelA*$^{-/-}$ fibroblasts, the one that appears to be the most stringent in this regard is the spheroplast method ***(12)***. Spheroplast-mediated transfer, however, also has limitations in that it is rather labor intensive and only yields low transfection efficiency (i.e., 0.1–0.5%), compared with other methods ***(12,20)***.

11. For successful DNA transfer, key parameters must be optimized beforehand, using pLTP-GFP. These include (1) the density of $RelA^{-/-}$ 3T3 cells in 100-mm dishes, (2) the time of incubation with PEG-1000, and (3) the conditions of centrifugation (i.e., time and acceleration) as in **Subheading 3.8., step 2**. Furthermore, some practice is required for proper handling of tissue culture dishes and execution of the various steps.
12. Although for cycle 1 of library selection, episomal DNA should be pooled from at least 200–400 dishes of $RelA^{-/-}$ cells, with subsequent cycles (after the library has been partially enriched), fewer dishes are required: typically 100–200 dishes are needed for cycle 2, and approximately 100 dishes are needed for cycles 3 and 4.
13. Efficient induction of cell death is another key parameter determining the success of the screen. Cytotoxic treatment must yield minimal background viability ($< 1\%$); yet, it must enable protective cDNAs to rescue cells from death ***(12,15)***. With $RelA^{-/-}$ 3T3 cells, these conditions are met by a 21-h treatment with 300 U/mL TNFα and 0.25 μg/mL CHX (*see* **Subheading 3.1., steps 4** and **5**). These low doses of CHX are necessary in order to maximize cell death, due in part to the fact that these cells retain the expression of NF-κB-family members such as p50/p105, p52/p100, and Rel, which can partly compensate for the lack of RelA ***(1,3,14)***. Optimal concentrations of CHX (and TNFα) have to be precisely established in pilot experiments, using $RelA^{-/-}$ cells transfected with either pLTP-GFP or pLTP-GFP-RelA. It is imperative to define conditions enabling maximal killing of RelA-deficient cells (i.e., pLTP-GFP) while having minimal effects on survival of RelA-proficient cells (i.e., pLTP-GFP-RelA). An excess of CHX can in fact be detrimental to the ability of RelA (or its targets) to block cell death.
14. With episomal DNA, transformation efficiency may be low. If this is the case, concentrate DNA by standard ethanol precipitation. Another potential problem is the presence of shorter, truncated forms of pLTP-GFP in this DNA. This is often caused by treatment with CAP (*see* **Subheading 3.7., step 11**) and may become especially severe with latter cycles of library selection. One way to minimize this problem is to reduce either the concentration or the duration of the treatment with CAP (*see* **Subheading 3.7., step 11**) ***(20)***. To this end, perform dose–response and time–course experiments, verifying that modification to the CAP treatment conditions allows sufficient transfection efficiency of spheroplasts. The use of smaller vectors (e.g., pLTP) ***(15)*** may also contribute to attenuate this problem.
15. With libraries that do not express eGFP, such as pLTP-based libraries, cytoprotection assays are carried out by co-transfecting library plasmids together with insert-less pLTP-GFP at a 10:1 ratio. This system, however, is not as accurate as transfection of pLTP-GFP-based library plasmids.
16. Because the library is cloned into pLTP-GFP directionally, cytoprotection can occur with either "genuine" prosurvival genes or dominant-negative variants of death-inducing genes ***(12,13)***.

17. The screen does not select for genes that are transcriptionally controlled by NF-κB ***(12,13)***. Thus, once protective activity is established (**Subheading 3.12.**), in order to identify NF-κB targets, expression patterns of isolated genes must be assessed experimentally through a secondary screen.

Acknowledgments

We thank L. D'Adamio for the gift of pLTP and helpful advice with the library screen. We also thank A. Hofmann and D. Baltimore for the *RelA*$^{-/-}$ MEFs. This work was supported in part by NIH grants R01-CA84040 and R01-CA098583 to G.F.

References

1. Kucharczak, J., Simmons, M. J., Fan, Y., and Gelinas, C. (2003) To be, or not to be: NF-κB is the answer–role of Rel/NF-κB in the regulation of apoptosis. *Oncogene* **22,** 8961–82.
2. Papa, S., Zazzeroni, F., Pham, C. G., Bubici, C., and Franzoso, G. (2004) Linking JNK signaling to NF-κB: a key to survival. *J. Cell Sci.* **117,** 5197–208.
3. Hayden, M. S. and Ghosh, S. (2004) Signaling to NF-κB. *Genes Dev.* **18,** 2195–224.
4. Karin, M., Yamamoto, Y., and Wang, Q. M. (2004) The IKK NF-κB system: a treasure trove for drug development. *Nat. Rev. Drug Discov.* **3,** 17–26.
5. Alizadeh, A. A., Eisen, M. B., Davis, R. E., Ma, C., Lossos, I. S., Rosenwald, A., et al. (2000) Distinct types of diffuse large B-cell lymphoma identified by gene expression profiling. *Nature* **403,** 503–11.
6. Grumont, R. J., Rourke, I. J., and Gerondakis, S. (1999) Rel-dependent induction of A1 transcription is required to protect B cells from antigen receptor ligation-induced apoptosis. *Genes Dev.* **13,** 400–11.
7. Hinz, M., Lemke, P., Anagnostopoulos, I., Hacker, C., Krappmann, D., Mathas, S., et al. (2002) Nuclear factor κB-dependent gene expression profiling of Hodgkin's disease tumor cells, pathogenetic significance, and link to constitutive signal transducer and activator of transcription 5a activity. *J. Exp. Med.* **196,** 605–17.
8. Khoshnan, A., Tindell, C., Laux, I., Bae, D., Bennett, B., and Nel, A. E. (2000) The NF-κB cascade is important in Bcl-xL expression and for the anti-apoptotic effects of the CD28 receptor in primary human CD4+ lymphocytes. *J. Immunol.* **165,** 1743–54.
9. Wang, C. Y., Mayo, M. W., Korneluk, R. G., Goeddel, D. V., and Baldwin, A. S., Jr. (1998) NF-κB antiapoptosis: induction of TRAF1 and TRAF2 and c-IAP1 and c-IAP2 to suppress caspase-8 activation. *Science* **281,** 1680–3.
10. Zhou, A., Scoggin, S., Gaynor, R. B., and Williams, N. S. (2003) Identification of NF-κB-regulated genes induced by TNFα utilizing expression profiling and RNA interference. *Oncogene* **22,** 2054–64.

11. Zong, W. X., Edelstein, L. C., Chen, C., Bash, J., and Gelinas, C. (1999) The prosurvival Bcl-2 homolog Bfl-1/A1 is a direct transcriptional target of NF-κB that blocks TNFα-induced apoptosis. *Genes Dev*. **13,** 382–7.
12. De Smaele, E., Zazzeroni, F., Papa, S., Nguyen, D. U., Jin, R., Jones, J., et al. (2001) Induction of gadd45β by NF-κB downregulates pro-apoptotic JNK signalling.*Nature* **414,** 308–13.
13. Pham, C. G., Bubici, C., Zazzeroni, F., Papa, S., Jones, J., Alvarez, K., et al. (2004) Ferritin heavy chain upregulation by NF-κB inhibits TNFα-induced apoptosis by suppressing reactive oxygen species. *Cell* **119,** 529–42.
14. Beg, A. A. and Baltimore, D. (1996) An essential role for NF-κB in preventing TNF-α-induced cell death. *Science* **274,** 782–4.
15. Vito, P., Lacana, E., and D'Adamio, L. (1996) Interfering with apoptosis: Ca(2+)-binding protein ALG-2 and Alzheimer's disease gene ALG-3. *Science* **271,** 521–5.
16. Hoffman, R. M. (2005) The multiple uses of fluorescent proteins to visualize cancer in vivo. *Nat. Rev. Cancer* **5,** 796–806.
17. Gruber, C. E. (1995) Production of cDNA libraries by electroporation. *Methods Mol. Biol.* **47,** 67–79.
18. Rassoulzadegan, M., Binetruy, B., and Cuzin, F. (1982) High frequency of gene transfer after fusion between bacteria and eukaryotic cells. *Nature* **295,** 257–9.
19. Sandri-Goldin, R. M., Goldin, A. L., Levine, M., and Glorioso, J. (1983) High-efficiency transfer of DNA into eukaryotic cells by protoplast fusion. *Methods Enzymol.* **101,** 402–11.
20. Schaffner, W. (1980) Direct transfer of cloned genes from bacteria to mammalian cells.*Proc. Natl. Acad. Sci. U. S. A.* **77,** 2163–7.
21. Belt, P. B., Groeneveld, H., Teubel, W. J., van de Putte, P., and Backendorf, C. (1989) Construction and properties of an Epstein-Barr-virus-derived cDNA expression vector for human cells. *Gene* **84,** 407–17.
22. Makrides, S. C. (1999) Components of vectors for gene transfer and expression in mammalian cells. *Protein Expr. Purif.* **17,** 183–202.
23. Barquinero, J., Eixarch, H., and Perez-Melgosa, M. (2004) Retroviral vectors: new applications for an old tool.*Gene Ther.* **11 (Suppl 1),** S3–9.
24. Verma, I. M. and Weitzman, M. D. (2005) Gene therapy: twenty-first century medicine. *Annu. Rev. Biochem.* **74,** 711–38.

9

Functional Cloning of Genes Regulating Apoptosis in Neuronal Cells

Roberta Visconti and Luciano D'Adamio

Summary

Here, we describe the use of a functional cloning approach, based on the screen of a genome-wide short hairpin RNA (shRNA) library, to identify novel genes regulating apoptosis in neuronal cells. Apoptosis is induced by doxorubicin and is detected with a fluorometric caspase 3 assay. Moreover, we describe also the screen of the library to identify genes regulating the processing of the β-amyloid (Aβ) precursor protein (APP), the protein associated with the pathogenesis of Alzheimer's disease. The levels of the peptide Aβ, produced by the APP processing, are detected with ELISA based on the innovative Delfia method developed by PerkinElmer.

Key Words: Apoptosis; Alzheimer's disease; amyloid precursor protein; RNA interference; genome-wide shRNA library screening.

1. Introduction

The discovery of RNA interference (RNAi) has provided a powerful tool to generate loss-of-function phenotypes ***(1)***. Indeed, in *Caenorhabditis elegans* and *Drosophila melanogaster*, RNAi has extensively been utilized in large-scale, genome-wide screens to switch off every gene of these animal models ***(2,3)***. Very recently, large-scale RNAi-based screens utilizing short hairpin RNA (shRNA) libraries have also been reported in mammalian cells ***(4,5)***. One of these libraries, the mouse Expression Arrest™ shRNA library, developed by Paddison et al. and supplied by Open Biosystems (Huntsville, AL, USA), consists of about 61,000 shRNA constructs, targeting about 28,000 mouse genes. The constructs have been designed, cloned into retroviral vectors, and

From: *Methods in Molecular Biology, vol. 399: Neuroprotection Methods and Protocols*
Edited by: T. Borsello © Humana Press Inc., Totowa, NJ

arrayed in 96-well plates, ready for gene-silencing experiments by RNAi in mammalian cells. Here, we describe the methods used in our laboratory to screen this library for identifying novel genes regulating apoptosis in mouse neuronal cells. Moreover, we describe the screen of the library aimed at identifying genes involved in the cleavage of the β-amyloid (Aβ) precursor protein (APP), a process firmly associated with the pathogenesis of Alzheimer's disease (AD) and thus with the neuronal degeneration characterizing this disease ***(6)***.

2. Materials

2.1. Transfection

1. 96-Well plates (Becton Dickinson Labware, Franklin Lakes, NJ, USA).
2. Dulbecco's modified Eagle's medium (DMEM) (Cambrex, East Rutherford, NJ, USA).
3. Fetal bovine serum (FBS) (HyClone, Logan, UT, USA).
4. Arrest-In Transfection Reagent (Open Biosystems) (*see* **Note 1**).

2.2. Induction and Detection of Apoptosis

1. Doxorubicin (Sigma-Aldrich, St. Louis, MO, USA).
2. 2× Caspase lysis buffer: 60 mM Tris–HCl (pH 7.5), 300 mM NaCl, 2% Triton X-100, 20% glycerol, and protease inhibitors.
3. Black 96-well plate (Corning Inc., Corning, NY, USA).
4. 10× Caspase reaction buffer: 200 mM HEPES, 100 mM NaCl, 10 mM ethylenediaminetetraacetic acid (EDTA), and 1% CHAPS.
5. Dithiothreitol (DTT).
6. Sucrose.
7. Caspase 3 substrate: *N*-Acetyl-Asp-Glu-Val-Asp-AFC (7-amino-4-trifluoromethyl coumarin) (BIOMOL International, Plymouth Meeting, PA, USA).
8. 96-well plate fluorescence reader (EnVision, PerkinElmer, Wellesley, MA, USA).

2.3. Measurement of Aβ Levels (See Note 2)

1. Maxisorp black 96-well plate (Nalge Nunc International, Rochester, NY, USA).
2. 6E10 antibody (Signet Laboratories, Dedham, MA, USA).
3. Aβ ELISA coating buffer: 2.27 g K_2HPO_4, 0.372 g EDTA, 3.48 g KH_2PO_4, 8 g NaCl, 0.1 g NaN_3 in 1 L H_2O (pH 7.4).
4. 20 × Aβ ELISA washing buffer: 464 g NaCl, 98.6 g Tris, 40 mL Tween-20 in 4 L H_2O (pH 7.4).
5. StartingBlock blocking buffer (Pierce, Rockford, IL, USA).

6. 4G8-Biotin antibody (Signet Laboratories).
7. SuperBlock blocking buffer (Pierce).
8. Europium-labeled streptavidin (PerkinElmer).
9. Delfia assay buffer (PerkinElmer).
10. Delfia wash solution (PerkinElmer).
11. Delfia enhancement solution (PerkinElmer).

3. Methods

As outlined in **Fig. 1**, we describe the methods used in the screening of a genome-wide shRNA library to identify genes regulating apoptosis and APP processing in neuronal cells. Briefly, the shRNA constructs derived from the library are transfected into a murine neuroblastoma cell line, Neuro2A (N2a),

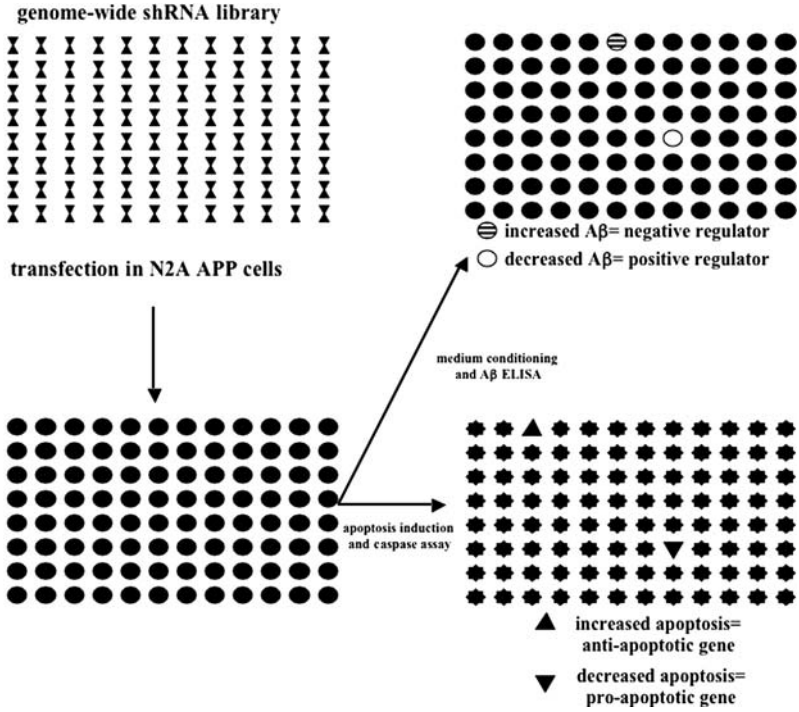

Fig. 1. Scheme illustrating the strategy for the identification of novel genes regulating apoptosis and β-amyloid precursor protein (APP) processing, by screening a genome-wide short hairpin RNA (shRNA) library.

overexpressing human APP, plated in 96-well plates. Sixty-nine hours posttransfection, the growth medium is replaced with fresh medium, allowing for 3 h the accumulation in the conditioned medium of Aβ, a peptide derived from the cleavage of APP. After 3 h, we proceed with the detection of Aβ levels by ELISA (**Fig. 2**). We reason that in the wells where the N2a cells produce Aβ levels higher than the plate average levels, the transfected shRNA construct is targeting and silencing a gene that physiologically downregulates APP processing. On the contrary, in the wells where the N2a cells produce Aβ levels lower than the plate average levels, the transfected shRNA is targeting and silencing a gene that physiologically upregulates APP processing. Three hours postconditioning and 72 h posttransfection, in each well the medium removed for the Aβ ELISA is replaced with new growth medium containing doxorubicin to induce apoptosis. Caspase activity is, then, determined by assaying for the cleavage of a fluorescent substrate. We reason that in the wells where we detect an increase in doxorubicin-induced apoptosis, the shRNA construct is targeting and silencing an antiapoptotic gene; on the contrary, in the wells where we detect a decrease in doxorubicin-induced apoptosis, the shRNA construct is presumably targeting and silencing a proapoptotic gene. In **Fig. 3**, we show a representative caspase assay, demonstrating that doxorubicin induces apoptosis in N2a cells in a dose-dependent manner.

Here, we describe in detail the methods used.

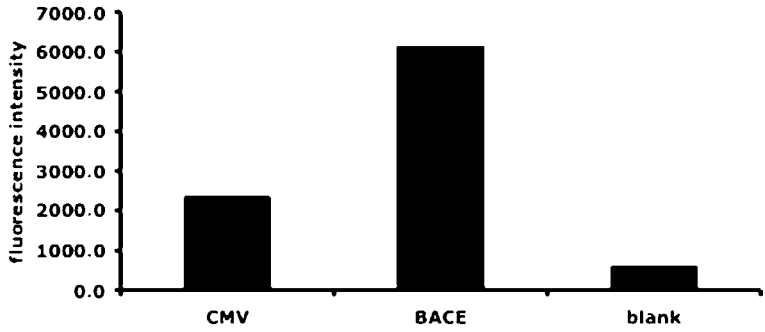

Fig. 2. ELISA detecting Aβ production in murine neuroblastoma cell line (N2a) β-amyloid precursor protein (APP) cells. The basal Aβ levels of the N2a APP cells transfected with a control vector cDNA (CMV) are shown. Moreover, as a positive control, we show the great enhancement of the Aβ levels induced by the transfection of a vector encoding BACE, one of the enzymes responsible for APP processing. The background level of the assay (blank) is also shown.

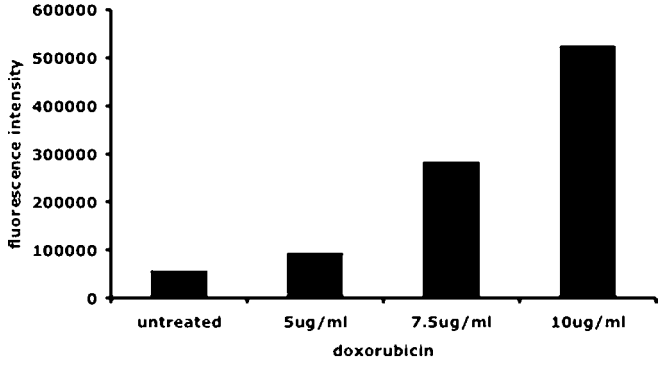

Fig. 3. Assay detecting caspase 3 activation in doxorubicin-treated murine neuroblastoma cell line (N2a) β-amyloid precursor protein (APP) cells. N2a APP cells were stimulated with increasing concentrations of doxorubicin for 7 h. Dose-dependent increase in caspase activity is demonstrated by the intensification of the fluorescence signal emitted at 535 nm following the cleavage of a specific caspase substrate linked to the AFC fluorophore.

3.1. Transfection

1. Seed 0.5×10^4 N2a cells per well in a 96-well plate in 100 μL DMEM with 10% FBS, without antibiotics.
2. Twenty-four hours later, dilute, for each well, 100 ng DNA in 25 μL serum-free DMEM.
3. Dilute, for each well, 2 μg Arrest-In in 25 μL serum-free DMEM (*see* **Note 1**).
4. Mix the diluted DNA with the diluted Arrest-In reagent.
5. Incubate for 10 min at room temperature.
6. Add the DNA/Arrest-In complexes to the cells.

3.2. Induction and Detection of Apoptosis

1. Seventy-two hours posttransfection, stimulate the cells in 25 μL DMEM + 10% FBS with 7.5 μg/mL doxorubicin for 7 h.
2. Add to each well 25 μL 2× caspase lysis buffer.
3. Freeze the lysate plate at −80° C for 30 min.
4. Warm the lysate plate to room temperature.
5. Transfer 20 μL of the lysates in a black 96-well plate.
6. Add to each well 20 μL H_20, 9 μL 10× caspase reaction buffer, 1 μL DTT, 50 μL 20% sucrose, and 0.2 μL caspase 3 substrate.
7. Incubate the reaction plate for 1 h at 37° C in the dark.
8. Read the reaction plate in a 96-well plate fluorescence reader (excitation filter 405 nm; emission filter 535 nm).

3.3. Measurement of Aβ Levels (See Note 2)

1. Coat a maxisorp black 96-well plate with a 1:500 dilution of the 6E10 antibody (100 μL per well) in coating buffer and leave at 4° C for 24 h on a shaker. The 6E10 antibody reacts with the amino acid residues 1–17 of human Aβ peptide.
2. Wash the plate three times with 300 μL 1× washing buffer per well.
3. Block with 300 μL 100% StartingBlock blocking buffer, either 1 h at room temperature or longer at 4° C.
4. Discard the block by inverting the plate. Do not wash.
5. Add to each well 50 μL conditioned growth medium.
6. To all wells, immediately following the addition of the test samples, add 50 μL of a biotinylated 4G8 antibody (1:2000 dilution made up in 20% SuperBlock blocking buffer). The 4G8 antibody is reactive to amino acid residues 17–24 of the human Aβ peptide. Incubate overnight at 4° C on a shaker.
7. Wash the plate five times with 300 μL 1× washing buffer.
8. To each well, add 100 μL europium-labeled streptavidin (1:1000 dilution in Delfia assay buffer) and incubate 1 h at room temperature.
9. Wash the plate five times with 300 μL 1× Delfia wash solution.
10. To each well, add 100 μL Delfia enhancement solution (warmed at room temperature). Shake for 5 min.
11. Read the reaction plate in a 96-well plate fluorescence reader (excitation filter 340 nm; emission filter 615 nm).

4. Notes

1. Several reagents can be utilized to obtain high transfection efficiencies. We tested several of them on N2a APP cells. We choose Arrest-In because it resulted in the highest efficiency (> 80%). Moreover, Arrest-In was less toxic than the other reagents tested, allowing the DNA/Arrest-In complex mixture to be incubated overnight.
2. We set up the Aβ ELISA utilizing the Delfia method developed by PerkinElmer. In particular, we use streptavidin labeled with europium. Europium, as other lanthanide metals such as samarium and terbium, has unique fluorescence characteristics. In particular, the fluorescence decay time of the specific signal is much longer than the nonspecific background. Thus, the specific signal can be read when the background has already decayed. Moreover, the specific signal can be distinguished from the background, also because of the large difference between excitation and emission wavelengths and because of a very sharp emission peak. Finally, the lanthanide-based ELISA ensures high fluorescence intensity. The europium-labeled streptavidin is, in fact, nonfluorescent in basal condition. However, the addition of the Delfia enhancement solution allows the fluorescence to be developed, dissociating the europium from the streptavidin. The free europium forms a highly fluorescent compound in complex with components of the Delfia enhancement solution, resulting in a great amplification of the fluorescence signal and therefore of the sensitivity of the assay.

Acknowledgments

The authors thank Cristiana Noviello, Emilio Cusanelli, Carolina Tarantino, and Anna Lucia Galiero for their essential contribution in setting up all the methods described here.

References

1. Hannon, G.J. (2002) RNA interference. *Nature* **418**, 244–251.
2. Kamath, R.S., Fraser, A.G., Dong, Y., Poulin, G., Durbin, R., Gotta, M., Kanapin, A., Le Bot, N., Moreno, S., Sohrmann, M., Welchman, D.P., Zipperlen, P., and Ahringer, J. (2003) Systematic functional analysis of the Caenorhabditis elegans genome using RNAi. *Nature* **421**, 231–237.
3. Kiger, A.A., Baum, B., Jones, S., Jones, M.R., Coulson, A., Echeverri, C., and Perrimon, N. (2003) A functional genomic analysis of cell morphology using RNA interference. *J Biol* **2**, 27.
4. Berns, K., Hijmans, E.M., Mullenders, J., Brummelkamp, T.R., Velds, A., Heimerikx, M., Kerkhoven, R.M., Madiredjo, M., Nijkamp, W., Weigelt, B., Agami, R., Ge, W., Cavet, G., Linsley, P.S., Beijersbergen, R.L., and Bernards, R. (2004) A large-scale RNAi screen in human cells identifies new components of the p53 pathway. *Nature* **428**, 431–437.
5. Paddison, P.J., Silva, J.M., Conklin, D.S., Schlabach, M., Li, M., Aruleba, S., Balija, V., O'Shaughnessy, A., Gnoj, L., Scobie, K., Chang, K., Westbrook, T., Cleary, M., Sachidanandam, R., McCombie, W.R., Elledge, S.J., and Hannon, G.J. (2004) A resource for large-scale RNA-interference-based screens in mammals. *Nature* **428**, 427–431.
6. Mattson, M.P. (2004) Pathways towards and away from Alzheimer's disease. *Nature* **430**, 631–639. Addendum in (2004) *Nature* **431**, 107.

10

Characterization of mRNA Expression in Single Neurons

David M. Lin, Brandon Loveall, John Ewer, David L. Deitcher, and Nikolaus J. Sucher

Summary

How neurons differ from each other is largely determined by their specific repertoire of mRNAs. The genes expressed by a given neuron reflect its developmental history, its interaction with other cells, and its synaptic activity. Since the introduction of reverse transcription polymerase chain reaction (RT–PCR), it has been possible to identify specific mRNAs present in small samples of total RNA. But isolating RNA from only those cells of interest, and not others, represents a significant challenge. Several approaches can be used to isolate RNA from selected neurons. Following whole-cell patch-clamp recording, mRNA can be harvested from living cells by aspirating the cytoplasm into the patch-clamp pipette. Transcripts expressed in the recorded neuron can then be amplified by RT–PCR. Another way of isolating identified neurons is to use cell-specific promoters to drive the expression of a marker gene such as green fluorescent protein (GFP). RNA can then be isolated from GFP-positive cells. In a tissue context, laser microdissection can also be used to excise the cells of interest directly into an RNA isolation solution. The above methods of RNA isolation can also be combined with RNA amplification and microarray technology to identify specific transcripts that are unique to the cell type being studied. Here we provide detailed protocols for harvesting RNA from single cells, methods for RNA purification, and PCR amplification.

Key Words: RT–PCR; microarray; GFP; laser microdissection; RNA amplification; patch-clamp.

1. Introduction

In the one and a half centuries since Rudolf Virchow postulated that "the cells are the loci of life and also the disease," a plethora of tools and techniques

From: *Methods in Molecular Biology, vol. 399: Neuroprotection Methods and Protocols*
Edited by: T. Borsello © Humana Press Inc., Totowa, NJ

have been developed which enable investigators to study the structure, function, and "behavior" of cells with ever-increasing sophistication. In particular, the invention of the polymerase chain reaction (PCR) ***(1,2)*** has made it possible to examine the genetic material of single cells ***(3)***. In clinical medicine, single-cell PCR is used in prenatal diagnosis for preimplantation genetic analysis and analysis of fetal cells for single-gene Mendelian disorders ***(4)***. By reverse transcribing mRNA into cDNA, PCR can also be applied to the analysis of gene expression. In basic research, the simplicity and sensitivity of reverse transcription RT–PCR has displaced Northern analysis and RNase protection assays as the method of choice in mRNA detection. The development of quantitative real-time RT–PCR ***(5–7)*** techniques and equipment has made possible the absolute quantification of mRNAs even at the single-cell level ***(8,9)***.

Identifying the range of mRNAs from a single cell or from small groups of cells can be helpful for determining why a neuron fires at the right time or secretes the appropriate signal or finds its correct synaptic target. For example, one may first record ionic or pharmacological responses from a single neuron, then isolate mRNA from the recorded cell and perform RT–PCR using primers for specific ion channel subunit genes to pinpoint the transcripts of candidate genes that might underlie the neuron's electrophysiological response ***(10,11)***. Similarly, one may study a neuroendocrine cell that secretes a crucial neuropeptide upon appropriate stimulation ***(12,13)***. By identifying the cell-specific signal transduction components from such a cell by RT–PCR, one may learn how cues in the circulation trigger that cell to secrete a neuropeptide at the correct time. In a developmental context, one may study a neuron that needs to sense the microenvironment in order to accurately synapse on the correct target. What cues present in the microenvironment allow an axon to find its way? Through isolating RNA from neurons at a specific developmental time point, it is possible to identify the key signaling molecules that direct axons to their target.

In the abovementioned examples, following RNA isolation, one may perform RT–PCR to detect whether specific candidate genes are involved in a particular process. How does one detect whether an mRNA is involved in a process when there is no candidate gene? Microarrays can be used to pinpoint candidate genes. Since their introduction more than a decade ago ***(14,15)***, microarrays have become a pervasive tool in biology ***(16)***.

The most common use for microarrays is to assay expression levels of RNA transcripts present within a sample. But it has long been recognized that microarrays used for this purpose possess a number of well-known limitations ***(17)***. First, microarray data is extremely noisy. It is rare to find a

published data set today which does not perform at least three separate, technically equivalent measurements to obtain a more reliable average estimate of a given gene's expression level. Second, microarrays are relatively insensitive. Common estimates range from 1:50,000 ***(14)*** to 1:300,000 ***(18)***. For some array formats, this detection limit can range up to 1:1,000,000 ***(19)***. In other words, in experiments where a known, unique RNA is "spiked" into a pool of RNAs, microarrays are capable of detecting one such transcript present in a pool of approximately 100,000 other transcripts ***(20)***. By comparison, PCR has a sensitivity limit of 1:1,000,000 and, in skilled hands, sometimes $1 : 10^{11}$ ***(21)***. This difference in sensitivity has an enormous impact on the biological relevance of the data that are obtained. There are an estimated 300,000 RNA transcripts present within a given cell ***(22)***. More than half represent low-copy genes expressed at 5 copies/cell or less ***(22,23)***.

Assuming these estimates are correct, and given that the average sensitivity of microarrays is approximately 1:100,000, it should be possible to detect most of the expressed transcripts present within a given cell. Thus, when using microarrays to compare, for example, yeast raised under various conditions ***(24)***, most of the changes that occur in the transcriptome will be detected. On the contrary, if the experiment involves a tissue that contains a mixture of distinct cell types, most, if not all, of the low-copy transcripts unique to an individual cell type might escape detection.

The mammalian brain is an extreme example of a complex tissue, with numerous specialized nuclei containing many different cell types. Multiple neuronal and glial subtypes exist which can be distinguished morphologically, histologically, electrophysiologically, and/or by the expression of various marker genes. Even neurons of the same subtype can differ electrophysiologically and molecularly based on synaptic input, experience, and plasticity. As a result, most microarray experiments performed with whole tissues can only detect those genes, which are strongly induced in response to a particular stimulus. The more heterogeneous the sample, the more likely that unique transcripts will fail to be detected. As these genes comprise a significant percentage of an individual cell's RNA population, this represents an important limitation of such experiments.

To reduce the effect of contaminants on this analysis, we can use various mechanical processes to separate individual cell types away from one another. A wide range of homemade and commercial tools is available, including hole-punching syringes, arrays of razor blades or gold-wire, and the like. Manual microdissection can be very precise, as even individual chromosomes can be teased out ***(25)***, but throughput is low and depends on the skill of the

individual operator. Fluorescence-activated cell sorting (FACS) can also be used to separate cell types from one another, but mechanical dissociation of the tissue and the time needed to stain and process the sample contribute to potential changes in gene expression (e.g., see **ref. *16***).

In the last 20 years, the convergence of a number of technical developments has made it possible to examine gene expression in single cells that are part of a complex tissue ***(3,10–12,26–38)***. Examples of this convergence of complementary techniques and technology are the combination of patch-clamp recording and single-cell RT–PCR ***(10,11)*** or RNA amplification ***(32)*** and laser microdissection coupled with RT–PCR ***(31)***. In addition, the rapid increase in the number of transgenic animals where desired cells can be labeled with GFP has made it possible to consistently identify cell types without the need for staining or histological techniques ***(38)***.

In the following section, three separate, exemplary protocols are provided for the harvest of RNA from single cells and its reverse transcription (RT) into cDNA for subsequent PCR or synthesis of amplified RNA (aRNA). The PCR products and the aRNA can then be analyzed using various techniques. In the first protocol, total RNA is harvested from single cells following whole-cell patch-clamp recordings. The RNA is subsequently reverse transcribed into cDNA, which is then used as template for PCR with primers corresponding to the sequences of specific genes of interest ***(10,11)***. In the second protocol, the mRNA from *Drosophila* peritracheal (neuroendocrine) cells is used in an optimized RT–PCR procedure ***(12)***. In the third example, small patches of olfactory bulb neurons are excised by laser microdissection, RNA is isolated, cDNA is prepared, and then RNA is amplified. The general work flow for these procedures is schematically illustrated in **Fig. 1**.

2. Materials

2.1. Silanation of Patch-Clamp Pipettes

1. Borosilicate glass pipettes (e.g., catalog #PG52150-4, PG52151-4, and PG52165-4, World Precision Instruments Inc., Sarasota, FL).
2. Dimethyldichlorosilane (catalog #440272, Sigma-Aldrich, St. Louis, MO).
3. Chloroform (catalog #02487, Fluka, Sigma-Aldrich).
4. Silanation solution: In a chemical fume hood, prepare a 5% (v/v) solution of dimethyldichlorosilane in chloroform.

2.2. RNA Isolation From Single Cells

1. Thin-walled RNase-free PCR Tubes (e.g., catalog #12250, Ambion, Austin, TX).
2. TRIZOL® reagent (catalog #15596-026, Invitrogen, Carlsbad, CA).

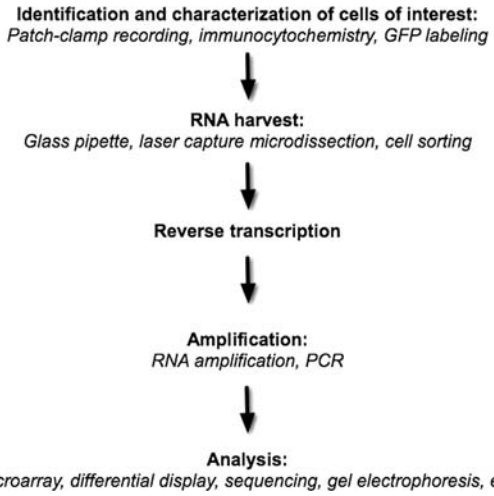

Fig. 1. Workflow for mRNA characterization experiments in single neurons. Cells are first characterized by performing patch-clamp recordings and/or immunocytochemistry or identified based on expression of a green fluorescent protein (GFP)-transgene driven by a cell-type-specific promoter. Single cells are harvested by using glass pipettes or laser capture microdissection. RNA is reverse transcribed into cDNA which can then be used in the polymerase chain reaction (PCR) or the synthesis of amplified RNA. The PCR amplicons or the amplified RNA can be analyzed using microarrays, DNA sequencing, or gel electrophoresis.

3. Glycogen solution (20 mg/ml catalog #10901393001, Roche Applied Sciences, Indianapolis, IN). Glycogen is used as an inert carrier for the precipitation of the small amounts of RNA.
4. DNA-free™ (catalog #AM1906, Ambion) can be used to remove contaminating genomic DNA from the RNA pellet if intron-flanking PCR primers are not used.
5. Diethylpyrocarbonate (DEPC)-treated H_2O. In a fume hood, add DEPC (e.g., catalog #32490-100ML, Fluka, Sigma-Aldrich) to a bottle of deionized water to 0.1%, tightly cap the bottle, and shake to disperse the DEPC. Let the bottle sit at room temperature for 2 h, then autoclave for 1 h. Wear gloves and use DEPC only in a fume hood, as DEPC is a potential carcinogen until it is autoclaved.

2.3. Reverse Transcription of RNA From Single Cells

1. For patch-clamp single-cell RT–PCR: Moloney murine leukemia virus (MMLV) or avian myeloblastosis virus (AMV) reverse transcriptase (multiple vendors).

2. For expression profiling of Inka cells and laser capture microdissection: SuperScript™ III First-Strand cDNA Synthesis (Invitrogen).
3. Isopropanol (Sigma-Aldrich) for purification of cDNA.
4. Random hexamer primers (e.g., catalog #48190-01, Invitrogen).
5. 2′-Deoxynucleoside 5′-triphosphate (dNTP) mix (10 mM, e.g., catalog #R0192, Fermentas Inc., Hanover, MD).
6. Solution for harvesting single-cell RNA containing 50 mM Tris–HCL (pH 8.8 at 25 °C), 5 μM random hexamer primers, and 1 mM dNTP mix.
7. 10× PCR buffer containing 0.5 M Tris–HCL (pH 8.8 at 25 °C), 100 mM MgCl, 10 mM dithiothreitol, 10 mM EDTA, and 100 μg/mL bovine serum albumin.
8. RNase inhibitor (e.g., catalog #03335399001, Roche Applied Sciences).
9. Sodium acetate (3 M, pH 5.2). Dissolve 24.6 g NaOAc (catalog #71183-250G, Fluka, Sigma-Aldrich) in 80 mL double distilled (dd) H_2O, adjust to pH 5.2 with glacial acetic acid (Sigma-Aldrich) and add ddH_2O to 100 mL. Filter (Nalgene No.: 150 0020, capacity: 150 mL, pore size: 0.2 μm) to sterilize.

2.4. Polymerase Chain Reaction

1. Taq (*Thermus aquaticus*) DNA polymerase (with license for PCR, many vendors, store following manufacturer's recommendation). The polymerase is usually distributed with additional vials containing a 10× PCR buffer (200 mM Tris–HCl, pH 8.4, 500 mM KCl, with or without 15 mM $MgCl_2$). In cases where 10× PCR buffer without magnesium is provided, a 50 mM $MgCl_2$ stock solution is usually also provided for convenience.
2. Ultrapure deoxyribonucleotides (dNTPs, many vendors, store at – 20 °C).
3. FailSafe™ PCR System (catalog #FS99060, Epicentre, Biotechnologies Madison, WI).

2.5. Collagenase/Dispase Enzyme Mix

1. Crude collagenase type XI (catalog #C7657, Sigma-Aldrich) and dispase II (catalog #10295825001, Roche Applied Sciences).
2. For 1 mL collagenase/dispase enzyme mix, combine 0.3 mL dispase II, 0.2 mL crude collagenase type XI (1 mg/mL PBS), and 0.5 mL PBS.

2.6. Slide and Tissue Preparation for Laser Microdissection (LMD)

1. PENfoil slides (Leica Microsystems, Wetzlar, Germany).
2. Agarose (ultrapure molecular biology grade, many vendors).
3. Cryostat.

2.7. Laser Microdissection

1. Leica AS LMD system (Leica). *See* **Table 1** for a list of microdissection systems.

Table 1
LMD Machines

Manufacturer	System	Website URL
Arcturus	PixCell, Veritas	arctur.com
Cell Robotics International	LaserScissors	cellrobotics.com
Leica	AS LMD	light-microscopy.com
Molecular Machines	CellCut/SmartCut	molecular-machines.com
P.A.L.M.	EasyBeam, MicroBeam	palm-mikrolaser.com
Zeiss	Clonis	zeiss.com

2.8. mRNA Isolation From Tissue Sections

1. Gentra PureScript kit (catalog #R5110A).
2. Linear polyacrylamide (catalog #9520, Ambion).
3. Agilent 2100 Bioanalyzer and RNA 6000 Pico Labchip (catalog #5065-4473).
4. Nanodrop ND-1000 spectrophotometer (Nanodrop).

3. Methods

3.1. Combined Patch-Clamp and Single Cell RT–PCR

3.1.1. Silanation of Glass Capillaries for Manufacturing of Patch-Clamp Pipettes (see Note 1)

1. In a chemical fume hood, prepare a 5% (v/v) solution of dimethyldichlorosilane in chloroform and add to a glass beaker.
2. Add glass capillaries to the beaker containing the silanation solution. Ensure that the capillaries are entirely submerged and soak the capillaries for 20 min.
3. Pour off the silanation solution and allow remaining liquid to evaporate in the fume hood.
4. Autoclave (15 min) and steam dry (15 min) the capillaries. The capillaries can be stored in an airtight container for several weeks.
5. Manufacture patch-clamp pipettes using the silanized capillaries using standard procedures.

3.1.2. Harvest and Reverse Transcription of RNA From Single Cells

1. Before starting the experiment, prepare on ice several RNase-free PCR tubes containing 4 μL of a solution containing 50 mM Tris–HCl (pH 8.8 at 25 °C), 5 μM random hexamer primers, and 10 mM dNTP mix (dATP, dCTP, dGTP, and dTTP).

2. Harvest single-cell RNA (*see* **Note 2**). Apply suction to the interior of the patch-pipette and verify by visual inspection that the cell's cytoplasm is entering the tip of the pipette. When only the shrunken cell membrane and the cell nucleus remain outside of the pipette tip, remove the pipette under continuous suction from the recording chamber across the liquid–air interface. Pressure-eject the contents of the pipette consisting of the internal solution used for recording and the harvested cellular cytoplasm into a PCR tube containing the previously prepared hexamer primer and dNTP mix for later use in the RT reaction. Store on ice until proceeding to the next step.
3. Heat the RNA/hexamer/dNTP mixture at 70 °C for 10 min and then chill on ice for 5 min. On ice, add 2 μL 10× reaction buffer (containing 0.5 M Tris–HCL [pH 8.8 at 25 °C], 100 mM MgCl, 10 mM dithiothreitol, 10 mM EDTA, and 100 μg/mL bovine serum albumin), 40 U RNase inhibitor, and 100 U MMLV or 32 U of AMV reverse transcriptase. Incubate for 1 h at 37 or 42 °C, respectively, and then 5 min at 95 °C. Chill on ice until proceeding with the next step.
4. Purify cDNA by isopropanol precipitation (*see* **Note 3**). At room temperature, add 2 μL of glycogen (from the 20 mg/ml stock solution), 2.5 μL 3 M sodium acetate (pH 5.2), and 15 μL of isopropanol. Mix well. Centrifuge immediately at 10,000–15,000 × g for 30 min at 4 °C. Carefully remove the supernatant without disturbing the pellet (cDNA and glycogen). Add 100 μL of 70% ethanol and centrifuge for 15 min at 4 °C. Carefully remove the supernatant, air-dry the pellet for 5 min and re-dissolve in 5 μL of Tris–HCl (10 mM) (pH ≥ 8).

3.1.3. Polymerase Chain Reaction (see ***Note 4***)

1. Prepare the oligonucleotide primers for PCR (*see* **Note 5**).
2. Prepare the PCR mix (*see* **Note 6**).
3. Insert the PCR tubes into the thermocycler.

Reagents	Final concentration
Ultrapure ddH_2O	Up to final volume (*see* **Note 6**)
10× PCR buffer	1×
50 mM $MgCl_2$	1.5 mM (*see* **Note 7**)
1.25 mM dNTP mix	–
Forward primer (10 μM)	0.2–1.0 μM (*see* **Note 8**)
Reverse primer (10 μM)	0.2–1.0 μ M (*see* **Note 8**)
Template DNA	Purified cDNA from single cell RT reaction
Taq polymerase (5 U/μL)	1.25 U

4. Program the PCR cycles and run PCR (*see* **Note 9**) .
5. Remove the reaction tubes upon completion of the PCR. The reaction products can be analyzed by gel electrophoresis, DNA sequencing, microarray hybridization, or by other techniques. If necessary, the PCR products can be purified using a commercially available PCR purification kit. Alternatively, the entire reaction can be stored in a freezer for later use.

3.2. Expression Profiling of Inka Cells

3.2.1. Dissociation of Inka Cells

1. In the larval stage, seven pairs of Inka cells are distributed along the tracheae ***(39)***. The Inka cells produce the peptide ecdysis-triggering hormone (ETH), which is secreted at each ecdysis ***(40)***. To visualize the Inka cells, we use a UAS-atrial natriuretic factor-emerald (ANF-EMD) reporter construct that treats the ANF-EMD fusion protein as an endogenous neuropeptide ***(41)***. The expression of this transgene can then be driven in the Inka cells with the c929 enhancer trap ***(42)***. The larval progeny from a UAS-ANF-EMD × c929-Gal4 cross-expresses GFP fluorescence, in a pattern which co-localizes with the ETH-immunoreactive Inka cells ***(12)***. Inka cells can be removed from the tracheae with a collagenase/dispase enzyme mix.
2. Progeny from the cross will be heterozygous for the two transgenes. Dissect third instar "wandering" larvae in Ca^{2+}-free HL3 and remove the two main tracheal trunks.
3. Incubate tracheae in 500-μL collagenase/dispase enzyme mix in an Eppendorf tube; two complete sets of tracheae (comprising a maximum of 28 Inka cells) are sufficient.
4. Dissociation of Inka cells can be optimized by setting up several tubes of tracheae in collagenase/dispase enzyme mix and varying the incubation time. At the end of each incubation period, remove the tracheae from the enzyme mix, mount on a slide, and place a coverslip.
5. Slide preparations of tracheae from the various incubation periods can be compared through fluorescent microscopy to mounted, untreated tracheae to establish the point at which the fluorescent Inka cells dissociate from the tracheae. However, digested tracheae can result from a longer incubation and should be avoided.
6. Any dissociated Inka cells should remain in the tube with the enzyme mix. Centrifuge tubes for 5 min at 7500 × *g* to pellet Inka cells. Remove supernatant and proceed to RNA isolation step.

3.2.2. Reverse Transcription Polymerase Chain Reaction

1. Isolate total RNA from Inka cells using TRIZOL reagent, following manufacturer's instructions. For the initial homogenization, 100 μL of TRIZOL reagent is sufficient;

all other reagents should be scaled down similarly. Aliquots of 2-μL glycogen can be added before RNA precipitation with isopropanol. The RNA pellet can be re-dissolved in 20 μL DEPC H_2O.

2. One issue with RNA isolation using the TRIZOL reagent is the presence of contaminating genomic DNA in the RNA pellet. For this reason, PCR primers should be designed to flank an intron. If the gene structure is unknown or it is not possible to design intron-flanking primers, then we suggest using Ambion's DNA-free™ kit (*see* **Note 10**).
3. Convert RNA to cDNA using SuperScript III First-Strand cDNA Synthesis System for RT–PCR, following manufacturer's instructions (*see* **Note 11**). For one reaction, 8 μL total RNA can be converted. The addition of RNaseH is not necessary.
4. For amplification of cDNA product, use FailSafe™ PCR PreMix Selection Kit, following manufacturer's instructions for "Suggested PCR Protocol." For a 30-μL amplification reaction, 1.2-μL template cDNA can be used. If contaminating genomic DNA was not removed with DNase, then intron-flanking primers should be used. To amplify the ETH gene, we used the forward primer 5′-AGTCCTGTCTGTTTCGCTCTTG-3′ and the reverse primer 5′-AGGAGCGTATTCGAGTTGACG-3′ which produce a 309 bp cDNA product and a 367 bp genomic DNA product (**Fig. 2**).
5. A suitable thermocycler program for amplification of ETH cDNA product is: (94 °C, 3 min, 1 cycle) ([94 °C, 15 s; 47 °C, 30 s; 72 °C, 1 min] × 40 cycles) (72 °C, 5 min, 1 cycle).

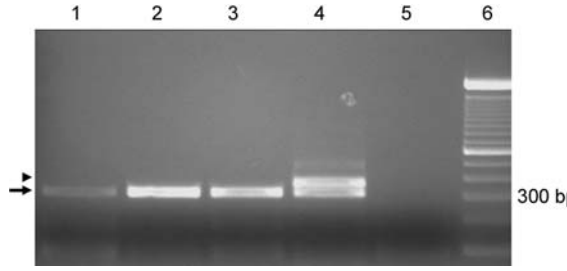

Fig. 2. Gel electrophoresis of ecdysis-triggering hormone (ETH) reverse transcription polymerase chain reaction (RT–PCR) product from Inka cells. Lanes 1–3 reflect differences in incubation times of Inka cells in collagenase/dispase enzyme mix. Lane 1: 15 min-incubation. Lane 2: 30-min incubation. Lane 3: 60-min incubation. Lane 4: whole larva cDNA. Lane 5: negative control. Lane 6: 100 bp ladder. The primers span an intron in the ETH gene. Arrow: ETH cDNA (309 bp). Arrowhead: ETH genomic DNA (367 bp). The observed 309 bp PCR product is amplified from cDNA corresponding to less than one Inka cell's sample of mRNA.

3.3. Laser Capture Microdissection

3.3.1. Slide and Tissue Preparation for LMD

1. While PENfoil slides are available for purchase from Leica, they are quite costly. Instead, these slides can easily be made in bulk in the laboratory. To produce PENfoil slides, standard glass microscope slides are first cleaned in ethanol and dried, and a sheet of PENfoil is cut that is slightly smaller than the width and diameter of the slide. To minimize any wrinkles in the surface of the foil, the PENfoil must be applied wet, which can easily be done by putting a few milliliters of sterile water onto the slide first and floating the PENfoil on top. Using gloved fingers, we smooth the PENfoil out over the surface of the slide. The water is then drained off, and the slide is left to air-dry. (*see* **Note 12**).
2. To embed the tissue, we recommend using 3% agarose as a supporting medium. The agarose (standard UltraPure molecular biology grade) should be dissolved in water, melted, and cooled in a 50 °C water bath. When the tissue samples are ready for embedding, a small amount of the agarose is poured into the mold. The sample is placed into the agarose and held steady in the desired orientation until the agarose hardens. As a 3% agarose solution is significantly less viscous than OCT or TFM, the tissue will tend to fall over unless it is held in place until the agarose solidifies. Additional agarose can then be poured over the sample to stabilize the sample, and the blocks stored at −80 °C until ready to use. Agarose blocks should be brought up to temperature prior to sectioning by equilibrating the block in the cryostat for approximately 20 min. The blocks are then sectioned on a cryostat (we have successfully used sections from 5 to 20 μm) onto the PENfoil slides. Ideally, no further processing (histological or immunohistochemical) would be needed to identify appropriate cells for dissection. We have found that the optics on the Leica AS LMD can allow us to identify regions of interest using brightfield alone. To obtain maximal contrast, we should allow the section to air-dry (~15 min) prior to visualizing the tissue on the microscope.

3.3.2. Laser Microdissection (see **Note 13**)

Sectioning controls available for user manipulation in the Leica software include intensity, speed, aperture, and offset. The optimal settings will need to be empirically determined for each tissue. In cutting sections from the olfactory system and brain, we have found that the intensity is best left at 100%. Given that the laser is not continuously active, but rather is pulsed in 4 ns bursts, the surrounding tissue does not heat up appreciably. We have also discovered that a relatively slow speed (three of nine) works well for cutting through tissue bounded by cartilage or connective tissue (e.g., in the nasal epithelium). Aperture plays a small role if the goal is to excise relatively large (tens to hundreds of cells) LMD samples. The larger the aperture, the wider the beam,

and the more surrounding tissue is ablated. Of all the user-defined settings, the offset setting is in our view the most critical parameter to optimize. For each objective, the focal position of visible light and that of the UV laser microbeam are not precisely equivalent. The offset enables the laser microbeam to be focused in the same plane as what is being visualized on the microscope. Without correcting for offset, the beam may in fact be focused above or below the sample and will not dissect with maximal efficiency.

3.3.3. mRNA Isolation of Tissue Section (see **Note 14**)

1. We have essentially followed the manufacturer protocol for the Gentra PureScript kit (for a list of mRNA purification kits *see* **Table 2**) with the following modifications. After LMD has been completed, the samples are collected in the collection cap in 50 μL lysis buffer and pipetted 10 times to dissolve the tissue. Gentra recommends minimal (two to three times) pipetting, as additional mechanical agitation can release genomic DNA. While we have observed this to be the case, the yield of RNA is improved by pipetting multiple times. After addition and incubation with the DNA/protein precipitation solution, the mixture is centrifuged and the supernatant transferred to a fresh tube. This supernatant is centrifuged a second time to remove any remaining DNA/protein precipitate. Prior to precipitating the RNA, 5–10 μg linear polyacrylamide (Ambion) is added as carrier. After addition of isopropanol, the RNA is precipitated overnight at −20 °C before being collected by centrifugation and resuspended.
2. From 50 to 100 isolated cells, we test one tenth of the resuspended RNA using a Picochip on Agilent's BioAnalyzer. We have found that quantities as low as 100 pg can be detected with the BioAnalyzer, but as the amount of RNA drops below 500 pg, the 28S/18S ratio values are no longer accurate. Thus, integrity of the RNA, as defined by the 28S/18S ratio, cannot be determined from very small amounts of RNA with this assay. However, as a means of detecting presence or absence

Table 2
Nano and Micro RNA Isolation Kits

Manufacturer	System	Website URL
Ambion	RNAqueous micro	ambion.com
Arcturus	PicoPure	arctur.com
Gentra	PureScript	gentra.com
Qiagen	RNEasy micro	qiagen.com
Stratagene	Absolutely RNA Nanoprep	stratagene.com

of RNA in the purified samples, the Picochip is very useful. For assessing RNA integrity from fewer than 10 cells, we have primarily used RT–PCR to determine the expression of various highly expressed genes (e.g., β-actin, GAPDH). In these instances, primers designed to bind the 5′ and 3′ end of these genes can be used to estimate the integrity of the RNA.

3.3.4. cDNA Synthesis and Amplification of RNA (see **Note 15**)

1. We use standard 20-μL reactions using Superscript III (Invitrogen) for RT of the purified RNA. The RT reaction can be directly used for RNA amplification. However, the cDNA should be purified (e.g., by ethanol or isopropanol precipitation) before it is used as template in PCR. We have had great success using T7-based amplification protocols to amplify RNA from LMD samples obtained and purified as described in **Subheading 3.3.2**. While we have predominantly used our own protocol for this process ***(35)***, an increasing number of vendors provide commercial kits to amplify this RNA (**Table 3**).

4. Notes

1. Silanation of the glass capillaries prevents adsorption of RNA to the interior of the patch-clamp pipette.)
2. Isolation of single-cell mRNA by aspiration of the cytoplasm into the patch-pipette is relatively easy and avoids aspiration of contaminants from the cell's surroundings. It is also possible, however, to aspirate the entire cell using a pipette with a larger mouth ***(8,37)***.
3. Direct addition of the RT mix to the PCR can decrease the efficiency of the amplification. Therefore, we recommend purifying the cDNA before addition to the PCR. Glycogen is a useful addition to precipitate small amounts of RNA as it increases the size of the pellet making it more easily visible. As an alternative

Table 3
RNA Amplification Kits

Manufacturer	System	Website URL
Agilent Technologies	Low RNA Input Linear Amplification kit	chem.agilent.com
Affymetrix	Two-cycle target labeling	genechip.com
Ambion	Message Amp aRNA	ambion.com
Arcturus	RiboAmp	arctur.com
ArrayIt	miniAmp	arrayit.com

to the "traditional" isopropanol precipitation method, the use of a commercially available DNA purification kit has been described recently *(8)*.

4. Fully optimized, successful PCR amplification of a single DNA template can be achieved. The accumulation of product (P) during PCR is governed by the equation

$$P = N_0 \times (1 + Y)^{n-1}$$

where N_0 is the number of duplex template copies at the start of the PCR, n equals the number of cycles, and Y the efficiency of the reaction. In general, the efficiency is ≤ 1. This formula does not apply for very low copy numbers ($N_0 \ll 100$) when amplification becomes stochastic. Nonetheless, this very high sensitivity of PCR poses a formidable problem because of the constant danger of contaminating samples with previously amplified DNA, which can yield false-positive results. Appropriate laboratory practice is of utmost importance. For example, it is good practice to use filtered pipette tips whenever possible to avoid contamination.

5. Information needed to prepare primers for PCR is provided in the "Analysis Report" included by the manufacturer of the oligonucleotides. To calculate the extinction coefficient (E), use the formula:

$$E_{\mathrm{M}} = (n \times \mathrm{A} \times 16,000) + (n \times \mathrm{G} \times 12,000) + (n \times \mathrm{C} \times 7000) + (n \times \mathrm{T} \times 9600)$$

with n denoting the number of the bases A, C, G, and T. Using E_{M} (concentration in M) of each oligonucleotide, one can calculate the volume (V; in μL) needed to prepare the primer stock solution using the formula:

$$V = \frac{\mathrm{OD}_{260}}{E_{\mathrm{mM}}}$$

with E_{mM} (concentration in mM). Please note that primer stock solutions are usually 100–500 μM. Store at −20 °C.

6. PCR is generally performed in volumes between 20 and 50 μL using special thin-walled reaction tubes (0.2 mL). For several PCRs, a master mix is usually prepared containing all reagents except reaction-specific primers and DNA template. The volume of the master mix (V_{MM}) is calculated by the formula:

$$V_{\mathrm{MM}} = V_{\mathrm{PCR}} \times (n_{\mathrm{PCR}} + 1)$$

where V_{PCR} is the final reaction volume and n_{PCR} the number of reactions. The number of actual reactions is increased by one in order to account for small pipetting errors.

7. Amplification efficiency is influenced by the magnesium concentration in the PCR. Although most primer/template combinations work well at the "standard"

magnesium concentration of 1.5 mM, the "best" concentration has to be determined empirically by varying the magnesium content of the reaction. A range of 0.5–3 mM is usually sufficient for finding the optimal concentration.

8. Well-chosen and designed primers are essential for the success of the PCR ***(43)***. In our own experience, primers between 20 and 24 nucleotides with a similar G/C content between 50 and 65% have worked very well ***(10,11)***. The 5′ and 3′ ends of the primers should not be complementary in order to prevent the formation of hairpins or primer dimers. "Primer 3" ***(44)***, one of the best software tools for computer-assisted design of primers, is available online free of charge (http://frodo.wi.mit.edu/cgi-bin/primer3/primer3_www.cgi). Multiple primer pairs aimed at different targets can be added in the same PCR to perform so-called "multiplex PCR" ***(43)***. The optimal annealing temperature depends on the G/C content of the primers and the template and has to be determined empirically.
9. One PCR cycle normally includes three basic steps: (1) denaturation (typically performed at 95 °C for 20 s to 5 min depending on the amount of expected secondary structure and complexity of the template), (2) annealing (the annealing temperature depends on the CG content of the primer and template. For example, for GC content < 50%, try annealing temperatures between 37 ° and 55 °C, but for GC content > 50%, try annealing temperatures between 48 and 70 °C), and (3) extension. In most cases, 25–35 cycles should be sufficient for amplification. Typically, a denaturation step of 1–5 min precedes the actual PCR cycles and an extra extension step (10 min) is sometimes added at the end of the PCR in order to extend incomplete amplicons to their final size.
10. The DNA-free™ kit contains DNase I, DNase I buffer, and DNase Removal Reagent. The advantage of this kit is that it does not require a phenol extraction or heat denaturation to eliminate or inactivate the DNase after DNA digestion.
11. This kit consists of an enzyme mix, plus 12 premix buffers to choose from to optimize the PCR. We have found that buffers D, J, K, and L give the best results. For the purposes of ETH cDNA amplification, buffer J has been the most consistently reliable.
12. It is critical that all of the water has evaporated from underneath the PENfoil, or it will be difficult to both visualize and laser microdissect the tissue. Any remaining water can be removed by drying the sample overnight at room temperature or in a warm (37 °C) oven and then using nail polish to seal the PENfoil to the slide. We have found that leaving the sealed slides overnight in a tissue culture hood with the UV light on (membrane side up) helps to ensure minimal residual RNase activity on the slide.
13. In an ideal scenario, methanol-fixed or fresh-frozen tissue would be used for LMD to best maintain the integrity of the RNA; however, fixation prior to embedding or after sectioning may be unavoidable (e.g., if immunohistochemistry is required to identify cell types of interest). Once the tissue sample has been excised from the animal, it should be embedded as soon as possible. If RNALater is used to preserve

the excised tissue, the tissue should be rinsed with PBS prior to embedding, as it can be very difficult to laser microdissect tissue soaked in RNALater. Cryosectioning through agarose can be tricky, as the agarose will shear and flake. While this does not affect the tissue, it can make collecting sections difficult. However, we believe the additional difficulty is well worth the effort given the improved integrity of the RNA. Counterstaining, if absolutely required, can be accomplished with hematoxylin and eosin. The excess residual water remaining on the slide after staining should be evaporated by allowing the slide to air-dry for 30 min or so. After this time, it should be obvious if the PENfoil membranes have been properly sealed and dried. Any water underneath the membrane (between the membrane and slide) will make it very difficult to visualize and laser microdissect samples. While the laser is capable of cutting through damp sections, this process is very inefficient.

Even after all settings have been determined, some tissues may be much more difficult to microdissect with a laser than others. Tissues with high stromal content, in particular, are very difficult templates for LMD. It may be necessary to perform two or more passes with the laser to completely cut through the surrounding tissue. Optimizing the settings for performing LMD does take some time, but once optimized, they can essentially be standardized for samples isolated from the same tissue-type collected on different days.

After the laser has completed ablation of tissue surrounding the sample, the membrane and sample fall away into a waiting collection cap. While the Leica AS LMD allows you to easily change focal positions to visualize the surface of the cap, it can be quite tedious to actually confirm that the sample lies within the cap. The sample may be attracted to the rim of the cap (which is well outside the plane of focus and not easily visualized) or to points unknown outside of the cap. As static electricity can have a strong effect on where the sample ultimately lands, we clean all exposed surfaces with 70% ethanol. This (we hope) helps to maximize the chance that a sample will end up within the collecting cap. One of the advantages of laser microdissection is the ability to rapidly excise large areas (100,000 μm^2) of tissue. Thus, hundreds, if not thousands, of cells can be isolated at a single sitting. It is, however, more difficult to isolate single cells. While this can be done with a $\times 63$ or $\times 100$ objective, a real problem in isolating single cells is finding an aperture setting that does not accidentally ablate the desired cell while removing the surrounding contaminating cells. However, with the new XT objectives available from Leica, the company claims that cutting diameters as low as 1 μm can be achieved with the $\times 63$ objective. This in principle will greatly improve the ability to excise individual cells.

14. While a variety of kits can be used to purify RNA from LMD samples (*see* **Table 2**), we prefer the Gentra kit for ease of use and high recovery rates. No matter which RNA isolation kit is chosen, we recommend that a small volume ($\sim$ 50 μL) of the lysis buffer be pipetted into the collecting cap. This will help to immediately

inactivate any RNases within the excised sample. While the lysis solution tends to evaporate as the sectioning proceeds, sections can be collected for at least 45 min.

15. Enough RNA can be produced in two rounds of amplification to hybridize Affymetrix GeneChips that normally require greater amounts of labeled material than spotted arrays for the hybridization. In addition to these technical considerations, one important statistical issue is to determine how many arrays are needed to reliably identify differentially expressed genes within a sample set ***(17)***. For example, although it is possible to isolate individual cells, it is still difficult to guarantee that no contaminating material has been isolated along with the desired cell type. Isolating multiple such cells and comparing the observed transcriptional profiles can sometimes be used as a measure of the degree of sample contamination. In addition, an important theoretical question is whether RNA from an individual cell should be amplified and compared against other individual cells or whether multiple cells should be isolated, the RNA pooled, and this population amplified. The advantage of the latter approach is to reduce the variance caused from any one cell and to identify general trends among cells exposed to the same stimulus. But this very reduction may hide important differences that exist among seemingly similar cells. Consideration of these statistical design issues is best accomplished prior to performing the LMD, RNA isolation, amplification, and microarray analysis.

References

1. Mullis, K., Faloona, F., Scharf, S., Saiki, R., Horn, G., and Erlich, H. (1986) Specific enzymatic amplification of DNA in vitro: the polymerase chain reaction. 1986. *Cold Spring Harb Symp Quant Biol 51 (Part 1)*: 263–273.
2. Mullis, K. B. (1990) The unusual origin of the polymerase chain reaction. *Sci Am* **262**, 56–61, 64–65.
3. Li, H. H., Gyllensten, U. B., Cui, X. F., Saiki, R. K., Erlich, H. A., and Arnheim, N. (1988) Amplification and analysis of DNA sequences in single human sperm and diploid cells. *Nature* **335**, 414–417.
4. Hahn, S., Zhong, X. Y., Troeger, C., Burgemeister, R., Gloning, K., and Holzgreve, W. (2000) Current applications of single-cell PCR. *Cell Mol Life Sci* **57**, 96–105.
5. Bustin, S. A. (2000) Absolute quantification of mRNA using real-time reverse transcription polymerase chain reaction assays. *J Mol Endocrinol* **25**, 169–193.
6. Freeman, W. M., Walker, S. J., and Vrana, K. E. (1999) Quantitative RT-PCR: pitfalls and potential. *Biotechniques* **26**, 112–122, 124–125.
7. Wilhelm, J., and Pingoud, A. (2003) Real-time polymerase chain reaction. *Chembiochem* **4**, 1120–1128.
8. Durand, G. M., Marandi, N., Herberger, S. D., Blum, R., and Konnerth, A. (2005) Quantitative single-cell RT-PCR and Ca^{2+} imaging in brain slices. *Pflugers Arch* **451**, 716–726.

9. Hillman, K. L., Knudson, C. A., Carr, P. A., Doze, V. A., and Porter, J. E. (2005) Adrenergic receptor characterization of CA1 hippocampal neurons using real time single cell RT-PCR. *Brain Res Mol Brain Res* **139**, 267–276.
10. Sucher, N. J., and Deitcher, D. L. (1995) PCR and patch-clamp analysis of single neurons. *Neuron* **14**, 1095–1100.
11. Sucher, N. J., Deitcher, D. L., Baro, D. J., Warrick, R. M., and Guenther, E. (2000) Genes and channels: patch/voltage-clamp analysis and single-cell RT-PCR. *Cell Tissue Res* **302**, 295–307.
12. Husain, Q. M. and Ewer, J. (2004) Use of targetable gfp-tagged neuropeptide for visualizing neuropeptide release following execution of a behavior. *J Neurobiol* **59**, 181–191.
13. Shakiryanova, D., Tully, A., Hewes, R. S., Deitcher, D. L., and Levitan, E. S. (2005) Activity-dependent liberation of synaptic neuropeptide vesicles. *Nat Neurosci* **8**, 173–178.
14. Schena, M., Shalon, D., Davis, R. W., and Brown, P. O. (1995) Quantitative monitoring of gene expression patterns with a complementary DNA microarray. *Science* **270**, 467–470.
15. Fodor, S. P., Rava, R. P., Huang, X. C., Pease, A. C., Holmes, C. P., and Adams, C. L. (1993) Multiplexed biochemical assays with biological chips. *Nature* **364**, 555–556.
16. Dougherty, J. D. and Geschwind, D. H. (2005) Progress in realizing the promise of microarrays in systems neurobiology. *Neuron* **45**, 183–185.
17. Churchill, G. A. (2002) Fundamentals of experimental design for cDNA microarrays. *Nat Genet* **32 Suppl**, 490–495.
18. Lockhart, D. J., Dong, H., Byrne, M. C., Follettie, M. T., Gallo, M. V., Chee, M. S., Mittmann, M., Wang, C., Kobayashi, M., Horton, H., and Brown, E. L. (1996) Expression monitoring by hybridization to high-density oligonucleotide arrays. *Nat Biotechnol* **14**, 1675–1680.
19. Hughes, T. R., Mao, M., Jones, A. R., Burchard, J., Marton, M. J., Shannon, K. W., Lefkowitz, S. M., Ziman, M., Schelter, J. M., Meyer, M. R., Kobayashi, S., Davis, C., Dai, H., He, Y. D., Stephaniants, S. B., Cavet, G., Walker, W. L., West, A., Coffey, E., Shoemaker, D. D., Stoughton, R., Blanchard, A. P., Friend, S. H., and Linsley, P. S. (2001) Expression profiling using microarrays fabricated by an ink-jet oligonucleotide synthesizer. *Nat Biotechnol* **19**, 342–347.
20. Chudin, E., Walker, R., Kosaka, A., Wu, S. X., Rabert, D., Chang, T. K., and Kreder, D. E. (2002) Assessment of the relationship between signal intensities and transcript concentration for Affymetrix GeneChip arrays. *Genome Biol* **3**(1):RESEARCH0005. *Epub 2001 Dec 14, http://genomebiology.com/2001/3/1/research0005*.
21. Iscove, N. N., Barbara, M., Gu, M., Gibson, M., Modi, C., and Winegarden, N. (2002) Representation is faithfully preserved in global cDNA amplified exponentially from sub-picogram quantities of mRNA. *Nat Biotechnol* **20**, 940–943.

22. Velculescu, V. E., Madden, S. L., Zhang, L., Lash, A. E., Yu, J., Rago, C., Lal, A., Wang, C. J., Beaudry, G. A., Ciriello, K. M., Cook, B. P., Dufault, M. R., Ferguson, A. T., Gao, Y., He, T. C., Hermeking, H., Hiraldo, S. K., Hwang, P. M., Lopez, M. A., Luderer, H. F., Mathews, B., Petroziello, J. M., Polyak, K., Zawel, L., Kinzler, K. W., et al. (1999) Analysis of human transcriptomes. *Nat Genet* **23**, 387–388.
23. Mahadevappa, M. and Warrington, J. A. (1999) A high-density probe array sample preparation method using 10- to 100-fold fewer cells. *Nat Biotechnol* **17**, 1134–1136.
24. DeRisi, J. L., Iyer, V. R., and Brown, P. O. (1997) Exploring the metabolic and genetic control of gene expression on a genomic scale. *Science* **278**, 680–686.
25. Ludecke, H. J., Senger, G., Claussen, U., and Horsthemke, B. (1989) Cloning defined regions of the human genome by microdissection of banded chromosomes and enzymatic amplification. *Nature* **338**, 348–350.
26. Dixon, A. K., Richardson, P. J., Pinnock, R. D., and Lee, K. (2000) Gene-expression analysis at the single-cell level. *Trends Pharmacol Sci* **21**, 65–70.
27. Eberwine, J., Kacharmina, J. E., Andrews, C., Miyashiro, K., McIntosh, T., Becker, K., Barrett, T., Hinkle, D., Dent, G., and Marciano, P. (2001) mRNA expression analysis of tissue sections and single cells. *J Neurosci* **21**, 8310–8314.
28. Eberwine, J., Yeh, H., Miyashiro, K., Cao, Y., Nair, S., Finnell, R., Zettel, M., and Coleman, P. (1992) Analysis of gene expression in single live neurons. *Proc Natl Acad Sci USA* **89**, 3010–3014.
29. Freeman, T. C., Lee, K., and Richardson, P. J. (1999) Analysis of gene expression in single cells. *Curr Opin Biotechnol* **10**, 579–582.
30. Ginsberg, S. D. and Che, S. (2004) Combined histochemical staining, RNA amplification, regional, and single cell cDNA analysis within the hippocampus. *Lab Invest* **84**, 952–962.
31. Hahn, S., Zhong, X. Y., and Holzgreve, W. (2002) Single cell PCR in laser capture microscopy. *Methods Enzymol* **356**, 295–301.
32. Hinkle, D., Glanzer, J., Sarabi, A., Pajunen, T., Zielinski, J., Belt, B., Miyashiro, K., McIntosh, T., and Eberwine, J. (2004) Single neurons as experimental systems in molecular biology. *Prog Neurobiol* **72**, 129–142.
33. Kacharmina, J. E., Crino, P. B., and Eberwine, J. (1999) Preparation of cDNA from single cells and subcellular regions. *Methods Enzymol* **303**, 3–18.
34. Kelz, M. B., Dent, G. W., Therianos, S., Marciano, P. G., McIntosh, T. K., Coleman, P. D., and Eberwine, J. H. (2002) Single-cell antisense RNA amplification and microarray analysis as a tool for studying neurological degeneration and restoration. *Sci Aging Knowledge Environ* **2002**, re1.
35. Lin, D. M., Yang, Y. H., Scolnick, J. A., Brunet, L. J., Marsh, H., Peng, V., Okazaki, Y., Hayashizaki, Y., Speed, T. P., and Ngai, J. (2004) Spatial patterns of gene expression in the olfactory bulb. *Proc Natl Acad Sci USA* **101**, 12718–12723.

36. Monyer, H. and Lambolez, B. (1995) Molecular biology and physiology at the single-cell level. *Curr Opin Neurobiol* **5**, 382–387.
37. Van Gelder, R. N., von Zastrow, M. E., Yool, A., Dement, W. C., Barchas, J. D., and Eberwine, J. H. (1990) Amplified RNA synthesized from limited quantities of heterogeneous cDNA. *Proc Natl Acad Sci USA* **87**, 1663–1667.
38. Young, P. and Feng, G. (2004) Labeling neurons in vivo for morphological and functional studies. *Curr Opin Neurobiol* **14**, 642.
39. Park, Y., Filippov, V., Gill, S. S., and Adams, M. E. (2002) Deletion of the ecdysis-triggering hormone gene leads to lethal ecdysis deficiency. *Development* **129**, 493–503.
40. Zitnan, D., Zitnanova, I., Spalovska, I., Takac, P., Park, Y., and Adams, M. E. (2003) Conservation of ecdysis-triggering hormone signalling in insects. *J Exp Biol* **206**, 1275–1289.
41. Rao, S., Lang, C., Levitan, E. S., and Deitcher, D. L. (2001) Visualization of neuropeptide expression, transport, and exocytosis in Drosophila melanogaster. *J Neurobiol* **49**, 159–172.
42. O'Brien, M. A. and Taghert, P. H. (1998) A peritracheal neuropeptide system in insects: release of myomodulin-like peptides at ecdysis. *J Exp Biol* **201**, 193–209.
43. Dieffenbach, C. and Dveksler, G. (2003) *PCR Primer: A Laboratory Manual*. 2 ed., Cold Spring Harbor Laboratory Press, Cold Spring Harbor, NY.
44. Rozen, S. and Skaletsky, H. (2000) Primer3 on the WWW for general users and for biologist programmers, in *Bioinformatics Methods and Protocols: Methods in Molecular Biology* (Krawetz, S. and Misener, S., eds.), Humana Press, Totowa, NJ, pp. 365–386.

11

Brain on a Chip: A Method to Detect Novel Neuroprotective Candidate Targets

Yang Tang and Myriam Bernaudin

Summary

The search of potential novel therapeutical targets for neuroprotection has been widely intensified since the usefulness of microarray techniques. Indeed, this recent technology (also called Gene chip) provides a powerful tool to examine gene expression changes of thousands of genes at the same time, on a single chip in the brain. Arrays can paint a picture or "profile" (gene profiling, gene expression patterns) of which genes in the genome are active in a particular cell type and under a particular condition. In this chapter, we will describe the methods to perform microarrays and analyze the following data using GeneChip® technology (Affymetrix, Inc., Santa Clara, CA, USA), to identify, for example, potential brain neuroprotective targets. Moreover, step-by-step explanations of software operation will be provided. Finally, methods are presented to validate the gene expression changes revealed from the microarray analyses.

Key Words: Chip; microarray; brain; neuroprotection; genomic.

1. Introduction

A number of methods currently exist to measure the mRNA abundance and therefore to study gene expression changes. Besides conventional methods that are used to measure the expression levels of specific genes, such as northern blots, reverse transcriptase-polymerase chain reaction (RT–PCR), and nuclease protection, several novel approaches have been developed to characterize global gene expression profiles or screen for significant differences in mRNA abundance, including differential display, subtractive hybridization, cDNA fragment fingerprinting, serial analysis of gene expression (SAGE),

From: *Methods in Molecular Biology, vol. 399: Neuroprotection Methods and Protocols*
Edited by: T. Borsello © Humana Press Inc., Totowa, NJ

and microarrays. Microarray technology makes use of the sequence resources created by the genome projects and other sequencing efforts to study which genes are expressed in a particular cell type or tissue of an organism, at a particular time, under particular conditions. This technology is based on the principle of hybridization between two strands of complementary nucleic acids, one is fixed into a solid membrane and the other is the sample to analyze.

In addition to the term "DNA microarray," several additional terminologies are used in the literature to describe this technology including, but not limited to, DNA chip, gene array, biochip, or simply chip. Affymetrix, Inc. owns a registered trademark, GeneChip®, which refers to its high-density, oligonucleotide-based DNA arrays. Although the name GeneChip is a trademark of Affymetrix, this term is often used to refer to any microarray. Compared with other technologies, microarrays have recently received a great deal of attention because they have the capability to measure the expression of the whole genome in a single experiment, on a single chip, so that researchers can have a better picture of the interactions among thousands of genes simultaneously. Therefore, more recently, the term "genome chip" appeared, indicating that this technology could monitor the whole genome on a single chip.

There are two major applications for the DNA microarray technology: (1) identification of sequence (gene/gene mutation) and (2) determination of expression level (abundance) of genes. Knowing when, where, and how much a gene is expressed is useful to deduce biological functions. Furthermore, coordinated changes of expression pattern can provide clues about gene regulatory networks. Thus, microarrays serve many fields, including gene discovery, disease diagnosis, toxicological research (toxicogenomics), and drug discovery (pharmacogenomics). This last application will be further detailed in this chapter. Indeed, we ***(1–3)*** and others ***(4–7)*** have used microarrays to detect novel potential neuroprotective targets to counteract brain damage induced by hypoxia–ischemia.

Hypoxia and/or ischemia to the brain is a major cause of morbidity and mortality in both perinatal and adult periods, often resulting in cognitive impairment, seizures, and other neurological disabilities. Though hypoxia–ischemia animal models have increased our understanding of the processes leading to cell death, there are still no pharmacological treatments available to reduce cell death in ischemic brain. Interestingly, cells can be protected when a noninjurious hypoxic stress is performed several hours or days before a lethal hypoxic–ischemic stress (preconditioning). This phenomenon is called tolerance. Ischemic tolerance can be achieved in brain by several preconditioning sublethal stresses including hypoxia and ischemia itself. As ischemic

tolerance models might be a useful paradigm to understand the mechanisms that lead to brain protection against ischemia and consequently to identify new therapeutic targets for stroke, we ***(2,3)*** and several groups ***(5,6,8)*** have studied the genomic response to hypoxic or ischemic preconditioning by microarray analysis. The results gave rise to numerous potential neuroprotective targets.

This chapter discusses the methods to perform microarrays and to analyze microarrays' data with the example of GeneChip® (Affymetrix, Inc.) to identify, for example, potential brain neuroprotective targets. In addition, methods are presented to validate the gene expression changes revealed from the microarray analyses.

2. Materials

2.1. Gene Chip

1. Although many microarray systems have been developed, the most commonly used systems can be divided into two groups based on the property of arrayed DNA sequence: (1) *cDNA microarrays* and (2) *oligonucleotide genechips*. In the former, the probe cDNA (500–5000 bases long) is immobilized to a solid surface such as glass using robot spotting and exposed to a set of targets either separately or in a mixture. This method is "traditionally" called DNA microarray. In the latter, concerning the oligonucleotide probes, Affymetrix arrays use for example short oligonucleotide reporters of 25 or fewer bases. Other varieties of microarrays use longer (35–70 bases) oligonucleotides.
2. The array is exposed to labeled sample DNA and hybridized, and the identity/abundance of complementary sequences are determined. This method, "historically" called DNA chips, was developed at Affymetrix, Inc., which sells its photolithographically fabricated products under the GeneChip® trademark. Many companies are manufacturing oligonucleotide-based chips using alternative in situ synthesis or depositioning technologies.
3. See the different types of arrays and corresponding references (rat, mouse, human, etc.) on the Affymetrix web site: http://www.affymetrix.com.

2.2. RNA Sampling

1. Animals are purchased from a commercial breeder of the appropriate country.
2. Different types of anesthesic and analgesic are used depending on the species and the protocols: ketamine (Phoenix Pharmaceutical, Inc., St. Joseph, MO); xylazine (Phoenix Pharmaceutical); isofluorane (Abbott Laboratories, N. Chicago, IL); or others.
3. Small animal surgical instruments: scalpel, forceps, and scissors are useful for brain tissue isolation.

4. Disposable sterile 1-mL syringes (Becton Dickinson and Co., Franklin Lakes, NJ), needles (Becton Dickinson), or 1-mL homogenizer are necessary to homogenize the brain for RNA isolation.
5. Reagents needed for RNA isolation: Trizol® (Life Technology, Rockville, MD) and acidic-phenol: chloroform mixture, pH 4.5 (Ambion, Austin, TX), diethyl-pyrocarbonate (DEPC)-treated water (Life Technology), and RNeasy mini kit (Qiagen, Valencia, CA, USA).
6. Materials needed for RNA isolation: Rnase-free microtubes (0.5 and 1.5 mL), tips and PCR 96-well microplates with caps (USA Scientific, Germany), visible-wavelength spectrophotometer (Molecular Devices, SpectraMax Plus, Sunnyvale, CA, USA).

2.3. cDNA and cRNA Preparation and Hybridization to the Chip

All the reagents are widely listed in the Affymetrix Expression Analysis Technical Manual (GeneChip® Expression Analysis Technical Manual). For cDNA preparation, Affymetrix, Inc. sells a convenient package containing all required labeling and control reagents to perform 30 one-cycle labeling reactions (P/N 900493). Each of these components may be ordered individually as well as in this complete kit which contains: 1 IVT (in vitro transcription reaction) Labeling Kit (Affymetrix, P/N 900449); 1 one-Cycle cDNA Synthesis Kit (Affymetrix, P/N 900431); 1 sample Cleanup Module (Affymetrix, P/N 900371); 1 hybridization Control Kit (Affymetrix, P/N 900454); cRNA is fragmented with 5× RNA fragmentation buffer consisting of 200 mM Tris–acetate (pH 8.1) (Affymetrix, P/N T1503), 500 mM potassium acetate (KOAc; Affymetrix, P/N P5708), and 150 mM magnesium acetate (MgOAc; Affymetrix, P/N M2545).

2.4. Microarray Data Analysis

1. Affymetrix MAS5 software (Affymetrix, Inc.).
2. GeneSpring 6.0 software (Silicon Genetics, which is now part of Agilent Technologies, Palo Alto, CA, USA).

2.5. Real-Time RT–PCR

1. Reagents needed for RT–PCR experiments: two primers and one probe (TaqMan probe labeled with VIC on the 5′ nucleotide and TAMRA on the 3′ nucleotide; Applied Biosystems, Foster City, CA) and the TaqMan Gold RT–PCR kit (Applied Biosystems). Other companies such as Eurogentec (Angers, France) or Biorad (Marnes-la-Coquette, France) also sell their own real-time RT–PCR reagents.

2. Materials needed for RT–PCR: tips and PCR 96-well microplates with caps (USA Scientific), a real-time PCR cycler (Perkin-Elmer, ABI 5700), and Perkin-Elmer PrimerExpress software (Applied Biosystems). Other companies, such as Biorad, also sell their own real-time RT–PCR materials (real-time PCR cycler iCycler, Biorad).

3. Methods

RNA is extracted from cells or tissues, and converted to cDNA and then to cRNA. The newly synthesized cRNA contains tags (biotin-labeled cRNA). A cRNA molecule that contains a sequence complementary to one of the single-stranded probe sequences on the array will hybridize, via base pairing, to the spot at which the complementary reporters are affixed. The spot will then fluoresce (after staining with fluorescent streptavidin) when examined using a microarray scanner. The intensity of the fluorescence is roughly proportional to the number of copies of a particular mRNA that were present and thus roughly indicates the activity or expression level of that gene. All these different steps are summarized in **Figs. 1** and **2**.

3.1. Microarray: Oligonucleotide Genechips

Although many microarray systems have been developed, the most commonly used systems can be divided into two groups, as mentioned in the introduction: cDNA microarrays and oligonucleotide genechips. We will present only the latter one.

1. Oligonucleotide genechips (Affymetrix, Inc.) are different from cDNA microarrays in several ways. First, the method of array fabrication is different. Instead of using robotic spotting, genechips are synthesized through a light-directed process, which combines two techniques: photolithography and solid-phase DNA synthesis. Synthetic linkers modified with photochemically removable protecting groups are attached to a glass substrate. The first of a series of chemical building blocks, hydroxyl-protected deoxynucleosides, is incubated with the glass substrate, and chemical coupling occurs at sites that have been illuminated. Next, light is directed to different regions of the substrate by a new mask, and the chemical cycle is repeated. Second, the probe design and tiling strategy are different. In Affymetrix, expressed sequences from databases, including GeneBank, Refseq, dBEST, and UniGene, are collected and clustered into groups of similar sequences, which are further subdivided into subclusters representing distinct transcripts.
2. Each transcript represented on the array is assessed using 11–16 probe pairs with each consisting of an oligomer (25 base long) that is designed to be perfectly complementary to a particular message (called the perfect match or PM) and a

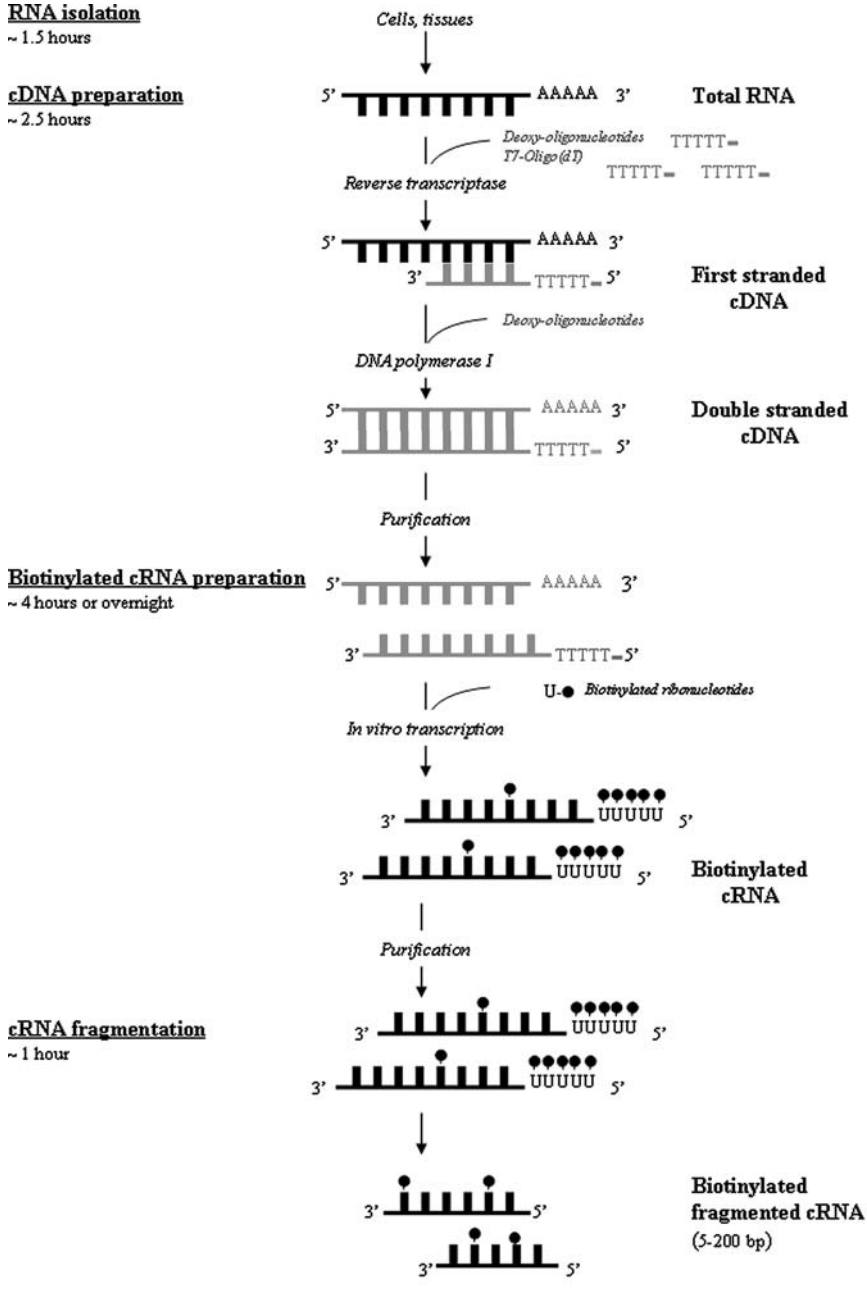
RNA isolation
~ 1.5 hours
Cells, tissues
cDNA preparation
~ 2.5 hours
5' AAAAA 3'
Total RNA
Deoxy-oligonucleotides
T7-Oligo(dT)
TTTTT-
TTTTT- TTTTT-
Reverse transcriptase
5' AAAAA 3'
3' TTTTT- 5'
First stranded cDNA
Deoxy-oligonucleotides
DNA polymerase I
5' AAAAA 3'
3' TTTTT- 5'
Double stranded cDNA
Purification
Biotinylated cRNA preparation
~ 4 hours or overnight
5' AAAAA 3'
3' TTTTT- 5'
U-● Biotinylated ribonucleotides
In vitro transcription
3' UUUUU 5'
3' UUUUU 5'
Biotinylated cRNA
Purification
cRNA fragmentation
~ 1 hour
3' UUUUU 5'
3' UUUUU 5'
3' 5'
3' 5'
Biotinylated fragmented cRNA
(5-200 bp)

companion oligomer that is identical to PM probe except for a single base difference in a central position (called the mismatch or MM probe).
3. The MM probe serves as a control for hybridization specificity and helps subtract nonspecific hybridization.

Thereafter, major steps involve RNA isolation and purification followed by data analysis and interpretation using advanced bioinformatic techniques. The final step consists of validation results with other methods such as real-time RT–PCR method.

3.2. RNA, cRNA Preparation and Hybridization to the Chip

1. All animal experiments should be approved and performed in strict accordance with the local ethics committee and governed by the pertinent national legislation. Animals should be acclimated to the animal quarters at least 3 days prior to study. The animals, maintained on a 12-h light/dark cycle, are given food and water ad libitum. In addition, all experimental and control animals are housed in the same room prior to and until the conclusion of the study. All surgical procedures described should be performed by aseptic technique with sterilized instruments and materials.
2. RNA isolation: Total RNAs from test and reference are extracted and double-stranded cDNAs are synthesized from total RNA. Brain or only a specific region of the brain is removed as rapidly as possible for RNA isolation (*see* **Notes 1–3**). Total RNA is isolated with Trizol® reagent (Life Technology) according to the manufacturer's protocol. Briefly, the tissue pellets are homogenized in Trizol Reagent using a syringe or homogenizer. After extraction with chloroform (an additional step of phenol/chloroform extraction is added to the manufacturer's protocol), RNA is precipitated by isopropyl alcohol and subjected to further purification using an RNeasy mini kit (Qiagen). The quality and quantity of extracted total RNA samples are examined by loading 5 μg of each sample on a denaturing agarose gel. The OD 260/280 ratio should be close to 2.0 for pure RNA (between 1.9 and 2.1

◄

Fig. 1. Schema summarizing the different steps (and their approximate duration) of the target preparation from RNA for future target hybridization to oligonucleotide arrays. Double-stranded cDNAs are synthesized from isolated RNAs from test and reference samples. To synthesize the first cDNA strand, an HPLC-purified oligo-dT primer is annealed to the RNA, and extension by reverse transcriptase is performed in the presence of deoxyoligonucleotides. The second strand is synthesized using DNA polymerase I. Double-stranded cDNAs are purified, and an in vitro transcription is performed to produce biotin-labeled cRNA. cRNAs are purified, fragmented, and then incubated at 94° C for 35 min before to put them on ice and stored at −20° C until ready to perform the hybridization.

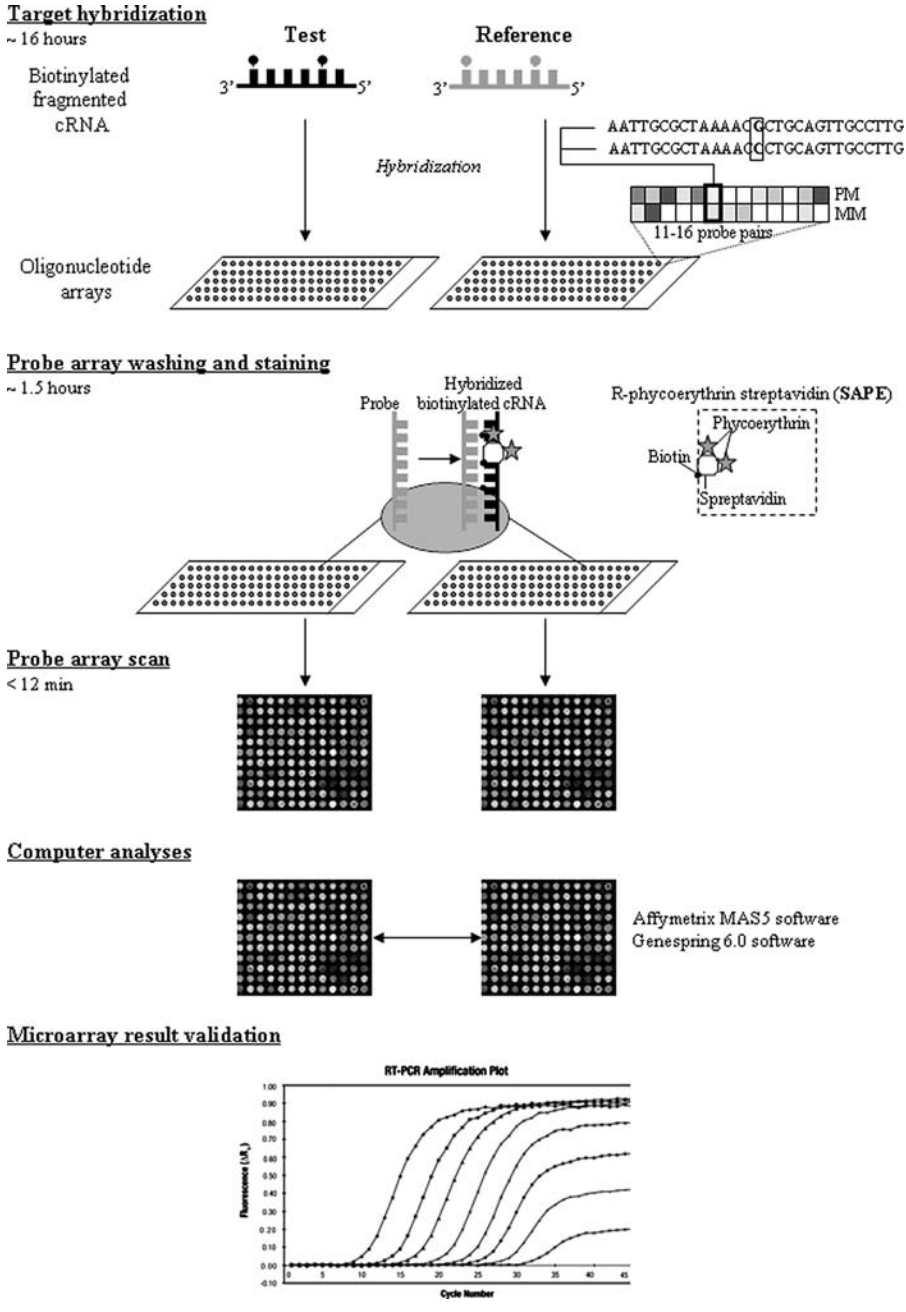
Target hybridization
~ 16 hours
Test
Reference
Biotinylated fragmented cRNA
3'
5'
3'
5'
AATTGCGCTAAAAGCCTGCAGTTGCCTTG
AATTGCGCTAAAAGCCTGCAGTTGCCTTG
Hybridization
PM
MM
11-16 probe pairs
Oligonucleotide arrays
Probe array washing and staining
~ 1.5 hours
Probe
Hybridized biotinylated cRNA
R-phycoerythrin streptavidin (SAPE)
Phycoerythrin
Biotin
Spreptavidin
Probe array scan
< 12 min
Computer analyses
Affymetrix MAS5 software
Genespring 6.0 software
Microarray result validation
RT-PCR Amplification Plot
Fluorescence (ΔRn)
Cycle Number

is acceptable) (*see* **Note 4**). Then, sample labeling, hybridization to arrays, and image scanning are carried out as described in the Affymetrix Expression Analysis Technical Manual. Approximately, 10 μg is enough in a maximal volume of 10 μL for microarray proceeding.

3. cDNA preparation: Double-stranded cDNA is synthesized from total RNA. To synthesize the first cDNA strand, an HPLC-purified oligo-dT primer is annealed to the RNA and extension by reverse transcriptase is performed in the presence of deoxyoligonucleotides. The second strand is synthesized using DNA polymerase I. Double-stranded cDNA was purified using a modified phenol/chloroform extraction procedure (Eppendorf-5 Prime, Boulder, Colorado), followed by ethanol precipitation.
4. Biotinylated labeled cRNA preparation: An IVT reaction is performed to produce biotin-labeled cRNA from the purified cDNA using the ENZO BioArray™High-Yield RNA Transcript Labeling kit. The cRNA is purified with affinity columns (Qiagen) followed by ethanol precipitation. No amplification procedure is performed to produce the final cRNA. The amount of product is quantified by spectrophotometric analysis, and the quality of the cRNA is assessed by gel electrophoresis.
5. After the biotin labeling, cRNA is fragmented with 2 μL of 5× RNA fragmentation buffer for every 8 μL RNA plus H_2O with a final concentration of RNA ranging from 0.5 to 2 μg/μL. Then, cRNA are incubated at 94° C for 35 min and then put on ice. The quality of the cRNA fragmentation is assessed by gel electrophoresis: the fragmentation procedure should produce RNA fragment sizes from approximately 5 to 200 bases. Fragmented-labeled cRNA can be stored at −20° C until ready to perform the hybridization.

Fig. 2. Schema summarizing the different steps from the hybridization of the target to the Affymetrix oligonucleotide chip to the analyses of results (PM, perfect match; MM, mismatch probes). cRNA was hybridized to Affymetrix arrays (Affymetrix, Inc.) automatically in a chamber at 45° C for 16 h while being rotated at 60 rpm. The hybridized probe array is then automatically washed, stained, dried, and scanned two times at an excitation wavelength of 488 nm. The staining is realized using R-phycoerythrin streptavidin (SAPE) and can be amplified with antibody amplification (anti-streptavidin antibody biotinylated and SAPE again). After hybridization, intensity data are captured, and the Affymetrix Genechip software MAS 5.0 automatically calculates intensity values for each probe cell and uses these probe cell intensities to calculate an average intensity for each gene, which directly correlates with mRNA abundance. After other possible computer analyses with GeneSpring 6.0 software, for example, one major step is to validate with other methods the gene expression changes. This can be done at the mRNA level using for example real-time reverse transcriptase-polymerase chain reaction (RT–PCR) to quantitate mRNA levels for selected genes.

6. Hybridization: In contrast to cDNA microarrays, test and reference samples are hybridized to separate arrays. Once prepared, cRNA was hybridized to Affymetrix arrays (Affymetrix, Inc.). The hybridization cocktail, containing the cRNA sample, acetylated bovine serum albumin (BSA), and herring sperm DNA, is incubated at 99° C, transferred to 45° C, and then injected into the microarray chamber (Affymetrix, Inc.). Hybridization is performed automatically in a chamber at 45° C for 16 h while being rotated at 60 rpm.
7. Washing, staining, and scanning probe arrays: The hybridized probe array is then automatically washed, stained, dried, and scanned two times at an excitation wavelength of 488 nm. The staining is realized using R-phycoerythrin streptavidin (SAPE) and can be amplified with antibody amplification (anti-streptavidin antibody biotinylated, and SAPE is added again).

3.3. Microarray Data Analysis

1. After hybridization, intensity data are captured; the Affymetrix Genechip software MAS 5.0 automatically calculates intensity values for each probe cell and uses these probe cell intensities to calculate an average intensity for each gene (called average difference), which directly correlates with mRNA abundance.
2. Affymetrix software also gives each gene a qualitative assessment of "present" or "absent" based on a "voting scheme," using the number of instances in which the PM signal is significantly larger than the MM signal across the whole probe set.
3. Prior to comparing any two measurements, a scaling procedure is performed so that all signal intensities on an array are multiplied by a factor that makes the mean PM–MM value for each array equal to a preset value. The scaling corrects for any inter-array differences or small differences in sample concentration, labeling efficiency, or fluorescence detection and makes inter-array comparisons possible.
4. In the case of a pair-wise comparison of two array results, the patterns of change of the whole probe set (with consistent voting) is used to make a qualitative call of "Increase," "Decrease," "Marginally increase," "Marginally decrease," or "No change." The fold change is derived by the ratio of Average Differences from one "test" compared to a "reference" array. The typical process of data analysis is screen (by calls), statistical test (*t*-test or permutations), and then cluster analysis to find co-regulated gene groups.
5. Therefore, the first step in most analyses is to determine whether changes in gene expression are experimentally significant. When the number of sample replicates is limited, the fold-change threshold alone or combined with other empirical criteria is usually adopted ***(9,10)*** (*see* **Note 5**).
6. When more replicates (at least three) are available, statistical analyses are usually adopted to determine what genes are significantly regulated (*see* **Note 6**). Methods based on conventional parametric or nonparametric tests provide the probability that a difference in gene expression occurred by chance. However, although $P < 0.01$ is significant in the experiments designed to evaluate small numbers of genes, a

microarray experiment surveying 50,000 genes would identify 500 genes just by chance, which will produce a large number of false-positives, that is, genes falsely called differentially expressed when they are not. This limitation has led to introduction of statistical methods using multiple testing corrections such as Benjamini–Hochberg False Discovery Rate, Bonferroni test, and Westfall and Young permutation tests that can been found in the GeneSpring software 6.0. Methods based on permutation have also been developed such as significance analysis of microarray (SAM).

7. The hierarchical ***(11)*** and K-means clustering algorithms ***(12)*** as well as self-organizing maps ***(13)*** have all been successfully used for deciphering expression profiles. Hierarchical clustering works by iteratively joining the two closest clusters starting from singleton clusters. A hierarchical cluster analysis is applied to organize the expression data such that genes and conditions so that similar expression profiles are grouped together. This process results in a phylogenetic tree, the branch lengths of which reflect the degree of similarity between genes or treatments. The cluster analysis is performed on all the genes that are regulated by any of the conditions. Then all of the conditions are normalized to the "reference" samples, and the normalized values are graphed in log scale and subjected to a hierarchical cluster algorithm using GeneSpring software and a standard correlation coefficient of 0.95 as the measure for significant statistical similarity. Genes having similar expression patterns across all the groups are grouped, while conditions causing similar genomic responses are clustered together. The branching behavior of the tree is controlled using a separation ratio setting. The K-means and self-organizing maps clustering algorithm typically use the Euclidean distances of the vector space. In contrast to hierarchical clustering, the desired number of clusters in these algorithms has to be chosen before the clustering is performed. After the initial partitioning of the vector space into K parts, the algorithm calculates the center points in each subspace and adjusts the partition so that each vector is assigned to the cluster, the center of which is the closest. This is repeated iteratively until either the partitioning stabilizes or the given number of iterations is exceeded ***(14,15)***.

Thereafter, one major step is to validate with other methods the gene expression changes. This can be done at the mRNA level using for example real-time RT–PCR to quantitate mRNA levels for selected genes.

3.4. Real-Time RT–PCR

1. Two primers and one probe (TaqMan probe) (Applied Biosystems) are designed for each gene using Perkin-Elmer PrimerExpress software (Applied Biosystems).
2. Probes are labeled with VIC on the 5′ nucleotide and TAMRA on the 3′ nucleotide. Assays should be run in triplicates on the Perkin-Elmer ABI 5700 instrument under default conditions (RT: 48° C for 30 min; AmpliTaqGold activation: 95° C for 10 min and then PCR: 40 cycles of 95° C, 15 s and 60° C, 1 min). The RT–PCR

protocol is done according to the manufacturer's protocol using the TaqMan Gold RT–PCR kit (Applied Biosystems) with 50 ng RNA for each sample.
3. The abundance of genes of interest is determined relative to a reference housekeeping gene such as the glyceraldehyde-3-phosphate dehydrogenase (GAPDH) transcript using TaqMan GAPDH RNA control reagents kits (Applied Biosystems) (*see* **Note 7**).
4. To verify the presence and the predicted size of amplified fragments, PCR products are separated by electrophoresis and visualized in 3% agarose gels with ethidium bromide.

It is generally concerned that since mRNA is only an intermediate to the ultimate product, the correlation between the mRNA and protein abundance may not exist ***(16,17)*** (*see* **Note 8**).

4. Notes

1. Details for the experimental procedures to induce brain neuroprotection with models of hypoxia-induced ischemic brain tolerance in vivo are given in **ref.** ***(18)***.
2. Only a specific area of the brain and not the whole brain may be isolated for RNA extraction if necessary (when lesion is localized to a specific area for example) in order not to dilute the signal.
3. Importance of the sampling time-point choice (short time/long time kinetics) depending on which type of gene is targeted (early/delay gene responses).
4. High quality RNA is the single most important determinant of successful microarray experiments. Care should be taken to provide pure, nondegraded total RNA samples. For example, the Affymetrix Core in Cincinnati (USA) runs each sample through quality control testing using the Agilent 2100 Bioanalyzer prior to beginning labeling procedures. The RNA 6000 Nano and Pico Assays are available, which consume as little as 25–500 ng and 200–5000 pg per sample, respectively. The Bioanalyzer separates the total RNA by size, and high quality samples should produce sharp, distinct 28S and 18S rRNA peaks, with a 28S to 18S ratio of 1.9–2.1.
5. Classifying regulated genes into stringent and less-stringent lists can provide an index of the reliability of data. For example, in previous studies ***(3)***, we have chosen the following criteria for the stringent list: (1) the average fold change of the means is at least 1.5-fold; (2) P values, obtained with parametric Student's t-test with global error model correction, is inferior to 0.05; (3) there are four increase calls for the four comparisons and at least five increase calls for the six or nine comparisons as determined by the Affymetrix GeneChip software (marginally increase and marginally decrease are treated as increase or decrease). Genes in the stringent list are more reliable than genes in the less-stringent list as based on the Affymetrix algorithm. However, somewhat less reliable genes, for example genes with a low abundance, or very high abundance genes that only change by 50%,

may also have important biological significance. Indeed, typically it is assumed that abundance ratios of 1.5–2 are indicative of a change in gene expression, but such estimates can be very crude, and the reliability of ratios highly depends on the absolute intensity. If the baseline intensity is low, fold change may be high, but the measurement may not be reliable. The reliability of ratio also varies from gene to gene due to specificity of the sequence and cross-hybridization of homologous sequences ***(19)***.

6. For each of the experimental conditions, at least three arrays should be used corresponding to three animals in each experimental group (triplicate arrays for each group).
7. Caution with housekeeping genes should be taken. Indeed, some genes are not appropriated as housekeeping genes in some experimental conditions. Thus, various "housekeeping" genes should be used.
8. Caution should be mentioned for negative results. Indeed, some false-negative results may be due to some oligonucleotides that are not optimal at the unique hybridization temperature used. We had this case for erythropoietin probe in our previous studies ***(2,3)***.

References

1. Tang, Y., Lu, A., Aronow, B. J., Wagner, K. R., and Sharp, F. R. (2002) Genomic responses of the brain to ischemic stroke, intracerebral haemorrhage, kainate seizures, hypoglycemia, and hypoxia. *Eur J Neurosci* **15**, 1937–1952.
2. Bernaudin, M., Tang, Y., Reilly, M., Petit, E., and Sharp, F. R. (2002) Brain genomic response following hypoxia and re-oxygenation in the neonatal rat. Identification of genes that might contribute to hypoxia-induced ischemic tolerance. *J Biol Chem* **277**, 39728–39738.
3. Tang, Y., Pacary, E., Freret, T., Divoux, D., Petit, E., Schumann-Bard, P., and Bernaudin, M. (2005) Effect of hypoxic preconditioning on brain genomic response before and following ischemia in the adult mouse: Identification of potential neuroprotective candidates for stroke. *Neurobiol Dis* **21**, 18–28.
4. Jin, K., Mao, X. O., Eshoo, M. W., Nagayama, T., Minami, M., Simon, R. P., and Greenberg, D. A. (2001) Microarray analysis of hippocampal gene expression in global cerebral ischemia. *Ann Neurol* **50**, 93–103.
5. Stenzel-Poore, M. P., Stevens, S. L., Xiong, Z., Lessov, N. S., Harrington, C. A., Mori, M., Meller, R., Rosenzweig, H. L., Tobar, E., Shaw, T. E., Chu, X., and Simon, R. P. (2003) Effect of ischaemic preconditioning on genomic response to cerebral ischaemia: similarity to neuroprotective strategies in hibernation and hypoxia-tolerant states. *Lancet* **362**, 1028–1037.
6. Kawahara, N., Wang, Y., Mukasa, A., Furuya, K., Shimizu, T., Hamakubo, T., Aburatani, H., Kodama, T., and Kirino, T. (2004) Genome-wide gene expression analysis for induced ischemic tolerance and delayed neuronal death following transient global ischemia in rats. *J Cereb Blood Flow Metab* **24**, 212–223.

7. Lu, X. C., Williams, A. J., Yao, C., Berti, R., Hartings, J. A., Whipple, R., Vahey, M. T., Polavarapu, R. G., Woller, K. L., Tortella, F. C., and Dave, J. R. (2004) Microarray analysis of acute and delayed gene expression profile in rats after focal ischemic brain injury and reperfusion. *J Neurosci Res* **77**, 843–857.
8. Dhodda, V. K., Sailor, K. A., Bowen, K. K., and Vemuganti, R. (2004) Putative endogenous mediators of preconditioning-induced ischemic tolerance in rat brain identified by genomic and proteomic analysis. *J Neurochem* **89**, 73–89.
9. Mirnics, K., Middleton, F. A., Marquez, A., Lewis, D. A., and Levitt, P. (2000) Molecular characterization of schizophrenia viewed by microarray analysis of gene expression in prefrontal cortex. *Neuron* **28**, 53–67.
10. Sandberg, R., Yasuda, R., Pankratz, D. G., Carter, T. A., Del Rio, J. A., Wodicka, L., Mayford, M., Lockhart, D. J., and Barlow, C. (2000) Regional and strain-specific gene expression mapping in the adult mouse brain. *Proc Natl Acad Sci USA* **97**, 11038–11043.
11. Eisen, M. B., Spellman, P. T., Brown, P. O., and Botstein, D. (1998) Cluster analysis and display of genome-wide expression patterns. *Proc Natl Acad Sci USA* **95**, 14863–14868.
12. Tavazoie, S., Hughes, J. D., Campbell, M. J., Cho, R. J., and Church, G. M. (1999) Systematic determination of genetic network architecture. *Nat Genet* **22**, 281–285.
13. Tamayo, P., Slonim, D., Mesirov, J., Zhu, Q., Kitareewan, S., Dmitrovsky, E., Lander, E. S., and Golub, T. R. (1999) Systematic determination of genetic network architecture. *Proc Natl Acad Sci USA* **96**, 2907–2912.
14. Brazma, A. and Vilo, J. (2000) Gene expression data analysis. *FEBS Lett* **480**, 17–24.
15. Sherlock, G. (2000) Analysis of large-scale gene expression data. *Curr Opin Immunol* **12**, 201–205.
16. Anderson, L. and Seilhamer, J. (1997) A comparison of selected mRNA and protein abundances in human liver. *Electrophoresis* **18**, 533–537.
17. Gygi, S. P., Rochon, Y., Franza, B. R., and Aebersold, R. (1999) Correlation between protein and mRNA abundance in yeast. *Mol Cell Biol* **19**, 1720–1730.
18. Bernaudin, M. and Sharp, F. R. (2004) Methods to detect hypoxia-induced ischemic tolerance in the brain. *Methods Enzymol* **381**, 399–416.
19. Claverie, J. M. (1999) Computational methods for the identification of differential and coordinated gene expression. *Hum Mol Genet* **8**, 1821–1832.

12

Intracerebral Infusion of Neurotrophic Factors

Theo Hagg

Summary

Neurotrophic factors are among the most potent neuroprotective and neuroregenerative agents known. However, they cross the adult mammalian blood–brain barrier very poorly and can have serious peripheral side effects. These problems can be solved by using chronic infusions with small pumps to directly deliver known quantities of these proteins into selected regions of the brains of small experimental animals such as rats and mice. The method consists of commercially available Alzet osmotic pumps that are placed under the skin and are connected to commercially available metal infusion cannulas whose tip can be stereotactically placed in virtually any location of the brain. Different models of pumps that fit comfortably in rodents can be selected for infusion between 1 and 28 days and at infusion rates ranging between 8 and 0.25 μL/h, respectively. Methodological details are provided for the successful use of proteins and to minimize the time of the surgery.

Key Words: Alzet; central nervous system; chronic infusion; degeneration; growth factor; mouse; intraventricular; pharmacological; rat; regeneration.

1. Introduction

Neurotrophic factors have been widely used to promote survival of cells in the central nervous system (CNS) and to promote sprouting and regeneration of axons in adult rodent models of neurological disorders ***(1–5)***. However, these sizable proteins do not normally cross the adult mammalian blood–brain barrier ***(6,7)***. Moreover, as with many growth factors and cytokines, they can have serious peripheral side effects ***(5)***. These are two of the reasons why systemically delivered neurotrophic factors have failed in clinical trials for

From: *Methods in Molecular Biology, vol. 399: Neuroprotection Methods and Protocols*
Edited by: T. Borsello © Humana Press Inc., Totowa, NJ

neurological disorders *(5)*. In experimental rodent models, these problems can be solved by using chronic infusions with Alzet osmotic pumps to deliver known quantities of these proteins into selected brain regions. The method can also be used to deliver other molecules and to determine whether a therapeutic agent that is effective after systemic administration acts directly through mechanisms in the CNS, rather than indirectly by inducing changes in the rest of the body.

The chronic intracerebral infusion method uses commercially available Alzet osmotic pumps that are filled with a solution containing the test reagent. Different types of pumps exist and can be used to infuse almost anywhere in the CNS from a few hours to 28 days, or longer if replaced with fresh pumps. The pump is placed under the skin, which reduces the chance of infections, and is connected to a metal infusion cannula (catheter) encased in a plastic platform. The tip of the cannula can be stereotactically placed in virtually any location of the brain, and the platform is quickly glued to the skull. At the end of the infusion period, the test reagent can be retrieved from the pump to determine the remaining biological activity. This chapter replaces an outdated version that dealt with this intracerebral infusion technology *(8)*.

2. Materials

2.1. Infusion Device

1. Alzet pumps with flow moderators (Durect Corporation, Cupertino, CA, http://www.alzet.com) (*see* **Fig. 1** and **Note 1**).
2. Brain infusion kits (Durect Corporation or Plastics One, Roanoka, VA) consisting of metal cannulas embedded in a plastic platform and their connecting lines (*see* **Note 2**).
3. If the cannulas need to be shortened (*see* **Note 2** and **Subheading 3.1., steps 3** and **4**): use Dremel drill (Dremel, Racine, WI) with fine grinding wheels (Dremel cut-off wheel no. 409), dissecting microscope, and a 30-ga needle.
4. Cyanoacrylate fluid glue also called superglue (e.g., Instant Krazy glue Advanced Formula; Elmers Products, Columbus, OH) can be purchased in most hardware stores (*see* **Note 3**).
5. Single-sided razor blade.
6. Petri dishes (9 cm) with holes in the lid (*see* **Note 4**), poster putty, and gas sterilization pouches.
7. Clear tubes (15 mL) filled with 3 mL sterile saline in a tube rack (as many as the number of pumps).

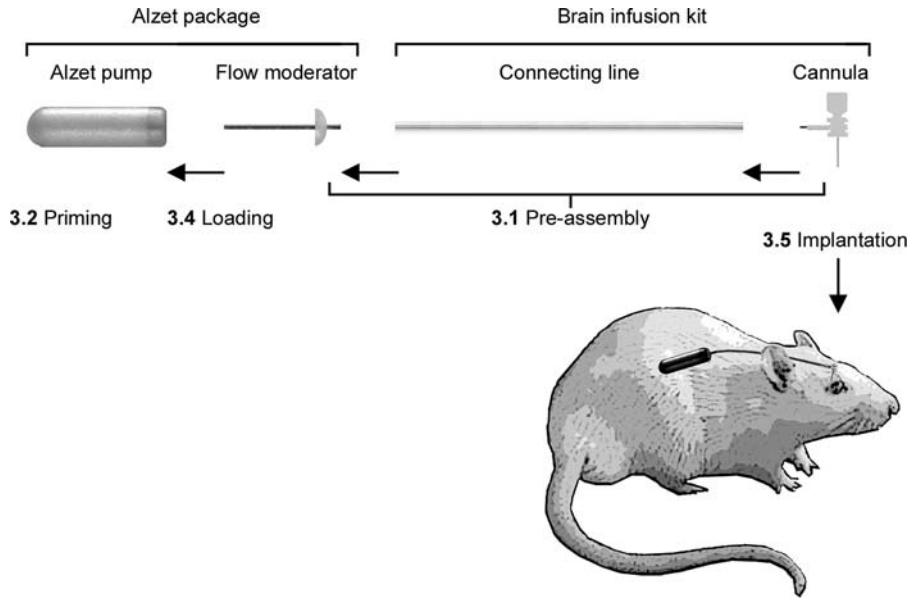

Fig. 1. Alzet pump and infusion device. Shown here are the parts of the infusion device and the steps that are described in **Heading 3.** with the corresponding section numbers. Also, shown is the final subcutaneous placement of the device in an adult rat.

2.2. Infusion Solution or Vehicle

1. Phosphate buffered saline (PBS) or appropriate other solution (depends on trophic factor; *see* **Note 5**) in a 5-mL or 15-mL polypropylene or other low-protein-binding tube.
2. Rat serum albumin (Cat. #A6272, Sigma-Aldrich, St. Louis, MO).
3. Gentamicin antibiotic solution (e.g., Cat. #G1272).
4. One's favorite sterile neurotrophic factor (*see* **Note 6**).

2.3. Filling Materials

1. Laminar tissue culture flow hood.
2. A few sterile 0.5-mL to 1.5-mL Eppendorf tubes in a small tube rack.
3. Sterile pipette tips and 20-μL and 200-μL pipetters.
4. A few 1-mL or 3-mL syringes and 0.2-μm Acrodisc low-protein-binding syringe filters (Pall Life Sciences, Ann Arbor, MI).
5. Medium-sized hemostatic forceps (e.g., FST 13009-12, Fine Science Tools, Foster City, CA) and Alzet pump filling tube from the Alzet pump package.
6. Ethanol, kimwipes, and latex or similar gloves.

2.4. Surgical Tools

1. Small animal clippers appropriate for the species (e.g., rats: Golden A5 model, Oster, McMinnville, TN; mice: GMT180TP plus CB-01, Conair Corporation, Glendale, AZ) and Betadine surgical scrub (Purdue Frederick Company, Norwalk, CT).
2. Stereotaxic apparatus with stereotaxic micromanipulator arm (*see* **Note 7**) and cannula holder (e.g., MH-300 or MH-300/SPC, Plastics One).
3. Instruments: No. 10 scalpel blade and holder (e.g., FST10003-12), blunt scissors (FST14512-15 for rats and FST14079-10 for mice), four small towel clamps (FST11095-09), low-heat electrocautery system (e.g., Gemini, Harvard Apparatus, Holliston, MA), Dremel or surgical drill with fine round-tip carbide drill burs (e.g., round HP-1 or HP-2, REF14823, SS White Burs, Lakewood, NJ), fine forceps (FST Dumont #5 and #7), sterile 30-ga needle, and two medium-sized forceps (FST11000-14 and FST110021-14).
4. Sterile surgical supplies: sterile drapes, sterile cotton applicators, gauze, small pieces of Gelfoam (Pharmacia & Upjohn, Kalamazoo, MI) presoaked in saline in Eppendorf tubes, and surgical or regular latex gloves.
5. Cyanoacrylate fluid glue.
6. Sodium bicarbonate powder (Cat. #S6014, Sigma-Aldrich) in 15-mL polystyrene or similar tube; Pasteur pipettes with rubber bulb.
7. Syringe (5 mL) filled with saline containing 0.1 mg/mL gentamicin.
8. Metal wound clips for rats (FST12040-01) with clip applying forceps (RS9290, Roboz, Gaithersburg, MD). Ethicon 5-0 silk sutures with attached needle for mice (Johnson and Johnson, Piscataway, NJ) and needle holder (e.g., FST12002-12 or hemostat FST13009-12).

3. Methods

The infusion method consists of five steps that are performed at different times and most likely in different locations of the laboratory (**Fig. 2**). These are designed to make the overall procedure efficient, to minimize the duration of the surgery, and to maintain sterility of the infusion solution. The latter is of particular importance when using proteins, which would otherwise be degraded inside the pump by organisms that grow well at the 36–37° C of the animal. The first step is to preassemble and gas-sterilize the infusion device consisting of the cannula, the connecting line, and the metal flow moderator, which will later be inserted into the Alzet pump. This preassembly can be done at any time before the surgery, and large numbers of devices can be made well in advance of large experiments. Alternatively, the assembly can be performed in a laminar flow hood just before loading the pumps. The second step is to prime the Alzet pumps by incubating them in saline, which will get the osmotic process to an equilibrium, and is needed to drive the flow. This is done overnight before the

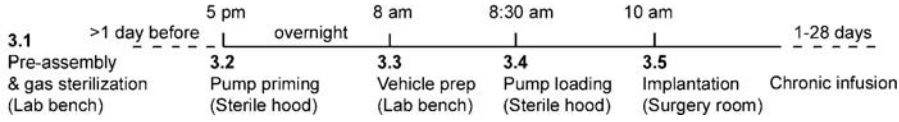

Fig. 2. Time-line of a typical experiment in the Hagg laboratory. Shown here are the steps of a typical infusion study in the laboratory as indicated by the numbers mentioned in **Heading 3.**, the locations where they are performed, and the approximate times when they are started.

day of surgery. The third step is to make the vehicle solution and is performed at the bench. The preassembled infusion device, preconditioned pumps, and vehicle solution are then taken to a laminar tissue culture flow hood for the fourth step, which consists of filling the pump and the final assembly of the infusion device. The fifth step is to implant the infusion device into the animal. Finally, if needed, the pump can be collected after the infusion period and the remaining fluid collected to measure the remaining biological activity of the neurotrophic factor.

3.1. Preassembly of the Infusion Device

1. The metal cannulas come embedded in a plastic platform that has a small cylinder attached on top to hold the platform for stereotaxic implantation. Do not remove that yet. There are two types of platforms. One has a much lower but wider profile that is well suited for mice with their less rigid skull. The wide platform can obstruct the view during surgery, and it can be helpful to cut off or trim one side of the flatter part. The other platform has a cylindrical shape and is appropriate for rats.
2. If a laboratory expects to infuse in various locations within the brain in different experiments, it is useful to purchase a large number of 11-mm cannulas and trim them to any desired length in the future. To do this, follow **steps 3–4**. If not, go to **step 5**.
3. Hold on to the platform and cut the metal cannula part to half a millimeter from the desired length. This can be done with a cut-off wheel and a Dremel or similar drill. Wear protective eye-gear. Next, using a dissecting scope, lightly bevel the tip of the cannula at a 45° angle with a fresh grinding wheel. This is best done with a sweeping motion against the direction of the spin of the cut-off wheel. If too much pressure is exerted or the wheel is old, the hole of the cannula will fill with too much metal. Afterward, any metal or other debris is removed with the tip of a 30-ga needle.
4. To test whether the cannula is open, attach the metal/plastic connector at the other end of the platform to an appropriately sized vinyl line and syringe and inject 95% ethanol through it. Afterward, remove the ethanol by injecting air through the

cannula. If the cannula is not open, check the opening of the metal cannula for additional debris.

5. One end of the connecting line (*see* **Note 2**) that is packaged with the cannula of the brain infusion kit (or alternative tubing) is attached to the platform via the short connector protruding from the platform and is secured with a small drop of Krazy glue (*see* **Note 8**). This glue is dry in about 10 min. For adult rats, the length of the connecting line generally needs to be 6–7 cm for placement of the Alzet pump between the shoulder blades. For mice, it is approximately 3 cm. This can more accurately be determined by measuring the required length in the particular strain used by the laboratory. The line can easily be cut with a single-sided razor blade.
6. The other end of the connecting line is attached to the short end of the flow moderator and secured by applying a small amount of Krazy glue. These moderators are the metal tubes that are located in the Alzet pump package. In some models (the 200# and 2ML# series), a small removable rubber guard needs to be removed first. For some models of flow moderators (the 100# series), the white tab needs to be broken off, for example, using sturdy forceps.
7. After the glue is dry, the assembled cannula-line-moderators are placed in a 9-cm Petri dish. The platforms (as many as are needed for an experiment, up to four to six per dish) can be pushed into a strip of poster putty on the bottom of the dish, which helps in taking them out for final assembly with the pumps (*see* **Subheading 3.4.**).
8. The Petri dish with the infusion devices (not the pumps) is placed in a gas sterilization bag for gas sterilization. Do not autoclave, as this will melt the plastic of the devices and the dish.

3.2. Priming of the Alzet Pump

1. In order for the pump flow rate to equilibrate, the pumps need to be primed by placing them into saline. Therefore, fill 15-mL sterile polystyrene or other clear tubes each with 3–5 mL sterile saline in a laminar flow hood. Next, open the packages of the Alzet pumps and put the pumps into the saline with the hole facing up. To maintain the sterility of the pumps, handle them with ethanol-sterilized forceps after opening the individual pump packages. The pumps will float in the saline and fluid will not get into the inside of the pumps. Close the tubes and keep them straight up in a tube rack. (For a choice of pumps, *see* **Note 1**.)
2. The manufacturer recommends incubating the pumps for at least 4 h at 37° C. Alternatively, they can be incubated overnight at room temperature that helps improve the efficiency of the experiment (*see* **Note 9**).

3.3. Preparation of the Vehicle Solution

1. Measure out 1 mL more PBS than is needed for the experiment and dissolve 1 mg/mL serum albumin of the species of the experimental animal, for example, rat

serum albumin for rats (*see* **Note 10**). The same vehicle should be used to dissolve the neurotrophic factor and for the control group in the experiment.
2. To further reduce the chances of bacterial growth, add 0.1 mg/mL gentamicin to the vehicle.
3. Up to this point, the solution is not sterile and can be made at the bench on the day before loading the pumps or on the day itself. Do not dissolve the neurotrophic factor yet.

3.4. Loading of the Alzet Pump and Final Assembly

1. Decontaminate the working area in a laminar tissue culture hood with 70% ethanol using a spray bottle and kimwipes. Throughout the loading procedure, wear latex or similar gloves and decontaminate them after touching nonsterile surfaces. Arrange materials in the hood for convenient access while maintaining sterile areas for later placement of the pumps and infusion devices.
2. Filter-sterilize the vehicle through a 0.2-μm low-protein-binding Acrodisc filter into sterile 0.5-mL or 1.5-mL Eppendorf tubes using a 1-mL or 3-mL syringe.
3. Connect the sterile filling tube that came with the Alzet pump package to a sterile 1-mL syringe and fill it with sterile vehicle to prime it for 2 min (*see* **Note 5**). Afterward, express the vehicle back into the Eppendorf tube.
4. Take up more than enough fresh vehicle to fill one or more of the pumps of the vehicle group plus what is required to fill the infusion device. This amount depends on the volume of the pump and the length of the connecting line.
5. Take the Alzet pump out of the saline with forceps and while holding it between the fingers with its opening facing up, insert the filler tube, and slowly inject the vehicle until the pump is filled. This is noticeable by the slight darkening of the shell, by the appearance of a fluid bubble at the top, or by the ending of small air bubbles that may form on the top of the pump during loading. Place the pump horizontal on a sterile surface.
6. Pick up a sterile infusion device at the metal part of the flow moderator end using the hemostatic forceps and keep the device horizontal. Insert the filler tube all the way into the moderator and fill the device up to approximately 3 mm from the cannula platform. Withdraw the filler tube while holding the moderator almost vertical with the opening pointing down.
7. Insert the flow moderator approximately four-fifths into the Alzet pump (*see* **Note 11**) and place the Alzet pump back into the tube with saline, with the rest of the infusion device positioned above the saline. Close the tube. This will keep the assembled infusion device pump sterile until use at the surgery later in the day.

3.5. Stereotaxic Implantation Into Rats or Mice

1. After anesthetizing the animal (*see* **Note 12**), the head and dorsal neck area are shaved and the surgical area cleaned with Betadine. The head of the animal is placed securely and straight in the stereotaxic apparatus with the tooth bar set at a

level appropriate for the stereotaxic atlas that was used to determine the coordinates for the tip of the cannula, for example, rats ***(9)*** and mice ***(10)*** (*see* **Note 7**).

2. Make a mid-sagittal (in the middle along the long axis of the animal) skin incision from behind the level of the eyes to the back of the skull. Insert a pair of blunt medium-sized scissors through the back of the incision under the skin of the neck area up to one-third or halfway along the length of the body. Spread the scissors and withdraw in that position to create a subcutaneous pocket for later placement of the Alzet pump.
3. Cover the animal with a sterile drape and make a slit in the middle over the skull area to access the surgical area. Attach the sides of the drapes to the skin using the towel clamps, which are retracted to the sides to open up the surgical field for easy access to the skull.
4. Remove the membrane covering of the skull by scraping it to the sides with the back of the scalpel holder. Clean the skull by lightly scraping it with the sharp edge of the scalpel blade held at a 45° angle. Remove all blood with cotton applicators and stop any remaining bleeding from the skull with the low-heat cautery device (*see* **Note 13**).
5. Measure out the mediolateral and rostrocaudal coordinates from Bregma (*see* **Note 14** and **Fig. 3**) using a pin that is inserted into the cannula holder attached to the micromanipulator. Drill a small (approximately 1 mm) burr hole through the skull without penetrating the dura. Make a small incision in the dura with a bent 30-ga needle.

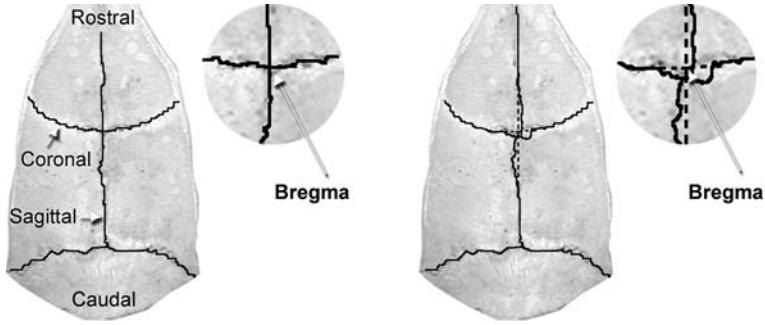

Fig. 3. Two examples of Bregma. The intersection between the sagittal and coronal sutures between the skull plates is named Bregma and is used as a reference point to determine the coordinates where the tip of an infusion cannula is inserted. On the left is the ideal Bregma; on the right, one variation that is often seen. The broken lines indicate the imaginary lines that can be drawn from the caudal and rostral portions of the sagittal suture, which are more consistent, and the projection of the coronal suture, to determine Bregma in cases where the sutures are aberrant.

6. Clean and completely dry (*see* **Note 15**) the skull area where the platform will touch, by scraping with the scalpel blade or cotton applicators and/or by cauterizing blood vessels. If bleeding occurs from the burr hole, fill it with a small piece of Gelfoam for a minute, remove the Gelfoam, and clean off the skull again. Do not cauterize the burr hole.
7. Ensure that the glue can be expressed from the tip of its container. Next, secure the removable tab of the plastic platform of the infusion device in the cannula holder of the micromanipulator, with the connecting line and attached Alzet pump located over the midline of the animal and on top of the drape. Insert the rest of the flow moderator into the Alzet pump and check that a droplet forms at the tip of the cannula. Wipe this off with a sterile cotton applicator. Ensure that the cannula is positioned vertical by optically aligning it with the vertical parts of the stereotaxic apparatus by looking from the back and the side.
8. Again measure out the mediolateral and rostrocaudal coordinates, now using the tip of the cannula, without touching the skull. Ensure that the skull is still dry and the burr hole is filled with a small amount of fluid (*see* **Note 16**). Insert the cannula through the burr hole until the platform touches the skull, making sure the cannula does not touch the side of the burr hole (*see* **Note 17**).
9. Apply a drop of cyanoacrylate in the corner between the platform and the skull on one side, enough for the glue to penetrate to the other side of the platform. Next, deposit a small amount of sodium bicarbonate powder all around the sides and front (not the back) of the platform, using a Pasteur pipette (*see* **Note 18**). This will immediately polymerize (harden) the glue. Repeat application of glue and powder if needed to build up a small rim of glue around the sides of the platform. A small amount of glue and powder can be applied underneath the caudal end of platform while ensuring that the clear part of the connecting line remains free.
10. Place the Alzet pump under the skin all the way between the scapula or farther, using forceps to pull up the skin of the neck and another forceps to hold on the Alzet pump. Ensure that the connecting line does not have kinks by palpating through the skin.
11. Open the cannula holder and raise the micromanipulator. Cut off the removable tab of the platform using the cauterizer. Clean the wound by removing debris and flushing it with sterile saline containing 0.1 mg/mL gentamicin. Inject 0.1 mL (mice) or 1 mL (rats) of this saline–gentamicin solution around the pump through the open neck area.
12. Close the skin of rats with removable wound clips or metal staples or of mice with silk sutures (*see* **Note 19**). Return animals to a cage placed on a heating pad for recovery. Remove clips or sutures after 7–10 days.
13. At the end of the experiment, the pump can be retrieved, the flow moderator removed, and the remaining fluid collected with a syringe and filler tube to measure remaining biological activity, if necessary. Please note, the Alzet pump cannot be reused.

4. Notes

1. Alzet pumps have a hard semipermeable outer shell filled with a gel-like substance that attracts water from the subcutaneous location in the animal through osmosis. As the osmotic substance swells, it compresses an internal bag containing the infusion fluid to expel the latter through the opening of the pump into the infusion device. There are currently 10 different types of Alzet pumps available. Because of their size, the 100# series is most suitable for mice and the 200# series for rats. They readily fit under the skin. The 2ML# series is large and fits under the skin only with some difficulty in adult rats or can be placed into the peritoneal cavity of larger rats (preferably over 300 g). Some of the pumps have a seemingly high infusion rate, for example, the 2001D infuses at 8.0 μL/h to achieve a maximal delivery time of 1 day. This may be considered too high for intraparenchymal infusions. If a 1-day infusion is required, one can use a 3-day 1 μL/h pump and process the animal after 1 day. The only disadvantage in case of expensive neurotrophic factors is the wasted fluid.
2. Durect offers two precut cannula lengths that will place the tip in the lateral ventricle of rats or mice. Plastics One offers customized lengths up to 11 mm to fit the particular depth needed for any particular location in the brain. The length should be measured from the top of the skull. There are two types of platforms. One has a much lower but wider profile that is intended for mice. The other platform has a cylindrical shape and is appropriate for rats. If a laboratory expects to use various locations, it is useful to purchase a large number of 11-mm cannulas and trim them to any desired length in the future using the Dremel drill and cut-off wheel (*see* **Subheading 3.1., step 3**). The lines that come with the platform may not be kink resistant (e.g., polyethylene), meaning the line can fold in the animal and thus obstruct the flow. In most cases, the line will be straight in the animal and this would not be a problem. When infusing agents into the fourth ventricle or intrathecally into or around the spinal cord, the placement of the pump might require bending the line. In such cases, one can purchase kink-resistant polyvinyl tubing (V-3A, Scientific Commodities Inc., Lake Havasu City, AZ).
3. Cyanoacrylate glue comes in many types, including fluid and gel. I prefer the fluid, as it can enter into small spaces easier and faster, which is particularly important for the surgery.
4. The lid of the dish should have holes, which can be made with the hot (flamed) thick end of a glass Pasteur pipette.
5. The choice of vehicle is essential for the success of the experiment. For most neurotrophic factors, a pH-neutral solution like PBS is suitable. If not, this most likely is indicated on the data sheet that came with the factor. If unsure, the easiest is to check what others have done. Alzet maintains a bibliography of agents tested and the vehicles (carriers) used. Like most proteins, neurotrophic factors have the potential to "stick" to charged surfaces they come into contact with, such as the tubes, loading syringes, and infusion device. The albumin helps protect the

much less abundant trophic factor. Albumin should not sequester the neurotrophic factors. Some neurotrophic factors or other proteins might require nonphysiological vehicles. If so, it is important to include another control group, in addition to the vehicle group, which is infused with a physiological solution.

6. Most commercially available neurotrophic factors are already filter-sterilized and come as a single amount. If the factor will be used for different experiments or at different times, it is best to aliquot it into sterile Eppendorf tubes with as much per tube as is expected to be used for one animal. Freeze them at −70 to −80° C. If the factor is not sterile, filter it through a 0.2-μm low-protein-binding Acrodisc filter, which could first be primed with a solution containing 1 mg/mL serum albumin.
7. We use a David Kopf stereotaxic apparatus (David Kopf Instruments, Tujunga, CA), which is sufficiently precise and reliable. For rats, we use the standard ear bars and penetrate the eardrums to ensure a precise centering of the skull. For mice, there are two options. One is to use the same rat ear bars, but this requires a skilled person to be able to feel the superficial entry into the ear canal. The other is to use mouse-specific ear bars that are positioned externally over the lower caudal end of the skull. These are less precise but can achieve a reasonably centered position of the skull. The toothbar for the rat is standard. For mice, a smaller toothbar is needed and is preferable over bars that are not placed into the mouth.
8. When applying the fluid glue, take off the excess with a kimwipe leaving only a small amount at the connection between the line and the platform. This will prevent the fluid from going into the platform in the rare cases that the line does not fit tightly. Too much glue also can make the polyvinyl lines brittle. Do not glue your fingers together.
9. The manufacturer's recommendation is based on their findings that the pump rate accelerates from zero to a constant rate over 4 h at 37° C, the approximate core temperature of an adult rodent. Some types of pumps require a longer preincubation (see Alzet recommendations on their website). In the laboratory, we incubate them overnight at room temperature for several reasons. First, this increases the efficiency of larger experiments; for example, pumps can be loaded early in the morning without having to wait another 4 h for the pumps to get ready. Second, when changing the pump from a 37° C to a room temperature environment for filling, the fluid in the pump shrinks. If this happens after the final assembly of the pump, this results in air being drawn into the cannula and connecting line. Third, in our approach, when going from room temperature to the animal, the flow rate increases for a while, which will deliver a small "burst" of fluid, which reduces the potential backflow of blood into the cannula.
10. Measuring out small amounts of albumin can be challenging, as it can stick to the spatula and can readily be blown away. Steady hands help. To maintain accuracy, we do not measure out less than 1 mg.
11. Small air bubbles may appear in the connecting line. These will be resorbed into the vehicle or will not harm the nervous tissue if infused. If air pockets larger than

3 mm form, remove the flow moderator from the pump, remove the fluid from the infusion device, and refill the device. This is most likely caused by inadvertently injecting air into the moderator or because the moderator is not held up straight while withdrawing the filler tube. The remaining one-fifth of the moderator is inserted just before implantation in the animal. This ensures that the entire infusion device is filled in case the fluid level withdraws between filling and implantation.

12. A good anesthetic for rats is an intramuscular injection of 3 mL/kg of a mixture containing 25 mg/mL ketamine hydrochloride (e.g., Abbott Laboratories, North Chicago, IL), 1.2 mg/mL acepromazine maleate (e.g., The Butler Company, Columbus, OH), and 0.25 mg/mL xylazine (e.g., The Butler Company) in 0.9% saline. This provides deep anesthesia within 15 min and lasts for at least 1 h. A 0.2-mL booster shot can be given after 45 min to ensure deep anesthesia for a longer time. For mice, we use an intraperitoneal injection of Avertin (0.4 mg per gram body weight; 2,2,2-tribromoethanol in 0.2 mL of 1.25% [v/v] 2-methyl-2-butanol in saline, Sigma-Aldrich), which induces anesthesia within 10 min and also lasts for at least an hour. Avertin should be stored in the dark. Both anesthetics should be stored in the refrigerator and should be replaced at least every 2 weeks to maintain their effectiveness.
13. When using the cautery device, do not place it too long in one place, as this will heat up the cortex through the skull, causing damage. For the same reason, do not use it close to exposed nervous tissue.
14. Bregma can be recognized by the sutures between the skull plates (**Fig. 3**). These will become clearly visible after scraping the skull or can be enhanced by applying a dye such as toluidine blue. These sutures often are aberrant and may not form a perfect cross at the intersection that defines Bregma. It is therefore necessary to double-check the position of Bregma by moving the tip of the measuring device (e.g., a pin) caudal and rostral over the sagittal suture, whose caudal and rostral ends are more consistent. In case the coronal suture (in the mediolateral plane) is aberrant, the position of Bregma can be determined by projecting imaginary lines through the more lateral portions of the suture toward the midline. Using a surgical microscope will greatly enhance the precision of the measurement and subsequent implantation of the infusion device.
15. The skull needs to be dry for the glue to bond well. There is often some bleeding and build up of fluid in the wound pockets on the side, which can be repeatedly removed by cotton applicators to prevent the fluids from entering the region where the platform will touch. This is easier than trying to stop all bleeding from the sides, which most often is difficult to locate.
16. Cyanoacrylate is toxic for the cortex, and we therefore leave a small amount of fluid in the burr hole, which will prevent the glue from entering. This most often occurs spontaneous with some cerebrospinal fluid.
17. There might be a small space on one side of the platform, if the cannula was not entirely vertical. This is not a problem, as the glue will fill the space. This is one

of the reasons for using the fluid form of the cyanoacrylate. If the cannula touches the sides of the burr hole anywhere along its length, the tip of the cannula will not end up at the intended coordinates, as it will be pushed to the opposite side when lowered further. The wide platforms with the low profile obstruct the view from above making it difficult to see when the platform touches the skull. If this is the case, one side of the flat part of the platform can be trimmed during preassembly (*see* **Subheading 3.1., step 1**).

18. Sodium bicarbonate changes the pH of the glue and causes its immediate polymerization. This is a great time-saver. Repeated layering can be used to build up substantial and strong structures, which can be useful. Note that the powder needs to be applied by very gentle squeezing of the bulb to prevent a large amount from being deposited onto the skull. Also, ensure that the powder does not touch fluid that may have built up in the sides of the wound, as the powder will quickly absorb the fluid. The next layer of glue will not bond. If this happens, remove the wet powder, dry the surface, and reapply.
19. We use metal clips/staples from Fine Science Tools for rats, as they are affordable and reliable. Make sure not to tighten the skin too much, which would prevent the eyes from closing which would cause unnecessary animal morbidity. For this reason, the staples are too big for mice. It is advised to check the sutures every couple of days.

Acknowledgments

This work was made possible by an Endowed Chair to T.H. supported by the Department of Neurological Surgery, Bucks for Brains, University of Louisville, Norton Healthcare and the Kentucky Spinal Cord and Head Injury Research Trust.

References

1. Hagg, T., Manthorpe, M., Vahlsing, H. L., and Varon, S. (1988) Delayed treatment with nerve growth factor reverses the apparent loss of cholinergic neurons after acute brain damage. *Exp. Neurol.* **101**, 303–312.
2. Oudega, M. and Hagg, T. (1996) Nerve growth factor promotes regeneration of sensory axons into adult rat spinal cord. *Exp. Neurol.* **140**, 218–229.
3. Lu, X., Maysinger, D., and Hagg, T. (2002) Tyrosine phosphatase inhibition enhances neurotrophin potency and rescues nigrostriatal neurons in adult rats. *Exp. Neurol*. **178**, 259–267.
4. Sofroniew, M. V., Howe, C. L., and Mobley, W. C. (2001) Nerve growth factor signaling, neuroprotection, and neural repair. *Annu. Rev. Neurosci.* **24**, 1217–1281.
5. Thoenen, H. and Sendtner, M. (2002) Neurotrophins: from enthusiastic expectations through sobering experiences to rational therapeutic approaches. *Nat. Neurosci.* **5 Suppl**, 1046–1050.

6. Liu, X. and Chen, C. (2005) Strategies to optimize brain penetration in drug discovery. *Curr. Opin. Drug Discov. Dev.* **8**, 505–512.
7. Wu, D. (2005) Neuroprotection in experimental stroke with targeted neurotrophins. *NeuroRx* **2**, 120–128.
8. Hagg, T. (1994) Continuous central nervous system infusion with Alzet osmotic pumps, in *Methods in Neurosciences, Vol. 21: Providing Pharmacological Access to the Brain: Alternate Approaches* (Flanagan T., Emerich D., and Winn S., eds.), Academic Press, San Diego, CA, pp. 201–213.
9. Paxinos, G. and Watson, C. (2005) *The Rat Brain in Stereotaxic Coordinates, The New Coronal Set*. 5 ed., Academic Press, San Diego, CA.
10. Paxinos, G. and Franklin, K. (2002) *The Mouse Brain in Stereotaxic Coordinates*. 2 ed., Academic Press, San Diego, CA

13

Synthesis of Cell-Penetrating Peptides and Their Application in Neurobiology

Gunnar P.H. Dietz and Mathias Bähr

Summary

Short basic amino acid sequences, often called cell-penetrating peptides (CPPs), allow the delivery of proteins and other molecules into cells and across the blood–brain barrier (BBB). Although the ability of basic proteins to facilitate such trafficking is known for a long time, only the application of genetic methods and overexpression of fusion proteins in *Escherichia coli* has lead to a wide application of CPP in many research areas, including signal transduction, cancer, angiogenesis, apoptosis, bone development, cardioprotection, cell cycle, neurobiology, and many others. For the neuroscientist, CPPs are particularly attractive, as a number of articles in the last 5 years have reported their use for neuronal rescue in a number of models for neurodegenerative diseases in vitro and in vivo in rats, mice, or gerbils. Here, we give a detailed description of the protein purification methodology and applications in neuroscience.

Key Words: Protein delivery; Trojan horse peptide; arginine-rich peptide; ischemia; trauma; apoptosis; excitotoxicity; cell-penetrating peptides (CPP); protein transduction domain (PTD); transactivator of transcription (Tat).

1. Introduction

Over a decade ago, Fawell et al. ***(1)*** showed that a variety of enzymes, chemically linked to amino acids 37–72 or 1–72 of HIV-transactivator of transcription (Tat), are delivered across biological membranes in vitro and in vivo. S.F. Dowdy's group was the first to generate an in-frame Tat bacterial expression vector and to report the purification of recombinant, transducible proteins ***(2)***. They used this approach to deliver large, enzymatically active

From: *Methods in Molecular Biology, vol. 399: Neuroprotection Methods and Protocols*
Edited by: T. Borsello © Humana Press Inc., Totowa, NJ

proteins throughout the body and even into the mouse brain *(3)*. Besides Tat cell-penetrating peptides (CPP), many others have been used. The transduction efficiency mediated by Tat is in some cases higher as compared to the Antp-derived penetratin *(4)*. Which CPP for a given cargo (1) is the most permeant for the plasma membrane or the blood–brain barrier (BBB); (2) is released most efficiently from endosomes; and (3) shows the highest enzymatic or blocking activity is likely to remain a partly empirical process for some more time *(5)*.

Extensive reviews of the various CPPs, their mechanisms of transduction and applications, with about 600 references on the topic *(6)*, or a specific focus on neuroscience *(7)* have recently been published. Here, we focus on the methodology and applications in neuroscience in the growing field of protein transduction technology. For the neuroscientist, such strategies are of particular interest, as current gene vectors or proteins do not cross the BBB, and only few brain diseases respond well to small-molecule drugs. CPPs have been used to examine β-amyloid function and toxicity *(8,9)*, apoptotic processes *(10–16)*, axon guidance, regeneration and growth *(8,17–20)*, ischemia *(13,21–27)*, multiple sclerosis *(28)*, memory *(29)*, LTP *(30)*, lysosomal storage disease *(31,32)*, cell signaling *(33)*, cell survival *(34)*, cell cycle *(35)*, Parkinson's disease *(36,37)*, pneumococcal meningitis *(38)*, and nerve trauma *(15,39)*, to give just a few examples. The gene of interest is cloned into an *Escherichia coli* expression vector and expressed in LB medium. The protein is purified by affinity chromatography and gel filtration and can be applied in cell culture or in the intact animal. Besides proteins, siRNA can also be delivered using the Tat CPP *(40)*.

2. Materials

2.1. Expression Constructs

The gene of interest without the initiation codon should be cloned into an expression plasmid in frame with the Tat CPP sequence. For instance, the pTat-HA *(2,3)* and several control construct vectors are available from Stephen Dowdy at the University of California in San Diego (sdowdy@ucsd.edu), who is generous with reagents and support. These vectors are derived from the pRSET™ expression plasmid from Invitrogen™ and contain a His_6 sequence to facilitate purification by metal-affinity chromatography, and the Tat sequence 5′ of the polylinker, under the control of a T7 promoter. The His_6 tag also enhances cell penetration *(5)*. Alternatively, clone the Tat CPP into your favorite prokaryotic expression vector and insert the cDNA of interest 3′ or 5′ of that CPP. Whether the linking of the CPP to the N-terminus or the C-terminus of

the protein leads to a more soluble, efficiently delivered protein needs to be determined empirically ***(41)***. In addition, several control constructs are needed. One should contain only your gene without the CPP. For instance, for the pTat-HA vector from the Dowdy laboratory, the pRSET vector is a wise choice, because it will render a similar protein without the CPP. Ideally, one would also want to produce a control protein that contains a mutant, nonfunctional form of the gene of interest. If this is not known or available, a protein that consists of only the His_6-Tat-HA domain would be an acceptable choice. This control is important, as full-length HIV-Tat is neurotoxic, partly responsible for AIDS-associated dementia ***(42)***, and has many biological effects (for review, *see* **ref. *43***). Although the Tat-derived basic CPP is not toxic for cells, this control protein should be included in the experiments, if possible.

2.2. Cells

For maintenance of the plasmid, it is mandatory to use a recombination-deficient bacterial strain, for instance those which carry a *recA* mutation. Constructs verified by sequencing are then transfected into a strain that allows expression. For instance, if you cloned your gene into a plasmid with a T7 promoter, a variant of the BL21 (DE3) strain is the most common choice. In this strain, expression of protein is high. They require isopropylthiogalactosidase (IPTG) or lactose to induce expression of T7 RNA polymerase from the *lac*UV5 promoter. Some proteins, such as many eukaryotic membrane proteins, are toxic for *E. coli*. In such instances, a strain that suppresses leaky expression of the T7 polymerase should be used, such as BL21(DE3)pLysS or BL21(DE3)pLysE, which are, for instance, available from Invitrogen™ or Novagen™. They produce T7 lysozyme to reduce basal expression, which is particularly recommended when the heterologous genes are expressed from a high copy number T7-based plasmid. The pLysE strain produces more of the T7 lysozyme and therefore more firmly reduces leaky expression; however, it may render lower protein yields.

As many eukaryotic genes require codons that are rarely used in *E. coli*, a higher expression can often be obtained with strains that express rare *E. coli* tRNAs, such as the Rosetta™ strains from Novagen™. BL21 Star™ cells have an increased mRNA stability, which may also enhance protein yield.

2.3. Solutions and Reagents

1. LB medium, made up from powder (*see* **Note 1**).
2. Ampicillin, 100 mg/mL stock solution in water, 1000×, store at −20° C (*see* **Note 2**).

3. Chloramphenicol (34 mg/mL stock solution in ethanol, 1000×, store at −20° C).
4. Lactose (powder) or IPTG (0.5 M stock, 1000×–5000× in water, store at −20° C).
5. 2× SDS sample buffer: 0.125 M Tris (pH 6.8), 4.1% SDS, 20% glycerol, 2% β-mercaptoethanol, and 0.001% bromphenol blue ***(44)***.
6. GuHCl buffer: 6 M guanidine hydrochloride, 100 mM NaCl, and 20 mM HEPES (pH 8.0).
7. Buffer Z: 8 M urea, 100 mM NaCl, and 20 mM HEPES (pH 8.0).
8. Ni-NTA (Quiagen, Hilden, Germany).
9. 5, 1, 0.5, 0.25, or 0.1 M, 0.01 mM imidazol in buffer Z.
10. Reagents for SDS polyacrylamide gel electrophoresis (PAGE) and Coomassie Blue staining ***(44)***.
11. Protein molecular weight marker (e.g., from Amersham™ Biosciences, Uppsala, Sweden or BioRad, Hercules, CA).
12. Antibody against the HA tag (BAbCO, Richmond, CA) or against the protein to be delivered.
13. Silicone solution (SERVA Electrophoresis GmbH, Heidelberg, Germany).
14. PD-10 pre-packed desalting columns (Amersham™ Biosciences).
15. Protease inhibitor cocktail for use with bacterial extracts (Sigma-Aldrich, Taufkirchen, Germany).
16. Phosphate buffered saline (PBS) ***(45)***.
17. Autoclaved glycerole.
18. MobiFairy™ cryoprotectant (MoBiTec, Göttingen, Germany).

2.4. Glass Plastic, and Instruments

1. Sonicator.
2. Polypropylene columns (Quiagen, Hilden, Germany).
3. Amicon™ Ultra Centrifugal Filter Device (Millipore™, Bedford, MA).
4. Silanized microcentrifuge tubes, 1.5 and 2 mL.
5. Apparatus for SDS PAGE and Western blotting.

3. Methods

3.1. Purification of Recombinant Protein

3.1.1. Safety Measures

Tat proteins penetrate biological membranes. Thus, if the protein to be purified might have an oncogenic or toxic activity, obviously measures must be taken not to allow contact with mucous membranes, the lungs, or skin.

Adhere to guidelines for the use of low-level radionuclide, for example, ^{35}S. Wear a laboratory coat, safety goggles, and gloves. Change gloves often, and do not touch door handles and other equipment with gloves that might be contaminated. Autoclave all solutions and glassware that might contain bacteria with the expression plasmid.

3.1.2. Purification of Fusion Proteins by Nickel-Affinity Chromatography

The basic method has largely been worked out and reviewed by the Dowdy laboratory, of which experience we have highly benefited ***(46,47)*** (*see* **Note 3** for alternative procedures).

3.1.2.1. Test of Different E. *coli* Clones

1. Transform competent BL21 *E. coli* with T7-based plasmid (or any other expression system).
2. Late next evening, pick 6 colonies and inoculate 2 mL cultures; in addition, as a control, also inoculate one culture with a nontransformed BL21 strain.
3. Early next morning, take a 20 µL sample from each culture, spin 1 s at full speed, discard supernatant, freeze the pellet.
4. To the rest of the overnight culture, add IPTG to a final concentration of 100 µM. Continue incubation for another 4 h.
5. Take a 20-µL sample, collect bacteria in step 3.
6. Add 20-µL 2× SDS loading buffer to all samples, sonicate 10 s, boil 5 min.
7. Analyze 2–4 µL on an SDS minigel by Coomassie staining. Note that the 5′ sequence of the pTat-HA vector includes the Xpress™ epitope, besides the polyhistidine region, the T7 gene 10 leader, the HA tag, and the Tat domain, which increases the size of the protein by 8 kDa.
8. Some proteins are not expressed efficiently enough to be easily detected by Coomassie staining among the other *E. coli* proteins. If no additional band of the expected size is seen after IPTG induction, perform Western analysis of the gel, using an antibody against the gene of interest or against a tag included in the construct, such as the HA domain 3′ of the Tat sequence in the pTat-HA vector.
9. Choose the bacterial clone that renders the highest expression of the recombinant protein for large-scale protein purification (Section 3.1.2.2).

3.1.2.2. Large-Scale Recombinant Gene Expression

1. Inoculate 200 mL LB/Ampicillin/Chloramphenicol (the latter only in case pLys E por pLys S strains are used) with a single colony or a −80° C stock overnight.
2. Early next morning, inoculate 1 L pre-warmed LB/ampicillin (no chloramphenicol) with the 200 mL culture.
3. At an OD_{600} of 0.4–0.8, which is usually reached after 20 min, induce with 9 g lactose. Although IPTG is a stronger inducer of the *lac*UV5 promoter, it is expensive, and induction with lactose is, in many cases, more than sufficient to reach high protein production.
4. At the time of induction, and about every hour thereafter, take another 20 μL bacterial sample as described in **Subheading 3.1.2.1.** for gel analysis (**Fig. 1**). Often, a 4-h induction will lead to a high level of protein synthesis; however, for certain constructs, induction times between 2 h and overnight are optimal.

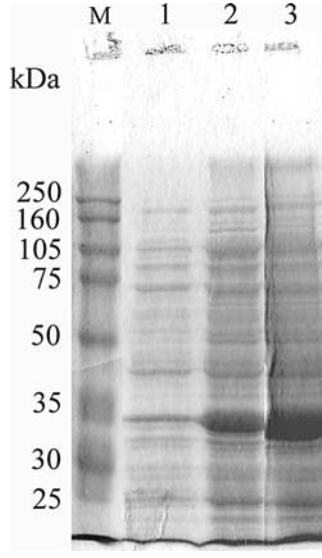

Fig. 1. Tat-Bcl-x_L expression induced with lactose. SDS polyacrylamide gel electrophoresis (PAGE) of crude bacterial lysates at the time of induction with lactose (lane 1), 2 h 30 min after induction (lane 2) and at the time of harvest, 5 h 30 min after induction (lane 3). The recombinant protein, Tat-Bcl-x_L, is 34 kDa in size.

3.1.2.3. Harvest of Bacteria and Immobilized Metal-Affinity Chromatography

1. While harvest of bacteria, centrifugation, and so on, is ongoing, as described below, pack polypropylene gravity columns with 2–10 mL Ni-NTA (*see* **Note 4**). Equilibrate with 5 bed volumes of 10 mM imidazole (*see* **Note 5**) in buffer Z. To start column flow, you may apply *slight* air pressure using a latex-gloved thumb or finger on the top of the column.
2. Harvest bacteria by centrifugation at 3500 *g*, 5 min.
3. Wash once with 10 mL ice-cold PBS, transfer to 50-mL screw cap tube, spin again as in step 2.
4. Resuspend pellet in 10 mL 6 M GuHCl buffer or buffer Z. In most cases, GuHCl buffer dissolves inclusion bodies more efficiently than 8 M urea. Sometimes, protein purification under nondenaturing conditions may be necessary, as explained in **Note 6**.
5. Sonicate pellet until all bacterial clumps are completely dissolved. Make sure the solution does not heat up; intermittent incubation of the protein solution on ice may be required.
6. Spin at 12, 000 *g* for 5 min. Take off supernatant, set aside. Take a 20-μL sample of the pellet and the supernatant for later gel analysis.
7. Add another 10 mL of GuHCl buffer to the pellet, sonicate, spin as in step 6. Combine supernatant with the first supernatant. If later SDS gel electrophoresis reveals that there is still a lot of protein extracted in the second supernatant, and/or if there is still much of the recombinant protein left in the bacterial pellet, it is worth to go through the whole sonication/spin procedure repeatedly (**Fig. 2**).
8. Spin combined supernatants again, this time at 30,000*g* for 20 min, to remove all residual bacterial debris, which will clog the Ni-NTA column.
9. Take off supernatant, filter through a kimwipe tissue: fold the tissue around your gloved index finger, carefully insert it into a 50-mL screw cap tube without tearing it and pour the centrifuged protein solution inside, and allow the solution to drip into the 50 mL tube.
10. Bring to 10 mM imidazole using the 5 M stock solution (or to a higher concentration for increased specificity, or a lower concentration for higher yield, cf. **Note 5**).
11. Suspend the equilibrated Ni-NTA in 10 mM imidazole/buffer Z and pour that resin slurry into the protein solution.
12. Incubate in a head-over-end shaker for 1 h at room temperature.
13. Pour protein–Ni-NTA slurry onto the column. Collect a 20 μL sample of the flow-through for SDS gel analysis.

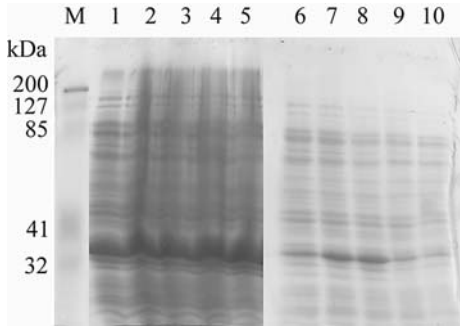

Fig. 2. Repeated extraction of Tat-Bcl-x_L from bacterial debris enhances protein yields. SDS polyacrylamide gel electrophoresis (PAGE) of pellets (lanes 1–5) and soluble protein fractions (lanes 6–10) after treatment with denaturing buffer and repeated extraction and centrifugation. After the second and third extractions, a lot of additional protein is brought into solution (lanes 7 and 8). Note that even after five cycles of sonication in GuHCl, centrifugation, and harvesting of the supernatant, a lot of the recombinant protein could not be brought into solution (band at 34 kDa, lane 5). Solubization from inclusion bodies seems to be the limiting step in protein yield.

14. Wash column with 10 bed volumes of 10 mM imidazole in buffer Z.
15. After collecting 2 mL fractions, elute protein consecutively with 5 mL 100 mM imidazole in buffer Z, followed by 5 mL of 250 mM imidazole, 5 mL 0.5 M imidazole, 5 mL 1 M imidazole, 1 mL 5 M imidazole, and 1 bed volume 1.1% acetic acid, to push out all imidazole/buffer Z solution that still remains in the column (**Fig. 3**) . Nickel columns can be regenerated according to manufacturer's instructions at least 5 times.
16. Store fractions at 4° C, rather than on ice, which would cause precipitation of urea.
17. Analyze the preparation by SDS PAGE. Load the bacterial lysates (*see* **Subheading 3.1.2.1.**0, step 6), the pellet from centrifugation after sonication, the supernatant, the flow-through and the wash samples, and 2 μL each of the fractions from Ni-affinity chromatography. Dilute all GuHCl-containing samples 10× with buffer Z before loading on an SDS gel to perform Coomassie staining. This analysis will allow you to determine the best time point of bacterial harvest after induction with lactose, (1) whether induction with IPTG might be necessary; (2) whether the imidazole concentration in the Ni-NTA incubation buffer and the wash buffer should be increased or decreased; (3) which imidazole concentration is necessary for elution of the protein from the column, and, of

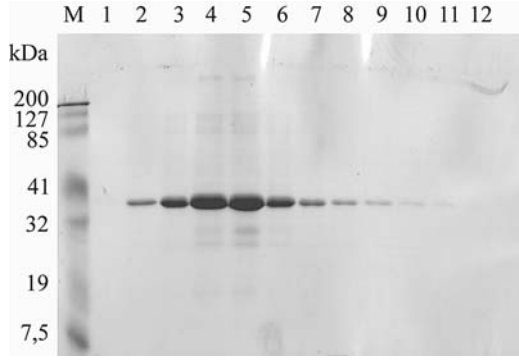

Fig. 3. Purification of Tat-Bcl-x_L by elution of the His_6-tagged protein from the Ni-NTA column. To purify Tat-Bcl-x_L, 12 fractions (2 mL each) to elute the 34-kDa protein from the resin are collected. Other recombinant proteins may require collecting more fractions. Two microliters of each fraction was loaded on the gel.

course, (4) which fractions contain the bulk of the protein. If protein is not visible by Coomassie staining, the yield is probably too little for in vitro or in vivo experiments; however, *see* **Note 7**.

18. Pool protein fractions that contain recombinant protein free of contaminating *E. coli* proteins.
19. Concentrate proteins to 2–5 mL volume using Amicon™ Ultra Centrifugal Filter Device or a similar system with a molecular weight cut-off 3× smaller than the total size of the protein. Use 500 µL to 2.5 mL for gel filtration as described in **Subheading 3.2**. Rapidly removing salt and urea in a single step will render better soluble protein than buffer exchange by dialysis (*see* **Note 8**).

3.2. Removal of Salt and Denaturant From Affinity-Purified Protein Samples and Protein Storage

1. Equilibrate PD-10 columns with 25 mL autoclaved PBS or, if the protein is to be used in cell culture, cell culture medium without serum. If the sample is sensitive to degradation, work in a cold room.
2. You will later collect 3.5 mL of protein solution. We recommend to collect 0.5 mL fractions in 1.5-mL microcentrifuge tubes. Thus, label 7 tubes with "PD-10 fraction 1 to 7," add 20 µL bacterial protease inhibitor into each tube and place on ice (*see* **Note 9**).

3. Add concentrated protein in a volume of 2.5 mL onto the equilibrated PD-10 column. Discard the flow-through.
4. Place microcentrifuge tube "PD-10 fraction 1" under the column. Add 0.5 mL PBS to the top of the column. When the 0.5 mL have dripped through, put tube "PD-10 fraction 1" back on ice and collect 6 additional 0.5 mL fractions in the other tubes. Usually, most of the protein will be in fractions 2–4; however, we recommend to collect fractions 1 and 5–7 also, because different proteins pass the column at a variable rate.
5. Spin all fractions for 2 min at maximum speed in a microcentrifuge. Check for a pellet indicating precipitation of protein, which is a common problem (*see* **Note 10**) and may in part be due to a neutralization of the charged CPP with its cargo protein ***(48)***.
6. Load 2 μL of each fraction plus 2 μL2× SDS sample buffer on an SDS minigel, together with BSA standards to estimate protein concentration (**Fig. 4**). The Tat fusion protein is now ready for use.
7. Store protein at 4° C. Stability is highly variable and needs to be determined for each protein. Some proteins lose their activity over time even when they appear not degraded by SDS PAGE.
8. For long-term storage, add 20% glycerol or other cryoprotectant, such as MobiFairy™. Quickly freeze an aliquot of the protein in liquid nitrogen. Thaw again, centrifuge for 2 min at maximum speed to check for precipitation. Compare an aliquot of the frozen/thawed sample with non-frozen

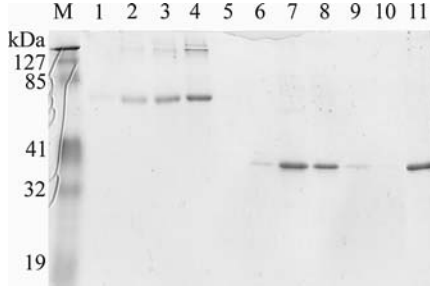

Fig. 4. Removal of salt and urea by gel filtration on PD-10 column and estimation of protein concentrations. Lanes 1–4: protein standards of 20, 40, 100, 200 ng BSA. Lanes 5–10: fractions collected from PD-10 column. Two microliters of each 0.5 mL fraction was loaded on the gel. Lane 11: for comparison, 1 μL of metal-affinity purified protein was loaded, which still contained salt and urea.

sample on an SDS gel. Even proteins that do not precipitate after freezing might lose their enzymatic activity, which again needs to be determined empirically. Do not refreeze thawed proteins.

3.3. Application of Cell-Penetrating Proteins in Neurobiology

To unambiguously demonstrate that the recombinant proteins have transduced cells can be somewhat tricky. Fluorescence-activated cell sorting (FACS) of cells treated with a fluorescently labeled protein might detect those cells that have bound the positively charged proteins on their plasma membrane, which is usually negatively charged. To estimate the number of cells that have taken up the CPP, they need to be extensively treated with protease, to degrade all protein that is attached to the outside of the cells. Only protein that has been internalized is protected against protease degradation. However, protease treatment might cleave off the fluorophore from the protein and, if small enough, the dye might be taken up by the cells without the protein. Immunohistochemistry, on the contrary, is also prone to artifacts ***(49,50)***. For instance, methanol or acetone, which is often used for fixation, can cause relocalization of the antigen to the nucleus ***(51)***. One option is to immunolabel cells without fixing and compare protein-treated with nontreated cells. The best proof demonstrating transduction is a quantifiable enzymatic activity within the cells, such as Cre recombinase ***(5,52)***.

In many cases, biologic effects have been observed with 100 nM concentrations of protein in the medium ***(15)***. However, in other cases, protein concentrations as low as 0.3 pM ***(16)*** or up to 10 μM have been used (*see* **Note 11**). Note that not only the molarity of the protein in the medium needs to be held constant in a particular experiment but also the peptide-to-cell ratio ***(53)***.

A negative result, that is, no apparent biologic effect is hard to interpret. It might be due to the fact that an insufficient amount of protein has been taken up by the cells; that too little protein got released from endocytic vesicles and reached its target compartment; or that the protein was not folded into its active conformation. As a rule of thumb, a small protein cargo linked to the CPP is more likely be transducible and biologically active than a large one.

For in vivo applications, Tat-linked functional protein can be delivered into the brain by intraperitoneal ***(3,16,22)***, intravenous ***(13,23,24)***, intraventricular ***(22)***, or direct injection into a particular brain region ***(29)***. The protein can be detected in the brain within a few hours. Intraperitoneal application may lead to a better distribution of CPPs when a small amount of SDS (0.25% final concentration) is added to the protein ***(54)***. This increases solubility of the protein and may mask positive charges on the protein surface, delaying the

uptake of the protein in the abdominal cavity, and possibly enhancing a steady delivery across the BBB. Remember to equilibrate the protein solution to room temperature and to add the SDS immediately before injection. In our hands, CPP did not distribute well in the organism after subcutaneous injection ***(60)***.

4. Notes

1. Many commercially available LB media contain lactose, which induces expression of T7 RNA polymerase from the *lac*UV5 promoter. Such expression before the bacteria have reached the desired OD may lead to poor yields, if the protein is toxic for *E. coli*. If toxicity of the protein for *E. coli* is a concern, you may treat the autoclaved LB medium with a sterile-filtered solution of lactase (e.g., lactrase™ from ProNatura™, Frankfurt am Main) for a few hours at 37° C before inoculation with the bacterial stock.
2. *E. coli* cultures with ampicillin selection can easily be overgrown with bacteria that have lost their plasmid, because β-lactamase is released into the medium and degrades the antibiotic. Moreover, acidification through *E. coli* metabolism also causes its degradation. Carbenicillin is more resistant against acidic conditions; however, it is also more expensive than ampicillin.
3. For short peptides, chemical synthesis may be advantageous as compared to genetic methods, because it avoids contamination with traces of *E. coli* proteins that might still be present in the preparation and which might, for instance, lead to immune reactions when applied in vivo. Moreover, it allows the use of the retro-inverso CPP sequence, which is more stable against degradation than the natural L-isomers ***(55)***. If the CPP is coupled to the protein through disulfide bonds, the cargo is released from its vector after transduction into the cytoplasm ***(48)***. This decreases a possible influence of the CPP on the protein and also traps it inside the cell. An additional option to the production in *E. coli* is the synthesis of secretable Tat fusion proteins in mammalian cells ***(56)***.
4. As shown in **Fig. 5**, in our hands, using cobalt-based affinity columns instead of Ni-NTA rendered pure protein, however, with painfully slow flow rates and low yields.
5. If protein does not bind well to the column in 10 mM imidazole, the imidazole concentration in the equilibration buffer, in the protein solution, and in the wash buffer can be lowered to 1 mM. If binding is sufficient, but the preparation is contaminated with *E. coli* proteins, the imidazole concentration can be elevated up to 25 mM.
6. Some proteins irreversibly lose their enzymatic activity after denaturation. In that case, sonicate the bacterial pellets in PBS with protease inhibitors and proceed as in 3.1.2.3. As it is difficult to isolate proteins from inclusion bodies under native conditions, decrease inclusion body formation by inducing protein production at 30° C and by adding 2% ethanol to increase chaperone activity.

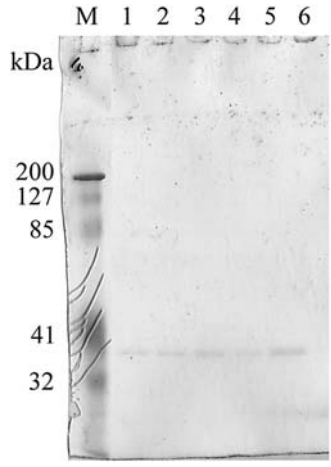

Fig. 5. Purification of Tat-Bcl-x_L by cobalt-based immobilized metal-affinity chromatography leads to pure protein, but considerably lower yields as compared to Ni-NTA. SDS polyacrylamide gel electrophoresis (PAGE) of the first six fractions (2 mL each), collected from the metal-affinity column is shown. Two microliters were loaded on each lane.

7. When purifying proteins smaller than 10 kDa, such as the Xpress™-His_6-Tat-HA control protein, use 18% SDS gels and fix them in 40% methanol with 10% trichloracetic acid for 1 h before Coomassie staining.
8. The Steve Dowdy laboratory recommends an additional FPLC ion exchange step after Ni-affinity chromatography, using Mono Q or Mono S resin ***(46)***. For the proteins used by our group, this step decreased total yield significantly and has not been necessary.
9. Tat proteins stick to plastic and glass surfaces ***(57)***. Therefore, we recommend to siliconize or poly(ethylenimine)-coat ***(58,59)*** microcentrifuge tubes before adding CPP-fusion protein solutions. Under a fume hood, add 50 µL silicone solution into each tube. Shake or vortex at high speed for about 1 h. Open tube lids and allow the remainder of the solution to evaporate at 37° C under a fume hood.
10. If the protein precipitates during the gel filtration step, immediately remove supernatant after centrifugation and check its concentration by SDS PAGE as in **Fig. 4**. For the next gel filtration, try a buffer other than PBS. Calculate isoelectric point of the protein. If the protein—including the Tat fusion—is acidic, use a 1–10 mM Tris buffer at a basic pH, or an acidic pH if the protein is basic. This will increase the charge of the protein and thus the repulsion between the protein molecules. Also, try adding up to 500 mM NaCl, 0.1% EDTA, 0.1% pluronic, and/or 0.02% Tween-80, or a small percentage of DMSO, all of which is well tolerated by cells

if the dilution of the protein solution is sufficiently high. Moreover, use up to 50% glycerole. In that case, the protein can be stored at −20° C without freezing. Note, however, that such viscous solutions do not disperse well in the cell culture medium and need to be diluted before in vivo application. If the protein is to be frozen at −80° C for long-term storage, 20% glycerole should be added anyway.

11. Dying cells often release (negatively charged) DNA, which will bind basic peptides. Therefore, small amounts of DNAse in the cell culture medium might enhance transduction of the protein. Moreover, in some cases we observed that protein uptake is better in serum-free medium.

Acknowledgments

We thank Birgit Kramer for technical assistance and for preparing the Figures. Supported by the Research Center for Molecular Physiology of the Brain (CMPB) of the Deutsche Forschungsgemeinschaft (DFG).

References

1. Fawell, S., Seery, J., Daikh, Y., Moore, C., Chen, L.L., Pepinsky, B., Barsoum, J. (1994) Tat-mediated delivery of heterologous proteins into cells. *Proc Natl Acad Sci USA* **91**, 664–8.
2. Nagahara, H., Vocero-Akbani, A.M., Snyder, E.L., Ho, A., Latham, D.G., Lissy, N.A., Becker-Hapak, M., Ezhevsky, S.A., Dowdy, S.F. (1998) Transduction of full-length TAT fusion proteins into mammalian cells: TAT-p27Kip1 induces cell migration. *Nat Med* **4**, 1449–52.
3. Schwarze, S.R., Ho, A., Vocero-Akbani, A., Dowdy, S.F. (1999) In vivo protein transduction: delivery of a biologically active protein into the mouse. *Science* **285**, 1569–72.
4. Saalik, P., Elmquist, A., Hansen, M., Padari, K., Saar, K., Viht, K., Langel, U., Pooga, M. (2004) Protein cargo delivery properties of cell-penetrating peptides. A comparative study. *Bioconjug Chem* **15**, 1246–53.
5. Lin, Q., Jo, D., Grebre-Amlak, K.D., Ruley, H.E. (2004) Enhanced cell-permeant Cre protein for site-specific recombination in cultured cells. *BMC Biotechnol* **4**, 25.
6. Dietz, G.P.H., Kilic, E., Bähr, M. (2004) Delivery of bioactive molecules into the cell: the Trojan Horse approach. *Mol Cell Neurosci* **27**, 85–131.
7. Dietz, G.P.H., Bähr, M. (2005) Peptide-enhanced cellular internalization of proteins in neuroscience. *Brain Res Bull* 68(1–2), 103–14.
8. Allinquant, B., Hantraye, P., Mailleux, P., Moya, K., Bouillot, C., Prochiantz, A. (1995) Downregulation of amyloid precursor protein inhibits neurite outgrowth in vitro. *J Cell Biol* **128**, 919–27.
9. Pizzi, M., Sarnico, I., Boroni, F., Benarese, M., Steimberg, N., Mazzoleni, G., Dietz, G.P.H., Bähr, M., Liou, H.C., Spano, P.F. (2005) NF-kappaB factor c-Rel mediates neuroprotection elicited by mGlu5 receptor agonists against amyloid beta-peptide toxicity. *Cell Death Differ* **12**, 761–72.

10. Troy, C.M., Stefanis, L., Prochiantz, A., Greene, L.A., Shelanski, M.L. (1996) The contrasting roles of ICE family proteases and interleukin-1beta in apoptosis induced by trophic factor withdrawal and by copper/zinc superoxide dismutase down-regulation. *Proc Natl Acad Sci USA* **93**, 5635–40.
11. Liu, X.H., Castelli, J.C., Youle, R.J. (1999) Receptor-mediated uptake of an extracellular Bcl-x(L) fusion protein inhibits apoptosis. *Proc Natl Acad Sci USA* **96**, 9563–7.
12. Wu, H.Y., Tomizawa, K., Matsushita, M., Lu, Y.F., Li, S.T., Matsui, H. (2003) Poly-arginine-fused calpastatin peptide, a living cell membrane-permeable and specific inhibitor for calpain. *Neurosci Res* **47**, 131–5.
13. Kilic, E., Dietz, G.P.H., Hermann, D.M., Bähr, M. (2002) Intravenous TAT-Bcl-X_L is protective after middle cerebral artery occlusion in mice. *Ann Neurol* **52**, 617–22.
14. Cao, G., Pei, W., Ge, H., Liang, Q., Luo, Y., Sharp, F.R., Lu, A., Ran, R., Graham, S.H., Chen, J. (2002) In vivo delivery of a Bcl-xL fusion protein containing the Tat protein transduction domain protects against ischemic brain injury and neuronal apoptosis. *J Neurosci* **22**, 5423–31.
15. Dietz, G.P.H., Kilic, E., Bähr, M. (2002) Inhibition of neuronal apoptosis in vitro and in vivo using TAT-mediated protein transduction. *Mol Cell Neurosci* **21**, 29–37.
16. Asoh, S., Ohsawa, I., Mori, T., Katsura, K., Hiraide, T., Katayama, Y., Kimura, M., Ozaki, D., Yamagata, K., Ohta, S. (2002) Protection against ischemic brain injury by protein therapeutics. *Proc Natl Acad Sci USA* **99**, 17107–12.
17. Theodore, L., Derossi, D., Chassaing, G., Llirbat, B., Kubes, M., Jordan, P., Chneiweiss, H., Godement, P., Prochiantz, A. (1995) Intraneuronal delivery of protein kinase C pseudosubstrate leads to growth cone collapse. *J Neurosci* **15**, 7158–67.
18. Bertrand, J., McKerracher, L.J. (2003) Intravitreal injection of C3 – 05 promotes regeneration after intraorbital microlesion of the optic nerve in adult rat. *Abstract Viewer/Itinerary Planner. Washington, DC: Society for Neuroscience*, Program No. 678.11.
19. Winton, M.J., Dubreuil, C.I., Campenot, R.B., McKerracher, L. (2003) The effects of C3-05 treatment on sympathetic neurons plated in Campenot chambers. *Abstract Viewer/Itinerary Planner. Washington, DC: Society for Neuroscience*, Program No. 678.7.
20. Bertrand, J., Winton, M.J., Rodriguez-Hernandez, N., Campenot, R.B., McKerracher, L. (2005) Application of Rho antagonist to neuronal cell bodies promotes neurite growth in compartmented cultures and regeneration of retinal ganglion cell axons in the optic nerve of adult rats. *J. Neurosci.* **25**, 1113–21.
21. Asanuma, T., Inanami, O., Tabu, K., Waki, K., Kon, Y., Kuwabara, M. (2004) Protection against malonate-induced ischemic brain injury in rat by a cell-permeable peptidic c-Jun N-terminal kinase inhibitor, (L)-HIV-TAT48-57-PP-JBD20,

observed by the apparent diffusion coefficient mapping magnetic resonance imaging method. *Neurosci Lett* **359**, 57–60.
22. Borsello, T., Clarke, P.G., Hirt, L., Vercelli, A., Repici, M., Schorderet, D.F., Bogousslavsky, J., Bonny, C. (2003) A peptide inhibitor of c-Jun N-terminal kinase protects against excitotoxicity and cerebral ischemia. *Nat Med* **9**, 1180–6.
23. Kilic, Ü., Kilic, E., Dietz, G.P.H., Bähr, M. (2003) Intravenous TAT-GDNF is protective after focal cerebral ischemia in mice. *Stroke* **34**, 1304–10.
24. Aarts, M., Liu, Y., Liu, L., Besshoh, S., Arundine, M., Gurd, J.W., Wang, Y.T., Salter, M.W., Tymianski, M. (2002) Treatment of ischemic brain damage by perturbing NMDA receptor-PSD-95 protein interactions. *Science* **298**, 846–50.
25. Pardridge, W.M. (2002) Blood-brain barrier drug targeting enables neuroprotection in brain ischemia following delayed intravenous administration of neurotrophins. *Adv Exp Med Biol* **513**, 397–430.
26. Song, B.W., Vinters, H.V., Wu, D., Pardridge, W.M. (2002) Enhanced neuroprotective effects of basic fibroblast growth factor in regional brain ischemia after conjugation to a blood-brain barrier delivery vector. *J Pharmacol Exp Ther* **301**, 605–10.
27. Eum, W.S., Won Kim, D., Koo Hwang, I., Yoo, K.Y., Kang, T.C., Ho Jang, S., Soon Choi, H., Hyun Choi, S., Hoon Kim, Y., Young Kim, S., Yil Kwon, H., Hoon Kang, J., Kwon, O.S., Cho, S.W., Soo Lee, K., Park, J., Ho Won, M., Young Choi, S. (2004) In vivo protein transduction: biologically active intact pep-1-superoxide dismutase fusion protein efficiently protects against ischemic insult. *Free Radic Biol Med* **37**, 1656–69.
28. Diem, R., Taheri, N., Dietz, G.P.H., Kuhnert, A., Maier, K., Sättler, M.B., Gadjanski, I., Merkler, D., Bähr, M. (2005) HIV-Tat-mediated Bcl-xL delivery protects retinal ganglion cells during experimental autoimmune optic neuritis. *Neurobiol Dis* **20**, 218–26.
29. Blum, S., Dash, P.K. (2004) A cell-permeable phospholipase Cgamma1-binding peptide transduces neurons and impairs long-term spatial memory. *Learn Mem* **11**, 239–43.
30. Matsushita, M., Tomizawa, K., Moriwaki, A., Li, S.T., Terada, H., Matsui, H. (2001) A high-efficiency protein transduction system demonstrating the role of PKA in long-lasting long-term potentiation. *J Neurosci* **21**, 6000–7.
31. Elliger, S.S., Elliger, C.A., Lang, C., Watson, G.L. (2002) Enhanced secretion and uptake of beta-glucuronidase improves adeno-associated viral-mediated gene therapy of mucopolysaccharidosis type VII mice. *Mol Ther* **5**, 617–26.
32. Xia, H., Mao, Q., Davidson, B.L. (2001) The HIV Tat protein transduction domain improves the biodistribution of beta-glucuronidase expressed from recombinant viral vectors. *Nat Biotechnol* **19**, 640–4.
33. Kelemen, B.R., Hsiao, K., Goueli, S.A. (2002) Selective in vivo inhibition of mitogen-activated protein kinase activation using cell-permeable peptides. *J Biol Chem* **277**, 8741–8.

34. Williams, E.J., Doherty, P. (1999) Evidence for and against a pivotal role of PI 3-kinase in a neuronal cell survival pathway. *Mol Cell Neurosci* **13**, 272–80.
35. Zezula, J., Casaccia-Bonnefil, P., Ezhevsky, S.A., Osterhout, D.J., Levine, J.M., Dowdy, S.F., Chao, M.V., Koff, A. (2001) p21cip1 is required for the differentiation of oligodendrocytes independently of cell cycle withdrawal. *EMBO Rep* **2**, 27–34.
36. Zhang, Y., Calon, F., Zhu, C., Boado, R.J., Pardridge, W.M. (2003) Intravenous nonviral gene therapy causes normalization of striatal tyrosine hydroxylase and reversal of motor impairment in experimental parkinsonism. *Hum Gene Ther* **14**, 1–12.
37. Albani, D., Peverelli, E., Rametta, R., Batelli, S., Veschini, L., Negro, A., Forloni, G. (2004) Protective effect of TAT-delivered alpha-synuclein: relevance of the C-terminal domain and involvement of HSP70. *FASEB J* **18**, 1713–5.
38. Ebert, S., Dietz, G.P.H., Mitchell, T.J., Michel, U., Bähr, M., Nau, R. (2005) Limited protection of TAT-Bcl-X(L) against pneumolysin-induced neuronal cell death. *Neurosci Lett* **384**, 349–53.
39. Kilic, Ü., Kilic, E., Dietz, G.P.H., Bähr, M. (2004) The TAT protein transduction domain enhances the neuroprotective effect of GDNF after optic nerve transection. *Neurodegen Dis* **1**, 44–49.
40. Chiu, Y.L., Ali, A., Chu, C.Y., Cao, H., Rana, T.M. (2004) Visualizing a correlation between siRNA localization, cellular uptake, and RNAi in living cells. *Chem Biol* **11**, 1165–75.
41. Li, Y., Rosal, R.V., Brandt-Rauf, P.W., Fine, R.L. (2002) Correlation between hydrophobic properties and efficiency of carrier-mediated membrane transduction and apoptosis of a p53 C-terminal peptide. *Biochem Biophys Res Commun* **298**, 439–49.
42. Aksenov, M.Y., Hasselrot, U., Wu, G., Nath, A., Anderson, C., Mactutus, C.F., Booze, R.M. (2003) Temporal relationships between HIV-1 Tat-induced neuronal degeneration, OX-42 immunoreactivity, reactive astrocytosis, and protein oxidation in the rat striatum. *Brain Res* **987**, 1–9.
43. Pugliese, A., Vidotto, V., Beltramo, T., Petrini, S., Torre, D. (2004) A review of HIV-1 Tat protein biological effects. *Cell Biochem Funct* **7**, 7.
44. Ausubel, F.M., Brent, R., Kingston, R.E., Moore, D.D., Seidman, J.G., Smith, J.A., Struhl, K. (1997) *Current Protocols in Molecular Biology*. John Wiley, New York.
45. Sambrook, J., Russell, D.W. (2001) *Molecular Cloning. A Laboratory Manual*. Cold Spring Harbor Laboratory Press, Cold Spring Harbor, New York.
46. Becker-Hapak, M., McAllister, S.S., Dowdy, S.F. (2001) TAT-mediated protein transduction into mammalian cells. *Methods* **24**, 247–56.
47. Vocero-Akbani, A., Chellaiah, M.A., Hruska, K.A., Dowdy, S.F. (2001) Protein transduction: delivery of Tat-GTPase fusion proteins into mammalian cells. *Methods Enzymol* **332**, 36–49.

48. Derossi, D., Chassaing, G., Prochiantz, A. (1998) Trojan peptides: the penetratin system for intracellular delivery. *Trends Cell Biol* **8**, 84–7.
49. Melan, M.A., Sluder, G. (1992) Redistribution and differential extraction of soluble proteins in permeabilized cultured cells. Implications for immunofluorescence microscopy. *J Cell Sci* **101**, 731–43.
50. Richard, J.P., Melikov, K., Vives, E., Ramos, C., Verbeure, B., Gait, M.J., Chernomordik, L.V., Lebleu, B. (2003) Cell-penetrating peptides. A reevaluation of the mechanism of cellular uptake. *J Biol Chem* **278**, 585–90.
51. Moulton, H.M., Hase, M.C., Smith, K.M., Iversen, P.L. (2003) HIV Tat peptide enhances cellular delivery of antisense morpholino oligomers. *Antisense Nucleic Acid Drug Dev* **13**, 31–43.
52. Peitz, M., Pfannkuche, K., Rajewsky, K., Edenhofer, F. (2002) Ability of the hydrophobic FGF and basic TAT peptides to promote cellular uptake of recombinant Cre recombinase: a tool for efficient genetic engineering of mammalian genomes. *Proc Natl Acad Sci USA* **99**, 4489–94.
53. Hällbrink, M., Oehlke, J., Papsdorf, G., Bienert, M. (2004) Uptake of cell-penetrating peptides is dependent on peptide-to-cell ratio rather than on peptide concentration. *Biochim Biophys Acta* **1667**, 222–8.
54. Schutze-Redelmeier, M.P., Gournier, H., Garcia-Pons, F., Moussa, M., Joliot, A.H., Volovitch, M., Prochiantz, A., Lemonnier, F.A. (1996) Introduction of exogenous antigens into the MHC class I processing and presentation pathway by Drosophila antennapedia homeodomain primes cytotoxic T cells in vivo. *J Immunol* **157**, 650–5.
55. Snyder, E.L., Meade, B.R., Saenz, C.C., Dowdy, S.F. (2004) Treatment of terminal peritoneal carcinomatosis by a transducible p53-activating peptide. *PLoS Biol* **2**, E36.
56. Barka, T., Gresik, E.S., Henderson, S.C. (2004) Production of cell lines secreting TAT fusion proteins. *J Histochem Cytochem* **52**, 469–77.
57. Chico, D.E., Given, R.L., Miller, B.T. (2003) Binding of cationic cell-permeable peptides to plastic and glass. *Peptides* **24**, 3–9.
58. Brink, C., Österberg, E., Holmberg, K., Tiberg, F. (1992) Using poly(ethylene imine) to graft poly(ethylene glycol) or polysaccharide to polystyrene. *Colloids Surf B Biointerfaces* **66**, 149–156.
59. Persson, D., Thoren, P.E., Herner, M., Lincoln, P., Nordén, B. (2003) Application of a novel analysis to measure the binding of the membrane-translocating Peptide penetratin to negatively charged liposomes. *Biochemistry* **42**, 421–9.
60. Dietz, G. P. H, Valbuens, P. C., Dietz, B., Meuer, K., Müller, P., Weishanpt, J. H., Bähr, M. (2006) Application of a blood-brain bamir-penetrating from of SDNF in a more model for Parkinson's Disease. *Brain Res* **1082**, 61–66.

14

The Stem Cells as a Potential Treatment for Neurodegeneration

Ferrari Daniela, Angelo Luigi Vescovi, and Daniele Bottai

Summary

Cell degeneration and death, be it extensive and widespread, such as in metabolic disorders, or focal and selective as in Parkinson's disease (PD), is the underlying feature of many neurological diseases. Thus, the replacement of cells lost by injury or disease has become a central tenet in strategies aiming at the development of novel therapeutic approaches for neurodegenerative disorders. In addition to the in vivo recruitment of endogenous cells, which is now emerging as a promising novel strategy, the transplantation of new, exogenously generated brain cells is probably the most extensively studied methodology for cell replacement in the central nervous system, with the initial experimental clinical studies in PD dating back to the early 1970s (Bjorklund, A. and Stenevi, U., 1984, Intracerebral neural implants: neuronal replacement and reconstruction of damaged circuitries. *Annu Rev Neurosci* **7**, 279–308; Snyder, B. J. and Olanow, C. W., 2005, Stem cell treatment for Parkinson's disease: an update for 2005. *Curr Opin Neurol* **18**, 376–85). The need to generate the cells to be transplanted in large quantities and in a reproducible, steady, and safe fashion has long represented one of the major issues in this field, regardless of whether one was trying to produce specific cell subtypes or uncommitted and highly plastic neural precursors, which would respond to local, instructive cues, upon transplantation into the damaged area. Neural stem cells (NSCs), with their capacity for long-term expansion in vitro and their extensive functional stability and plasticity, allow now for the establishment of cultures of mature neural cells as well as highly undifferentiated precursors and are emerging as one of the most amenable cell sources for neural transplantation (Gage, F. H., 2000, Mammalian neural stem cells. *Science* **287**, 1433–8; McKay, R., 1997, Stem cells in the central nervous system. *Science* **276**, 66–71). This chapter illustrates the basic aspect of the handling and preparation of NSCs for experimental transplantation in two animal models of neurodegenerative disorders, namely, postcontusion spinal cord injury and multiple sclerosis.

From: *Methods in Molecular Biology, vol. 399: Neuroprotection Methods and Protocols*
Edited by: T. Borsello © Humana Press Inc., Totowa, NJ

Key Words: Neural stem cell; transplantation; spinal cord injury; multiple sclerosis; stereotaxic; endovenous injection; intraspinal injection; intracranial injection.

1. Introduction

Neurogenesis continues throughout adulthood and in selected brain regions, thanks to the persistence of remnants of the primary germinal embryonic layers within specific areas of the central nervous system (CNS) ***(1,2)***. The two largest germinal regions in the adult mammalian brain are the subventricular zone (SVZ) ***(3–5)***—which extends along the length of the lateral wall of the lateral ventricles—and the dentate gyrus of the hippocampus ***(6)***. The SVZ, most likely, represents the largest reservoir in the adult brain of cells that possess all of the defining characteristics of true neural stem cells (NSCs). In fact, a subpopulation of astroglial-like cells that reside within this area is endowed with an extensive capacity for self-renewal in vivo, as well as the ability to give rise to neurons and glial cells ***(7)*** that support life-long cell turnover in the cortex of the olfactory bulb ***(3)*** and, possibly, in other areas ***(8)***. When explanted and placed in culture, both these astrocyte-like stem cells and their earlier progeny—the transit-amplifying type C cells of the SVZ—adopt the functional properties expected by NSCs in vitro ***(9)***. They become actively proliferating in response to specific mitogens such as epidermal growth factor (EGF) and fibroblast growth factor 2 (FGF2), expand in number significantly, retain stable functional properties ***(10–13)***, and express multipotentiality (i.e., the ability to give rise to the three major neural cell lineages: astrocytes, oligodendrocytes, and neurons). In this view, these cells that have also been isolated from the fetal ***(14–16)*** and adult human brain ***(17)*** may provide a plentiful source of neural cells to be used for transplantation purposes in the CNS. NSC-based therapy in the damaged nervous tissues may be accomplished in at least three ways, which should not be viewed as necessarily mutually exclusive. For instance, the degenerated cells can be replaced by transplantation of exogenously generated cells of the very same phenotype. In this case, donor cells are expanded ex vivo and exposed to inductive agents or conditions, so as to steer their differentiation toward the desired phenotype, prior to implantation. Alternatively, uncommitted and highly plastic neural precursors—most often a mixture of NSCs and undifferentiated progenitors—can be implanted into the lesion site in an attempt to exploit the local, instructive cues to direct their differentiation toward the desired therapeutic phenotypes. Finally, NSCs and their early undifferentiated progeny may be exploited for their capacity to elicit a bystander effect through which NSCs may release tropic factors and cytokines

at the site of engraftment, therein eliciting survival, antiapoptotic effects while recruiting the pools of endogenous precursors into the regenerative process ***(18)***.

In this view, the main purpose of this chapter is to describe the technical procedures underlying the preparation of NSCs for their use in transplantation in rodent models of human pathologies. As an example, we describe the approaches used in the postcontusion, mouse spinal cord injury model, and in experimental, allergic encephalomyelitis, a mouse model of multiple sclerosis (MS) ***(19,20)***.

2. Materials

2.1. Instruments

1. Rocking platform: SpeciMix, PBI, Milano, Italy.
2. Dissecting microscope: Inverted microscope Zeiss, Thornwood, NY, USA.
3. Dissecting tools: Fine Science Tools Inc., Heidelberg.
4. STS-7 Stereotaxic Instrument outfitted with Compact Spinal Cord Clamping Device (Tritech research Inc., Los Angeles, CA).
5. Dental needle: 27 ga × 13/16 inch(0.40 mm × 21 mm).
6. Polyethylene tubing; inner diameter = 0.38 mm; outer diameter = 1.09 mm (Becton Dickinson, Franklin Lakes, NJ, USA).
7. Hamilton syringe (10 μL).

2.2. Plasticware

1. Flasks: 25, 75, and 162 cm^2, 0.2-μm vented filter cap (Corning Inc., Corning, NY, USA), and six-well plates (Costar Inc. Corning Inc., Corning, NY, USA).
2. Petri dishes: 100 and 36 mm Ø (Falcon, Becton Dickinson, Franklin Lakes, NJ, USA).
3. Chamberslides Permanox (Lab Tek, Nalge Nunc Int., Naperville, IL, USA).
4. Bottle-top filters: low protein binding, 0.22 μm (Corning Inc.).
5. Syringe filters: 25-μm cellulose acetate, 0.22 μm (Millipore, Bedford, MA, USA).
6. Pipettes: 2, 5, 10, and 25 mL (Costar Inc.).
7. Aerosol-resistant tips: 10, 30, 200, and 1000 μL (Corning Inc.).

2.3. Dissection and Culture Media

1. Neurocult® NS-A basal medium (Stemcell Technologies, Vancouver BC, Canada).
2. NeuroCult® NSC proliferation supplements (Stemcell Technologies).
3. L-Glutamine (GIBCO, Grand Island, NY, USA).
4. Penicillin/streptomycin (GIBCO).
5. Glucose (Sigma, St. Louis, MO, USA).
6. bFGF (PEPROTECH, London, UK).
7. EGF (PEPROTECH).

8. EBSS (Invitrogen, Carlsbad, CA, USA).
9. 10× Phosphate-buffered saline (PBS): without calcium and magnesium (Invitrogen).
10. Gentamicin (Invitrogen).
11. Papain (Worthington DBA, Lakewood, NJ, USA).
12. L-Cysteine (Sigma).
13. EDTA (Sigma).

2.4. EAE Induction

1. Myelin oligodendrocyte glycoprotein peptide aa35–55 (MOGp 35–55) (Sigma).
2. Freund's incomplete adjuvant (Difco, Becton Dickinson, Franklin Lakes, NJ, USA).
3. *Mycobacterium tuberculosis* (strain H37Ra), desiccated (Difco).
4. Pertussis toxin from *Bordetella pertussis* (Sigma).

2.5. Surgery and Postsurgery Treatments

1. 2,2,2-Tribromoethanol (tribromoethyl alcohol 97%) (Sigma).
2. 2-Methyl-2-butanol (*tert*-amyl alcohol, ReagentPlus™, ≥ 99%) (Sigma).
3. Ampicillin (Sigma).
4. Buprenorphine (Sigma).

2.6. Solutions

1. *Anesthesia.* To prepare 200 mL avertine solution, mix 2.5 g 2,2,2-tribromoethanol and 5 mL 2-methyl-2-butanol. Warm up the solution in a 37° C bath and mix until the solution is clear. Add distilled water to a final volume of 200 mL, final concentration 12.5 mg/mL. Keep protected from light (*see* **Note 1**).
2. *PBS–Glucose penicillin–streptomycin solution (Pg solution).* Prepare 500 mL of solution as follows: add 50 mL of sterile 10× PBS, 5 mL of penicillin–streptomycin (to reach a final concentration of 100 U/mL each), 10 mL 30% glucose (final concentration 0.6%), and 435 mL H_2O. Filter in a 0.2-μm filter and protect from light to avoid penicillin–streptomycin degradation.
3. *7.5% Sodium bicarbonate*. Mix 7.5 g of $NaHCO_3$ in 100 mL water. Filter-sterilize. Store at 4° C.
4. *30% Glucose*. Mix 30 g glucose in 100 mL water. Filter sterilize. Store at 4° C.
5. *Growth factors stock*. Reconstitute EGF and FGF2 in order to have a 500 μg/mL stock. Aliquot into sterile tubes and store at −20° C.
6. *Mouse growth medium*. Thaw one bottle containing 50 mL NeuroCult® NSC proliferation supplements. Add the entire volume of NeuroCult® NSC proliferation supplements to the bottle containing 450 mL NeuroCult® NSC basal medium and add 40 μL EGF stock (20 ng/mL EGF final concentration) or/and 20 μL FGF2 stock (10 ng/mL final concentration).

3. Methods

3.1. NSC Preparation

3.1.1. Primary Culture

Here, we describe the protocol for the isolation and the establishment of continuous NSC culture lines from the adult murine SVZ *(5,11,21)* (*see* **Note 2**).

3.1.1.1. Set-Up (*see* **Notes 3 and 4**)

1. Weigh out 50 mg papain in a 50-mL Falcon tube and 10 mg cysteine plus 10 mg EDTA in a separate 50-mL Falcon tube. Resuspend the contents of the two tubes in 25 mL EBSS medium, mix the two solutions, and filter to sterilize. Keep the tube at 4° C (for up to a week) until the start of the dissection procedure. Before starting the dissection, aerate with 75% N_2/20%O_2/5%CO_2 the papain/cysteine/EDTA medium in a 37° C incubator.
2. Add cold Pg solution to sterile plastic Petri dishes in which tissue specimens are placed; prepare ten 100-mm Ø dishes to wash tissues and five 35-mm Ø dishes to hold dissected tissues.
3. Select tools needed to remove brain (large scissors, small pointed scissors, large forceps, and a small spatula) (*see* **Note 5)** . Keep the tools in 70% ethanol in two beakers with gauze at the bottom to avoid spoiling the tips of the microforceps and scissors (*see* **Note 6)** .
4. Warm culture medium to 37° C in a thermostatic water bath.
5. Warm EBSS at room temperature.

3.1.1.2. Removal and Dissection of the Brain

1. Anesthetize mouse by injecting anesthetics (1 mL/100 g) and kill it by cervical dislocation.
2. Using large scissors, cut off the head just above the cervical spinal cord region. Rinse the head with 70% ethanol.
3. Using medium-sized pointed scissors, make a medial caudal–rostral cut to remove the skin of the head. Keep the skull and the brain wet using sterile PBS.
4. Using the same scissors, make a longitudinal cut through the skull along the sagittal suture. Keep the scissors away from the brain tissue in order to avoid damages of the brain.
5. Using curved, pointed forceps, grasp and peel the skull of the two hemispheres.
6. Turn upside down the animal head, cut the optical nerves, and let the brain gently slip into a 100-mm Ø Petri dish containing Pg solution.
7. Wash brain by sequentially transferring them to new Petri dishes containing fresh Pg solution. Repeat the wash three times.
8. To dissect the forebrain subventricular region, place dish containing the brain under the dissecting microscope. (The magnification of choice depends on

the type of microscope and the operator's skills.) Position the brain flat on its ventral aspect and hold it from the caudal side (*see* **Note 7)** , using fine forceps. Using a scalpel, make a coronal cut 6–8 mm from emergence of the olfactory bulb and make a second coronal cut 2–3 mm caudally, so as to make a coronal slice ($\sim$ 2 mm thick) containing both the lateral ventricles (*see* **Fig. 1**).

9. Verify that the coronal section contains the SVZ, if not, cut other section more rostrally.
10. Move to a higher magnification and put the slide flat on the dish. Using fine microscissors, cut the thin layer of tissue surrounding the ventricles, excluding as much of the striatal parenchyma as possible, as well as the corpus callosum (*see* **Fig. 1**). Be careful to avoid inclusion of meningeal tissues. Place dissected tissue into labeled 35-mm Ø Petri dishes containing cold sterile Pg solution. Tissues from two or three mice are generally pooled (*see* **Note 8)** .

3.1.1.3. Dissociation of Brain Tissue and Primary Culturing

1. Cut dissected tissue into small pieces using fine scissors.
2. Take the papain solution from the incubator and aliquot it in 15-mL Falcon tubes. Label tubes and add 10 mL papain/cysteine/EDTA solution to each.
3. Transfer the pieces of tissues into the 15-mL tubes containing the papain/cysteine/EDTA solution.
4. Transfer the tubes to the rocking platform. Incubate at 37° C for 30–60 min, depending on the amount of tissue and on its consistence. Thirty minutes is normally sufficient to obtain proper tissue digestion.
5. At the end of the enzymatic incubation, pellet tissues by centrifugation at $123 \times g$ for 10 min.
6. From this point on, use aseptic technique working in a laminar flow hood.
7. Remove almost all the supernatant overlaying the pellets (*see* **Note 9)** . Add 1 mL aerate EBSS solution kept at 37° C. Dissociate by triturating 20–30 times using a 1-mL aerosol-resistant tip with the Gilson pipette set at an aspiration volume of 800 µL. Finally, add 5 mL of fresh 37° C aerated EBSS.
8. Pellet the cells by centrifugation at $123 \times g$ for 10 min.
9. Remove the supernatant leaving behind about 200 µL. Using a Gilson pipette with the volume set at 180 µL, gently dissociate the pellet 20–25 times (*see* **Note 10)** . Add 5 mL EBSS medium and pellet cells by centrifugation at $123 \times g$ for 15 min.
10. Discard supernatant and resuspend cells in 0.5 mL growth medium. Dilute a 5-µL to 10-µL aliquot from each sample in Trypan blue and count in a hemocytometer (initially, try a 1:2 dilution).
11. Seed cells at a density of 3500 viable cells/cm^2 in growth medium, in untreated six-well tissue culture dishes (4 mL volume) or 25-cm^2 tissue culture flasks (6 mL volume) (*see* **Note 11)** .

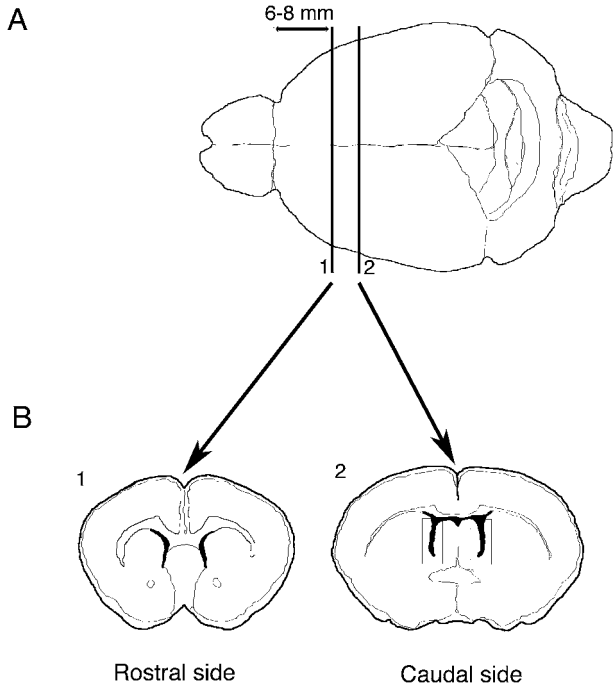

Fig. 1. (**A**) Dorsal vision of the mouse brain as it appears before the dissection. Lines 1 and 2 represent the positions at which the two coronal cuts were performed to obtain a 2-mm section containing the subventricular zone (SVZ). (**B**) Rostral and caudal sides of the dissected coronal section containing the SVZ. When the section is positioned flat on its rostral side, the two lateral ventricles should appear clearly. The boxed areas indicate the regions that need to be dissected to isolate the SVZ.

12. Incubate at 37° C, 5% CO_2 in a humidified incubator.
13. Cells should proliferate to form spherical clusters called neurospheres, which eventually lift off as they become bigger usually in 5–10 days.

3.1.2. Culture Propagation: Subculturing Protocols

Each step of the subculturing procedure should result in an increased overall cell number ranging from two to five times, depending on various parameters and operator's skills. The overall cell number increase is because of the simultaneous expansion of the NSCs pool as well as because of an augment in the number of more mature progenitors and differentiating cells. The latter two will die away at each subculturing step. The number of stem cells found in a

single sphere varies depending on the region of origin of the cells, age, species, or even animal strains.

1. To perform subculturing of the spheres, tap sides of flasks to be passaged to dislodge spheres and transfer content of the flask to 15-mL sterile plastic conical tubes using a sterile plastic pipette. Use 5 mL fresh medium to rinse flask and add them to the tube. Pellet the cells by centrifugation at 17–123 × *g* for 10 min. The centrifugation speed depends on the dimension of the spheres.
2. Remove the supernatant leaving behind approximately 200 μL.
3. Using a Gilson 200-μL pipette set at a volume of 180 μL, gently triturate pellet 40–50 times by passing the cells through the tip. The aim is to obtain a single-cell suspension to be replated. Rinse down the walls of the tube periodically to dislodge undissociated spheres.
4. Count viable cells by Trypan blue exclusion and reseed cells at the density of 1×10^4 cells/cm^2 in culture medium in untreated tissue flasks.
5. In a few days, when the spheres start to lift off and float in suspension, proceed with a new subculturing step. This will require approximately 3–6 days for adult murine cultures; at this time, they normally reach a diameter of approximately 100–150 μm.

3.2. NSCs for the Experimental Therapy in Acute Spinal Cord Injury

The lesions of the spinal cord, consequence of dislocations, or fractures of vertebrae are the most devastating injuries in humans and adversely affect multiple bodily systems, leading to severe or complete loss of respiratory, autonomic, and, particularly, sensorimotor functions. Between 1995 and 2005 we have seen the emergence of a number of experiments aimed at enhancing neurological function following posttraumatic spinal cord injury. Animal models include a large variety of animal species and have developed using a broad spectrum of injury paradigms ranging from sharp transections to blunt contusions ***(22)***. Here, we will discuss a postcontusion, spinal cord injury model developed in CD1 mice.

3.2.1. Animal Model

1. Anesthetize adult CD1 female or male Charles River mouse (25–30 g in body weight) with an intraperitoneal injection of avertine solution (*see* **Heading 2.**) 1 mL/100 g mouse (*see* **Note 12)** .
2. During surgery, maintain the animal at 37° C by a thermo-regulated heating pad.
3. Shave hair on the back of the animal.
4. Perform laminectomy at the T8–T9 level. With a medium-size scissor, cut the skin of the animal. Expose the spinal cord bones removing tendons and muscles by blunt dissection. Using forceps, pull the bone corresponding to T9 (grabbing the spiny

process) so as to make a small space between T9 and T10. Enter the space with a small scissor and make small cuts at the left and the right side of the bone. Repeat the same procedure for the bone corresponding to T8 (*see* **Note 13)** . Position the animal into the stereotaxic frame (such as Model STS-7). The spinal column is secured by up to four independent transverse process clamps, as well as a spinous process clamp.
5. Induce the injury using the weight-drop device impactor using a 0.1-N weight (1 mm diameter) dropped at a height of 1 mm from the spinal cord. Center the impact at the border between T8 and T9 (*see* **Note 14)** .
6. Perform the intraspinal transplantation (*see* **Subheading 3.2.3.**) or the intravenous transplantation (*see* **Subheading 3.2.4.**).

3.2.2. Preparation of the Adult Rodent Cells for Transplantation After Spinal Cord Injury

1. Transplant the lesioned animal with approximately 1×10^6 in two aliquots of 500,000 cells soon after the contusion and 18 h later. Monitor the animal in the days following the lesion.
2. Dissociate the cells the day before the transplantation and plate them growth medium at the density of 10,000 cells/cm^2 (*see* **Note 15)** . In order to have a sufficient amount of cells to complete the experiment, it is convenient to star from 1.5×10^6 cells per mouse.
3. Harvest the cells, the day of the transplantation, in a 15-mL Falcon tube and centrifuge at $123 \times g$ for 10 min (*see* **Notes 16 and 17)**
4. Remove the supernatant leaving 200 μL and gently disaggregate the pellet.
5. Transfer the suspension in a 2-mL Eppendorf and wash the Falcon tube with 1.6 mL sterile PBS; this PBS is then transferred to the 2-mL Eppendorf tube and spun at $123 \times g$ for 10 min.
6. Remove the supernatant and resuspend the cells in 1.5 mL PBS and pellet the cells at $123 \times g$ for 10 min.
7. Remove the supernatant and resuspend the cells in 200 μL PBS and put on ice and count the cells as already described.
8. Dilute the cells at concentration of 50,000 cells/μL and keep in ice.
9. In the case of intravenous transplantation, dilute the cells to a concentration of 10,000 cells/μL, and inject 50 μL of cell each time

3.2.3. Intraspinal Transplantation

1. Aspirate 10 μL of cells with a 10-μL Hamilton syringe and mount the latter into the appropriate holder on a microstereotaxic injection system.
2. Place the needle of the syringe 2 mm rostrally to the lesion site and enter 1 mm deep into the tissue.
3. Inject 5 μL of cells very slowly within 5 min.
4. Repeat the injection 2 mm caudal to the lesion.

5. Remove the animal from the stereotaxic apparatus and wash the wound with saline and inject the animal with ampicillin solution 0.1 mg/g.
6. Suture the animal skin.
7. Inject the mouse with buprenorphine s.c. (0.032 mg/kg), as analgesic.
8. After 18 h of lesion, anesthetize the animal and remove the clips on the skin, expose the surface of the contuse spinal cord and repeat the transplantation as in steps 3–6.
9. Inject the mouse with buprenorphine s.c. (0.032 mg/kg) as analgesic.

3.2.4. Intravenous Transplantation

1. Remove the animal from the stereotaxic apparatus and wash the wound with saline and inject the animal with ampicillin solution 0.1 mg/g.
2. Suture the animal skin.
3. Thirty minutes postcontusion, perform the first injection into the tail vein. Aspirate 50 μL of cells with a 1-mL insulin syringe; the temperature of the cells should rapidly equilibrate to the temperature of the syringe (room temperature). The injection in the tail vein can be also performed using a holding apparatus that adequately restrains an unanesthetized animal while having the tail vein straight in line with the operator eyes for a successful injection. The tail can also be put under a lamp to increase the tail temperature and allow for a better dilation of the tail veins, which significantly facilitates injection.
4. Inject the mouse with buprenorphine s.c. (0.032 mg/kg) as analgesic
5. Repeat the injection after 18 h with the same procedure as in steps 1–3.
6. Inject the mouse with buprenorphine s.c. (0.032 mg/kg) as analgesic.

3.3. NSCs for Experimental Therapy in an Animal Model of MS

MS is a chronic immune-mediated disease of the CNS that leads to the formation of demyelination plaques disseminated along the CNS, axonal loss, and severe neurological disability ***(23,24)***. The problem of targeting lesioned sites in such a multifocal disease emphasizes the importance of carefully evaluating not only the type of cells to be injected but also the delivery method to be used. In this case, cell therapy may perspectively be achieved by coupling a systemic delivery of the cells (intravenous or intrathecal injection) and the peculiar ability of NSCs to cross the blood–brain barrier and reach multiple lesion sites in the presence of an inflammatory reaction ***(19,20)***.

3.3.1. Animal Model

The experimental autoimmune encephalomyelitis (EAE) is a well-described animal model of T-cell-mediated autoimmune disease of the CNS ***(25)***, which mimics the main clinico-pathological features of human MS. EAE can be actively induced in a variety of animal species by immunization with different

myelin-related protein and peptides such as myelin basic protein (MBP), proteolipid protein (PLP), or myelin oligodendrocyte glycoprotein (MOG). The use of MOG peptides (MOGp) is critical to induce demyelinating forms of EAE ***(26)***. Immunization of C57BL/6 mice with the immunodominant MOGp spanning amino acids (MOGp 35–55) results in a chronic EAE, characterized by perivascular infiltration of mononuclear cells into the CNS and multifocal demyelination in the brain and spinal cord ***(27)***.

3.3.1.1. Disease Induction

1. Subcutaneously inject female C57BL/6 mouse (4–8 weeks old) with 200 μg of MOGp 35–55 emulsified in 300 μL incomplete Freund's adjuvant containing 8 mg/mL *M. tuberculosis* (strain H37Ra).
2. On the same day, inject i.v. 500 ng Pertussis toxin.
3. Two days after immunization, inject the mouse once more with Pertussis toxin (500 ng).
4. Diagnosis of EAE is based on the daily assessment of clinical symptoms of the disease, according to the following criteria: 0, no disease; 1, decreased tail tone; 2, hind limb weakness or partial paralysis; 3, complete hind limb paralysis; 4, front and hind limb paralysis; and 5, moribund state. Symptoms should appear between days 15 and 20 postimmunization (disease onset).
5. Transplant animal 1 week after the onset of the clinical signs, that is, approximately 22 days postimmunization.

3.3.2. Preparation of the Adult Rodent Cells for Transplantation in EAE

Follow steps 2–7 in **Subheading 3.2.2.** and dilute cells at a concentration of 10,000 cells/μL for intravenous transplantation and 200,000 cells/μL for intracisternal transplantation.

3.3.3. Intravenous Transplantation

1. Aspirate 100 μL of the cell suspension (10,000 cells/μL) with a 1-mL insulin syringe.
2. Inject in the tail vein as described in **step 3** of **Subheading 3.2.4**.

3.3.4. Transplantation of Cells Into the Cisterna Magna

Intracisternal injection is an easy method to deliver cells into the CNS avoiding the problem of inducing cells to cross the blood–brain barrier. Cells can be introduced directly into the cerebrospinal fluid with a technique that does not require the use of stereotactic devices. The method was developed by Ueda and collaborators ***(28)***, and it is also described by Furlan and collaborators ***(29)***.

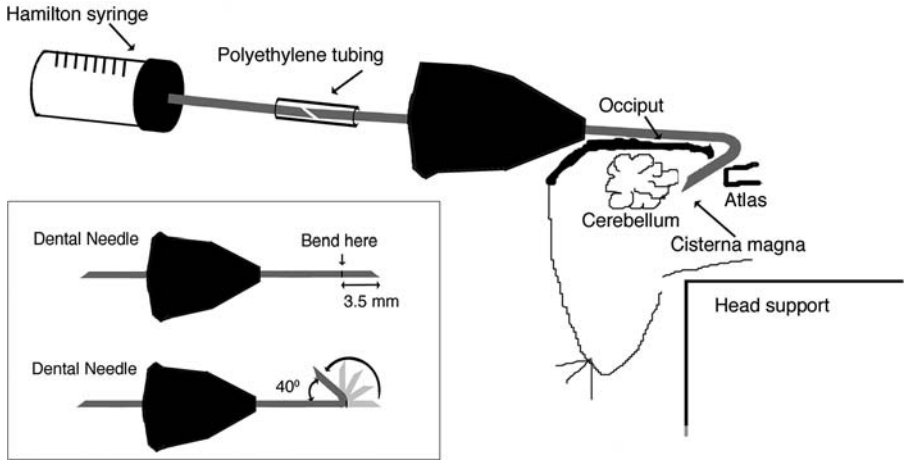

Fig. 2. Schematic of the position in which the animal should be held to perform the intracisternal transplantation. The dental needle is bent at 3.5 mm from the edge (boxed area) and connected to a Hamilton syringe through a polyethylene tubing before the injection.

1. Using forceps, bend the 27-ga dental needle to approximately 40° at 3.5 mm from the tip.
2. Connect the opposite end of the needle to the 10-μL Hamilton syringe through a 1-cm long polyethylene tubing (*see* **Fig. 2**).
3. Anesthetize C57BL/6 the mouse as in **step 1, Subheading 3.2.1**.
4. Fill the injection device with 5 μL of the single-cell suspension (200,000 cells/μL) (s*ee* **Note 16**).
5. Position the animal on top of a small box with the head leaning outside. Run the needle along the external surface of the occiput and insert it into the cleft between the occiput and the atlas vertebra in the midline at the back of the neck. The bent part of the needle has to be kept in close contact with the internal surface of the occiput for the entire length (3.5 mm) (*see* **Fig. 2**).
6. Inject the cells (5 μL); wait a few seconds before extracting the needle, to avoid cells backflow (*see* **Note 18)**.
7. Inject the mouse subcutaneously with buprenorphine (0.032 mg/kg).

4. Notes

1. Do not use this solution for more than 1 week.
2. Stem cells isolated from different animals have similar features; however, slight variations can be observed in their growth rate and differentiation capacity.

4. Killing of the animal and removal and dissection of brain and/or spinal cord are performed outside the laminar flow hood.
5. Different operators may prefer the use of alternative brands and tools.
6. Commercial, denatured ethanol may be used instead.
7. Leaving the cerebellum in place is preferable, because it allows for better handling of the brain with forceps.
8. A bulk culture can be produced from a single SVZ, which can be expanded for well over 40 passages. A theoretical total number of up to 1×10^{40} can be generated.
9. Do not use the vacuum suction. There is a substantial risk of sucking up and wasting the tissue together with the discarded medium.
10. Avoid bubbling and foaming.
11. If the counting of the cells is difficult because of the high amount of debris, try to plate the tissue derived from a single mouse in a 25-cm^2 flask.
12. This anesthesia should keep unconscious the animal for 20–30 min. It is possible to repeat it during the surgery, although this should be avoided if possible.
13. Be careful to make a complete cut through the bones and avoid that small pieces of bones are left on the dorsal surface of the cord.
14. At the time of impact, overextension of the hind limbs is observed. The impact site on the cord should quickly turn reddish. In many laboratories, the contusion is performed without holding the animal in a stereotaxic apparatus maintaining a high reproducibility of the experiments.
15. This procedure should produce an enrichment in the culture content of NSCs.
16. If the lesion and transplantation procedure are expected to take a significant time, make sure to perform separate cell-harvesting steps in order to avoid keeping the cells in PBS solution at 4° C for prolonged period of times, during which cell viability may drop significantly.
17. In order to avoid a sudden change in temperature of the buffer, it is convenient to slowly reduce the temperature of the PBS from room temperature to 4° C gradually. For instance, reducing the centrifuge temperature from 25 to 14° C and finally to 4° C.
18. Intracisternal injection might occasionally cause cerebellar lesion and ataxia in mice. If this becomes a recurrent problem, reduce the length of the bent part of the needle.

References

1. Gage, F. H. (2000) Mammalian neural stem cells. *Science* **287**, 1433–8.
2. McKay, R. (1997) Stem cells in the central nervous system. *Science* **276**, 66–71.
3. Lois, C. and Alvarez-Buylla, A. (1994) Long-distance neuronal migration in the adult mammalian brain. *Science* **264**, 1145–8.
4. Gritti, A., Cova, L., Parati, E. A., Galli, R., and Vescovi, A. L. (1995) Basic fibroblast growth factor supports the proliferation of epidermal growth factor-generated neuronal precursor cells of the adult mouse CNS. *Neurosci Lett* **185**, 151–4.

5. Gritti, A., Parati, E. A., Cova, L., Frolichsthal, P., Galli, R., Wanke, E., Faravelli, L., Morassutti, D. J., Roisen, F., Nickel, D. D., and Vescovi, A. L. (1996) Multipotential stem cells from the adult mouse brain proliferate and self-renew in response to basic fibroblast growth factor. *J Neurosci* **16**, 1091–100.
6. Galli, R., Gritti, A., Bonfanti, L., and Vescovi, A. L. (2003) Neural stem cells: an overview. *Circ Res* **92**, 598–608.
7. Lois, C. and Alvarez-Buylla, A. (1993) Proliferating subventricular zone cells in the adult mammalian forebrain can differentiate into neurons and glia. *Proc Natl Acad Sci USA* **90**, 2074–7.
8. Alvarez-Buylla, A. and Lois, C. (1995) Neuronal stem cells in the brain of adult vertebrates. *Stem Cells* **13**, 263–72.
9. Reynolds, B. A. and Weiss, S. (1992) Generation of neurons and astrocytes from isolated cells of the adult mammalian central nervous system. *Science* **255**, 1707–10.
10. Galli, R., Fiocco, R., De Filippis, L., Muzio, L., Gritti, A., Mercurio, S., Broccoli, V., Pellegrini, M., Mallamaci, A., and Vescovi, A. L. (2002) Emx2 regulates the proliferation of stem cells of the adult mammalian central nervous system. *Dev Suppl* **129**, 1633–44.
11. Gritti, A., Frolichsthal-Schoeller, P., Galli, R., Parati, E. A., Cova, L., Pagano, S. F., Bjornson, C. R., and Vescovi, A. L. (1999) Epidermal and fibroblast growth factors behave as mitogenic regulators for a single multipotent stem cell-like population from the subventricular region of the adult mouse forebrain. *J Neurosci* **19**, 3287–97.
12. Gritti, A., Bonfanti, L., Doetsch, F., Caille, I., Alvarez-Buylla, A., Lim, D. A., Galli, R., Verdugo, J. M., Herrera, D. G., and Vescovi, A. L. (2002) Multipotent neural stem cells reside into the rostral extension and olfactory bulb of adult rodents. *J Neurosci* **22**, 437–45.
13. Reynolds, B. A. and Rietze, R. L. (2005) Neural stem cells and neurospheres—re-evaluating the relationship. *Nat Methods* **2**, 333–6.
14. Vescovi, A. L., Gritti, A., Galli, R., and Parati, E. A. (1999) Isolation and intracerebral grafting of nontransformed multipotential embryonic human CNS stem cells. *J Neurotrauma* **16**, 689–93.
15. Svendsen, C. N., Caldwell, M. A., and Ostenfeld, T. (1999) Human neural stem cells: isolation, expansion and transplantation. *Brain Pathol* **9**, 499–513.
16. Carpenter, M. K., Cui, X., Hu, Z. Y., Jackson, J., Sherman, S., Seiger, A., and Wahlberg, L. U. (1999) In vitro expansion of a multipotent population of human neural progenitor cells. *Exp Neurol* **158**, 265–78.
17. Goldman, S. A. and Sim, F. (2005) Neural progenitor cells of the adult brain. *Novartis Found Symp* **265**, 66–80; discussion 82–97.
18. Bottai, D., Fiocco, R., Gelain, F., Defilippis, L., Galli, R., Gritti, A., and Vescovi, L. A. (2003) Neural stem cells in the adult nervous system. *J Hematother Stem Cell Res* **12**, 655–70.

19. Pluchino, S., Quattrini, A., Brambilla, E., Gritti, A., Salani, G., Dina, G., Galli, R., Del Carro, U., Amadio, S., Bergami, A., Furlan, R., Comi, G., Vescovi, A. L., and Martino, G. (2003) Injection of adult neurospheres induces recovery in a chronic model of multiple sclerosis. *Nature* **422**, 688–94.
20. Pluchino, S., Zanotti, L., Rossi, B., Brambilla, E., Ottoboni, L., Salani, G., Martinello, M., Cattalini, A., Bergami, A., Furlan, R., Comi, G., Constantin, G., and Martino, G. (2005) Neurosphere-derived multipotent precursors promote neuroprotection by an immunomodulatory mechanism. *Nature* **436**, 266–71.
21. Reynolds, B. A., Tetzlaff, W., and Weiss, S. (1992) A multipotent EGF-responsive striatal embryonic progenitor cell produces neurons and astrocytes. *J Neurosci* **12**, 4565–74.
22. Kwon, B. K., Oxland, T. R., and Tetzlaff, W. (2002) Animal models used in spinal cord regeneration research. *Spine* **27**, 1504–10.
23. Martino, G. and Hartung, H. P. (1999) Immunopathogenesis of multiple sclerosis: the role of T cells. *Curr Opin Neurol* **12**, 309–21.
24. Hemmer, B., Archelos, J. J., and Hartung, H. P. (2002) New concepts in the immunopathogenesis of multiple sclerosis. *Nat Rev Neurosci* **3**, 291–301.
25. Kuchroo, V. K., Anderson, A. C., Waldner, H., Munder, M., Bettelli, E., and Nicholson, L. B. (2002) T cell response in experimental autoimmune encephalomyelitis (EAE): role of self and cross-reactive antigens in shaping, tuning, and regulating the autopathogenic T cell repertoire. *Annu Rev Immunol* **20**, 101–23.
26. Lebar, R., Lubetzki, C., Vincent, C., Lombrail, P., and Boutry, J. M. (1986) The M2 autoantigen of central nervous system myelin, a glycoprotein present in oligodendrocyte membrane. *Clin Exp Immunol* **66**, 423–34.
27. Slavin, A., Ewing, C., Liu, J., Ichikawa, M., Slavin, J., and Bernard, C. C. (1998) Induction of a multiple sclerosis-like disease in mice with an immunodominant epitope of myelin oligodendrocyte glycoprotein. *Autoimmunity* **28**, 109–20.
28. Ueda, H., Amano, H., Shiomi, H., and Takagi, H. (1979) Comparison of the analgesic effects of various opioid peptides by a newly devised intracisternal injection technique in conscious mice. *Eur J Pharmacol* **56**, 265–8.
29. Furlan, R., Pluchino, S., Marconi, P. C., and Martino, G. (2003) Cytokine gene delivery into the central nervous system using intrathecally injected nonreplicative viral vectors. *Methods Mol Biol* **215**, 279–89.

15

In Vivo Tomographic Imaging Studies of Neurodegeneration and Neuroprotection: A Review

Rikki N. Waterhouse and Jun Zhao

Summary

Noninvasive tomographic imaging methods including positron emission tomography (PET) and single photon emission computed tomography (SPECT) are extremely sensitive and are capable of measuring biochemical processes that occur at concentrations in the nanomolar range. Inherent to neurodegenerative processes is neuronal loss. Thus, PET or SPECT monitoring of biochemical processes altered by neuronal loss (changes in neurotransmitter turnover, alterations in receptor, transporter or enzyme concentrations) can provide unique information not attainable by other methods. Such imaging techniques can also be used to longtitudinally monitor the effects of neuroprotective treatments. This review highlights current imaging probes used to evaluate patients with specific neurodegenerative disorders (e.g., Alzheimer's Disease, Parkinson's Disease, Huntington's Chorea), including those that image receptors of the dopaminergic, cholinergic and glutamatergic systems. Areas of future research focus are also defined. It is clear that monitoring the progression of neurodegenerative disorders and the impact of neuroprotective treatments are two different but related goals for which noninvasive imaging via PET and SPECT methods plays a powerful and unique role.

Key Words: Positron emission tomography, single photon emission computed tomography, neuroimaging, dopamine receptor, neurodegeneration, neuroprotection, Parkinson's Disease, Alzheimer's Disease, Huntington's Chorea, radiotracer, cholinergic receptor.

From: *Methods in Molecular Biology, vol. 399: Neuroprotection Methods and Protocols*
Edited by: T. Borsello © Humana Press Inc., Totowa, NJ

1. Introduction

Advances in noninvasive imaging methods recently afford previously unavailable opportunities for the study of central nervous system (CNS) function in living individuals. Two nuclear-based techniques, positron emission tomography (PET) and single-photon emission computed tomography (SPECT), have proven particularly powerful for measuring biochemical processes that occur in relatively low concentrations. PET and SPECT allow measurements of local neuronal activity, neurochemistry, and pharmacology in the living brain in a manner that does not disrupt ongoing endogenous processes. This chapter highlights the current state-of-the-art of these methodologies with respect to measurements of neurodegeneration and neuroprotection in clinical populations.

2. Noninvasive Tomographic Imaging of Neurodegeneration and Neuroprotection

Since the mid-1970s, PET and SPECT imaging techniques have been recognized as a vital tool in pathophysiological and neuropharmacological studies of the brain ***(1–5)***. For a given imaging paradigm, a photon-producing radionuclide is synthetically attached to a larger molecule, usually a compound with established pharmacological activity, in a way that it will bind to a protein of interest in the brain when administered normally intravenously to a patient ***(5,6)***. Radioactivity (gamma emission) originates from the radiotracer localized within the brain to provide a signal that is detected by the PET or SPECT camera. By a special type of reconstruction of the signal collected by the camera, the regional brain localization of the radiotracer is determined over time, and the resulting information provides a snapshot corresponding to the regional density of the protein or process of interest. In contrast to two-dimensional imaging methods, such as chest X-ray where externally generated radiation is transmitted through the subject to provide contrast images, PET and SPECT are tomographic in nature and are capable of providing three-dimensional images that correspond to regional brain target protein concentration in a highly sensitive manner (picomolar to femtomolar sensitivity).

During such an imaging procedure, the subject is taken to an examination room that houses a PET or SPECT scanner. The scanners have a hole in the middle and looks like a large doughnut. There is a long examination table on which the subject lies that can move in a way to place the head in the center for the camera. Within the camera are multiple rings of detectors that record the emission of energy from the radioactive substance in the brain to permit an image of the protein being measured. Before the image acquisition

begins, a transmission scan is taken to provide a map of the brain and to help in image reconstruction. The radioactive isotope is produced in a machine called a cyclotron and attached by a chemist to a compound that binds the protein of interest. Once this substance is administered to the patient, the radioactivity localizes in the appropriate areas of the brain and is detected by the PET or SPECT scanner. Blood samples (venous or arterial) may also be taken to determine the amount of radioactivity in the plasma and to measure the amount of metabolites present. These parameters are important for postscan quantification of the brain image data. Prescan restrictions placed on the subject are normally specific to the particular study design and patient population being studied.

Three most common measurements in brain imaging are regional cerebral blood flow, glucose metabolic rate, and neuroreceptor imaging. With respect to the neuroreceptor imaging, functional neuroimaging radiotracers are designed to selectively tag specific proteins including classical receptors, nonclassical sites (modulatory receptors), enzymes, and transporters. Although blood flow and metabolism have been monitored in studies to elucidate processes involved in neurodegeneration and neuroprotection, this chapter focuses on neuroreceptor class of imaging methodology because of its higher intrinsic sensitivity. Patients who benefit from neuroreceptor imaging techniques include, but are not limited to, those affected by Parkinson's disease (PD), stroke, Huntington's chorea, multiple sclerosis, epilepsy, traumatic brain injury, Alzheimer's disease (AD), and schizophrenia ***(7–9)***.

Membrane receptors and monoaminergic transporters are responsible for the homeostasis of neurotransmission and are often involved in the pathophysiology of neurological disease and also serve as targets for medications for such illnesses ***(10–12)***. During neurodegenerative processes, the densities of specific receptor and transporter proteins often decrease in proportion to increased cell loss. When effective neuroprotective drugs are administered, the rate of neuron loss is reduced. Such effects can be monitored using PET and SPECT neuroreceptor ligands by comparing baseline scans to those obtained some time after treatment. Indeed, the assessment of receptors and transporters can therefore provide a method for (1) detection of the loss of neurons, (2) monitoring the progression of the disease, and (3) validation of the neuroprotective potential of therapeutic strategies.

Brain imaging methods designed to monitor neurodegeneration are an important focus for this review because of their potential to assess over time the effects of clinical treatment on the rate of neuronal loss in patients. Imaging of neuroprotection obviously includes PET or SPECT evaluation of the same

proteins that are reduced in density because of neurodegenerative processes. Neuroprotective therapies are interventions that produce enduring benefits by favorably influencing underlying etiology or pathogenesis of neurodegenerative disorders. One would thus expect that the rate of reduced radiotracer signal over time that occurs because of neuron loss would be reduced with the successful application of neuroprotective therapies.

Although several neuroreceptor systems are affected by neurodegenerative processes, only a handful of these systems can be considered as targets for monitoring by PET and SPECT radiotracer methods. This is because relatively few radioligands are available for use in humans. Indeed, it is quite difficult to identify and validate radioligands that have appropriate characteristics of affinity, selectivity, lipophilicity, metabolic profile, and biological half-life for in vivo studies of neuroreceptor systems. Still, quite a bit of relevant research has been carried out, and much of it revealing important information. We provide here a review of the neuroimaging methods used to monitor neurodegeneration in specific patient populations, limiting our discussion to findings over the past 11 years (1995 onward). We also outline research involving PET and SPECT evaluation of neuroprotection and how such studies apply to the evaluation of putative therapeutic agents. We focus the discussion on specific neurotransmitter system proteins that have been successfully imaged in humans and those where postmortem evidence supports their usefulness for the study of neuroprotection and where suitable radioligands are available. Whenever possible, we also suggest future areas of research and development.

3. Dopaminergic System

One of neurological illnesses in which the degradation of the dopaminergic system has been most studied is PD. PD involves a progressive loss of the nigrostriatal dopaminergic neurons, leading to a functional decline and intellectual impairment (dementia) ***(13,14)***. A major goal of PD research is the development of treatments to slow the progressive degeneration of the dopaminergic system to alleviate the associated symptoms ***(10,13,15–17)***. But uncertainty often exists regarding the effect of therapy on disease progression, because clinical evaluation cannot directly assess the status of the nigrostriatal dopaminergic system, especially once therapy is underway. Thus, the field has sought to develop alternative measures of disease course, and much focus has been placed on the evaluation of dopamine system function. Neuroimaging with PET or SPECT radiotracers that interact with processes central to dopaminergic neurotransmission has proven very useful for this purpose ***(10,18–22)***.

Specifically, radioligand studies can report on the density of dopaminergic neurons as well as determine their metabolic status ***(23)***.

For example, the metabolic PET radiotracer [^{18}F]fluorodopa (L-3,4-dihydroxyphenylalanine; **Fig. 1**) ***(18,23–26)*** is used to monitor the conversion of levodopa to dopamine through aromatic amino acid decarboxylase in neuron axons. [^{18}F]fluorodopa is taken up by nigrostriatal neurons in a manner similar to L-dopa. It is then decarboxylated to fluorodopamine, which is subsequently metabolized like dopamine. The level of radioactivity during this process is measured, and the intensity of signal reflects the activity and density of active neurons. In PD, the [^{18}F]fluorodopa signal decreases over time as the disease progresses. Fluorodopa PET has been used alongside two clinical trials in early PD comparing new drugs with L-dopa to evaluate their relative effects on nigrostriatal neuron loss ***(20,26,27)***.

Another neuroimaging target that has been explored to follow neurodegeneration in PD and other illnesses is the presynaptic dopamine transporter (DAT) ***(7,11,18,28)***. The DAT is located on dopaminergic nerve terminals where it actively pumps synaptic dopamine back into neurons. DAT is reduced in number, as dopamine neurons are lost as a result of disease. Thus, a loss in DAT tracer signal indicates a loss of dopamine neurons. Several radioligands have been developed that are capable of imaging DAT in humans (*see* **Fig. 2** for examples). By far the most widely used DAT SPECT radioligand is 2β-carboxymethoxy-3-(4-iodophenyl)tropane ([^{123}I]β-CIT) ***(29–32)***. The uptake and clearance of [^{123}I]β-CIT are relatively slow, leading to image acquisition the day after injection. Newer ligands such as *N*-fluoropropyl-2-carboxymethoxy-3-(4-iodophenyl)tropane ([^{123}I]FP-CIT) and the PET tracer [^{18}F]FP-CIT equilibrate faster in the brain, and therefore, imaging can be performed several hours after injection ***(33–36)***. In the case of DAT imaging, the signal detected by the PET or SPECT camera reflects the uptake of the tracer into the striatum, its binding to the DAT, and its release. Thus, as PD progresses and dopamine neurons are lost, the signal associated with DAT tracer imaging becomes weaker. As one example, Winogrodzka et al. ***(37)*** investigated

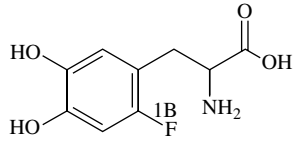

Fig. 1. Structure of [^{18}F]fluorodopa.

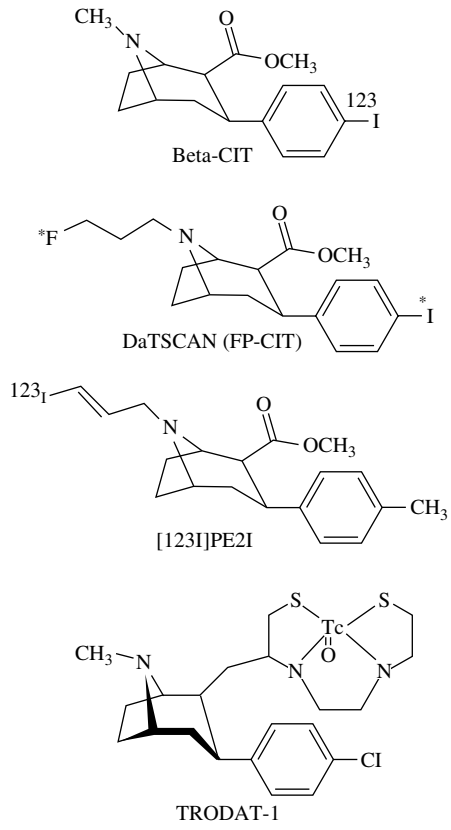

Fig. 2. Structures of select dopamine transporter tracers.

the applicability of [^{123}I]FP-CIT SPECT for the assessment of the rate of dopaminergic degeneration in 20 early-stage patients (age range 43–73 years; mean age 55.4 years). Each participant was scanned twice with the assessments approximately 12 months apart. A mean annual decrease in striatal [^{123}I]FP-CIT binding ratios was found to be about 8% of the initial baseline values. As an example of determination of therapeutic sparing of dopamine neurons, the "Parkinson Study Group" followed 82 patients with early PD who received either pramipexole or L-DOPA therapy for up to 4 years with [^{123}I]β-CIT SPECT ***(38)***.

The reduction in [^{123}I]β-CIT uptake over time from baseline normally associated with PD was significantly blunted in the group taking pramipexole compared with the group taking L-DOPA (7.1 versus 13.5% at 22 months,

$P = 0.004$; 10.9 versus 19.6% at 34 months, $P = 0.009$; 16.0 versus 25.5% at 46 months, $P = 0.01$). These results suggest that pramipexole is more neuroprotective than L-DOPA in patients with PD. Two other DAT tracers that are useful for studies of DAT in humans are [^{123}I]PE$_2$I ***(39,40)*** and [^{99m}Tc]TRODAT-1 ***(41–44)***. [^{123}I]PE$_2$I, which can also be labeled with carbon-11, binds to the DAT with high potency and, in contrast to β-CIT, has very low affinities for the serotonin and noradrenaline transporters. Autoradiographic studies support that [^{11}C]PE$_2$I and [^{123}I]PE$_2$I should be suitable for the in vivo visualization of the human DAT with PET or SPECT, respectively ***(39)***. [^{99m}Tc]TRODAT-1 is the first Tc-99m-labeled tracer for imaging CNS DATs in humans. This tracer displayed excellent specific binding to DATs in the basal ganglia region of the brain; thus, it is potentially useful for the diagnosis of the deficit of DATs in neurodegenerative diseases such as PD.

Finally, some studies to assess neuron loss in schizophrenia, PD, Huntington's chorea, AD, and other illnesses have utilized one of the many established dopamine D_2 receptor radioligands ***(31,45–55)***, such as [^{11}C]raclopride, [^{123}I]epidepride, and [^{123}I]iodobenzamide ([^{123}I]IBZM). In general, there is a loss of signal of these tracers with disease progression that typically corresponds with a loss of dopamine neurons. This paradigm is not quite as straightforward as those mentioned earlier because competition for receptor binding between the D_2 receptor radioligand and endogenous dopamine leads to a signal that is influenced by both receptor density and synaptic neurotransmitter concentration ***(56)***. Thus, a reduction in signal might be because of cell loss or increased dopamine, or a combination of the two.

4. Vesicular Monaminergic Transporters

Membrane and vesicular monoaminergic transporters (VMATs), responsible for the homeostasis of neurotransmitter pools at nerve endings, are very much involved in the physiology and diseases of CNS ***(57–62)***. The vesicular monoamine transporter subtype-2 ($VMAT_2$) has been proposed as an excellent imaging biomarker for dopamine neuron loss because of a high level of $VMAT_2$ expression in the healthy striatum along with stable expression levels during treatment ***(21,57,58)***. In vivo imaging and postmortem binding studies have revealed a loss in striatal $VMAT_2$ binding in PD. Highly precise and specific measures of human $VMAT_2$ are possible with PET employing the novel tracer [^{11}C]dihydrotetrabenazine ([^{11}C]DTBZ; **Fig. 3**) ***(57)***. In addition to PD, reductions in striatal $VMAT_2$ binding have been documented in patients with AD and Huntington's chorea compared with healthy individuals. Using [^{11}C]DTBZ PET, Bohnen et al. ***(59)*** found reduced striatal $VMAT_2$ binding,

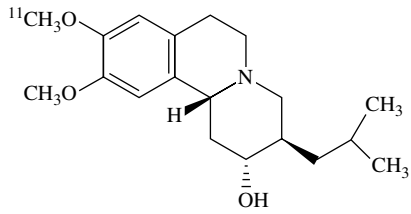

Fig. 3. Structure of (+)-[^{11}C]dihydrotetrabenazine.

suggesting nigrostriatal pathology in Huntington's chorea, and these abnormalities appeared in a phenotype-specific manner. Striatal reductions in tracer uptake were most prominent in the posterior putamen, a finding similar to that found in PD. In AD, autoradiographic studies have confirmed that $VMAT_2$ binding is significantly reduced (by 57%) in the ventral striatum but not in the caudate nucleus and putamen ***(63)***. The specific decrease in monoaminergic transporter levels in the ventral striatum confirms that this nucleus is selectively targeted area in AD. Thus, PET imaging of $VMAT_2$ could provide an effective way to monitor dopaminergic neurodegeneration as well as follow neuroprotective effects of therapy in these illnesses as well as in PD. Although at this time the use of $VMAT_2$ imaging to monitor a drug-induced decrease in cell loss in a clinical population has not been published, the potential for such a paradigm is certainly there.

5. Cholinergic System

One of the treatment strategies for AD is the use of drugs that enhance cholinergic brain function, because it is thought that the dysfunction of this system contributes to cognitive deterioration ***(64–68)***. Two receptor systems can currently be imaged in humans via PET and SPECT methods. These include specific subtypes, muscarinic and nicotinic receptors, as discussed in **Subheadings 5.1.** and **5.2**.

5.1. Muscarinic Receptors

Muscarinic receptors are known to be downregulated in patients with AD and other illnesses that involve the cholinergic system. The SPECT ligand, *Z*-(*R*)-1-azabicyclo[2.2.2]oct-3-yl-(*R*)-α-hydroxy-α-(1-iodo-1-propen-3-yl)-α-phenylacetate (*Z*-IQNP), exhibits high affinity to two muscarinic acetylcholine receptor (mAChR) subtypes (denoted M_1 and M_2) ***(69–71)***. In patients with AD, the radiolabeled SPECT analog [^{123}I]QNB (**Fig. 4**) has been

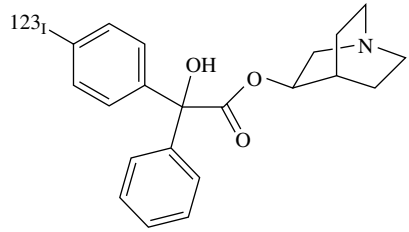

Fig. 4. Structure of ^{123}I-QNB.

used to demonstrate a significant relationship between reduced muscarinic receptor density and baseline psychometric impairment. In addition, the effects of cholinergic treatment on muscarinic receptor densities in AD patients have been measured with [^{123}I]QNB SPECT ***(72,73)***. In a first exploratory study, 12 patients with moderate-to-mild AD and 6 healthy individuals were scanned with [^{123}I]QNB ***(73)***. Both placebo and actively treated groups had reductions in [^{123}I]QNB uptake. However, greater reductions in [^{123}I]QNB receptor binding were demonstrated in the placebo group than in the group receiving active treatment. The results suggest that [^{123}I]QNB uptake is better preserved in AD patients on cholinergic treatment than in those on placebo. It was concluded that cholinergic drugs may be neuroprotective in patients with AD. Sequential [^{123}I]QNB imaging should prove a powerful tool in monitoring the response of the muscarinic cholinergic system to disease-modifying treatments.

5.2. Nicotinic Receptors

Consistent deductions in nicotinic acetylcholine receptors (nAChRs) have been measured in vitro in autopsy brain tissue of AD patients, as well as in vivo by PET. Measurement of the protein content of nAChRs showed reduced levels of the α-4, α-3, and α-7 nAChR subtypes ***(74)***. [^{123}I]5-iodo-3-(2[*S*]-azetidinylmethoxy)pyridine, [^{123}I]5-iodo-A-85380 (**Fig. 5**), a novel ligand for brain nAChRs, was evaluated in the rhesus monkey SPECT, and low nonspecific binding and lack of toxicity in animals were found for this tracer ***(75,76)***. [^{123}I]5-iodo-A-85380 also appears to be a promising ligand for SPECT imaging of nAChRs in the human brain ***(76–79)***. Very promising PET ligands measuring the α-4 nAChRs are currently being evaluated in clinical studies ***(80–82)***. In early studies, an improved binding of [^{11}C]nicotine was observed in the temporal cortex of AD patients in vivo by PET after treatment with tacrine, NXX-066, or rivastigmine ***(83–85)***. A parallel improvement in neuropsychological tests was observed after long-term treatment. The authors state that

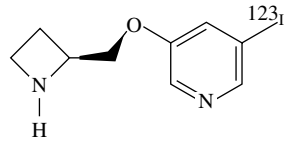

Fig. 5. Structure of 5-[^{123}I]iodo-A-85380.

the effects might be because of indirect stimulation of nicotinic receptors by endogenous acetylcholine in the synaptic cleft or because of direct upregulation of the nicotinic receptors. Further studies to assess the neuroprotective effects mediated through the modulation of nAChR subtypes using improved tracers such as [^{123}I]5-iodo-A-85380 should appear in the near future.

6. Glutamatergic System: NMDA Ion Channels

Ionotropic glutamate receptors of the *N*-methyl-D-aspartate (NMDA) ion channel are expressed throughout the brain and are involved in excitatory synaptic transmission and synaptic plasticity. Alterations in NMDA ion channel function have been implicated in the pathophysiology of several neurological and neuropsychiatric disorders, including AD, chronic pain syndromes, epilepsy, schizophrenia, PD, Huntington's disease, addiction disorders, major depression, and anxiety disorders. It is beyond the scope of this chapter to detail what is known about the roles of NMDA ion channels in these disorders, but several reviews are available ***(86–89)***. Prolonged activation of NMDA receptors leads to excitotoxicity, resulting in the pathogenesis of neurodegeneration that is related to several neurological illnesses (e.g., AD). In addition, neuroprotection involving modulation of the NMDA ion channel is a key strategy in patients with neurodegenerative disorders or who have suffered from stroke ***(86,87,89–92)***. Recent advances in understanding the function, pharmacology, genetics, and structure of NMDA receptors have promoted a search for new therapeutic compounds, including those thought to be neuroprotective ***(87–89,91)***. Of particular interest are the clinically used open channel blockers, such as memantine, which bind the PCP site that lies within the NMDA ion channel.

[^{123}I]CNS 1261 (**Fig. 6**) is a new SPECT PCP site ligand that is in the early stages of evaluation in humans ***(93,94)***. Tracer development for this site has proven particularly difficult, and most of the ligands including [^{123}I]CNS 1261 have not yet been fully validated ***(95)***. Nonetheless, the development of imaging probes and methods for the evaluation of NMDA ion channel status is important for studies of neuroprotection. Such techniques could be

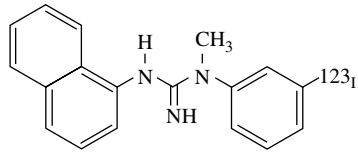

Fig. 6. Structure of [^{123}I]CNS 1261.

used to (1) follow over time the loss of NMDA ion channels because of the loss of glutamatergic neurons, (2) measure the degree of binding of memantine and other neuroprotective drugs targeted to NMDA ion channels, or (3) monitor the effect of neuroprotective therapies on NMDA system to determine whether glutamatergic neurons are spared. A review of the principles and possible applications of NMDA/PCP site imaging paradigms has been published ***(95)***.

7. Conclusion

Imaging tracers to monitor DAT density, dopamine metabolism, and the expression of specific cholinergic receptors have been successfully used to monitor neuron loss and neuroprotective properties of treatments for PD and other neurological illnesses. Other imaging biomarkers are coming to the forefront for such purposes, including NMDA ion channel receptors, α-4-β-2 nicotinic receptors, and $VMAT_2$. Certainly, this is one area of clinical research in which noninvasive imaging via PET and SPECT in patients will play a powerful and unique role.

References

1. Kessler, R. M. (2003) Imaging methods for evaluating brain function in man. *Neurobiol Aging* **24 Suppl 1**, S21–35.
2. Slifstein, M. and Laruelle, M. (2001) Models and methods for derivation of in vivo neuroreceptor parameters with PET and SPECT reversible radiotracers. *Nucl Med Biol* **28**, 595–608.
3. Lammertsma, A. (2001) PET/SPECT: functional imaging beyond flow *Vision Res* **41**, 1277–81.
4. Talbot, P. and Laruelle, M. (2002) The role of in vivo molecular imaging with PET and SPECT in the elucidation of psychiatric drug action and new drug development. *Eur Neuropsychopharmacol* **12**, 503–11.
5. Kegeles, L. and Mann, J. (1997) In vivo imaging of neurotransmitter systems using radiolabeled receptor ligands. *Neuropsychopharmacology* **17**, 293–307.

6. Halldin, C., Gulyas, B., Langer, O., and Farde, L. (2001) Brain radioligands—state of the art and new trends. *Q J Nucl Med* **45**, 139–52.
7. Piccini, P. (2004) Neurodegenerative movement disorders: the contribution of functional imaging. *Curr Opin Neurol* **17**, 459–66.
8. Costa, D., Pilowsky, L., and Ell, P. (1999) Nuclear medicine in neurology and psychiatry. *Lancet* **354**, 1107–11.
9. Blake, P., Johnson, B., and VanMeter, J. W. (2003) Positron emission tomography (PET) and single photon emission computed tomography (SPECT): clinical applications. *J Neuroophthalmol* **23**, 34–41.
10. Mandel, S., Grunblatt, E., Riederer, P., Gerlach, M., Levites, Y., and Youdim, M. B. (2003) Neuroprotective strategies in Parkinson's disease: an update on progress. *CNS Drugs* **17**, 729–62.
11. Kostrzewa, R. M. and Segura-Aguilar, J. (2003) Novel mechanisms and approaches in the study of neurodegeneration and neuroprotection. *Neurotox Res* **5**, 375–83.
12. Youdim, M. B. and Buccafusco, J. J. (2005) CNS targets for multi-functional drugs in the treatment of Alzheimer's and Parkinson's diseases. *J Neural Transm* **112**, 519–37.
13. Riederer, P., Gille, G., Muller, T., Przuntek, H., Reichmann, H., Riess, O., Schwartz, A., Schwarz, J., and Vogt, T. (2002) Practical importance of neuroprotection in Parkinson's disease. *J Neurol* **249**, 53–6.
14. Leenders, K. L. and Oertel, W. H. (2001) Parkinson's disease: clinical signs and symptoms, neural mechanisms, positron emission tomography, and therapeutic interventions. *Neural Plast* **8**, 99–110.
15. Hauser, R. A. and Zesiewicz, T. A. (1999) Management of early Parkinson's disease. *Med Clin North Am* **83**, 393–414.
16. Riederer, P., Sian, J., and Gerlach, M. (2000) Is there neuroprotection in Parkinson syndrome? *J Neurol* **247**, 8–11.
17. Stocchi, F. and Olanow, C. W. (2003) Neuroprotection in Parkinson's disease: clinical trials. *Ann Neurol* **53 Suppl 3**, S87–97.
18. Brooks, D. J., Frey, K. A., Marek, K. L., Oakes, D., Paty, D., Prentice, R., Shults, C. W., and Stoessl, A. J. (2003) Assessment of neuroimaging techniques as biomarkers of the progression of Parkinson's disease. *Exp Neurol* **184 Suppl 1**, S68–79.
19. Morrish, P. K. (2003) How valid is dopamine transporter imaging as a surrogate marker in research trials in Parkinson's disease? *Mov Disord* **18 Suppl 7**, S63–70.
20. Brooks, D. J. (2000) Monitoring neuroprotection and restorative therapies in Parkinson's disease with PET. *J Neural Transm Suppl* **60**, 125–37.
21. Guilloteau, D. and Chalon, S. (2005) PET and SPECT exploration of central monoaminergic transporters for the development of new drugs and treatments in brain disorders. *Curr Pharm Des* **11**, 3237–45.

22. Brooks, D. J. (2003) Imaging end points for monitoring neuroprotection in Parkinson's disease. *Ann Neurol* **53 Suppl 3**, S110–8.
23. Morrish, P. K., Rakshi, J. S., Bailey, D. L., Sawle, G. V., and Brooks, D. J. (1998) Measuring the rate of progression and estimating the preclinical period of Parkinson's disease with [18F]dopa PET. *J Neurol Neurosurg Psychiatry* **64**, 314–9.
24. Hilker, R., Schweitzer, K., Coburger, S., Ghaemi, M., Weisenbach, S., Jacobs, A. H., Rudolf, J., Herholz, K., and Heiss, W. D. (2005) Nonlinear progression of Parkinson disease as determined by serial positron emission tomographic imaging of striatal fluorodopa F 18 activity. *Arch Neurol* **62**, 378–82.
25. Heiss, W. D. and Hilker, R. (2004) The sensitivity of 18-fluorodopa positron emission tomography and magnetic resonance imaging in Parkinson's disease. *Eur J Neurol* **11**, 5–12.
26. Rakshi, J. S., Pavese, N., Uema, T., Ito, K., Morrish, P. K., Bailey, D. L., and Brooks, D. J. (2002) A comparison of the progression of early Parkinson's disease in patients started on ropinirole or L-dopa: an 18F-dopa PET study. *J Neural Transm* **109**, 1433–43.
27. Bohnen, N. I. and Frey, K. A. (2003) The role of positron emission tomography imaging in movement disorders. *Neuroimaging Clin N Am* **13**,791–803.
28. Booij, J., Tissingh, G., Winogrodzka, A., and van Royen, E. A. (1999) Imaging of the dopaminergic neurotransmission system using single-photon emission tomography and positron emission tomography in patients with parkinsonism. *Eur J Nucl Med* **26**, 171–82.
29. Carpinelli, A., Matarrese, M., Moresco, R., Simonelli, P., Todde, S., Magni, F., Galli, K. M., and Fazio, F. (2001) Radiosynthesis of [123I]betaCIT, a selective ligand for the study of the dopaminergic and serotoninergic systems in human brain. *Appl Radiat Isot* **54**, 93–5.
30. Staley, J., Krishnan-Sarin, S., Zoghbi, S., Tamagnan, G., Fujita, M., Seibyl, J., Maciejewski, P., O'Malley, S., and Innis, R. (2001) Sex differences in [123I]beta-CIT SPECT measures of dopamine and serotonin transporter availability in healthy smokers and nonsmokers. *Synapse* **41**, 275–84.
31. Wenning, G., Donnemiller, E., Granata, R., Riccabona, G., and Poewe, W. (1998) 123I-beta-CIT and 123I-IBZM-SPECT scanning in levodopa-naive Parkinson's disease. *Mov Disord* **13**, 438–45.
32. Berding, G., Brucke, T., Odin, P., Brooks, D. J., Kolbe, H., Gielow, P., Harke, H., Knoop, B. O., Dengler, R., and Knapp, W. H. (2003) [123I]beta-CIT SPECT imaging of dopamine and serotonin transporters in Parkinson's disease and multiple system atrophy. *Nucl Med* **42**, 31–8.
33. Berger, H., Cools, A., Horstink, M., Oyen, W., Verhoeven, E., and van der Werf, S. P. (2004) Striatal dopamine and learning strategy-an (123)I-FP-CIT SPECT study. *Neuropsychologia* **42**, 1071–8.

34. Booij, J., Tissingh, G., Boer, G., Speelman, J., Stoof, J., Janssen, A., Wolters, E., and van Royen, E. A. (1997) [123I]FP-CIT SPECT shows a pronounced decline of striatal dopamine transporter labelling in early and advanced Parkinson's disease. *J Neurol Neurosurg Psychiatry* **62**, 133–40.
35. Lavalaye, J., Linszen, D., Booij, J., Dingemans, P., Reneman, L., Habraken, J., Gersons, B., and van Royen, E. A. (2001) Dopamine transporter density in young patients with schizophrenia assessed with [123]FP-CIT SPECT. *Schizophr Res* **47**, 59–67.
36. Booij, J., Speelman, J. D., Horstink, M. W., and Wolters, E. C. (2001) The clinical benefit of imaging striatal dopamine transporters with [123I]FP-CIT SPET in differentiating patients with presynaptic parkinsonism from those with other forms of parkinsonism. *Eur J Nucl Med* **28**, 266–72.
37. Winogrodzka, A., Bergmans, P., Booij, J., van Royen, E. A., Janssen, A. G., and Wolters, E. C. (2003) [123I]FP-CIT SPECT is a useful method to monitor the rate of dopaminergic degeneration in early-stage Parkinson's disease. *J Neural Transm* **108**, 1011–9.
38. Parkinson Study Group. (2002) Dopamine transporter brain imaging to assess the effects of pramipexole vs levodopa on Parkinson disease progression. *JAMA* **287**, 1653–61.
39. Hall, H., Halldin, C., Guilloteau, D., Chalon, S., Emond, P., Besnard, J., Farde, L., and Sedvall, G. (1999) Visualization of the dopamine transporter in the human brain postmortem with the new selective ligand [125I]PE2I. *Neuroimage* **9**, 108–16.
40. Kuikka, J., Baulieu, J., Hiltunen, J., Halldin, C., Bergstrom, K., Farde, L., Emond, P., Chalon, S., Yu, M., Nikula, T., Laitinen, T., Karhu, J., Tupala, E., Hallikainen, T., Kolehmainen, V., Mauclaire, L., Maziere, B., Tiihonen, J., and Guilloteau, D. (1998) Pharmacokinetics and dosimetry of iodine-123 labelled PE2I in humans, a radioligand for dopamine transporter imaging. *Eur J Nucl Med* **25**, 531–4.
41. Choi, S., Kung, M., Plossl, K., Meegalla, S., and Kung, H. (1999) An improved kit formulation of a dopamine transporter imaging agent: [Tc-99m]TRODAT-1. *Nucl Med Biol* **26**, 461–6.
42. Kung, M., Stevenson, D., Plossl, K., Meegalla, S., Beckwith, A., Essman, W., Mu, M., Lucki, I., and Kung, H. (1997) [99mTc]TRODAT-1: a novel technetium-99m complex as a dopamine transporter imaging agent. *Eur J Nucl Med* **24**, 372–80.
43. Van Laere, K., De Ceuninck. L., Dom, R., Van den Eynder, J., Vanbilloen, H., Cleynhens, J., Dupont, P., Bormans, G., Verbruggen, A., and Mortelmans, L. (2004) Dopamine transporter SPECT using fast kinetic ligands: 123I-FP-beta-CIT versus 99mTc-TRODAT-1. *Eur J Nucl Med Mol Imaging* **31**, 1119–27.

44. Meegalla, S., Plossl, K., Kung, M., Stevenson, D., Mu, M., Kushner, S., Liable-Sands, L., Rheingold, A., and Kung, H. (1998) Specificity of diastereomers of [99mTc]TRODAT-1 as dopamine transporter imaging agents. *J Med Chem* **41**, 428–36.
45. Pan, T., Xie, W., Jankovic, J., and Le, W. (2005) Genetic analysis of parkin co-regulated gene (PACRG) in patients with early-onset parkinsonism. *Neurosci Lett* **377**, 106–9.
46. Stephenson, C., Bigliani, V., Jones, H., Mulligan, R., Acton, P., Visvikis, D., Ell, P., Kerwin, R., and Pilowsky, L. (2000) Striatal and extra-striatal D(2)/D(3) dopamine receptor occupancy by quetiapine in vivo. [(123)I]-epidepride single photon emission tomography (SPET) study. *Br J Psychiatry* **177**, 408–15.
47. Black, K. J., Hershey, T., Hartlein, J. M., Carl, J. L., and Perlmutter, J. S. (2005) Levodopa challenge neuroimaging of levodopa-related mood fluctuations in Parkinson's disease. *Neuropsychopharmacology* **30**, 590–601.
48. Prunier, C., Tranquart, F., Cottier, J., Giraudeau, B., Chalon, S., Guilloteau, D., De Toffol, B., Chossat, F., Autret, A., Besnard, J., and Baulieu, J. (2001) Quantitative analysis of striatal dopamine D2 receptors with 123 I-iodolisuride SPECT in degenerative extrapyramidal diseases. *Nucl Med Commun* **22**, 1207–14.
49. Kornhuber, J., Brucke, T., Angelberger, P., Asenbaum, S., and Podreka, I. (1995) SPECT imaging of dopamine receptors with [123I]epidepride: characterization of uptake in the human brain. *J Neural Transm Gen Sect* **101**, 95–103.
50. Pirker, W., Asenbaum, S., Wenger, S., Kornhuber, J., Angelberger, P., Deecke, L., Podreka, I., and Brucke, T. (1997) Iodine-123-epidepride-SPECT: studies in Parkinson's disease, multiple system atrophy and Huntington's disease. *J Nucl Med* **38**, 1711–7.
51. Cordes, M., Hierholzer, J., Schelosky, L., Schrag, A., Richter, W., Eichstadt, H., Schulze, P., Poewe, W., and Felix, R. (1996) Iodine-123-iodo-lisuride SPECT in Parkinson's disease. *J Nucl Med* **37**, 22–5.
52. Votaw, J., Ansari, M., Mason, N., Schmidt, D., de Paulis, T., Holburn, G., Clanton, J., Votaw, D., Manning, R., and Kessler, R. (1995) Dosimetry of iodine-123-epidepride: a dopamine D2 receptor ligand. *J Nucl Med* **36**, 1316–21.
53. Chalon, S., Emond, P., Bodard, S., Vilar, M., Thiercelin, C., Besnard, J., and Guilloteau, D. (1999) Time course of changes in striatal dopamine transporters and D2 receptors with specific iodinated markers in a rat model of Parkinson's disease. *Synapse* **31**, 134–9.
54. Pizzolato, G., Chierichetti, F., Rossato, A., Cagnin, A., Fabbri, M., Dam, M., Ferlin, G., and Battistin, L. (1995) Alterations of striatal dopamine D2 receptors contribute to deteriorated response to L-dopa in Parkinson's disease: a [123I]-IBZM SPET study. *J Neural Transm Suppl* **45**, 113–22.

55. Knudsen, G. M., Karlsborg, M., Thomsen, G., Krabbe, K., Regeur, L., Nygaard, T., Videbaek, C., and Werdelin, L. (2004) Imaging of dopamine transporters and D2 receptors in patients with Parkinson's disease and multiple system atrophy. *Eur J Nucl Med Mol Imaging* **31**, 1631–8.
56. Laruelle, M. and Huang, Y. (2001) Vulnerability of positron emission tomography radiotracers to endogenous competition. New insights. *Q J Nucl Med* **45**, 124–38.
57. Frey, K. A., Koeppe, R. A., and Kilbourn, M. R. (2001) Imaging the vesicular monoamine transporter. *Adv Neurol* **86**, 237–47.
58. Frey, K. A., Koeppe, R. A., Kilbourn, M. R., Vander Borght, T. M., Albin, R. L., Gilman, S., and Kuhl, D. E. (1996) Presynaptic monoaminergic vesicles in Parkinson's disease and normal aging. *Ann Neurol* **40**, 873–84.
59. Bohnen, N. I., Koeppe, R. A., Meyer, P., Ficaro, E., Wernette, K., Kilbourn, M. R., Kuhl, D. E., Frey, K. A., and Albin, R. L. (2000) Decreased striatal monoaminergic terminals in Huntington disease. *Neurology* **54**, 1753–9.
60. Miller, G. W., Erickson, J. D., Perez, J. T., Penland, S. N., Mash, D. C., Rye, D. B., and Levey, A. I. (1999) Immunochemical analysis of vesicular monoamine transporter (VMAT2) protein in Parkinson's disease. *Exp Neurol* **156**,138–48.
61. Suzuki, M., Desmond, T. J., Albin, R. L., and Frey, K. A. (2002) Striatal monoaminergic terminals in Lewy body and Alzheimer's dementias. *Ann Neurol* **51**, 767–71.
62. Suzuki, M., Desmond, T. J., Albin, R. L., and Frey, K. A. (2001) Vesicular neurotransmitter transporters in Huntington's disease: initial observations and comparison with traditional synaptic markers. *Synapse* **41**, 329–36.
63. Lehericy, S., Brandel, J. P., Hirsch, E. C., Anglade, P., Villares, J., Scherman, D., Duyckaerts, C., Javoy-Agid, F., and Agid, Y. (1994) Monoamine vesicular uptake sites in patients with Parkinson's disease and Alzheimer's disease, as measured by tritiated dihydrotetrabenazine autoradiography. *Brain Res* **659**, 1–9.
64. Aarsland, D., Sharp, S., and Ballard, C. (2005) Psychiatric and behavioral symptoms in Alzheimer's disease and other dementias: etiology and management. *Curr Neurol Neurosci Rep* **5**, 345–54.
65. Clader, J. W. and Wang, Y. (2005) Muscarinic receptor agonists and antagonists in the treatment of Alzheimer's disease. *Curr Pharm Des* **11**, 3353–61.
66. Riepe, M. W. (2005) Cholinergic treatment: what are the early neuropathological targets? *Eur J Neurol* **3**, 3–9.
67. Longo, F. M. and Massa, S. M. (2004) Neuroprotective strategies in Alzheimer's disease. *NeuroRx* **1**, 117–27.
68. Yan, Z. and Feng, J. (2004) Alzheimer's disease: interactions between cholinergic functions and beta-amyloid. *Curr Alzheimer Res* **1**, 241–8.
69. Bergstrom, K., Halldin, C., Savonen, A., Okubo, Y., Hiltunen, J., Nobuhara, K., Swahn, C., Karlsson, P., McPherson, D., Knapp, F., Larsson, S., Schnell, P., and Farde, L. (1999) Iodine-123 labelled Z-(R,R)-IQNP: a potential radioligand for visualization of M(1) and M(2) muscarinic acetylcholine receptors in Alzheimer's disease. *Eur J Nucl Med* **26**, 1482–5.

70. Knapp, F., McPherson, D., Luo, H., and Zeeburg, B. (1997) Radiolabeled ligands for imaging the muscarinic-cholinergic receptors of the heart and brain. *Anticancer Res* **17**, 1559–72.
71. Norbury, R., Travis, M., Erlandsson, K., Waddington, W., Owens, J., Pimlott, S., Ell, P., and Murphy, D. (2005) In vivo imaging of muscarinic receptors in the aging female brain with (R,R)[123I]-I-QNB and single photon emission tomography. *Exp Gerontol* **40**, 137–45.
72. Sunderland, T., Esposito, G., Molchan, S. E., Coppola, R., Jones, D. W., Gorey, J., Little, J. T., Bahro, M., and Weinberger, D. R. (1995) Differential cholinergic regulation in Alzheimer's patients compared to controls following chronic blockade with scopolamine: a SPECT study. *Psychopharmacology* **121**, 231–41.
73. Kemp, P. M., Holmes, C., Hoffmann, S., Wilkinson, S., Zivanovic, M., Thom, J., Bolt, L., Fleming, J., and Wilkinson, D. G. (2003) A randomised placebo controlled study to assess the effects of cholinergic treatment on muscarinic receptors in Alzheimer's disease. *J Neurol Neurosurg Psychiatry* **74**, 1567–70.
74. Nordberg, A. (2001) Nicotinic receptor abnormalities of Alzheimer's disease: therapeutic implications. *Biol Psychiatry* **49**, 200–10.
75. Saji, H., Ogawa, M., Ueda, M., Iida, Y., Magata, Y., Tominaga, A., Kawashima, H., Kitamura, Y., Nakagawa, M., Kiyono, Y., and Mukai, T. (2002) Evaluation of radioiodinated 5-iodo-3-(2(S)-azetidinylmethoxy)pyridine as a ligand for SPECT investigations of brain nicotinic acetylcholine receptors. *Ann Nucl Med* **16**,189–200.
76. Vaupel, D., Mukhin, A., Kimes, A., Horti, A., Koren, A., and London, E. (1998) In vivo studies with [125I]5-I-A-85380, a nicotinic acetylcholine receptor radioligand. *Neuroreport* **9**, 2311–7.
77. Chefer, S., Horti, A., Lee, K., Koren, A., Jones, D., Gorey, J., Links, J., Mukhin, A., Weinberger, D., and London, E. (1998) In vivo imaging of brain nicotinic acetylcholine receptors with 5-[123I]iodo-A-85380 using single photon emission computed tomography. *Life Sci* **63**, PL355–60.
78. Ueda, M., Iida, Y., Mukai, T., Mamede, M., Ishizu, K., Ogawa, M., Magata, Y., Konishi, J., and Saji, H. (2004) 5-[123I]Iodo-A-85380: assessment of pharmacological safety, radiation dosimetry and SPECT imaging of brain nicotinic receptors in healthy human subjects. *Ann Nucl Med* **18**, 337–44.
79. Staley, J., van Dyck, C., Weinzimmer, D., Brenner, E., Baldwin, R., Tamagnan, G., Riccardi, P., Mitsis, E., and Seibyl, J. (2005) 123I-5-IA-85380 SPECT measurement of nicotinic acetylcholine receptors in human brain by the constant infusion paradigm: feasibility and reproducibility. *J Nucl Med* **46**, 1466–72
80. Volkow, N. D., Ding, Y. S., Fowler, J. S., and Gatley, S. J. (2001) Imaging brain cholinergic activity with positron emission tomography: its role in the evaluation of cholinergic treatments in Alzheimer's dementia. *Biol Psychiatry* **49**, 211–20.

81. Abreo, M., Lin, N.-H., Garvey, D., Gunn, D., Hettinger, A.-M., Wasicak, J., Pavlik, P., Martin, Y., Donnelly-Roberts, D., Anderson, D., Sullivan, J., Williams, M., Arneric, S., and Holladay, M. (1996) Novel 3-pyridyl ethers with subnanomolar affinity for central neuronal nicotinic acetylcholine receptors. *J Med Chem* **38**, 817–25.
82. Schmaljohann, J., Gundisch, D., Minnerop, M., Joe, A., Bucerius, J., Dittmar, C., Jessen, F., Guhlke, S., and Wullner, U. (2005) A simple and fast method for the preparation of n.c.a. 2-[18F]F-A85380 for human use. *Appl Radiat Isot* **63**, 433–5.
83. Nordberg, A., Lundqvist, H., Hartvig, P., Andersson, J., Johansson, M., Hellstrom-Lindahi, E., and Langstrom, B. (1997) Imaging of nicotinic and muscarinic receptors in Alzheimer's disease: effect of tacrine treatment. *Dement Geriatr Cogn Disord* **8**, 78–84.
84. Nordberg, A., Lundqvist, H., Hartvig, P., Lilja, A., and Langstrom, B. (1995) Kinetic analysis of regional (S)(-)11C-nicotine binding in normal and Alzheimer brains—in vivo assessment using positron emission tomography. *Alzheimer Dis Assoc Disord* **9**, 21–7.
85. Nordberg, A., Lilja, A., Lundqvist, H., Hartvig, P., Amberla, K., Viitanen, M., Warpman, U., Johansson, M., Hellstrom-Lindahl, E., Bjurling, P. et al. (1992) Tacrine restores cholinergic nicotinic receptors and glucose metabolism in Alzheimer patients as visualized by positron emission tomography. *Neurobiol Aging* **13**, 747–58.
86. Molinuevo, J. L., Llado, A., and Rami, L. (2005) Memantine: targeting glutamate excitotoxicity in Alzheimer's disease and other dementias. *Am J Alzheimers Dis Other Demen* **20**, 77–85.
87. Waxman, E. A. and Lynch, D. R. (2005) N-Methyl-D-aspartate receptor subtypes: multiple roles in excitotoxicity and neurological disease. *Neuroscientist* **11**, 37–49.
88. Lipton, S. A. (2004) Paradigm shift in NMDA receptor antagonist drug development: molecular mechanism of uncompetitive inhibition by memantine in the treatment of Alzheimer's disease and other neurologic disorders. *J Alzheimers Dis* **6** S61–74.
89. Barnes, G. N. and Slevin, J. T. (2003) Ionotropic glutamate receptor biology: effect on synaptic connectivity and function in neurological disease. *Curr Med Chem* **10**, 2059–72.
90. Lipton, S. A. (2005) The molecular basis of memantine action in Alzheimer's disease and other neurologic disorders: low-affinity, uncompetitive antagonism. *Curr Alzheimer Res* **2**, 155–65.
91. Wang, C. X. and Shuaib, A. (2005) NMDA/NR2B selective antagonists in the treatment of ischemic brain injury. *Curr Drug Targets CNS Neurol Disord* **4**, 143–51.
92. Arundine, M. and Tymianski, M. (2004) Molecular mechanisms of glutamate-dependent neurodegeneration in ischemia and traumatic brain injury. *Cell Mol Life Sci* **61**, 657–68.

93. Bressan, R., Erlandsson, K., Mulligan, R., Gunn, R., Cunningham, V., Owens, J., Cullum, I., Ell, P., and Pilowsky, L. (2004) A bolus/infusion paradigm for the novel NMDA receptor SPET tracer [123I]CNS 1261. *Nucl Med Biol* **31**, 155–64.
94. Owens, J., Tebbutt, A., McGregor, A., Kodama, K., Magar, S., Perlman, M., Robins, D., Durant, G., and McCulloch, J. (2000) Synthesis and binding characteristics of N-(1-naphthyl)-N′-(3-[(125)I]-iodophenyl)-N′-methylguanidine ([(125)I]-CNS 1261): a potential SPECT agent for imaging NMDA receptor activation. *Nucl Med Biol* **27**, 557–64.
95. Waterhouse, R. N. (2003) Imaging the PCP site of the NMDA ion channel. *Nucl Med Biol* **30**, 869–78.

Index